Theses and Dissertations   1. Thesis and Dissertation Collection, all items

1990-06

High Frequency (HF) radio signal amplitude characteristics, HF receiver site performance criteria, and expanding the dynamic range of HF digital new energy receivers by strong signal elimination

Lott, Gus K., Jr.

Monterey, California: Naval Postgraduate School

http://hdl.handle.net/10945/34806

NAVAL POSTGRADUATE SCHOOL
Monterey, California

DISSERTATION

HIGH FREQUENCY (HF) RADIO SIGNAL AMPLITUDE CHARACTERISTICS,
HF RECEIVER SITE PERFORMANCE CRITERIA, and
EXPANDING THE DYNAMIC RANGE OF HF DIGITAL NEW ENERGY
RECEIVERS BY STRONG SIGNAL ELIMINATION

by

Gus K. Lott, Jr.

June 1990

Dissertation Supervisor: Stephen Jauregui

Prepared for: Commander
(PMW-143/144)
Space and Naval Warfare Systems Command
Washington, DC 20363-5100

Commander (G80/43)
Naval Security Group Command
3801 Nebraska Ave.
Washington, DC 20393-5213

Approved for public release; distribution is unlimited

THIS PAGE INTENTIONALLY LEFT BLANK

January 20, 2011

SUBJECT: Change in distribution statement for *High Frequency (HF) Radio Signal Amplitude Characteristics, HF receiver Site Performance Criteria, and Expanding the Dynamic Range of HF Digital New Energy Receivers by Strong Signal Elimination* – June 1990.

1. Reference: Lott, Gus K., Jr. *High Frequency (HF) Radio Signal Amplitude Characteristics, HF receiver Site Performance Criteria, and Expanding the Dynamic Range of HF Digital New Energy Receivers by Strong Signal Elimination*. Monterey, CA: Naval Postgraduate School, June 1990. UNCLASSIFIED [Distribution authorized to US. Government Agencies only; Critical Technology; June 1990].

2. Upon consultation with NPS faculty, the School has determined that this thesis may be released to the public and that its distribution is unlimited, effective December 16, 2010.

University Librarian
Naval Postgraduate School

THIS PAGE INTENTIONALLY LEFT BLANK

REPORT DOCUMENTATION PAGE		Form Approved OMB No. 0704-0188

1a. REPORT SECURITY CLASSIFICATION UNCLASSIFIED	1b. RESTRICTIVE MARKINGS		
2a. SECURITY CLASSIFICATION AUTHORITY	3. DISTRIBUTION/AVAILABILITY OF REPORT ~~Distribution limited to U.S. Government Agencies only to protect critical techno- logy: June 1990. Other requests for this~~		
2b. DECLASSIFICATION/DOWNGRADING SCHEDULE			
4. PERFORMING ORGANIZATION REPORT NUMBER(S) NPS62-90-006	5. MONITORING ORGANIZATION REPORT NUMBER(S)		
6a. NAME OF PERFORMING ORGANIZATION Naval Postgraduate School	6b. OFFICE SYMBOL (If applicable) EC	7a. NAME OF MONITORING ORGANIZATION Naval Postgraduate School	
6c. ADDRESS (City, State, and ZIP Code) Monterey, CA 93943-5100		7b. ADDRESS (City, State, and ZIP Code) Monterey, CA 93943-5100	
8a. NAME OF FUNDING/SPONSORING ORGANIZATION Space and Naval Warfare Systems Command	8b. OFFICE SYMBOL (If applicable) PMW-143/144	9. PROCUREMENT INSTRUMENT IDENTIFICATION NUMBER SPACETASKS 143-1-89-45BM-005 and 144-2-89-PGS-45BN-035	

8c. ADDRESS (City, State, and ZIP Code) Commander (PMW-143/144) Space and Naval Warfare Systems Command Washington, DC 20363-5100	10. SOURCE OF FUNDING NUMBERS			
	PROGRAM ELEMENT NO.	PROJECT NO.	TASK NO.	WORK UNIT ACCESSION NO.

11. TITLE (Include Security Classification)
HIGH FREQUENCY (HF) RADIO SIGNAL AMPLITUDE CHARACTERISTICS, HF RECEIVER SITE PERFORMANCE, and EXPANDING THE DYNAMIC RANGE OF HF DIGITAL NEW ENERGY RECEIVERS BY STRONG SIGNAL

12. PERSONAL AUTHOR(S)
Lott, Gus K.

13a. TYPE OF REPORT Doctoral Dissertation	13b. TIME COVERED FROM _____ TO _____	14. DATE OF REPORT (Year, Month, Day) 1990, June, 21	15. PAGE COUNT 257

16. SUPPLEMENTARY NOTATION
The views expressed in this dissertation are those of the author and do not reflect the official policy or position of the Department of Defense or the U.S. Government.

17. COSATI CODES			18. SUBJECT TERMS (Continue on reverse if necessary and identify by block number)
FIELD	GROUP	SUB-GROUP	HF Signals; HF Receiver; Wideband Receiver; Spectrum Survey; HF Signal Amplitude Probability Distribution; Log-normal; Receiver Site Performance;analog-to-digital

19. ABSTRACT (Continue on reverse if necessary and identify by block number)

The dissertation discusses High Frequency (HF) radio sources. It consolidates data from all available, published HF spectrum surveys. The author conducted a new HF survey using detection of new energy events. The first cumulative probability distribution function for the amplitude of detected non-broadcast HF signals is developed, and the distribution is log-normal. HF receiver site performance quantification is possible using the HF signal distributions. Site performance degradation results from noise, interference, and signal path attenuation. Noise examples are presented in a 3-D format of time, frequency, and amplitude. Graphs are presented that allow estimation of the percentage of HF non-broadcast signals lost as a function of noise and interferece levels. Limitations of HF search receivers using analog-to-digital converters as the receiver front-end are discussed. Derived bounds on A/D converter performance show that today's digital technology does not provide enough dynamic range, sensitivity, or

20. DISTRIBUTION/AVAILABILITY OF ABSTRACT ☒ UNCLASSIFIED/UNLIMITED ☐ SAME AS RPT. ☐ DTIC USERS	21. ABSTRACT SECURITY CLASSIFICATION UNCLASSIFIED	
22a. NAME OF RESPONSIBLE INDIVIDUAL Stephen Jauregui	22b. TELEPHONE (Include Area Code) (408) 646-2753	22c. OFFICE SYMBOL EC/Ja

3. continued

document must be referred to Superintendent, Code 043, Naval Postgraduate School, Monterey, CA 93943-5000 or Commander, PMW-143/144, Space and Naval Warfare Systems Command, Washington, DC 20363-5100 via the Defense Technical Information Center, Cameron Station, Alexandria, VA 22304-6145.

Warning - This document contains technical data whose export is restricted by the Arms Export Control Act (Title 22, U.S.C. Sec. 2751 et. seq.) or the Export Administration Act of 1979, as ammended, Title 50, U.S.C., App 2401, et. seq. Violations of these export laws are subject to severe criminal penalties. Disseminate in accordance with provisions of OPNAVINST 5510.161, reference (jj.).

Approved for public release; distribution is unlimited

11. continued

ELIMINATION

18. continued

converter; A/D; Electromagnetic compatability; dynamic range; new energy detection; strong signal elimination

19. continued

sampling rate. Alternative dynamic range extension methods are examined. A new method of dynamic range extension by removing the strongest signals present is presented. Greater receiver sensitivity results from changing the HF signal environment seen by the A/D converter. The new method uses a phase-tracking network and signal reconstruction techniques.

HIGH FREQUENCY (HF) RADIO SIGNAL AMPLITUDE CHRARCTERISTICS, HF RECEIVER SITE PERFORMANCE CRITERIA, and EXPANDING THE DYNAMIC RANGE OF HF DIGITAL NEW ENERGY RECEIVERS BY STRONG SIGNAL ELIMINATION

by

Gus K. Lott, Jr.
Lieutenant Commander, United States Navy
B.E.E., Auburn University, 1976
M.B.A., Corpus Christi State University, 1979
M.S., Naval Postgraduate School, 1988

Submitted in partial fulfillment of the requirements for the degree of

DOCTOR OF PHILOSOPHY IN ELECTRICAL ENGINEERING

from the

NAVAL POSTGRADUATE SCHOOL
June 1990

Author:_____
Gus K. Lott, Jr.

Approved by:

Glen A. Myers	Paul H. Moose
Associate Professor of	Associate Professor of
Electrical and Computer Engineering	Electrical and Computer Engineering
Hal M. Fredricksen	Michael J. Zyda
Department Chairman and	Associate Professor of
Professor of Mathematics	Computer Science

Stephen Jauregui
Adjunct Professor of
Electrical and Computer Engineering
Dissertation Supervisor

Approved by:_____
John P. Powers, Chairman, Department of Electrical and Computer Engineering

Approved by:_____
Harrison Shull, Provost/Academic Dean

iii

ABSTRACT

The dissertation discusses High Frequency (HF) radio sources. It consolidates data from all available, published HF spectrum surveys. The author conducted a new HF survey using detection of new energy events. The first cumulative probability distribution function for the amplitude of detected non-broadcast HF signals is developed, and the distribution is log-normal. HF receiver site performance quantification is possible using the HF signal distributions. Site performance degradation results from noise, interference, and signal path attenuation. Noise examples are presented in a 3-D format of time, frequency, and amplitude. Graphs are presented that allow estimation of the percentage of HF non-broadcast signals lost as a function of noise and interference levels. Limitations of HF search receivers using analog-to-digital converters as the receiver front-end are discussed. Derived bounds on A/D converter performance show that today's digital technology does not provide enough dynamic range, sensitivity, or sampling rate. Alternative dynamic range extension methods are examined. A new method of dynamic range extension by removing the strongest signals present is presented. Greater receiver sensitivity results from changing the HF signal environment seen by the A/D converter. The new method uses a phase-tracking network and signal reconstruction techniques.

TABLE OF CONTENTS

LIST OF TABLES

LIST OF FIGURES

ACKNOWLEDGEMENT

I. INTRODUCTION

The High Frequency (HF) band, 3 to 30 MHz, is the most densely populated part of the electromagnetic spectrum. HF is the least expensive media for world-wide communications, and military organizations continue to rely on HF for strategic and tactical data exchange.

With the advent of transmitting tubes capable of generating megawatts of power, HF has become a media with two classes of signals,

♦ the strong signals generated by international broadcasting stations, and

♦ all other signals.

Today the international broadcaster has enough power, high-gain antenna systems, and excellent propagation predictions to ensure that his listening audience receives a strong, clear signal. Despite predictions that satellite communications would make international HF broadcasting obsolete, the population and sophistication of HF broadcasting systems continue to grow.

The military user must share the HF spectrum with many others. Typically the military user has a kilowatt or less of transmitting power and uses an inefficient antenna. Clandestine transmission often requires operating near the edge of propagation limitations. Exploiting military signals requires searching through an environment where the target is about one billion times weaker than adjacent

international broadcasting signals. Direct-sequence spread spectrum, frequency-hopping, and compressed-data burst modulations can complicate detection. The HF listener will find every modulation type including voice, manual-morse, phase and frequency-shift keying, facsimile, television, and pulse.

Today's best analog receivers can barely cope with the HF signal environment. Trying to find new weak signals is hard enough, but the breadth of modulation types requires large investments in analog detection hardware. Digital receiver technology (i.e., receivers which change the analog radio-frequency (RF) voltage into digital codewords prior to detection) promises to allow improvements in detection.

The design of optimum, new-energy-detecting digital receivers requires an understanding of the dynamics of the signal population. Until the 1980's there was little, if any, data collection targeted on signal amplitude characteristics. Until designers have data describing the signal environment, optimal receiver design is not possible.

The first goal of this dissertation is to consolidate the separate HF spectrum studies into a statistical description. The result proposes a probability distribution function and places a range on values of the statistical moments.

The second goal is to develop a subset of the observations which describe the military-type signal population. New observations verify the description of this

important signal subset. The data collection site is one of the Navy's Wullenweber antenna facilities.

One can use the military-type signal descriptions to assess the performance of HF receiver facilities. This dissertation proposes performance functions to measure operational degradation. The resulting description projects the percentage of signals-of-interest lost due to noise, interference, and signal-path attenuation.

The analog-to-digital converter is the key link in digital receiver performance. This dissertation quantifies bounds on dynamic range resulting from the quantizer. The results express the number-of-bits of dynamic range as a function of bandwidth and other variables.

Other than the analog-to-digital converter itself, what other methods exist to improve quantizing receiver performance? An overview shows which techniques have potential for performance improvement.

Finally, this dissertation proposes a method of altering the voltage applied to the quantizer. A way to accommodate the dynamic range required by the digital receiver is by eliminating the signal or signals which are orders of magnitude stronger than signals-of-interest.

This dissertation is organized in chapters concentrating on each of the topics mentioned above. Within the chapters are original results of research including:

♦ Development of the first signal amplitude distribution function for the set of HF signals of military interest. Included are the first estimates for the mean and variance of this probability distribution.

- ◆ Verification of the signal amplitude distribution function by new observations of HF signals made at a European receiver site.

- ◆ Experimentation showing the effect on new signal detection caused by analog-to-digital converter saturation in a digital HF receiver.

- ◆ Development of the first HF receiver site performance criteria based on detailed HF signal observations.

- ◆ Development of the first HF receiver site performance criteria which details the differences between one and two ionospheric hop sites and between daytime and nighttime operation.

- ◆ First application of the new performance criteria to forms of man-made noise and signal path attenuation at a Navy CDAA receiver site. This allowed the best estimate to date of a receiver facility's performance in terms of percentage of signals lost.

- ◆ Derivation of the bounds on the dynamic range performance of a quantizer used in a wideband HF receiver system which shows that today's technology cannot meet the requirement.

- ◆ Description of a new technique to reduce the dynamic range requirement of the wideband HF receiver by eliminating the strongest signals.

Appendices provide an overview of collecting equipments, detail the newly collected data, briefly describe the types of analog-to-digital converters, and show MATHCAD computational work sheets.

II. HIGH FREQUENCY ENVIRONMENT

The High Frequency band is commonly known as shortwave (SW) radio. HF is the frequency decade from 3 MHz to 30 MHz [Ref. 1]. Regardless of the official designation, most spectrum users recognize HF as the span 1.7 MHz to 30 MHz. The lower-band limit is the edge of the medium wave AM broadcasting band. Ionospheric propagation, which allows long-distance worldwide communications, is the primary property which makes HF so important.

By international treaty, the International Telecommunications Union (ITU) allocates the international aspects of spectrum usage. The intent is to provide efficient allocation of limited spectrum and to minimize interference among spectrum users. Within the HF band, the ITU allocates space to the following services (with examples) [Ref. 2]:

- ◆ Fixed - radio communications between fixed land points (embassy to central government)

- ◆ Aeronautical Mobile - radio communications between an aircraft and a land station or between aircraft (air traffic control)

- ◆ Maritime Mobile - radio communications between a ship and a coastal station or between ships (public telegraph message service)

- ◆ Land Mobile - radio communications between a mobile land station and a stationary land station or between two mobile land stations (police dispatching)

5

- Aeronautical Radionavigation - determination of aircraft position for the purpose of navigation by means of the propagation properties of radio waves (Beacons)

- Maritime Radionavigation - determination of ship position for the purpose of navigation by means of the propagation properties of radio waves (LORAN)

- Radiolocation - determination of position for purposes other than those of navigation by means of the propagation properties of radio waves (Over-the-Horizon RADAR)

- Broadcasting - radio communications intended for direct reception by the general public (BBC World Service)

- Amateur - radio communications carried on by persons interested in radio technique solely with a personal aim without pecuniary interest (HAM radio)

- Earth-Space - radio communications between the earth and stations located beyond the earth's atmosphere (direct broadcast radio)

- Space - radio communications between stations beyond the earth's atmosphere (Tracking and Data Relay Satellite)

- Radio Astronomy - astronomy based on the reception of radio waves of cosmic origin

- Standard Frequency - radio transmissions on specified frequencies of stated high precision intended for general reception for scientific, technical, and other purposes (WWV, CHU, VNG, RWM, etc.).

Figure 2.1 shows how services share HF frequency allocations. Usually one service is considered primary; others are secondary on a not to interfere basis. ITU regulations have over 1000 footnotes which allow treaty members to deviate from strict spectrum allocation. In the footnotes most countries reserve the right to use HF within their borders for governmental uses as needed.
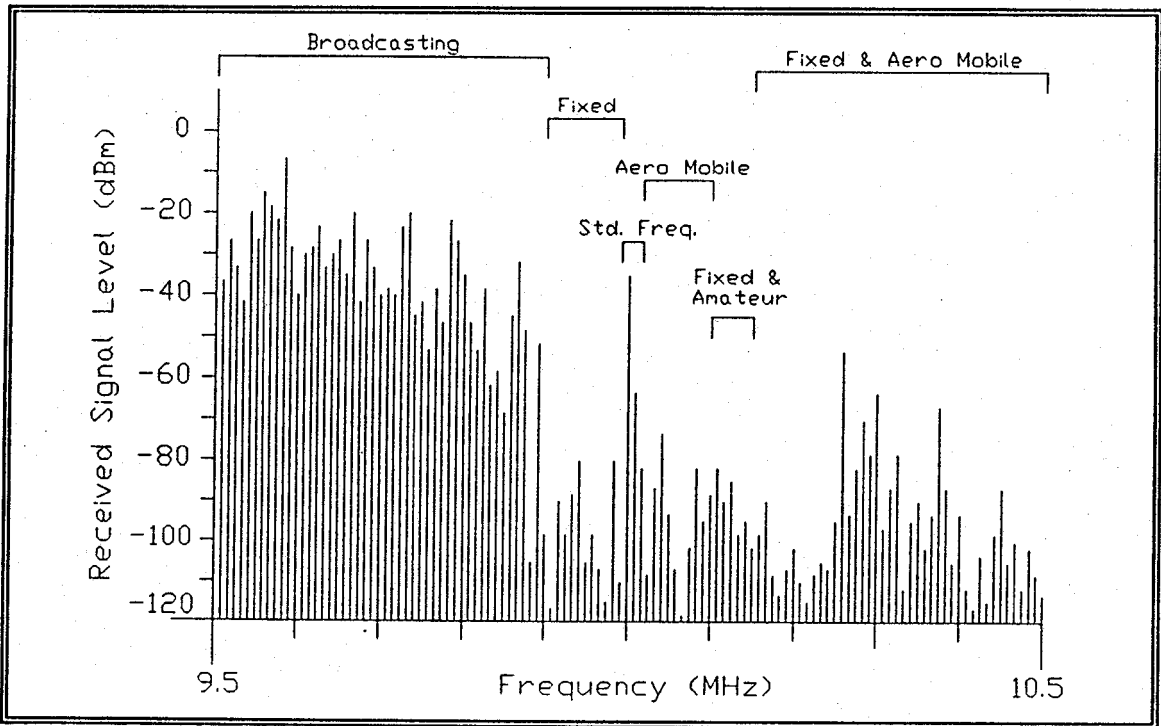
Figure 2.1 - HF Spectrum Sharing by Different Services

Propagation conditions govern military frequency selection, but military users customarily follow the ITU frequency allocations to limit interference to their own services. Military aeronautical mobile stations will use the ITU aeronautical mobile allocation which best supports the propagation between stations.

While the United States, Soviet Union, and China turn to satellite-relay military communication systems, third world military HF usage expands. High-quality, solid-state HF transceivers with one kilowatt or more of transmitting power are now commonplace, and many weigh less than 15 kilograms. Most have digitally synthesized tuning, and they are capable of operating over the entire HF band without circuit adjustment. These low-priced HF systems provide the navies of

7

small nations with their only communications when out of line-of-sight of their home base.

Within this crowded, growing signal environment, HF spectrum users must deal with several important questions:

- What are the strongest signals?

- What is the minimum-detectable signal level or noise floor?

- What dynamic range must an HF receiver have?

A. STRONGEST SIGNALS

1. International Broadcasting

International broadcasting occupies the most crowded and rapidly growing parts of the HF spectrum [Ref. 3]. Since the 1979 World Administrative Radio Conference, HF broadcasting has expanded rapidly. HF remains a major international broadcasting medium despite the enormous growth of satellite communication systems.

Smaller countries can afford several 50 to 100 kilowatt HF transmitter and simple antenna systems. A political leader can broadcast his message to the world over HF. To large-land-area countries such as Brazil, Mexico, China, Australia, and the Soviet Union, HF provides the least expensive way to broadcast to their population. In the tropical areas, HF broadcasting often rivals medium wave broadcasting because of lower atmospheric noise levels. In countries other

than the United States, most home and general-purpose radio receivers include a few SW bands. [Ref. 3]

There are 12 ITU allocated HF broadcasting bands. Table 2.1 lists these bands [Ref. 2]. As currently allocated, international broadcasting occupies some 3928 kHz of the HF spectrum. In reality, broadcasting operations extend 50 kHz or more on either side of the allocated bands. Broadcasting occupies approximately 16 percent of the limited HF spectrum, and international broadcasting is the source of most HF signals which exceed a level of -40 dBm at a given receiver site [Ref. 4].

Table 2.1 - INTERNATIONAL BROADCASTING ALLOCATIONS

Frequency Band	Meter Band
2300 - 2498 kHz	130
3200 - 3400 kHz	90
3900 - 4000 kHz	75
4750 - 4995 kHz	60
5005 - 5060 kHz	60
5950 - 6200 kHz	49
7100 - 7300 kHz	41
9500 - 9900 kHz	31
11650 - 12050 kHz	25
13600 - 13800 kHz	22
15100 - 15600 kHz	19
17550 - 17900 kHz	17
21450 - 21850 kHz	13
25670 - 26100 kHz	12

The largest international broadcasting organization is Radio Moscow, operated by the U.S.S.R. State Committee for Television and Radio Broadcasting.

Radio Moscow publicly lists some 38 home or foreign service transmitter locations within the U.S.S.R. with a published, combined transmitting power of 41.6 MW. There are at least 95 more Soviet domestic HF broadcasting frequencies. Radio Moscow has relay transmitters in Bulgaria, Cuba, and Mongolia. Adding to Radio Moscow's coverage, the U.S.S.R. has 11 HF broadcasting stations operating in the Soviet republics. [Ref. 3]

Most serious international broadcasters use multiple transmitters, power levels of 250 to 1000 kilowatts, relay stations, and large curtain array antennas. The British Broadcasting Corporation (BBC) World Service broadcasts 16 hours daily to Australia, New Zealand, Papua New Guinea, and the Pacific Ocean area. During certain hours, the BBC transmits on five frequencies to the Oceania target area (15360, 11955, 9640, 7150, and 5975 kHz) from transmitter locations outside the United Kingdom. The BBC uses HF relay stations in Singapore and Antigua, with 250 kW transmitters at each site on each frequency. [Ref. 5]

Strong signals within the international broadcast bands are the dominant signals in the HF band. Using an active, wideband, vertical monopole, Wong measured nighttime signal strengths exceeding -25 dBm. Signal strengths exceeding -40 dBm were common during daytime. Wong's survey shows nighttime international broadcast signals as much as 40 dB stronger than signals from all other HF services. Daytime signals were similarly stronger by about 20 dB. The

absorption of ionospherically propagated signals by the ionospheric D layer accounts for weaker daytime signals. [Ref. 4]

Signal strengths using large aperture antennas can be considerably higher than those received using simple antennas. Figure 2.2 shows a measurement made on the Circularly Disposed Antenna Array (CDAA), or Wullenweber antenna, at Adak, Aleutian Islands, Alaska. The Radio Moscow signal on 9580 kHz had a signal strength at the receiver input of +4 dBm. Nighttime observations at European CDAA sites routinely show strong international broadcasting signal strengths exceeding a level of -10 dBm. Appendix A describes the system used to make observations like that shown in Figure 2.2.

2. Over-the-Horizon Backscatter Radar

Another strong signal source is the Over-the-Horizon Backscatter (OTHB) radar. The primary countries using OTHB radar are the U.S. and the U.S.S.R., but France, Great Britain, the Federal Republic of Germany, and Australia are also OTHB users. HF listeners refer to the Soviet OTHB radar signal as the Woodpecker because of its periodic pulsing sound. The system uses high power transmitters (one megawatt or more) and remotely-located receiving sites. Figure 2.3 shows a typical OTHB radar system. Using ionospheric propagation, OTHB radar illuminates a large surface area. The receiver measures the backscatter wave which returns to the receiver over a similar ionospheric path.
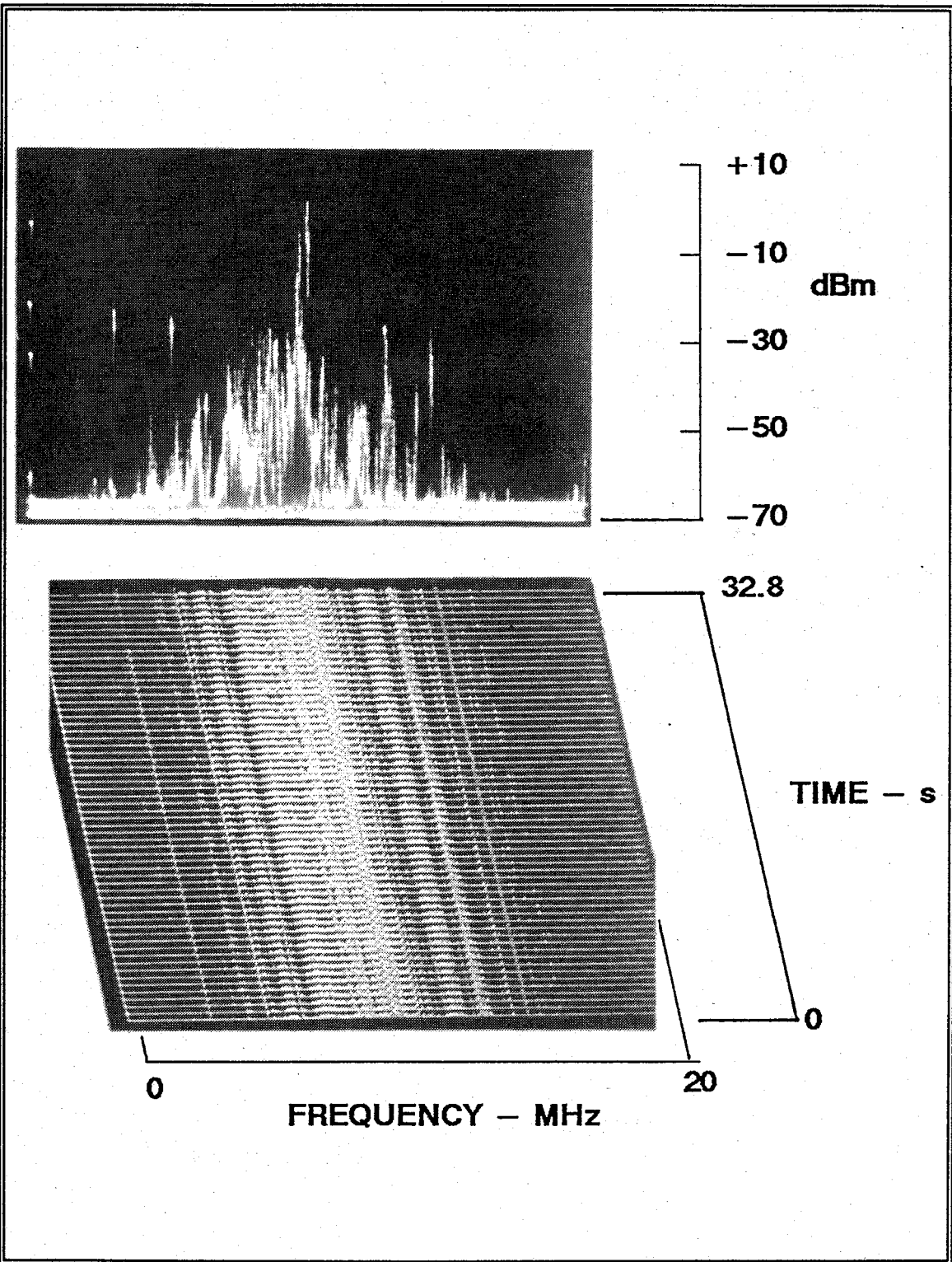
Figure 2.2 - Strong International Broadcasting Signals Received at Adak, Alaska
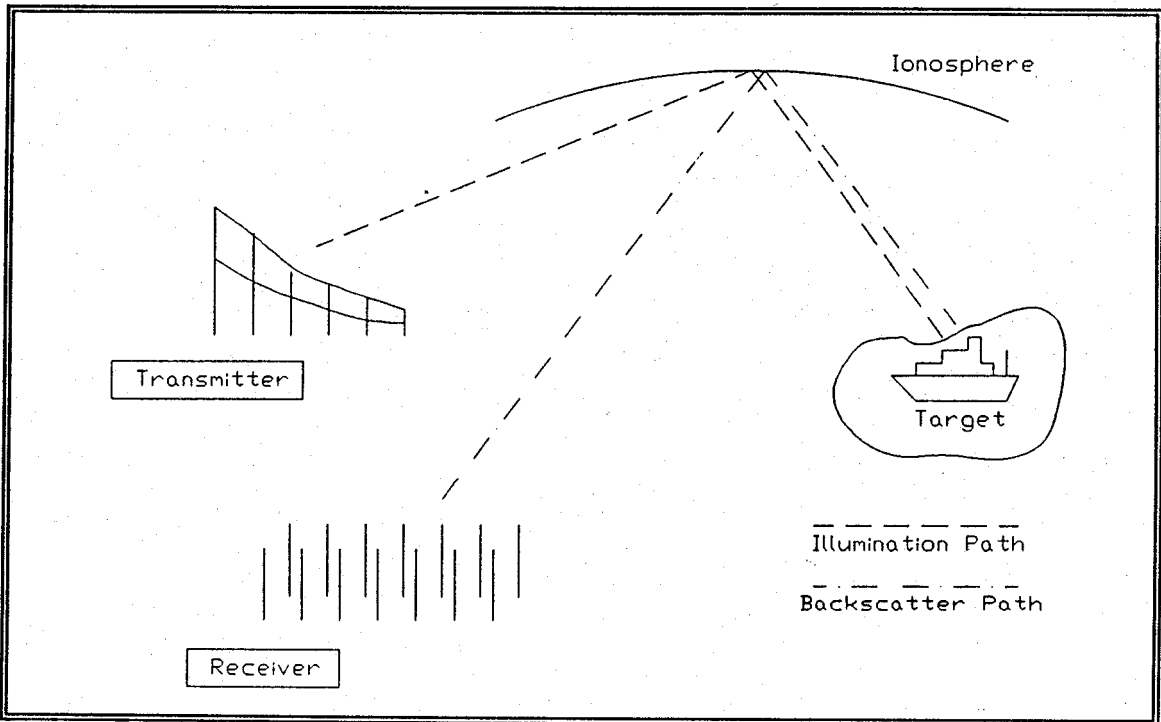
Figure 2.3 - Over-the-Horizon Radar Geometry

The primary search areas for OTHB radar are critical ocean regions out of reach of conventional radar. OTHB radar systems design utilizes a one-hop ionospheric path from the transmitter to the target which are 1000 to 4000 km in length.

The forward scatter signal from an OTHB system is a major interference source to many receiving systems. The first OTHB illumination zone is usually over water, but the second hop coverage is over a large land mass where receivers are located.

OTHB radar has a much wider bandwidth than broadcast signals, some 50 to 200 kHz compared to 10 kHz or less for broadcast systems. A receiver may

have all of its passband filled with this pulsed OTHB energy. The residence time for OTHB radars within a given allocation varies considerably. Observations show that a typical OTHB radar signal resides on one frequency for durations lasting from as short as two seconds to as long as two minutes.

Independent tests at numerous locations show that "...the strength of observed OTHB illumination did not appear to rival that of international broadcast stations...." [Ref. 6] This author's observations show otherwise. The OTHB radar signal strength may reach the 0 dBm level on large aperture arrays. In particular, the Soviet OTHB signal strength often exceeds the strongest international broadcaster's signal strength.

3. Harmful Interference

Harmful interference, commonly called jamming, uses radio signals to interfere deliberately with another radio transmission. Usually, the strongest HF harmful-interference signals are those interfering with signals in the international broadcasting bands.

Since World War II, most harmful interference to signals in the HF broadcasting service originate within the U.S.S.R. Other countries jamming HF broadcasting include Poland, Romania, Czechoslovakia, Bulgaria, China, Iraq, and Iran. [Ref. 7]

Much harmful interference involves ground-wave propagation paths where the jamming transmitters are near large population centers. This accounts

for most of the identified jammers being in the western U.S.S.R. Figure 2.4 shows the typical ground-wave interference geography.
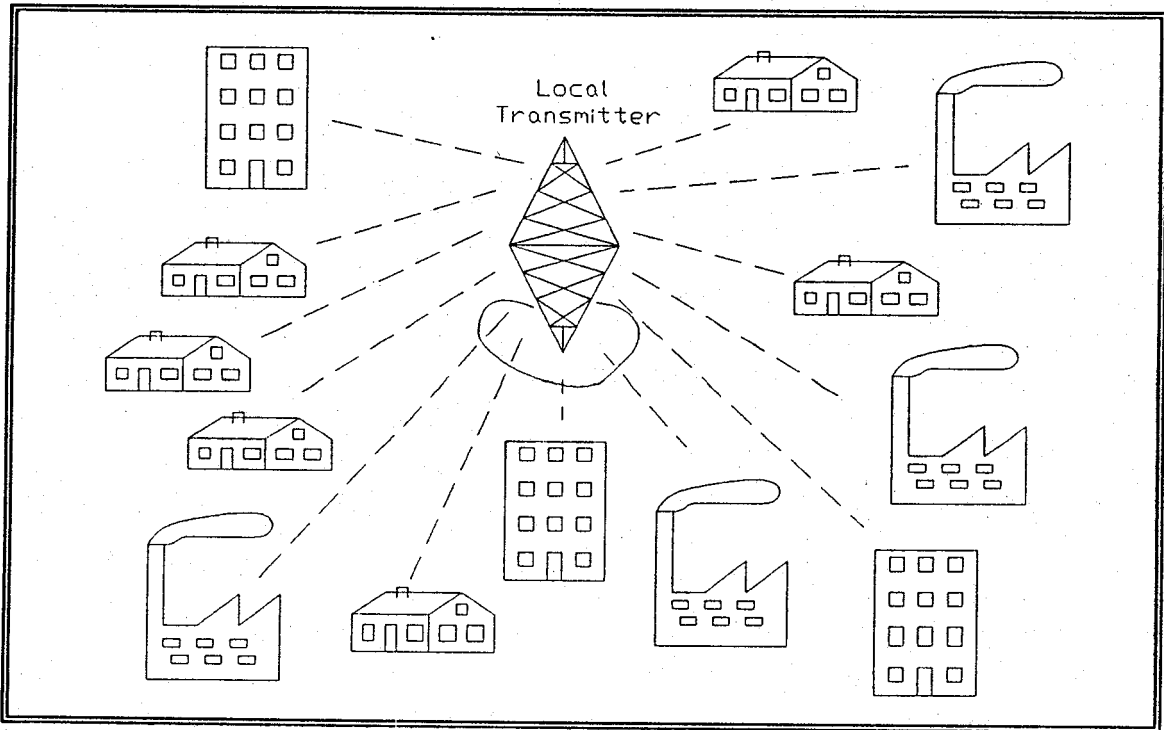
Figure 2.4 - Local Harmful Interference Operations

Some jamming occurs by sky-wave propagation modes. "It is likely that many of the emitters of harmful interference provide signals to large areas of the Soviet Union and the Bloc countries that are propagated via sky-wave ." [Ref. 7] Figure 2.5 diagrams sky wave interference operation.

Most harmful interference occurs against these international broadcasters:

♦ Voice of America

♦ Radio Free Europe

♦ Radio Liberty

15
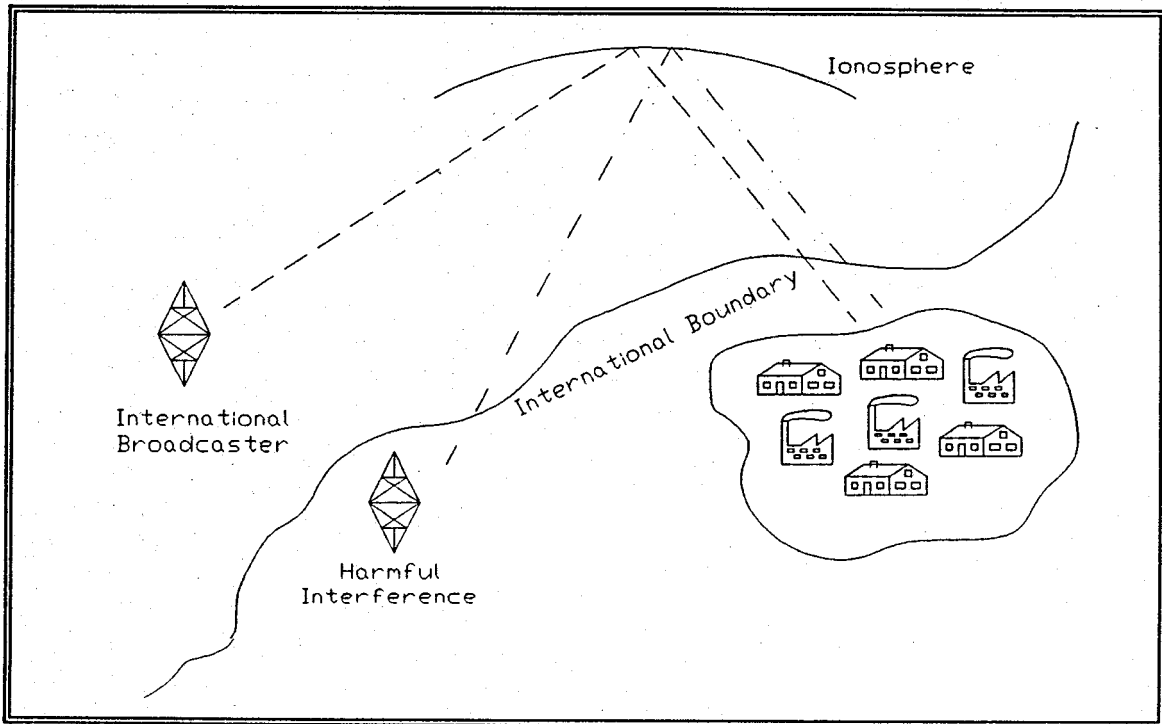
Figure 2.5 - Skywave Harmful Interference Operations

- British Broadcasting Corporation (BBC)

- Deutsche Welle

- KOL Israel.

The harmful-interference targets broadcasts in languages of the Soviet Union and Soviet Bloc countries. "... Radio Liberty and Radio Free Europe are targeted for harmful interference more than any other broadcasters...." [Ref. 7] Russian and Polish language broadcasts from all the above broadcasters are consistently jammed. Some transmissions are never without one or more harmful-interference sources. [Ref. 7]

16

With HF propagation, the harmful-interference signals also propagate into non-target areas. Many harmful-interference stations simultaneously transmit on the same frequency. The signal strengths are considerable, being greater than many HF broadcasting signals. [Ref. 8]

Sky-wave jamming signal levels may exceed -20 dBm. Because of the distribution of harmful-interference station location, most of the land mass of Europe and Asia are within one ionospheric hop from the jamming transmitters. Propagation conditions dictate that the broadcasters concentrate their transmissions within three or four international broadcasting bands. Harmful-interference stations usually concentrate on these same bands.

Since 1988, there has been a dramatic reduction in harmful-interference signals, particularly from the U.S.S.R. However, the Soviet Union has not dismantled the jamming facilities. The People's Republic of China began extensive jamming of Voice of America signals during the Spring of 1989. China's jamming coincided with the student demonstrations in Beijing. This demonstrates how quickly a country can turn to harmful interference. During hostilities, harmful interference will significantly contaminate HF spectrum, and receiver facilities throughout the world will feel the impact of the jamming.

B. MINIMUM-DETECTABLE SIGNAL

The usual definition of minimum-detectable signal (MDS) is the presence of a signal at least 3 dB above the received noise floor. The MDS will be different

for each receiver site and for each modulation system. In addition, the noise floor will vary with sunspot cycle, season, time-of-day, and the activity of man-made noise sources.

The ideal minimum noise floor is thermal noise, or the kTB noise level of -144 dBm per kHz of bandwidth. HF energy-detection receivers using Fast Fourier Transform spectral estimation techniques commonly use 1 kHz resolution bandwidth. "Measurements have shown that spectral occupancy measurements are approximately independent for frequency separations greater than 1 kHz." [Ref. 9] A 1 kHz bandwidth is a common reference bandwidth.

At HF, the noise components which set a realistic noise baseline are:

♦ Atmospheric

♦ Galactic

♦ Man-made.

Figure 2.6, adapted from Sosin's review of CCIR Report 322, summarizes the average effects of these noise sources. [Ref. 10]

1. Atmospheric Noise

Thunderstorm lightning discharges are the main source of HF atmospheric noise. Figure 2.7 shows the spectral emission characteristics of lightning noise. The line is the cubic-spline fit to data points from observations made at many locations by many researchers. [Ref. 11]
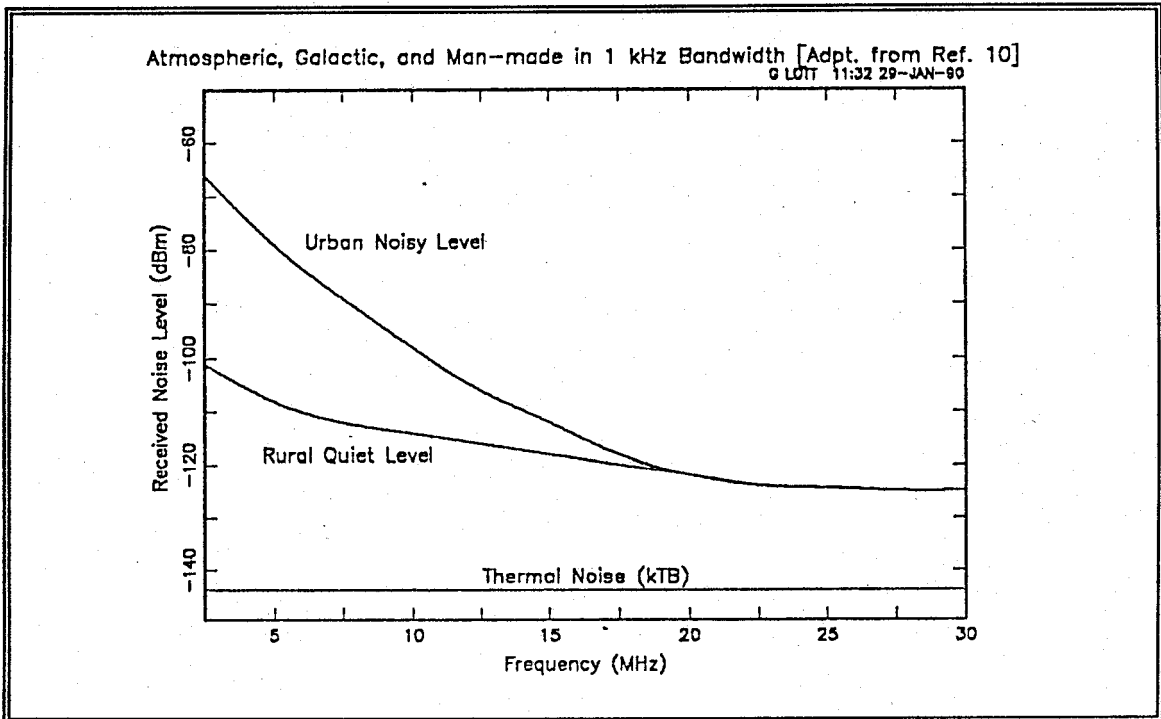
Figure 2.6 - Average Expected HF Noise Levels for Central Latitudes
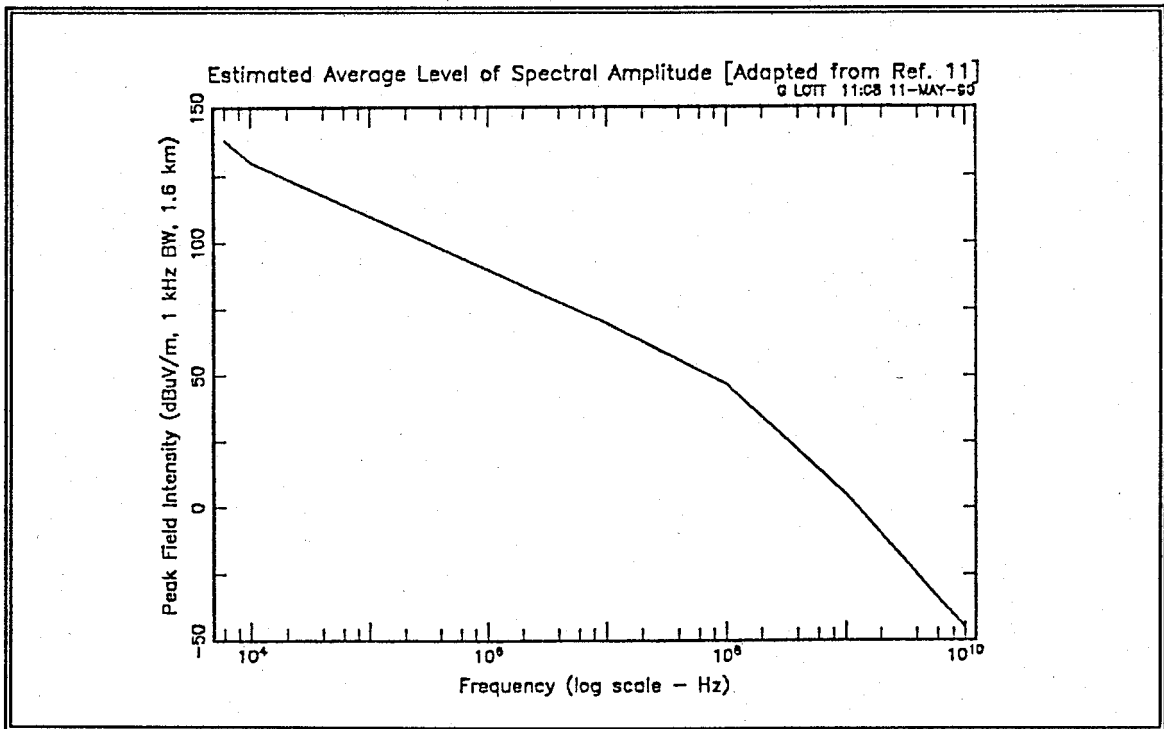
Figure 2.7 - Lightning Amplitude Characteristics

19

The highest levels of atmospheric noise are found in the tropics. Extreme atmospheric HF noise levels near Panama and Mozambique can reach -60 dBm. Atmospheric noise propagates via the ionosphere, so daytime, summer atmospheric noise levels may be 30 dB above kTB as far north as the Arctic Circle. Figure 2.8 shows the spectral width of an ionospherically propagated atmospheric noise (sferic) received at Adak, Alaska, from a distant lightning strike. The view shows the maximum and minimum propagating frequencies. [Ref. 12]
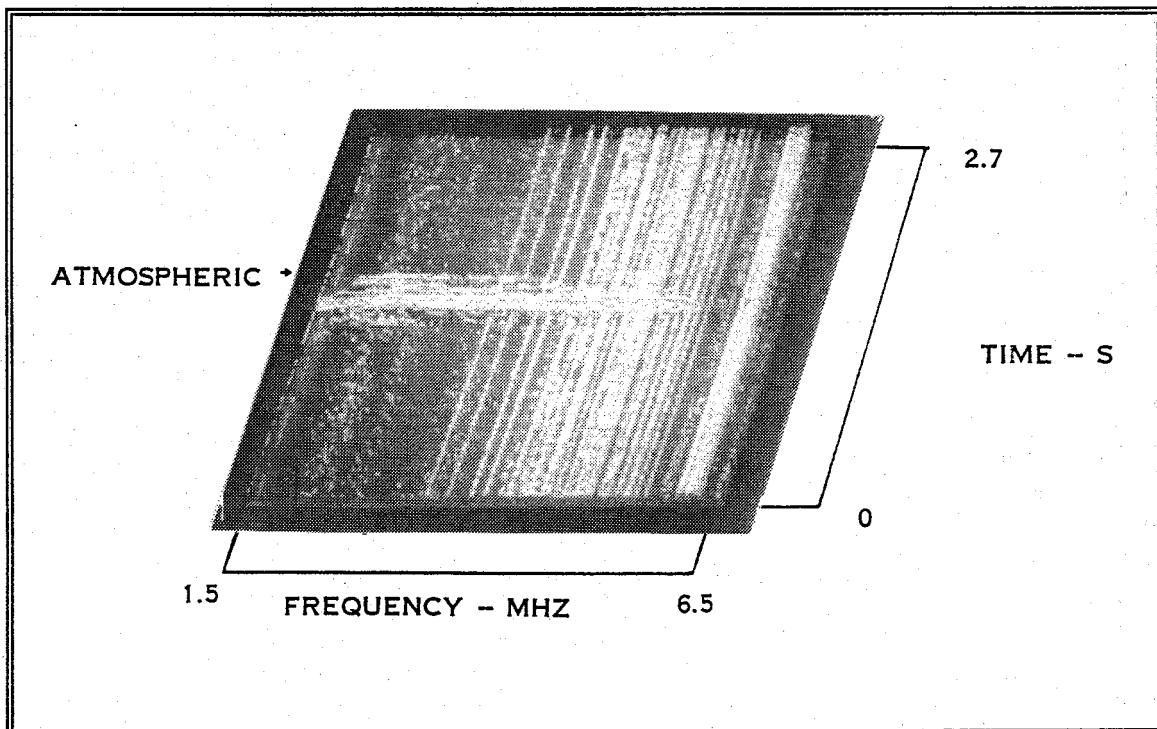
Figure 2.8 - Ionospherically Propagated Lightning Noise

2. Galactic Noise

Galactic noise is radio frequency noise originating from outside the earth's atmosphere. Galactic noise also contributes to HF noise levels. It is

strongest above 15 MHz, and it provides a background noise level about 20 dB above kTB. [Ref. 1]

3. Man-made Noise

Man-made noise is potentially the strongest HF noise source. It comes from many sources, including:

- Distribution Power Lines (Gap Noise)

- Transmission Power Lines (Corona Noise and Gap Noise)

- Motor Vehicles (Ignition and Alternator Noise)

- Industrial Processes

- RF Stabilized Arc Welders

- Industrial, Scientific, and Medical (ISM) Signals (out-of-band)

- Digital System Noise (computers and digital communications)

- Nearby HF Transmitters.

Many man-made noise sources are in line-of-site of the receiving antenna. For example, Figure 2.9 shows noise from a nearby overhead distribution power line. The peak noise level is -68 dBm in a 10 kHz bandwidth. "The most bothersome type of noise found at most (HF) sites was that emanating from electric power lines." [Ref. 13] Other noise, such as ISM, can propagate into a receiver site by ground-wave or by ionospheric modes of propagation. Figure 2.10 shows out-of-band ISM signals propagated by both means.
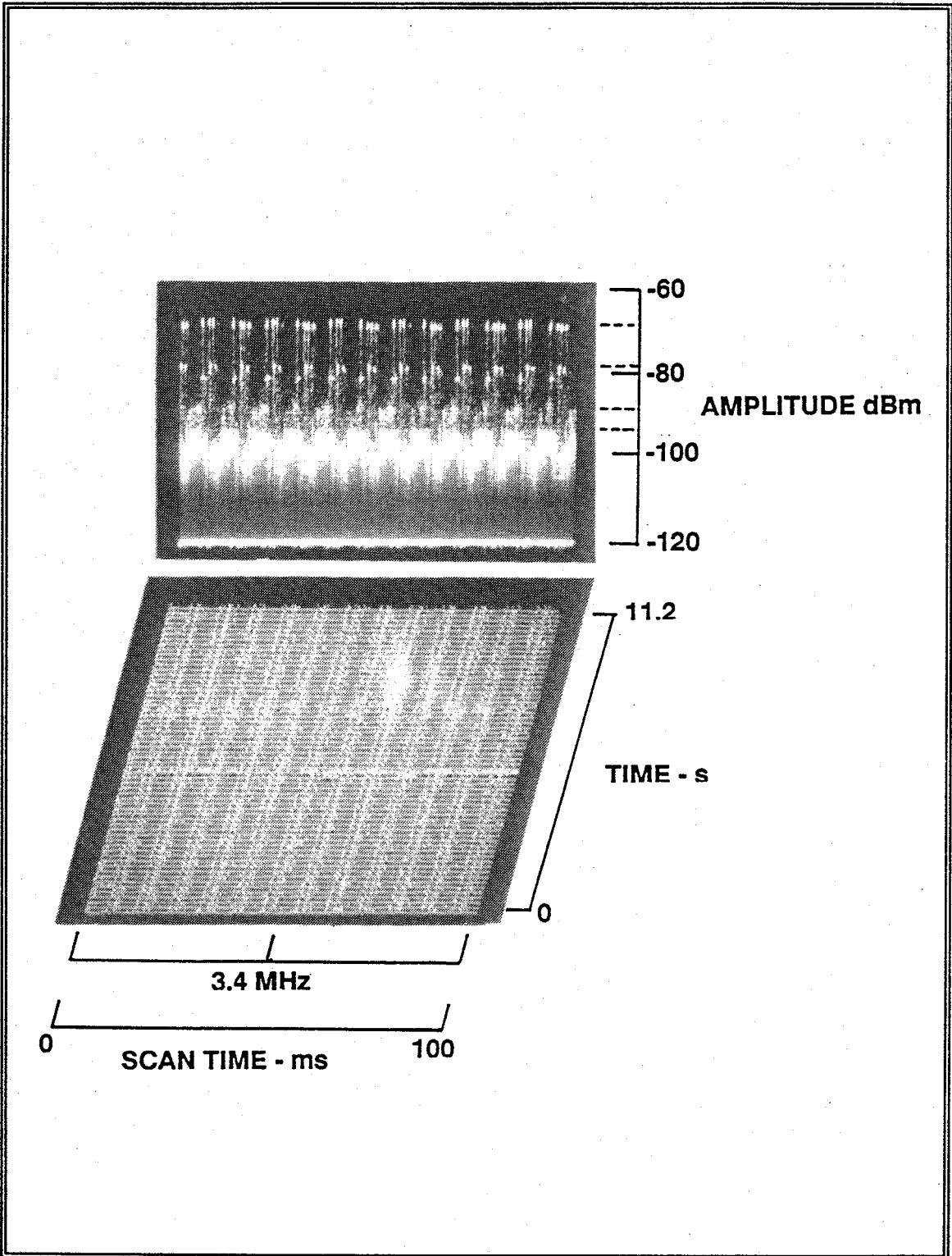
Figure 2.9 - Distribution Power-Line Related Noise
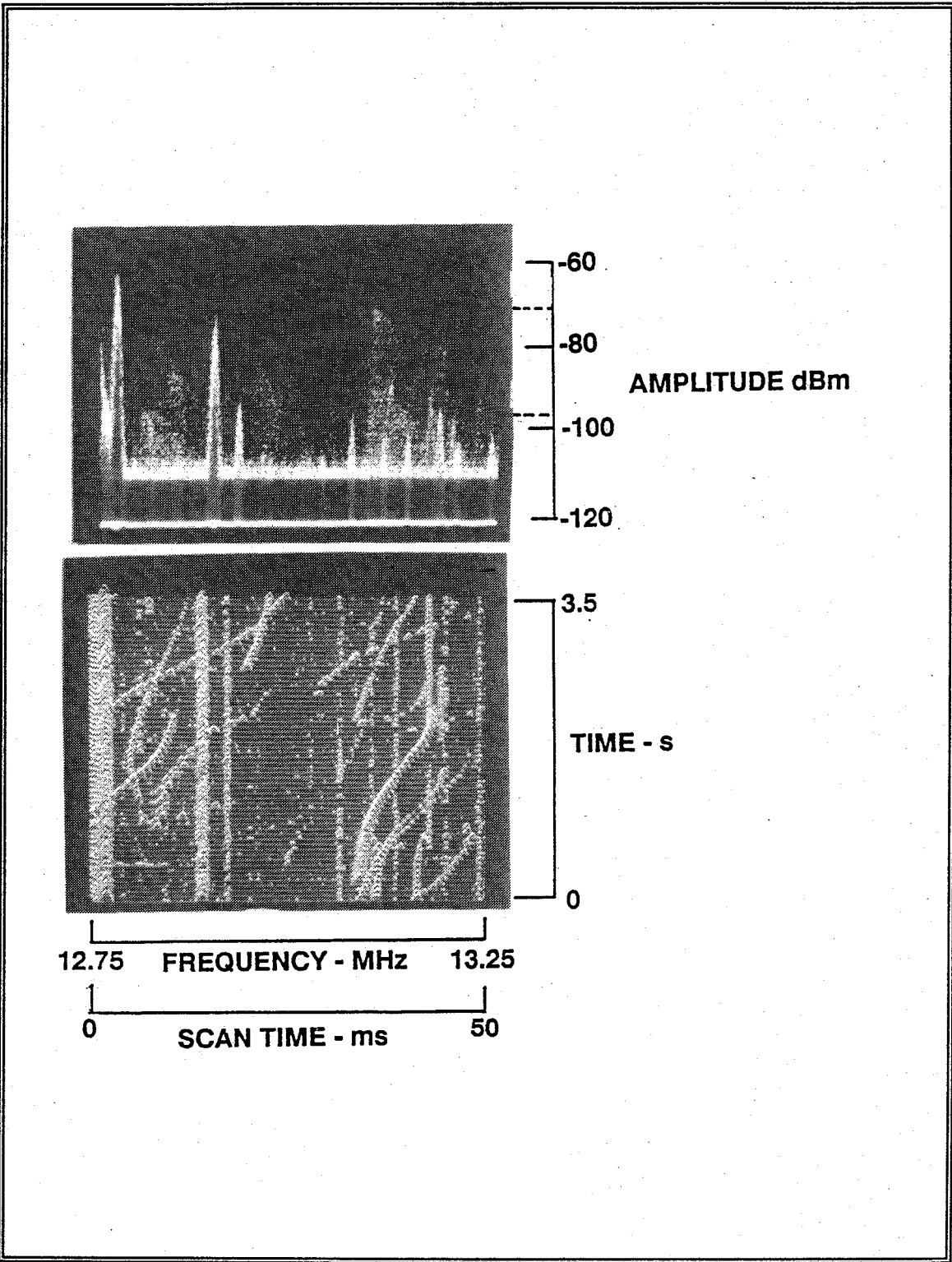
Figure 2.10 - Out-of-Band Industrial, Scientific, and Medical (ISM) Signals

Almost every HF receiver site will have some level and form of man-made noise. Some types of man-made noise cover a bandwidth of 5 MHz or more, while some have bandwidths of less than 10 kHz. Man-made noise also adds to the overall power received, so it affects both the upper and lower dynamic range limits of receiving systems.

4. Practical Noise Floor

Today's communications receivers have a sensitivity near 0.10 μV, or about -127 dBm. Table 2.2 summarizes the published sensitivities of common communication receivers. The value given is typically for 10 dB (S+N)/N, SSB mode, and approximately 3 kHz bandwidth.

Table 2.2 - MANUFACTURER SPECIFIED HF RECEIVER SENSITIVITIES

Receiver	Sensitivity
Kenwood R-5000	0.15 μV
Japan Radio NRD-525	0.50 μV
ICOM R-71	0.15 μV
ICOM R-9000	0.20 μV
RACAL R-2174	0.25 μV
Cubic R-3050	0.20 μV
Watkins Johnson WJ-8718A	0.56 μV

The three noise sources described above raise the noise floor by about 20 dB above kTB, resulting in a broad-band noise floor about -124 dBm in a 1 kHz bandwidth. Pearce and Baker propose "...a noise floor in the region of -15 dBμV (-122 dBm) in a 3 kHz bandwidth." [Ref. 14] A practical level of noise floor for

designing HF receiving systems, from antenna to receiver detector, should be at least -125 dBm in a 3 kHz bandwidth.

C. OVERALL HF DYNAMIC RANGE REQUIREMENTS

HF receiving systems with large aperture antennas must be capable of processing signal strengths as strong as -10 to 0 dBm without saturation. Signal levels above 0 dBm will be infrequent, and such extreme signal levels will be highly site dependent. The strongest signals will occur at night.

At Adak, Alaska, a receiver must be capable of processing a signal population which spans 130 dB (strong signals as high as +5 dBm to a noise floor of -125 dBm). Observations of signal population at CDAA receiver sites show that 120 dB is the antenna-to-receiver dynamic range design goal.

Pierce and Baker reached a similar conclusion. "Reception of the weakest signals, which may be as low as 0 dBμV, requires a receiver with a signal handling range of at least 120 dB (1 μV to 1 V)...." [Ref. 15]

Many of today's digitally operated HF receivers have front-end RF sections which process the entire HF spectrum without pre-selection filtering. The RACAL R-2174/U tri-service HF receiver covers 150 kHz to 30 MHz. The first stage RF amplifier covers this entire span. Yet the R-2174/U does not have a front-end amplifier with 120 dB dynamic range. The actual dynamic range is closer to 80 dB. This means that signals received by the RACAL are subject to distortion from

intermodulation processes, and spurious intermodulation products will be present in the receiver's output.

The dynamic range requirements apply to the entire RF distribution system at a receiving facility, from antenna to receiver. Multicouplers, beamformers, cables and connectors, transformers, amplifiers, filters, and switching systems must process the entire HF spectrum without distortion. This means that designers must use special care to preserve the dynamic range of received signals without increasing the noise floor.

Proper HF receiver site design should preclude the proximity of high power transmitters. This is not always possible on ships, aircraft, and at some limited-space locations. The island of Adak, Alaska, has HF transmitters within line-of-site of the receiving antenna, but the local transmitters are not the strongest signals received. Figure 2.2 shows signals from local transmitters that are 20 dB below an ionosphericly propagated international broadcast signal (Radio Moscow's transmitter some 1000 km away). The inverted cone antennas at the near-by transmitting site are approximately 5 km from the receiving CDAA, and local transmitter power is 10 kW.

Shipboard and aircraft transmitting antennas may be within 20 meters or less of the receiver antenna. In these extreme conditions, signal levels exceeding +20 dBm, or nearly 1 volt, will seriously degrade receiver performance. Adaptive attenuation, muting, and terrain shielding are mitigating techniques which strong

signal level environments require. This dissertation will not consider these special installations.

III. HF SIGNAL AMPLITUDE STATISTICS

This dissertation will use the random variable v_{in} as the root-mean-square (RMS) amplitude of the total, intercepted HF voltage applied to a receiver. In a wideband receiver searching the HF spectrum for new signals, v_{in} represents a voltage comprised of all broadcast signals, non-broadcast signals, and noise. Distortion in non-linear RF system components, losses in cables and connectors, and induced noise add an undesired component to v_{in}.

A wideband receiver and the first stages of many narrowband receivers must be capable of processing the maximum peak value of v_{in}. A narrowband receiver with pre-selection will reject signals and noise outside the pre-selector bandwidth. A much lower value of the input voltage will reach the front-end components of a narrowband receiver with pre-selector filtering.

The RMS voltage produced only by signals of military interest is considerably different than v_{in}. It will have a smaller dynamic range than v_{in}. Analog-to-digital (A/D) converters designed to optimally quantize signals of military interest should not waste limited quantization dynamic range on the high amplitude broadcast band signals. Instead, the A/D design should optimize the ability to receive and process the adversary's most clandestine transmitter.

A. HF SIGNAL STUDIES

As part of the Navy's Signal-to-Noise Enhancement Program, Prof. W. Ray Vincent and LT John O'Dwyer estimated an initial distribution of HF signal amplitudes. Using photographs taken of spectrum analyzer displays, they developed an amplitude distribution function by counting the number of signals exceeding threshold levels in 10 dB steps. This technique yielded a logarithmic distribution with a slope of approximately 0.1 per 10 dB of signal amplitude change. [Ref. 16]

In 1980, Dutta and Gott studied HF spectrum occupancy to determine the congestion levels. They compared the percentage of 1 kHz windows which had signals with amplitude greater than threshold slicing levels. This data, when viewed as an amplitude probability function, suggests a logarithmic distribution with a slope of 0.15 per 5 dB change between -125 and -110 dBm. [Ref. 17]

In 1981, Wong and others conducted an HF spectral occupancy study which provides spectrum occupancy information as a function of frequency. Their goal was to predict the probability of finding a vacant frequency for military use. A vacant frequency would have to have a signal level less than a specified amount. Wong's data includes the percentage of time a 1 kHz bandwidth has a signal level greater than specified thresholds. [Ref. 4]

Figure 3.1 displays Wong's data differently from that used in Reference 4. Figure 3.1 plots Wong's data as a two dimensional probability distribution of frequency and the amplitude as a random variable. Figure 3.2 is a plot of the 0.5
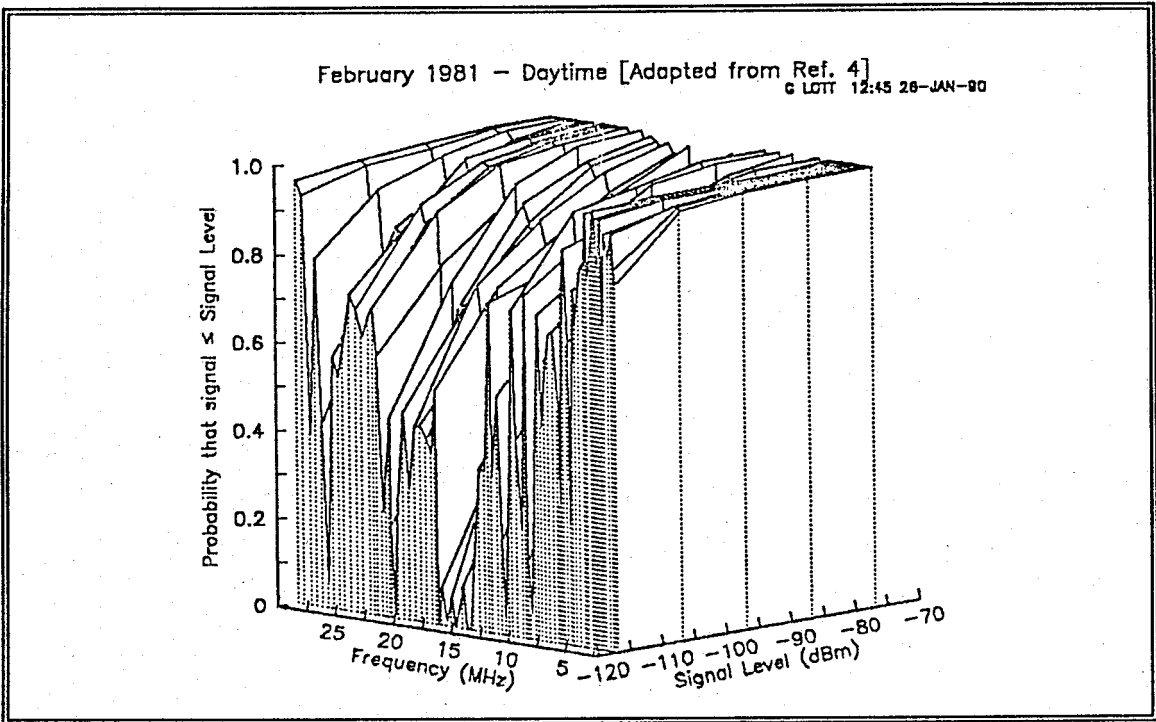
Figure 3.1 - Signal Amplitude Distribution as Function of Frequency
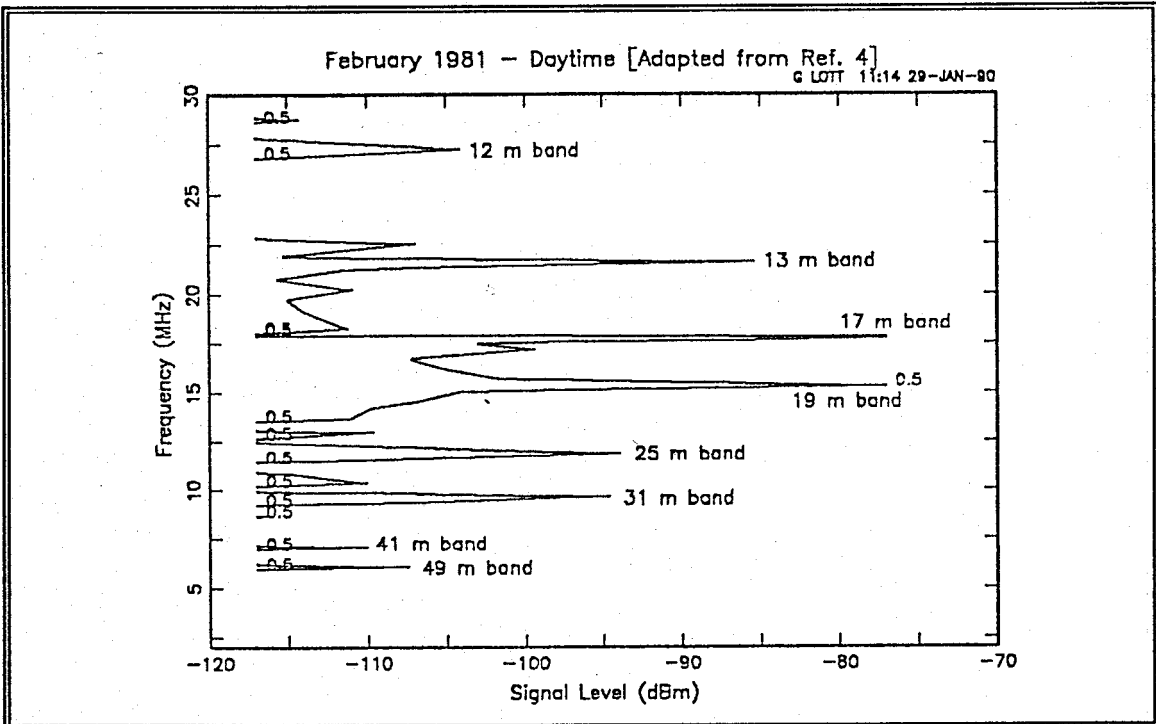
Figure 3.2 - Plot of 0.5 contours from Figure 3.1 Showing Dominance of International Broadcasting Bands

probability contours from the surface in Figure 3.1. It clearly shows the dominance of signals in the international broadcasting bands. Nearly all signals exceeding the 0.5 contours are within ITU allocated broadcasting bands.

P.A. Bradley, analyzing Wong's data, concluded "...that occupancy (or congestion) varies with the threshold level (expressed in dBm) approximately in accordance with a log-normal law." Of particular note is the limitation in Wong's measurement system that allowed it to revisit each 1 kHz frequency window only once every 3 to 5 days for one second duration. [Ref. 4]

Wilkinson performed a spectral occupancy study in which he separated data by frequency and receiver bandwidth. Figure 3.3 displays Wilkinson's data using the same type of presentation as that in Figure 3.1. He found that cumulative signal level distributions remain log-normally distributed for receiver bandwidths from 0.1 to 100 kHz. [Ref. 18]

Gibson and others conducted one of the few spectral occupancy studies using a large aperture antenna, namely a circularly disposed antenna array (CDAA) or Wullenweber antenna. After analysis, they concluded that the cumulative amplitude distributions "...are found generally to follow a log-normal law." [Ref. 19]

Moulsley used an active-antenna-based observation system to make his spectral observations. As shown in Figure 3.4, he found signals in the international broadcasting band to have power levels more than 20 dB higher than signals in the

31
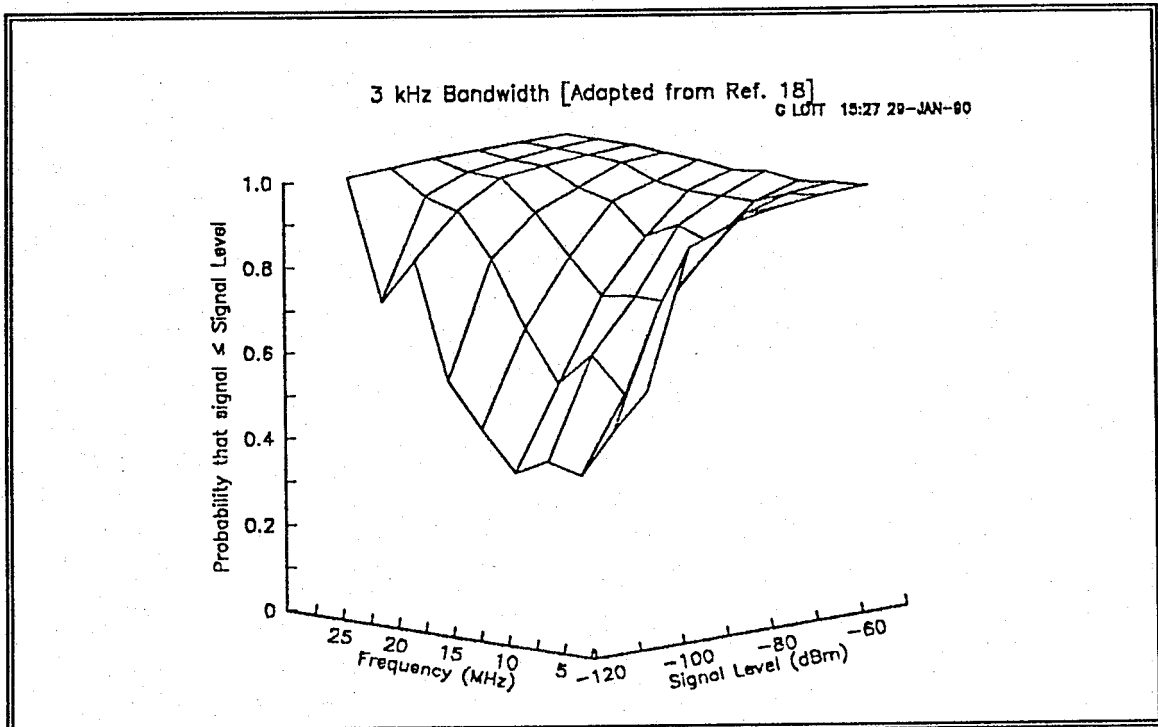
Figure 3.3 - Signal Amplitude Distribution as Function of Frequency
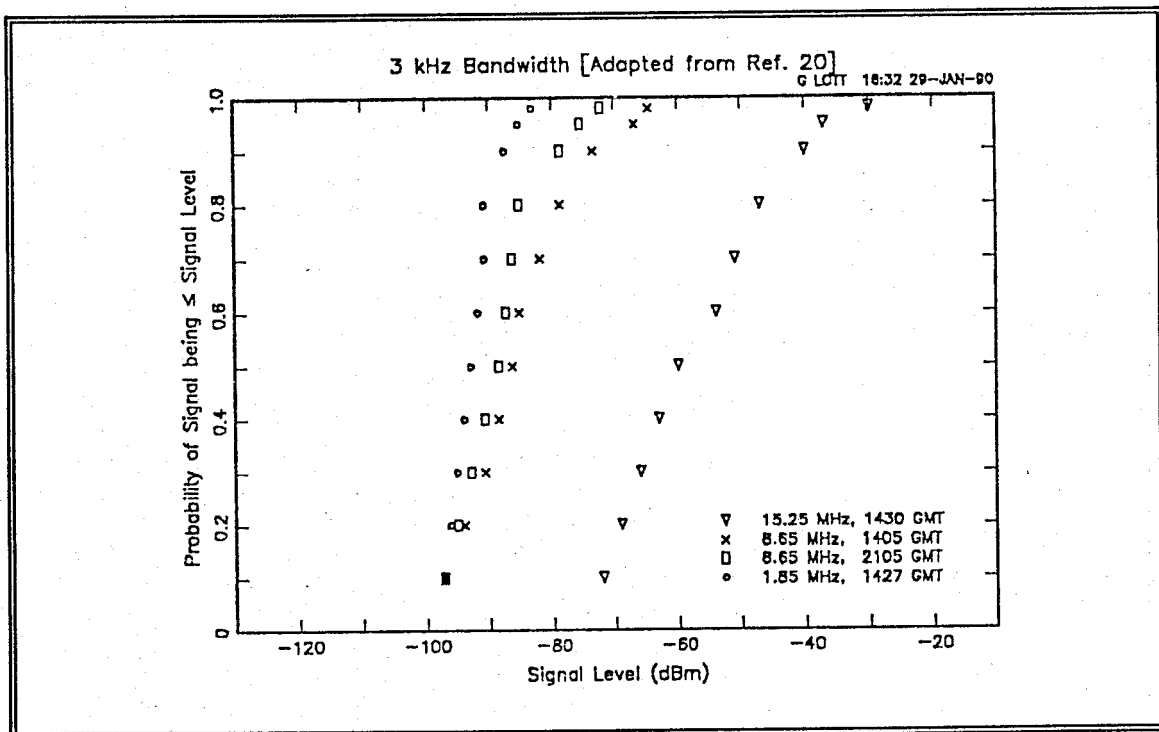
Figure 3.4 - Broadcasting vs. Non-Broadcasting Signal Amplitude Distributions

32

fixed, mobile, and maritime service bands. Moulsley's data shows an amplitude cumulative probability distribution which follows a log-normal law. [Ref. 20]

During the summer of 1987, Gibson performed a new spectral survey using a technique different from his 1981 observations. This study found little difference in spectrum occupancy from weekdays to weekends. Gibson modeled the noise floor as incident-external noise limited and distributed according to a Rayleigh law. Even with this projection, he found that the overall amplitude cumulative probability distribution followed a log-normal law. He eventually used a log-normal model for the noise floor. This survey considered specifically signals in non-broadcast portions of the HF band. This signal distribution should be similar to that expected from signals of military interest discussed earlier. Figure 3.5 displays the results. [Ref. 21]

Laycock and others made additional spectrum occupancy measurements in central England using a format similar to Wong's 1981 survey. From this they developed a model of channel occupancy, which is binomially distributed. While similar, channel occupancy is different from amplitude cumulative probability. Figure 3.6 shows the results of this study in a format similar to that used to show data from Wong's study. [Ref. 22]

Another study in 1987 by Perry and Abraham suggests that the channel occupancy statistics change when using bandwidths less than 150 Hz. The HF channel-occupancy to power-level relationship found in this study is log-log

Jul and Sep 1987 — 4.5 kHz Bandwidth [Adapted from Ref. 21]

Probability that signal ≤ Signal Level

+	13.4–13.9 MHz 1600–1800 Sunday Jul 87
∇	14.4–14.9 MHz 1600–1800 Sunday Jul 87
×	13.4–13.9 MHz 1615–1630 14 Sep 87
□	14.4–14.9 MHz 1630–1645 14 Sep 87
Δ	11.975–12.33 MHz 1800–1815 14 Sep 87
◦	11.975–12.33 MHz 1600–1615 14 Sep 87

Signal Level (dBm)
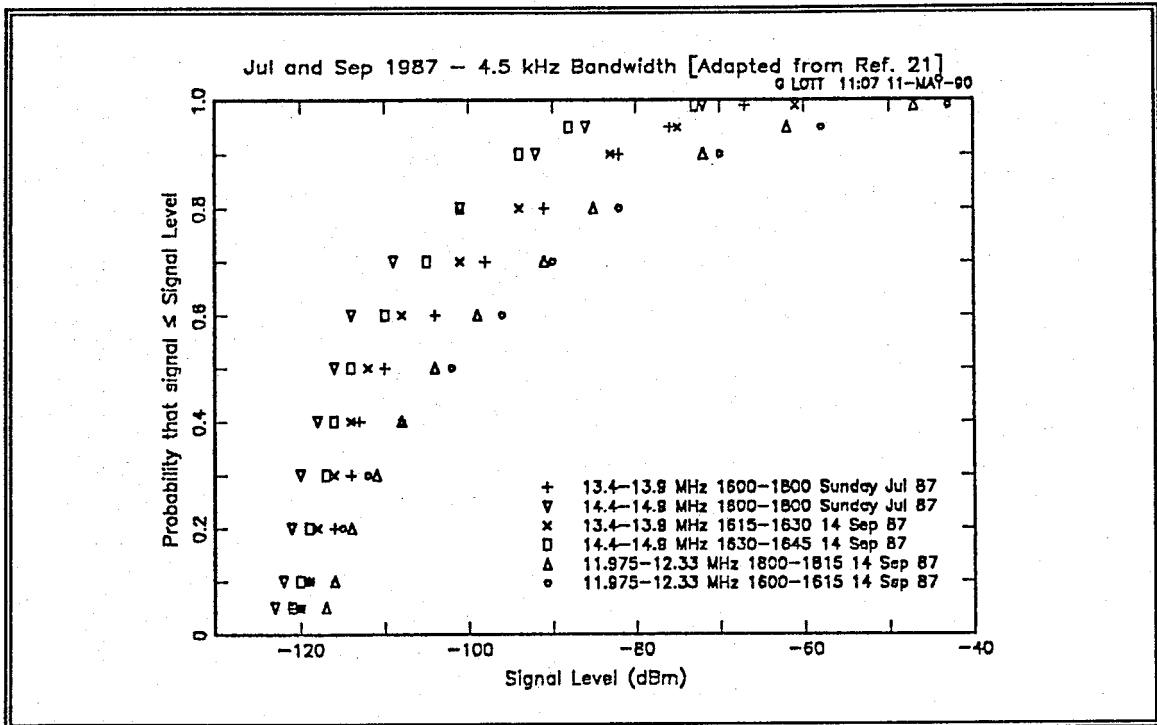
Figure 3.5 - Non-Broadcasting Signal Amplitude Distribution

July 82 — Nighttime — 3 kHz Bandwidth [Adapted from Ref.22]

Probability that signal ≤ Signal Level

Frequency (MHz)

Signal Level (dBm)
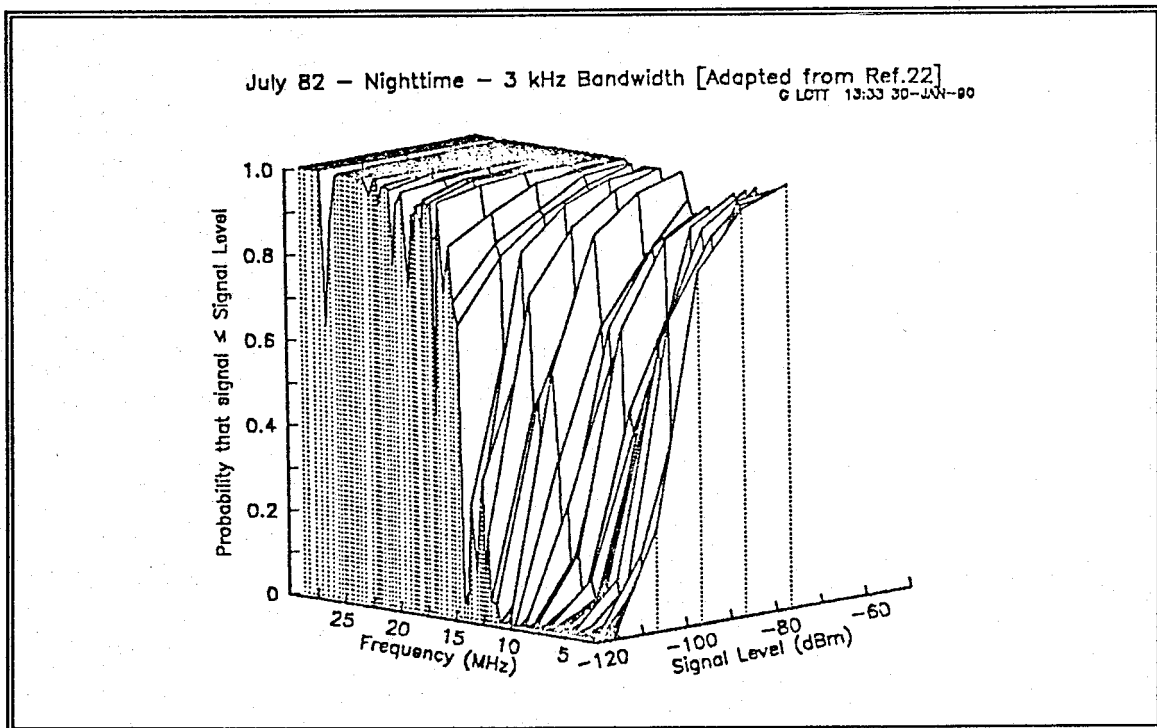
Figure 3.6 - Signal Amplitude Distribution as Function of Frequency

distributed. However, the model ignores curvature at the lower power levels due to external noise. To simplify the data required for their work, Perry and Abraham normalized all measurements to the largest interferer, or signal, present. This relationship is nearly log-normal after adding curvature on the extremes. [Ref. 23]

The most exhaustive HF signal level study published is that by Hagn and others using measurements from Europe and the U.S. taken during the Fall 1987. Most earlier studies used time averaged amplitude values, or they had long revisit times to each 1 to 3 kHz window. Hagn's survey used instrumentation that allowed rapid revisit. "Each of the 9333 3-kHz channels in the band from 2 to 30 MHz was sampled 150 times/hour...." [Ref. 24]

Figure 3.7 displays some of Hagn's data, and it reveals three significant results. First, Hagn's data follow a log-normal distribution. The slope, which indicates variance, is similar to the other tests conducted in Europe. However, the slope is steeper for the U.S. tests. The smaller variance indicates a smaller dynamic range requirement for receivers at sites in the continental U.S. environment.

Second, the mean signal level in the fixed and maritime service bands are about 20 to 30 dB below the mean of signals in the international broadcast bands. This agrees well with Moulsley's data as shown in Figure 3.4.

Third, there is a 10 to 30 dB difference in mean between signal levels in Europe and signals in the U.S.. One would expect this since most European area
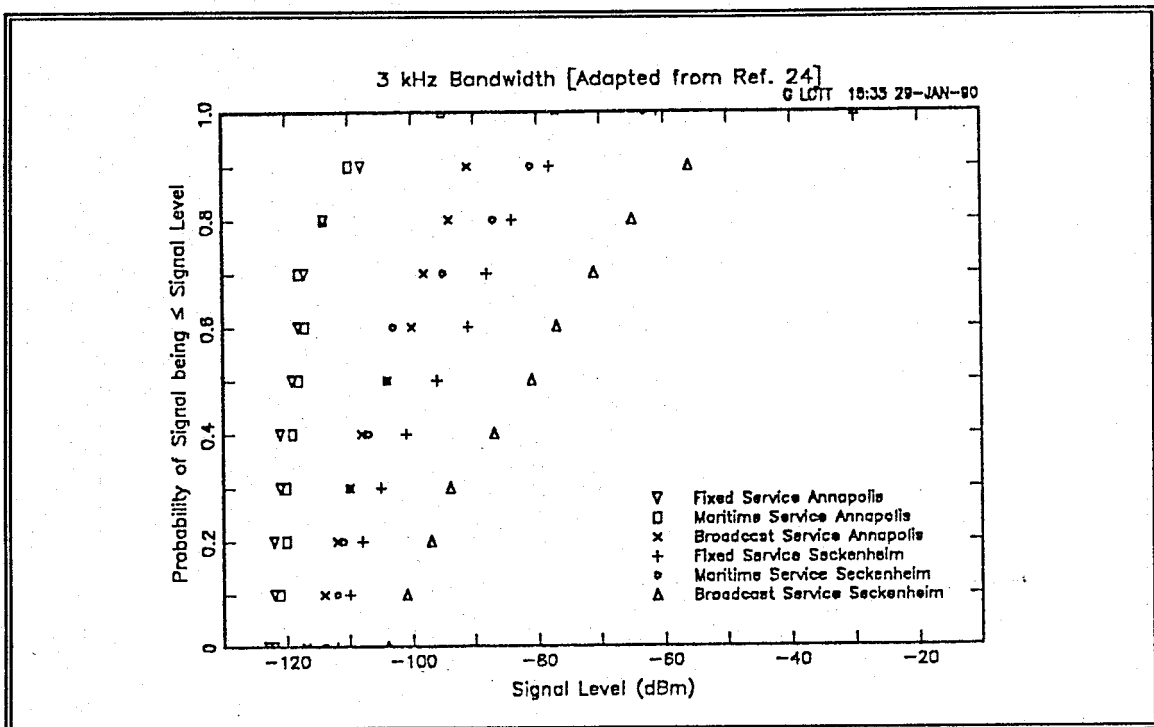
Figure 3.7 - European and CONUS Signal Amplitude Distributions

transmissions are a single ionospheric hop from many powerful transmitters, and many of the U.S. received signals are multi-hop from such sites.

Figure 3.8 shows the composite distributions from the various studies of non-broadcast signals. To reduce the number of data points displayed in Figure 3.8, the data representing Wong's and Laycock's studies (from References 4 and 22) are displayed as the arithmetic mean over all frequency bins calculated with each non-broadcast frequency bin as an independent observation.

B. THE LOG-NORMAL DISTRIBUTION

One common thread for all the studies is that they are normally distributed when plotted as a function of received signal power in dBm. This leads one to
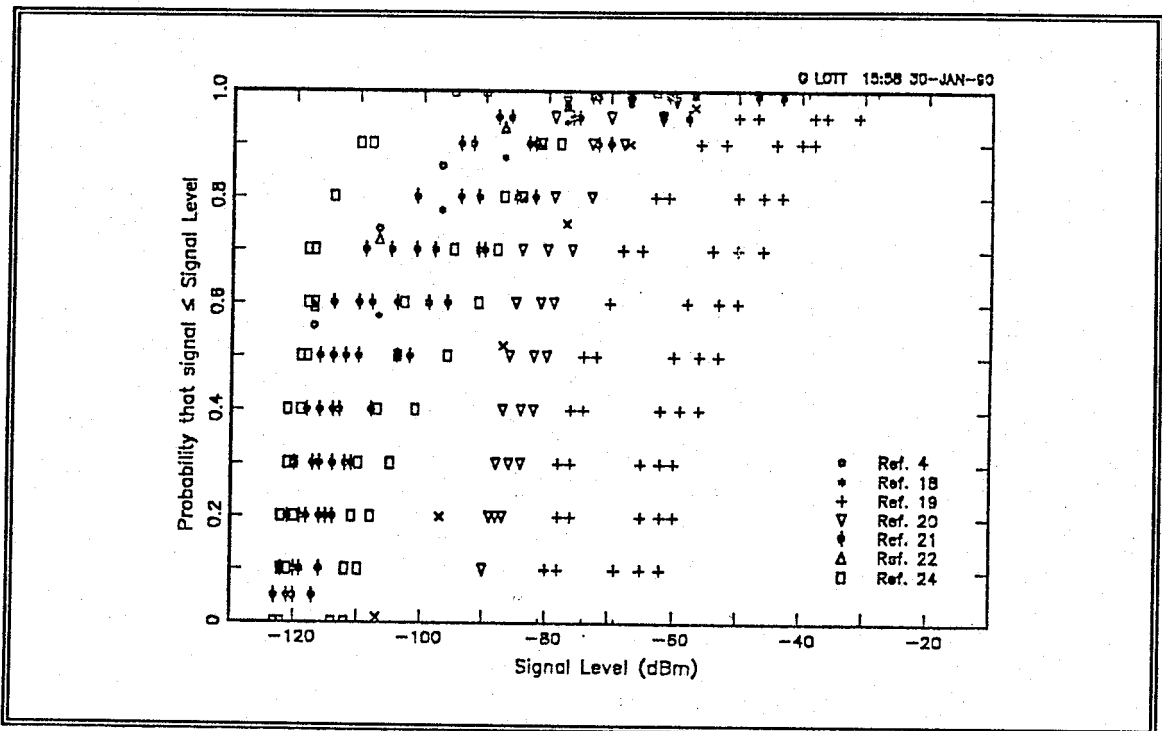
Figure 3.8 - Composite of Non-Broadcasting Signal Amplitude Distributions

the log-normal distribution for the RMS voltage v_{in} at the input to a wideband receiver.

The log-normal distribution is a positive, skewed distribution when plotted against a linear ordinate. Where the domain of the random variable for a normal distribution is all of the real numbers, the domain of the random variable for a log-normal distribution is all non-negative real numbers.

Economic trends, biological growth, and particle size commonly describe statistics that appear to be log-normally distributed [Ref. 25]. Reference 25 is the universally accepted reference on the subject. Many other references which

mention the log-normal distribution simply summarize the Aitchison and Brown [Ref. 25] work.

The random variable v_{in} represents the composite RMS voltage amplitude as described before, and w_{in} is the composite power received. With a 50 Ω load at the receiver, the relationship between w_{in} and v_{in} is given by the expression:

$$w_{in} = 20 \ \log_{10} \left[\frac{v_{in}}{\sqrt{(50)(10^{-3})}} \right] \tag{3.1}$$

where w_{in} is in dBm, v_{in} is in RMS volts such that $v_{in}>0$, and $\log_{10}$ is the logarithm to base 10.

When plotted as w_{in}, a normal distribution shape is the first indication that v_{in} may be log-normally distributed. The next step in fully describing the distribution is to calculate the mean and variance of the distribution of w_{in}, denoted as μ_{dBm} and σ^2_{dBm} respectively. Assuming normality in the dBm domain, the probability density of w_{in} is given by:

$$p_{w_{in}}(w_{in}) = \frac{1}{\sqrt{2\pi\sigma^2_{dBm}}} e^{-\frac{(w_{in}-\mu_{dBm})^2}{2\sigma^2_{dBm}}} . \tag{3.2}$$

To simplify calculations, one can write w_{in} as a natural logarithm rather than the decibel expression. Converting Equation 3.1 yields:

$$w_{in} = 8.69 \ \ln(v_{in}) + 13.01 . \tag{3.3}$$

Writing the density function of the RMS voltage amplitude v_{in} requires a change of variable. Using the transformation,

$$p_{V_{in}}(v_{in}) = p_{W_{in}}(w_{in}) \left| \frac{dw_{in}}{dv_{in}} \right| \tag{3.4}$$

and,

$$\frac{dw_{in}}{dv_{in}} = \frac{8.69}{v_{in}} \tag{3.5}$$

the probability density function for the RMS voltage amplitude v_{in} is given as:

$$p_{V_{in}}(v_{in}) = \frac{8.69}{v_{in}\sqrt{2\pi\sigma_{dBm}^2}} e^{-\frac{\left(8.69 \ln(v_{in})+13.01-\mu_{dBm}\right)^2}{2\,\sigma_{dBm}^2}} . \tag{3.6}$$

Making the substitutions

$$\mu_{\ln} = \frac{\left(\mu_{dBm}-13.01\right)}{8.69} \tag{3.7}$$

and

$$\sigma_{\ln} = \frac{\sigma_{dBm}}{8.69} , \tag{3.8}$$

the resulting distribution for the RMS voltage amplitude is:

$$p_{V_{in}}(v_{in}) = \frac{1}{v_{in}\sqrt{2\pi\sigma_{\ln}^2}} e^{-\frac{\left(\ln(v_{in})-\mu_{\ln}\right)^2}{2\sigma_{\ln}^2}} \tag{3.9}$$

which is the basic form of the log-normal distribution as used in Reference 25. The received RMS voltage amplitude will be positive since RMS implies the positive square root. Thus $v_{in}>0$ as required by the domain of the function.

Using the same notation as in Reference 25, one can write a mean and variance for the distribution of v_{in} which gives the mean, α, in rms volts as:

$$\alpha = e^{\left(\mu_{ln} + \frac{1}{2}\sigma_{ln}^2\right)} \tag{3.10}$$

and the variance, β^2, as:

$$\beta^2 = e^{\left(2\mu_{ln} + \sigma_{ln}^2\right)}\left(e^{\left(\sigma_{ln}^2\right)} - 1\right) . \tag{3.11}$$

The mean and variance, calculated using Equations 3.10 and 3.11, provide an intuitive feel for the average RMS voltage levels of the receiver input. Otherwise, most calculations remain in the logarithmic domain where the form of the distribution is well understood. The density function in Equation 3.9 involves both v_{in} and $\ln(v_{in})$. There is no simple closed-form expression for the density function in terms only of v_{in}. [Ref. 25]

An important result to be applied for the log-normal distribution is in the application of the central limit theorem. Simply stated, in non-logarithmically related distributions, the sum of independent random variables having the same probability distribution will asymptotically become a gaussian distribution.

A similar statement for the log-normal distribution is possible for the product of the random variables. In positive log-normal independent variates having the same means and variances, the product of the variates is asymptotically log-normally distributed. [Ref. 25]

This can be an important tool in estimating the products of the random variable v_{in} caused by non-linearities in the RF system. These products are the resulting intermodulation products which add as noise to the desired signal.

C. ESTIMATING MEAN AND VARIANCE

The problem here is to match an experimentally determined cumulative probability distribution function or probability density function to a theoretical function. The two dependent variables to be applied in the match are the mean and variance. To simplify calculations, the matching for HF signal studies is done in dBm. The goal is to match a normal distribution to the experimental observations. The following summarizes the mean and variance estimation methods.

1.   Quartile Estimation

A simple method exists to fit a normal probability density function to an experimentally derived histogram based on quartiles. Let N be the total number of observations. The observations are ordered in histogram form. Starting with the ordinate having the smallest value, the first quartile is the ordinate value corresponding to N/4 observations, etc. Stated differently, the first quartile is the ordinate value for which one-fourth of the observations have a value less than or equal that ordinate. The second, third, and fourth quartiles have similar definitions. The second quartile is the observational median.

Croxton used a quartile rule to provide an estimate of the mean and standard deviation of fitting a normal density based on these quartiles. [Ref. 26]

Following his derivation, we let Q_1, Q_2, and Q_3 be the quartiles of the experimental data where the data is already in logarithmic form (i.e., dBm). An estimate of mean and variance for the normal density are given as:

$$\mu = \frac{Q_1 + Q_2 + 1.2554 \; Q_3}{3.2554} \qquad (3.12)$$

and

$$\sigma^2 = 0.5495 \; (Q_3 - Q_1)^2 \; . \qquad (3.13)$$

This rule requires the data to be in histogram, or density, form. Quartile estimation provides a computationally efficient estimate. If the data are in distributional form, and if there is no exact ordinate value for 0.25, 0.5, and 0.75, interpolation error is possible. The ease in computation makes this estimation technique particularly well suited for field use.

2. Kullback-Leibler Information Measure Estimation

The Kullback-Leibler (KL) information measure is a probability density matching method. The KL test minimizes the information measure between observational statistics and a given density function. This estimation method is also a form of the Woolf-G estimation method. [Ref. 27]

Given the experimental density data p, and a theoretical density function model q, the KL test is given by:

$$I_{KL}(p;q) = \sum_{i=1}^{m} p_i \ln\left(\frac{p_i}{q_i}\right) . \qquad (3.14)$$

The goal in matching is to select the parameters which minimize the KL test distance value, given as $I_{KL}(p;q)$. Since p and q are probability distributions, $I_{KL}(p;q) \geq 0$.

3.   Kolmogoroff-Smirnoff Goodness of Fit Test

The Kolmogoroff-Smirnoff (KS) test determines how well an observed distribution fits a theoretically expected distribution. The KS test is most sensitive of these three estimating techniques to departures from the shape of the distribution function. [Ref. 27]

The goal in the test is to minimize the KS distance measure d_{ks}, which is given by:

$$d_{ks} = \min |Pr[p_i] - Pr[q_i]| \qquad (3.15)$$

where p is the experimental value and q is the theoretical model. The KS test searches for the minimum distance using the variables of the theoretical distribution. Compared to other estimating techniques, "The KS test is more likely to detect deviations from the normal distribution...." [Ref. 27] In a similar form, the KS test can match density functions.

D. MATCHED LOG-NORMAL DISTRIBUTIONS

Most of the published HF signal observations are in distributional form. The KS test is the best of the three methods to estimate the means and variances for matching theoretical distributions. The actual matching is done in the dBm domain. This results in the process of matching a normal distribution to the experimental distributions.

Figure 3.9 is a scatter plot of the means and variances used to match normal distributions to the distributions shown in Figure 3.8. The means cluster around the -100 to -120 dBm (with some higher), but the variance is widely scattered.
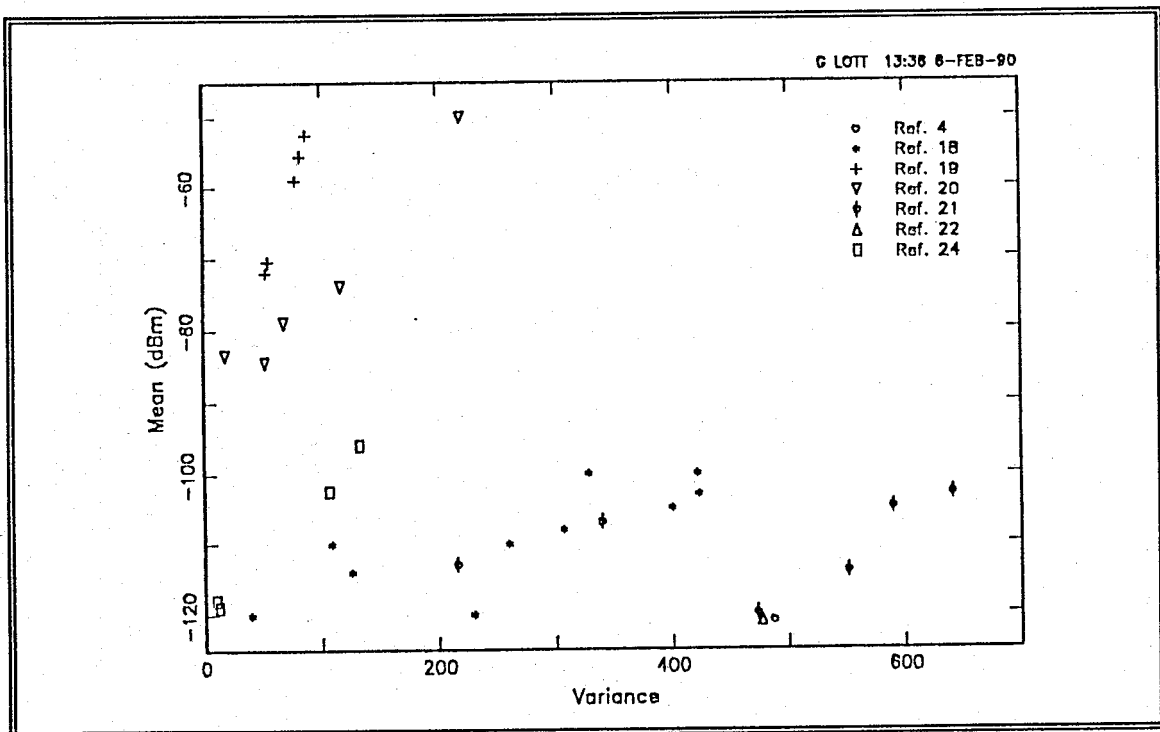
Figure 3.9 - Mean and Variance Matches Using the KS-Test

Most of the observations include day and night measurements. One should expect a smaller daytime mean and a larger nighttime mean and variance.

One can define a dynamic range requirement as the one percent to the 99 percent points on the distribution. Figure 3.10 is an example distribution using a -110 dBm mean and a variance of 100. This distribution leads to a design dynamic range of about 55 dB, and it shows the relatively small dynamic range of the received signals when one considers only signals of military interest.
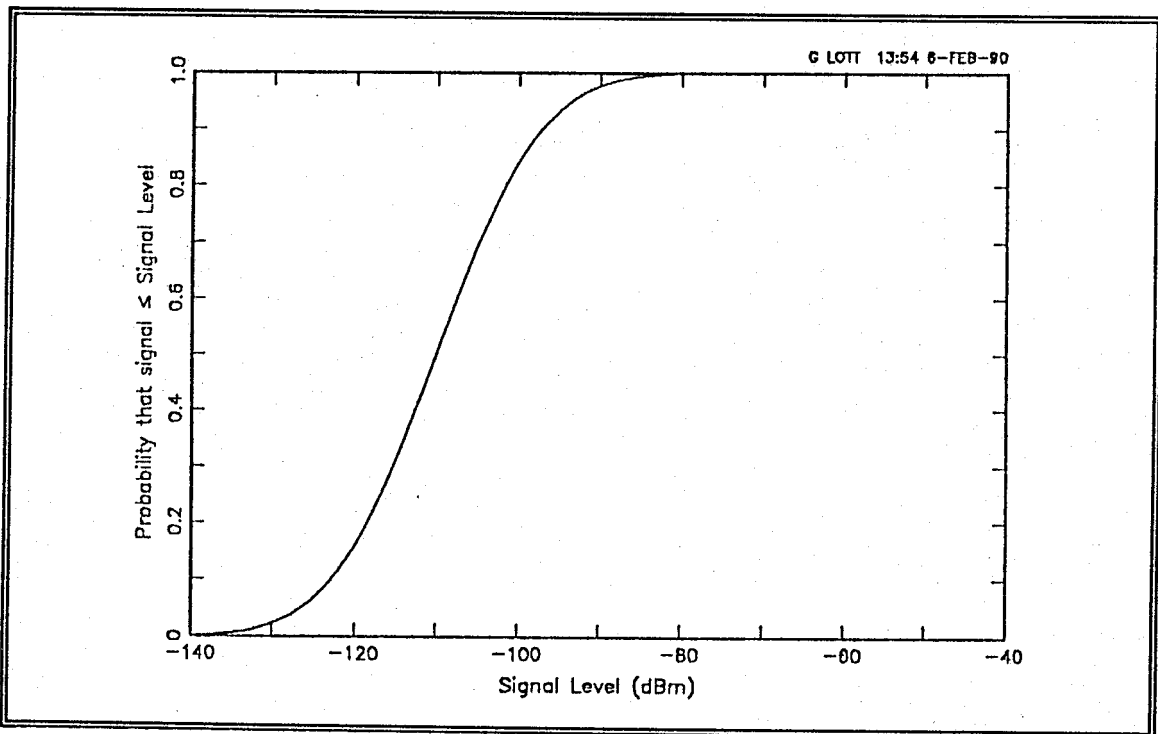
Figure 3.10 - Example Signal-of-Interest Distribution

IV. HF NEW-ENERGY OBSERVATIONS

The generalized, search receiver observes the entire HF spectrum and detects the presence of new energy. This new energy may be noise, a signal of interest, or another signal. The search receiver screens new energies using generalized parameters to create a set of new energies. These may include a subset consisting of signals of interest.

The search receiver decides if new energy is present based on certain measurements. Once screened, the search system assigns an analysis receiver to identify the new energy as a possible signal of interest. There are so many rapidly changing events in the HF spectrum that new-energy detection can, at times, be unmanageable.

When viewed as a composite voltage seen by the receiver, a voltage change alone is not an adequate indicator of a possible signal. The new-energy decision requires changes in measurable parameters including:

- Amplitude change exceeding a programmed threshold

- Duration

- Center frequency

- Bandwidth

- Identifiable frequency components (i.e., two specific frequencies used in frequency-shift keying)

- Identifiable temporal variations (i.e., spacing of amplitude-shift keying).

A new-energy system observes the entire HF spectrum before making new-energy decisions. The system usually uses an omnidirectional antenna system to allow reception from all directions.

A wideband receiving system rapidly samples the entire 2 to 30 MHz band, transforms the voltage into the frequency domain, and checks each frequency bin against programmed parameters. If the latest observation meets certain criteria, new energy is assumed to be present. There are usually many new energies present in each observation. The wideband system then assigns an analysis receiver to each new energy.

A narrowband new-energy system incorporates a different search approach. The system tunes a narrow-bandwidth receiver to a specific frequency, determines if a signal is present, and compares the frequency to a previously monitored frequency list. The frequency of the narrowband receiver may come from an established search list, or the frequency selection may be by a random process. If new energy is present, the same receiver used for new-energy detection becomes the analysis receiver by adding parameter recognizers as mentioned earlier.

The narrowband system can use either an omnidirectional or beam antenna depending on how well one can a priori define the geographic search area. The receiver component of the narrowband system is a typical HF communications

receiver with a 3 kHz IF bandwidth. Continuous narrowband monitoring of all frequencies in the HF band using a narrowband system requires nearly 9400 communications-type HF receivers. Random tuning systems may use ten or fewer receivers.

Random tuning of a narrowband search receiver is suitable for long duration signals. Frequency-hopping spread-spectrum, direct-sequence spread-spectrum, and compressed-data burst transmission detection requires either wideband or continuous narrowband coverage.

This dissertation discusses only the wideband search architecture. Figure 4.1 diagrams a generalized search receiver.
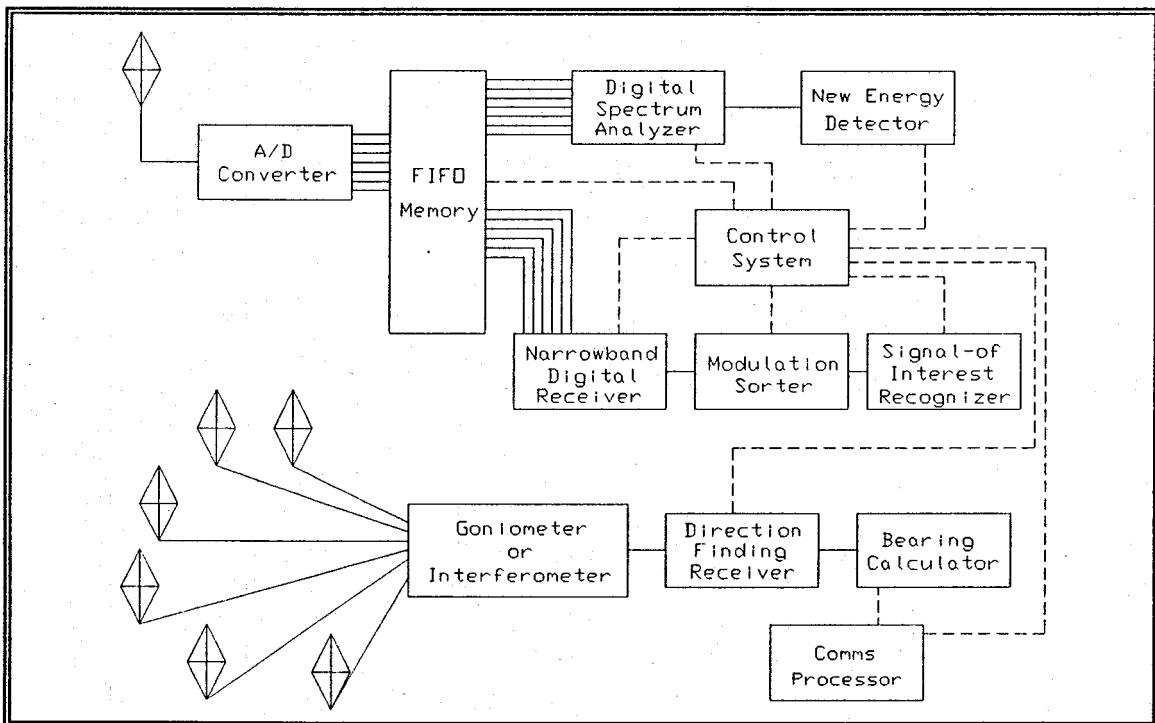
Figure 4.1 - Generalized Wideband Search Receiver

A. EXAMPLES OF NEW ENERGIES REQUIRING SEARCH SCREENING

There are thousands of potential HF new energies per second. The following are examples of potential new-energy events which require search screening. This list represents the large class of new energies, and it includes many noise sources discussed in Chapter II.

1. Sferics

Sferic is a term used to describe short burst of atmospheric electromagnetic energy. Convective, cumulonimbus cloud thunderstorm discharges account for nearly all sferics. Lightning associated with volcanic eruptions is the other source of sferics.

The average duration of a lightning stroke is approximately 30 μs, and each lightning flash averages four strokes. In a hemispheric satellite view, there is an average of 1000 thunderstorms visible, centered primarily in the tropics. Worldwide, an estimated 400 lightning strokes occur each second. With an average power per stroke of 10^{13} watts, each stroke can generate significant energy in the HF spectrum. [Ref. 28]

Since more storms containing lightning occur in the tropics, sferic energy is maximum in these regions. Sferic energy also propagates over ionospheric paths to far distant receivers.

Sferics are broadband, and each event lasts about 100 to 200 ms. These two characteristics, bandwidth and duration, can form a screening criteria in the search receiver to minimize new-energy decisions from sferics.

2. Broadband Man-Made Noise

Chapter II discusses numerous types of broadband man-made noise. The key to search screening is the broadband character. Broadband noise, from any source, will increase the noise floor and prevent weak signal reception.

Of particular concern is switching noise generated by RF switching systems employing digitally-controlled diode switches in matrix regimes. Switching transients caused by turning on and off the diodes in the switching matrix appear as new energy. For optimum performance, there should be no switching or other transient generating devices between the antenna and the search receiver. Switching noise is not necessarily broadband, so new-energy screening may be difficult.

3. Industrial, Scientific, and Medical (ISM) Noise

International agreements permit the operation of ISM devices in certain frequency bands. Yet, evidence shows that out-of-band ISM interference is increasing at receiver sites throughout the world. Many ISM signals are propagated by ionospheric modes to distant receiver sites.

A typical ISM signal appears as a repetitive signal which may sweep over a frequency band. ISM signal bandwidths range from a few kHz to hundreds of

kHz. Frequency change rates vary from 100 kHz per second to 1 kHz per minute. The repetitive signal characteristic results from the common use of ISM devices in production line manufacturing. Production line repetition rates vary widely from a few operations per second to one operation every few minutes. Narrowband and slow frequency changing ISM signals are extremely hard to screen by a new-energy receiver because the frequency-sweep rate and signal-repetition occurrence are random.

Figure 4.2 shows an ISM signal with a slowly changing frequency vs. time characteristic which lasts more than 20 seconds. The process generating the signal in Figure 4.2 is probably a large plastic forming mold. Figure 4.3 shows a much more rapidly repeating, frequency sweeping ISM signal. Figure 4.3 is archetypical of ISM signals generated by a production-line process such as plastic molding of small toys. The data shown in Figures 4.2 and 4.3 were collected at the CDAA sites at Guam and Homestead, Florida, respectively. The signals observed in Guam originated in the direction of China and Taiwan, and the signals observed in Florida were from Cuba or South America.

Other ISM signals are non-frequency sweeping pulses occupying bandwidths many kHz wide. Figure 4.4 shows a strong pulse-type ISM signal received via groundwave propagation at an HF receiver facility in Key West, Florida. The signal occupies about 20 kHz of bandwidth. The relatively rapid repetition rate and broadband nature are typical of an ISM device used in a heat-shrink plastic packaging process. Figure 4.4 also includes another ISM signal

51
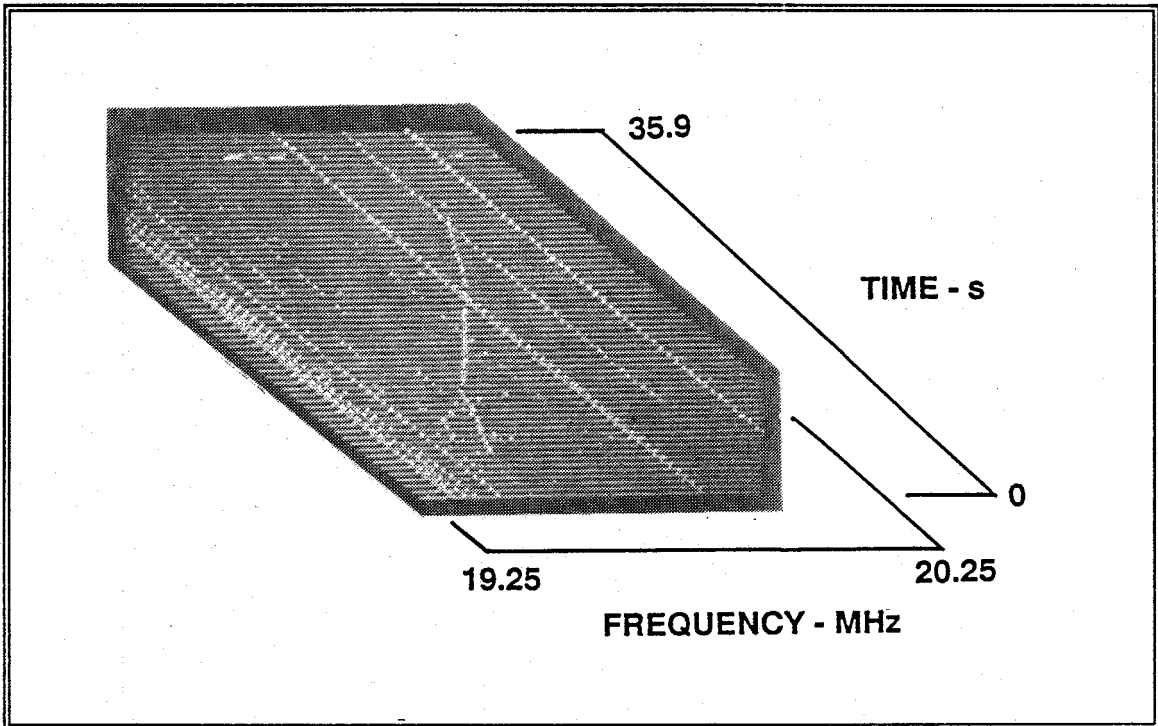
Figure 4.2 - Slowly Sweeping ISM Signal
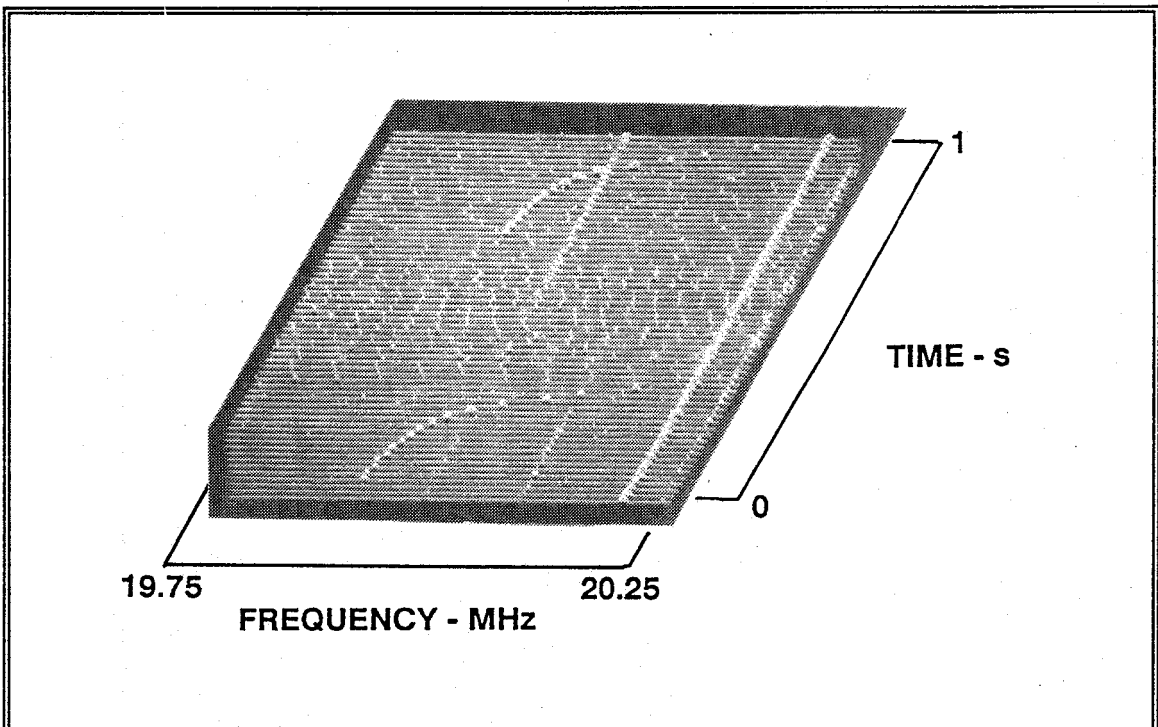
Figure 4.3 - Rapidly Frequency Sweeping ISM Signal
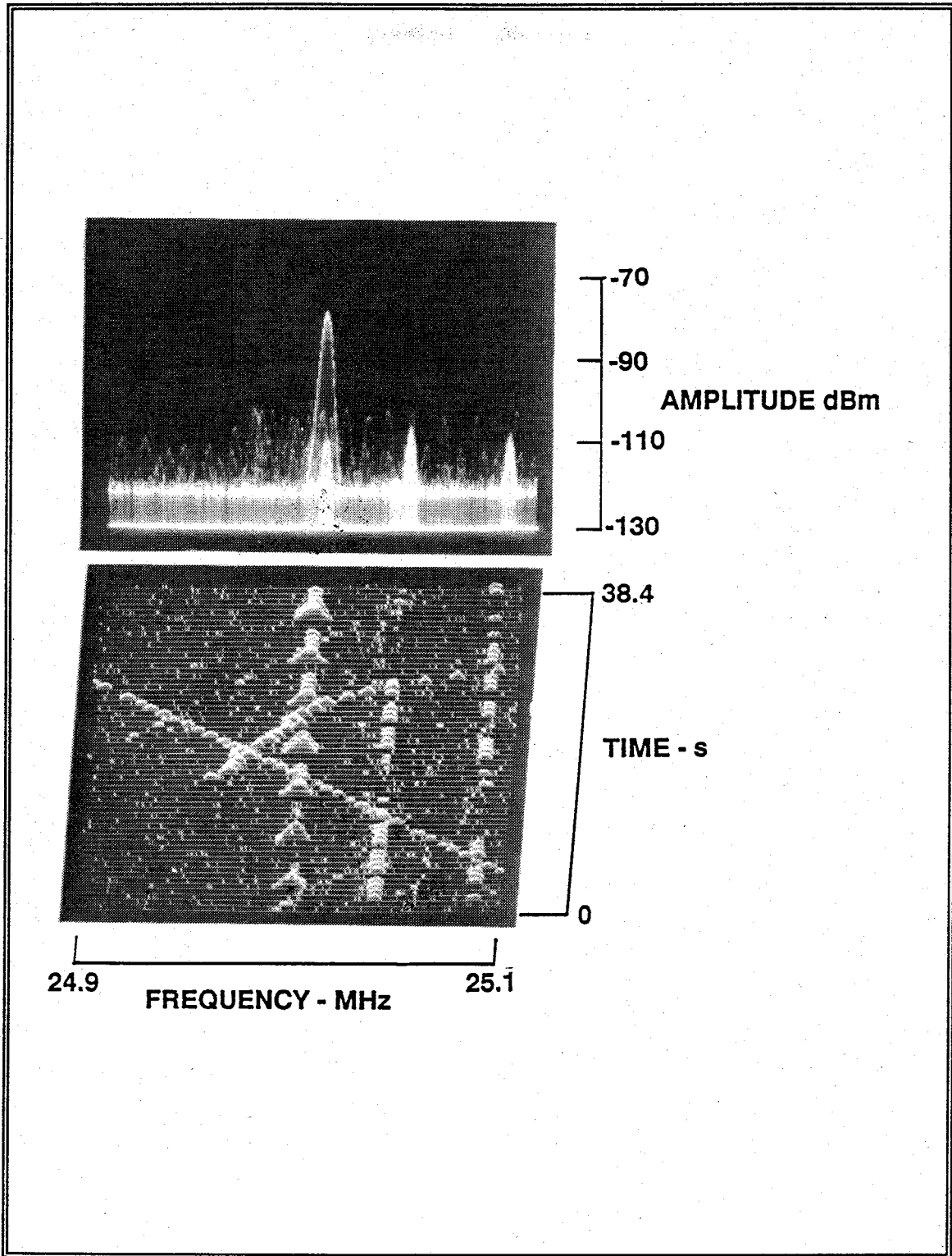
Figure 4.4 - Wideband, Pulse ISM Signal

53

similar to that shown in Figure 4.3. The diagonal straight line in Figure 4.4 is a signal from an ionospheric sounder which will be discussed in the next section.

One new-energy screening technique for ISM signals is to window search coverage around the narrow ISM allocations since all ISM equipment is designed to operate in ITU allocated bands. The HF ISM allocated bands are: [Ref. 2]

- ◆ 6780 kHz ± 15 kHz

- ◆ 13560 kHz ± 7 kHz

- ◆ 27120 kHz ± 163 kHz.

However, observations reveal that ISM interference exists throughout the HF band. Many ISM signals are far removed from the ITU allocated bands. Note the frequencies of the ISM signals in Figures 4.2 through 4.4. A likely reason for out-of-band operation is that ISM equipment users adjust the frequency of the equipment to maximize production rather than comply with unenforced regulation.

4. Ionospheric Sounders

Ionospheric sounders deliberately transmit signals to measure the propagation characteristics of the ionosphere. The various types of ionospheric sounders include: [Ref. 29]

- ◆ Vertical Pulse

- ◆ Oblique Pulse

- ◆ Linear Sweep (Chirp)

- ◆ Channel.

Signals from all these sounders are potential interferers since some portion of their energy will propagate to distant locations via the ionosphere. The sounder transmission interferes with the search receiver by providing a signal interpreted as new energy in adjacent frequency bins. As the sounder signal moves in frequency, more new-energy conditions occur.

How many sounders are there? During one data collection, 21 oblique sounders moved across the HF spectrum in as little as five minutes. While listening to the BBC World Service in Homestead, Florida, the signal level of one oblique sounder actually exceeded the strength of the BBC's signal.

Sounder activity appears to be maximum during the period five minutes before to five minutes after the hour. Other high activity periods are at each quarter hour. The population of chirp sounders is so high that some operators modify their sweep characteristics to reduce interference. Figure 4.5 shows two chirp sounders with different sweep patterns. One follows the normal low-to-high frequency sweep, but the other sweeps down in frequency.

One possible new-energy screening technique for oblique sounders is recognition of the characteristic linear sweep rate. The duration or residence screening parameter can be set longer than the sounder residence time, and the receiver can lock-out predicted frequencies at estimated times.

An effective screening tool for channel sounders requires that a receiver programmer lock-out all sounded frequencies from the search coverage.
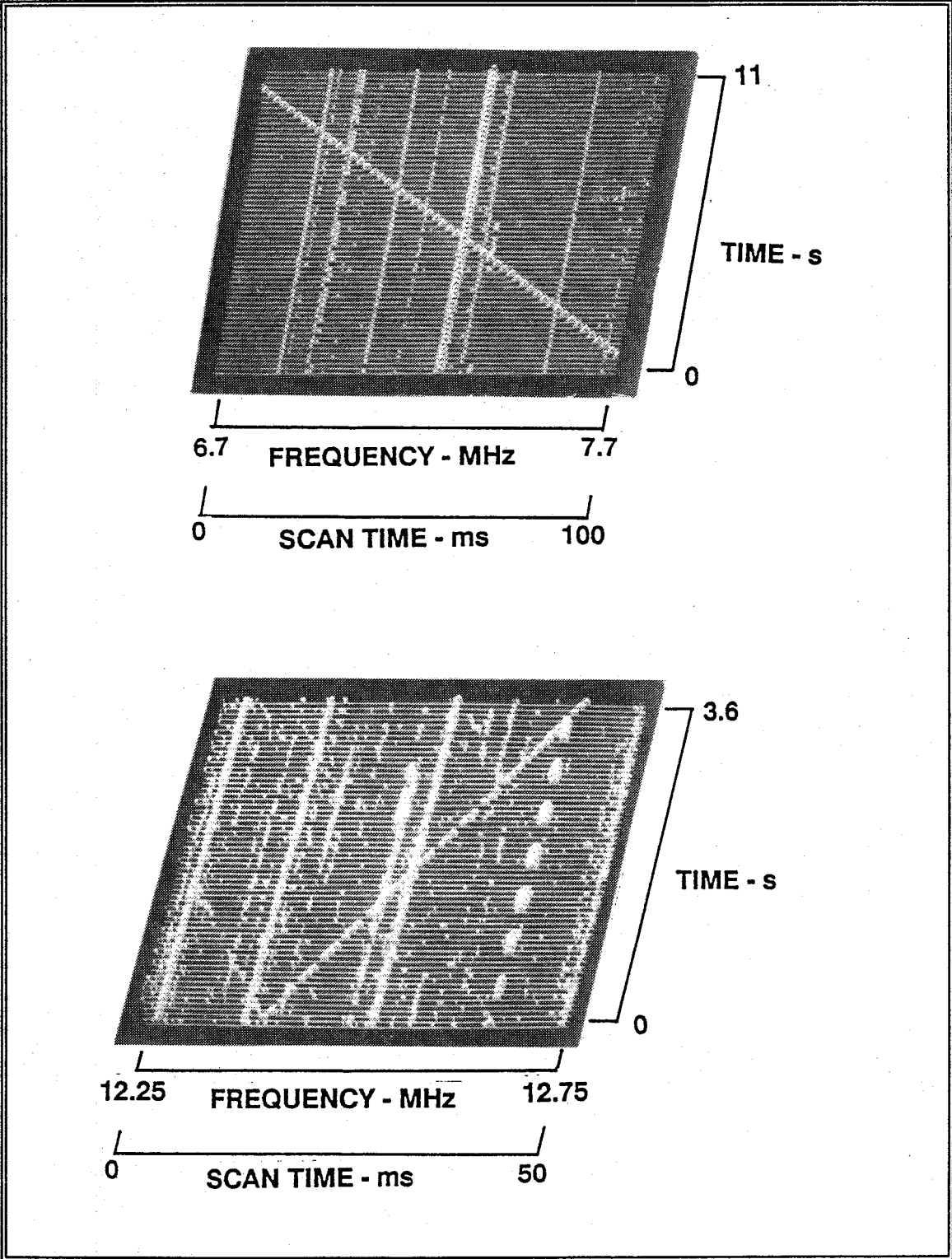
Figure 4.5 - Ionospheric Sounders

5. Amplitude Keying

The most common form of HF amplitude modulation is the common morse code transmission. Many morse code transmissions are signals of interest, so search screening should not eliminate them. The on-off characteristic of the signal will generate new-energy conditions, and the search process should recognize the start of a morse code transmission.

To prevent continuous new-energy alarms, the signal decay time from first new-energy detection should be longer than the spacing of slowly sent, manual morse signals. This same process applies to any modulation type or transmission profile which includes interrupted transmissions. However, a long decay parameter may interfere with the detection of random frequency-hop signals. This is due to the possibility of short frequency revisit times by the spread spectrum signal.

6. Spread-Spectrum Signals

Two frequency-hop spread-spectrum systems find use in the HF spectrum. These are the coherent and non-coherent slow-frequency-hop regimes. The second form is the more popular. HF slow-frequency-hop implies that the residence time on one frequency exceeds the duration of one information bit [Ref. 30]. Observations of HF spread-spectrum transmissions find signals with residence times exceeding 1 s.

The hopping spread is limited to a percentage of the maximum to minimum propagation frequency range for the path of interest. The necessary

signal strength at the receiver site determines the percentage. In most cases, the maximum frequency-hop range will be less than 1 MHz. Today's digital circuitry makes it possible to use extremely long hopping patterns.

Each frequency transmitted generates a new-energy-present condition. A single network of spread-spectrum, frequency-hopped stations could easily inundate a new-energy receiver. Search receiver screening requires prior knowledge of the specific hopping sequence and frequencies used.

B. HF NEW-ENERGY SURVEY

This author experimentally investigated the distribution of HF new-energy events during the period 10 - 23 April 1989. The receiver site was the circularly disposed antenna array, Wullenweber antenna, at Edzell, Scotland. The site is in the single ionospheric hop footprint of all the major European international broadcasting stations. Measurements during the period showed routine nighttime maximum received signal strengths between 0 and -10 dBm. The strongest signals were in the 49 and 31 meter international broadcast bands.

Because of the installation of an RF switching system, the new-energy survey did not use the combined-omni antenna of the CDAA. Instead, a conical monopole served as the omnidirectional search antenna.

1. System Description

Figure 4.6 is a block diagram of the search receiver system. The receiver is a hybrid analog and digital system. The attenuation, frequency

translation, and bandwidth limiting portions of the receiver are analog. The frequency transformation and decision processing portions are digital.
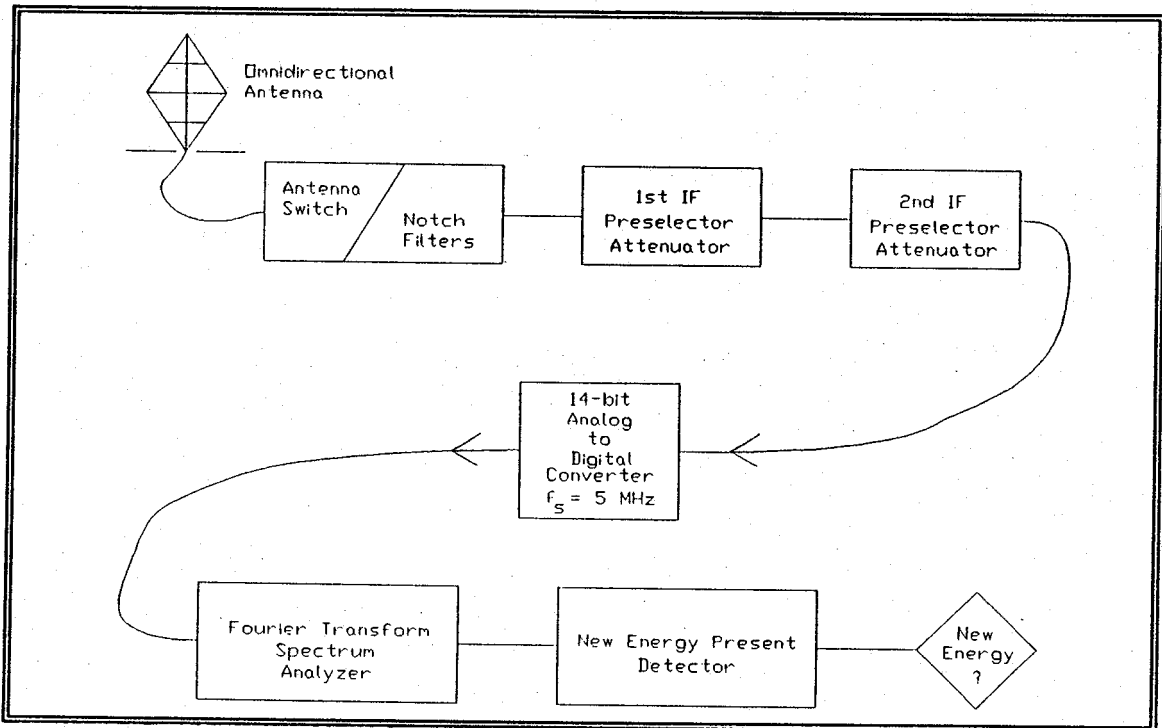
Figure 4.6 - Hybrid, New Energy Detection Receiver

The analog section employs two identical channels. In practice, the channels are not the same. The receiver is a dual conversion, superheterodyne type with first stage up-conversion to above 200 MHz and a second conversion down to baseband. Preselectors in each IF stage limit the bandwidth to 2.5 MHz. Attenuators, international broadcast band notch filters, and an antenna selector complete the analog end.

The key component in the receiver hardware is an Elsin 14-bit analog-to-digital converter operating at 5 MHz. The A/D includes an integral sample-and-hold. The theoretical maximum dynamic range is 84 dB using the expression:

$$\text{dynamic range in dB} = 20n \log_{10}(2) \approx 6n \tag{4.1}$$

where n is the number of bits of resolution in the analog-to-digital converter. The actual dynamic range, by whatever measurement used, will always be less than the theoretical value. A 12-bit Burr-Brown ADC-600 converter was also available as an alternative A/D device.

A single-tone measurement provided a 74 dB dynamic range for the 14-bit A/D. Site personnel consistently measure a dynamic range in the mid-seventies for the Elsin converter. Single tone measurement provided a 66 to 68 dB dynamic range for the Burr-Brown 12-bit converter.

The digital section includes a digital switching network, parallel Discrete Fourier Transform spectrum analyzers, and new-energy-event detectors. The Discrete Fourier Transform implementation is a Fast Fourier Transform algorithm that includes a minimum 4-sample Blackman-Harris window. An overall process controller manages detection identification, timing, control, and statistics. This controller records each new-energy-present condition by time, center frequency, and amplitude.

2. Detection parameters

The analog-to-digital converter produces 5 million samples per second (5-MSPS). The spectrum analyzer calculations require sample populations based in powers of two. Table 4.1 shows the processing configurations possible.

Table 4.1 - SPECTRUM ANALYZER SAMPLE PROCESSING SIZES

Number of Samples	Sample Period (ms)	Frequency Resolution (Hz)
$2^{11} = 2048$	0.41	2441
$2^{12} = 4096$	0.82	1220
$2^{13} = 8192$	1.64	610
$2^{14} = 16384$	3.28	305
$2^{15} = 32768$	6.56	153

The search receiver does not make a new-energy-present decision on each sweep of the analyzer. The times in Table 4.1 are for the sampling time only. Each sample also includes clocking overhead.

To reduce background noise, the system averages spectrum results into three longer periods. The short term average (STA) is in multiples of 26 ms; the medium term average (MTA) is four times the STA; the long term average (LTA) is four times the MTA or 16 times the STA.

The fundamental new-energy-present parameter is a change in amplitude over time. Amplitude decision subsystems compare the absolute value of the amplitude spectral density value computed by the Discrete Fourier Transform for

each frequency bin. As described in part A above, there are many potential energies that are not of interest to the search process that the amplitude parameter screening alone will not adequately eliminate. Amplitude screening by the search receiver produces a first subset of the new energies present. To improve the probability that the new energy is a signal of interest, additional parameter screening is necessary. The two additional screening parameters are time and bandwidth.

The time screening process requires that the new energy be present for a programmable number of STA's. Otherwise, it is not of interest. The time parameter also screens repetitive new energies such as those from amplitude shift keying or pulsed noise. Once a new energy disappears for at least one STA, the receiver allows energy in that bin to decay. During the decay period of one LTA, the receiver assumes that an amplitude change exceeding the new-energy threshold in the same bin to be from the same source as the previous new energy.

The bandwidth screening process assumes that all signals of interest (i.e., communications signals) are bandwidth limited. This should screen out new energies from lightning and impulsive noise which typically are several megahertz wide. The bandwidth window must be large enough for data communications using multiple tones and data rates as high as 1200 BAUD. Another bandwidth screening requires a minimum bandwidth to reduce noise effects.

3. Data Collection

The data collection included a series of 34 individual sets ranging in time duration from 15 minutes to 14½ hours. Data file oversize errors in the system control processor resulted in losing four data sets before accomplishing histogram processing, and the failure of one A/D converter resulted in losing another data set. In the remaining 29 data sets, 4,317,021 total new-energy-present conditions were obtained. The largest collection period had 1,373,554 new energies, and the smallest collection period had 1236 new energies. The receiver created a log of each new-energy event.

The data collection used both A/D channels, separate spectrum analyzers, and separate detectors. In all cases, the same analog receiver portion fed both A/D's. The sets included daytime, transition, and nighttime periods.

Most sets used an 8 dB amplitude detection threshold level. A new energy may be present when the STA amplitude calculated for a given frequency bin exceeds the amplitude level calculated in the last LTA for the same frequency bin by an amount greater than the amplitude detection threshold level.

Data sets 1 through 7 used a single 14-bit A/D converter. Sets 8 through 18 (daytime) and sets 19 through 26 (nighttime) used a 14-bit A/D on one channel and a 12-bit A/D on the parallel channel. Sets 8 through 26 employed the different word size A/D's provided data to compare dynamic range and saturation effects. Sets 27 through 34 utilized two 14-bit A/D's. Tests 32 through 34 used an

8 dB amplitude detection threshold on one channel and a 16 dB threshold on the parallel channel. Data sets 3, 10, 27, 28, and 29 were lost.

In general, data set collection used the minimum preselector/IF stage attenuation needed to prevent A/D overload. The data sets comparing the different word-length A/D's varied the attenuation from test to test. The best indicator of A/D overload was a sudden jump in the new-energy activity.

To reduce the data, the control processor produced an amplitude histogram for each data set from the new-energy-event log. The amplitude value used in histogram production for each new energy was the maximum amplitude spectral density value calculated for the MTA associated with that event. The control processor also produced amplitude histograms of the new energies unique to each channel and of new energies common to both channels. The control processor performed all data reduction off-line.

4.   Histogram Results

Figure 4.7 shows the histogram for data identified as set 34. Appendix B contains histogram presentations of the data obtained for the remaining sets.

The shape of the probability density functions in the dBm domain suggest a log-normal distribution of the received voltage amplitude. Following this assumption, the dB-domain normal distribution estimation of mean and variance were calculated using the three techniques described in Chapter III.
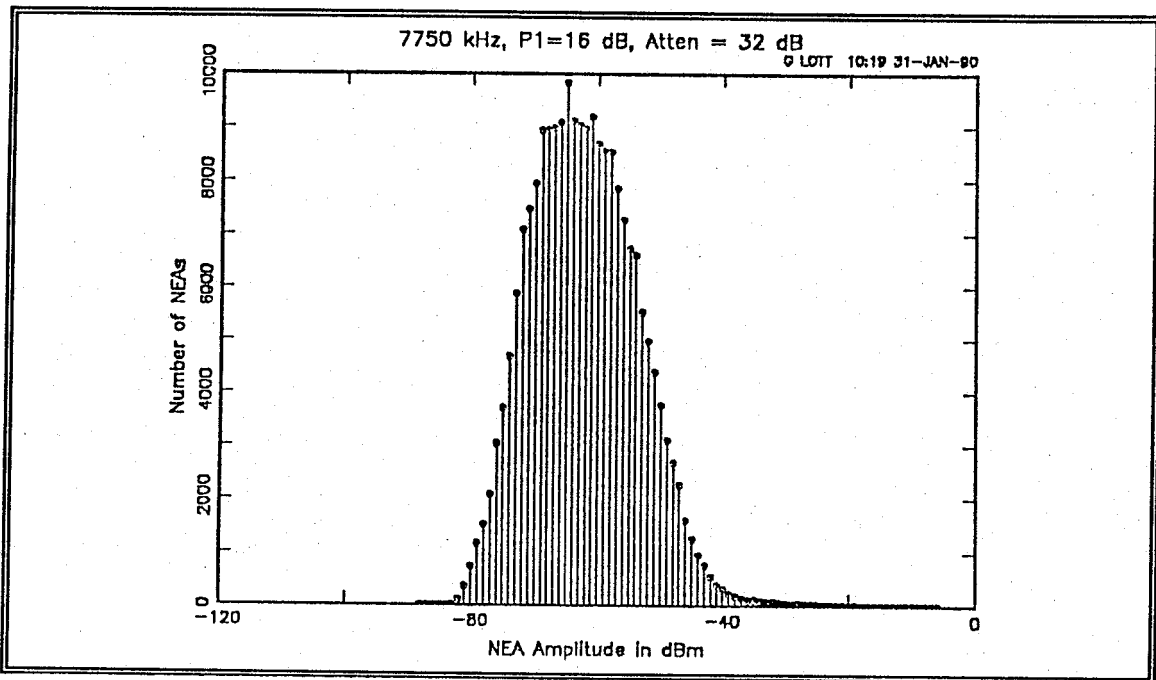
Figure 4.7 - Amplitude Histogram Results for Test 34

The classical means and variances serve as the basis for model comparison. Figures 4.8 shows the classical mean and variance calculations for all the tests. Figures 4.9, 4.10, and 4.11 show the mean and variance estimates using the three techniques for matching a normal distribution.

The estimates calculated using the Kullback-Leibler test more closely match the set of classical means and variances. Figure 4.12 shows the probability density functions using the mean and variance estimates compared to the experimental probability density obtained from set 34.
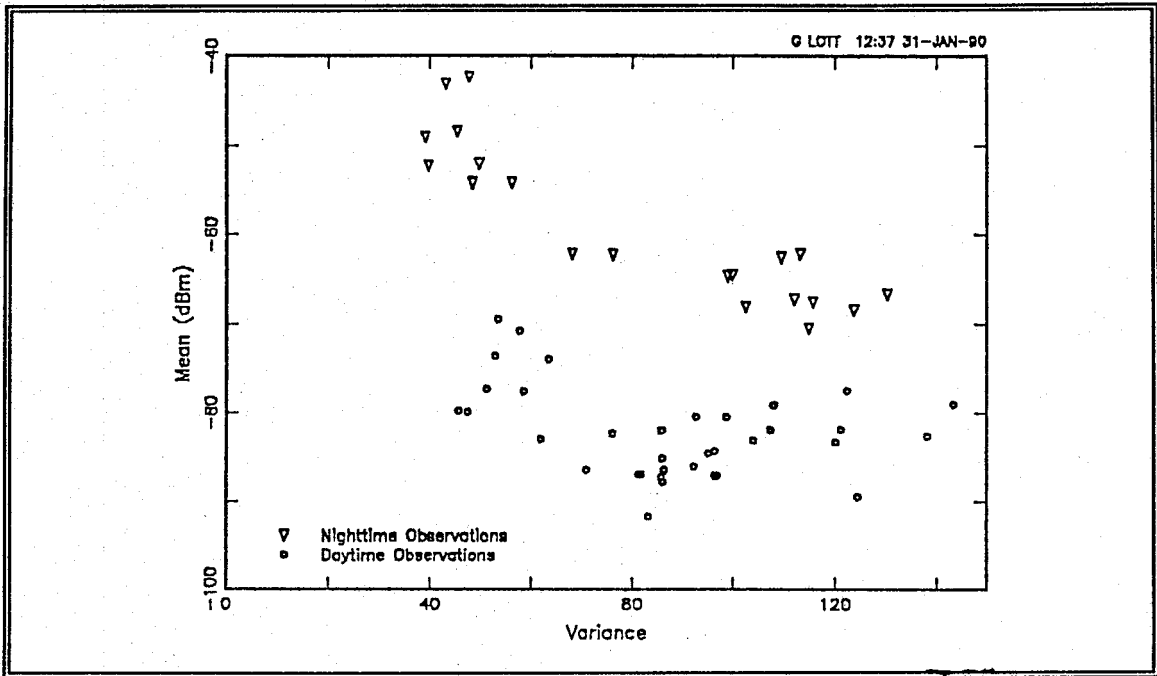
Figure 4.8 - Mean and Variance Using Classical Calculations for All Tests
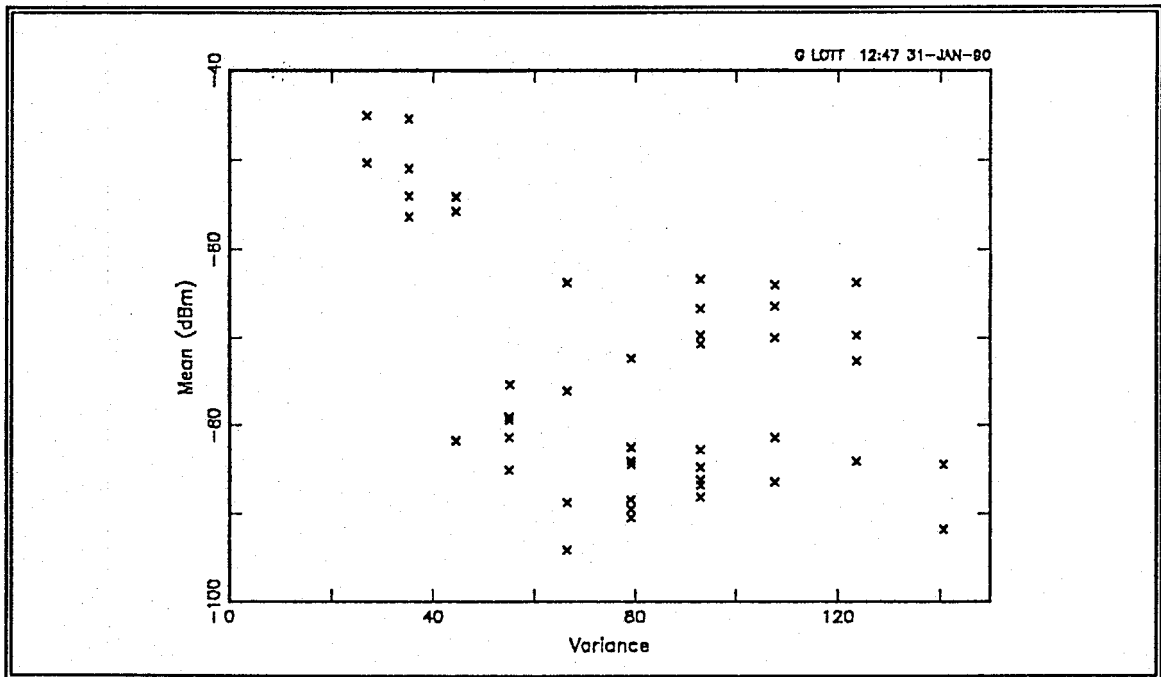
Figure 4.9 - Mean and Variance Estimation Using the Croxton-Quartile Method for All Tests
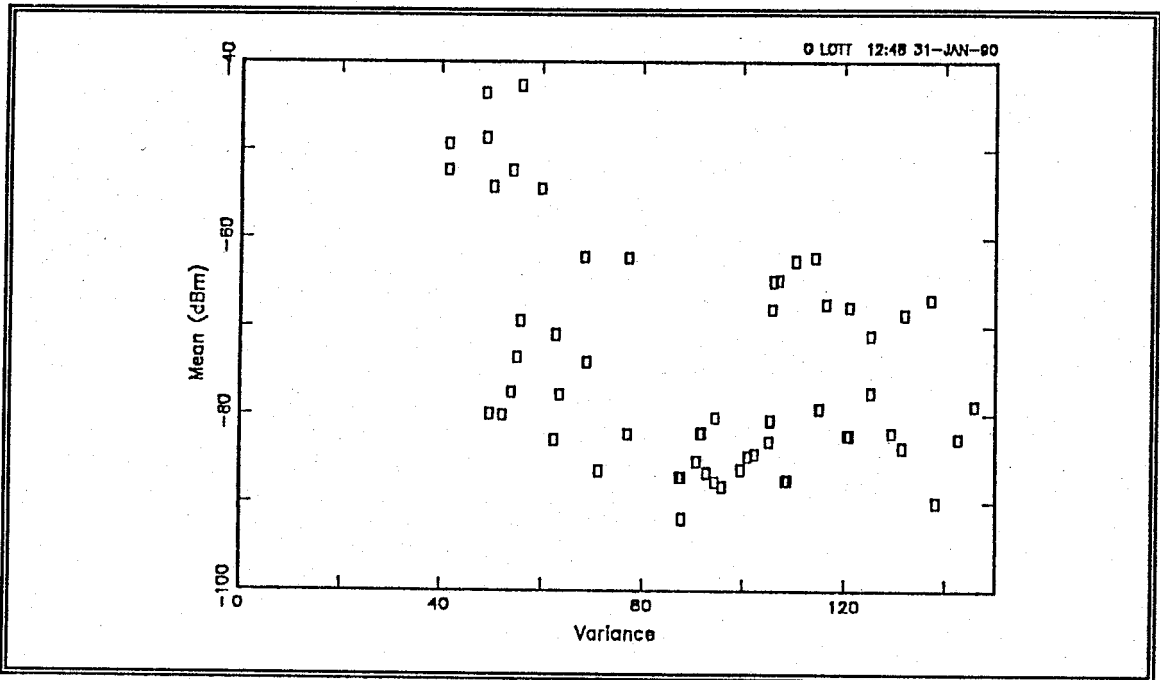
Figure 4.10 - Mean and Variance Estimation Using the Kullback-Leibler Method for All Tests
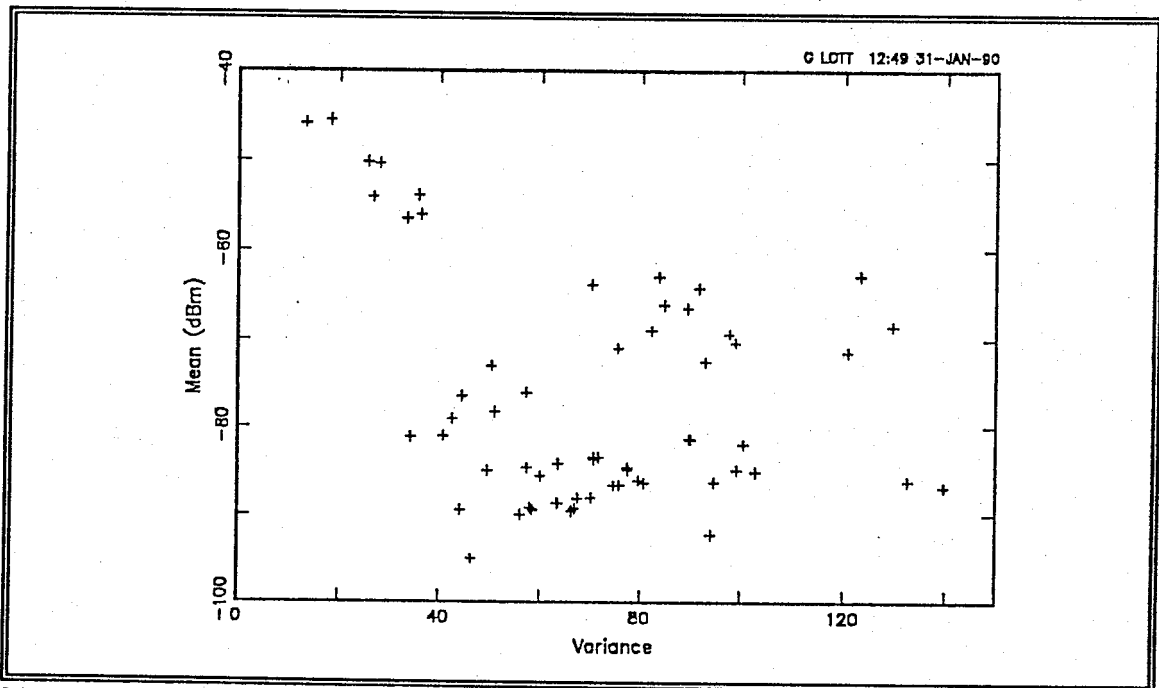
Figure 4.11 - Mean and Variance Estimation Using the Kolmogoroff-Smirnoff Method for All Tests
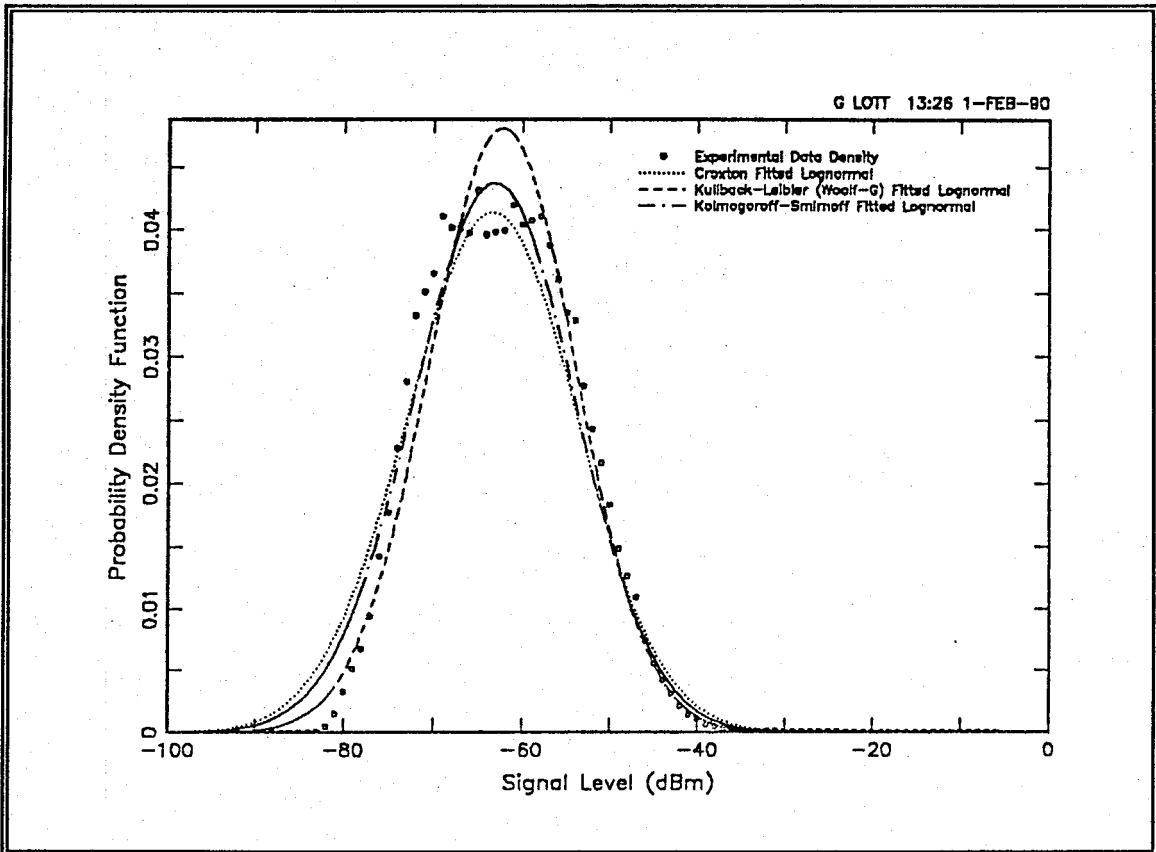
Figure 4.12 - Comparison of Density Functions Using All Four Mean and Variance Calculations for Test 34

There appear to be two clusters of data, one with a mean of approximately -85 dBm and another with a mean of approximately -65 dBm. Comparison of the data set time-of-day shows that this clustering is caused by the inclusion of both daytime and nighttime observations. Figures 4.8 shows day and night observations with different symbols to show the day and night clustering.

The 20 dB difference between the means of the daytime and nighttime data sets corresponds directly with the attenuation required prior to the receiver's analog front-end. During the day, separate observations show that the strongest

signals were in the 19 and 17 meter international broadcast bands with peak levels of -30 dBm. With the receiver dynamic range near 75 dB and without front-end attenuation, distortion products would appear in the receiver if the receiver's sensitivity was kept at the measured minimum sensitivity of -116 dBm. Thus daytime receiver operation required 12 to 28 dB of front-end attenuation to prevent the generation of distortion products.

At night, the strongest signals were in the 31 and 49 meter international broadcast band with peak signal levels of 0 dBm. Nighttime receiver operation required 36 to 54 dB of front-end attenuation to prevent distortion products. Routine receiver operation proves that there is a 20 to 30 dB difference in receiver front-end attenuation requirements between day and night operation.

The limited receiver dynamic range and the resulting receiver front-end attenuation requirements prevents detection of the weakest signals. One can see the result of lost receiver sensitivity in the sharp rise on the weaker signal side of the experimental density functions. The weaker signals are there, but they are not detectable by the system.

Even with this skew in the low end of the experimental density functions, the log-normal assumption appears valid. In fact the less-steep weaker signal slope of the theoretical densities fitted using the estimation techniques may more accurately represent the true signal population. The less-steep slope would come from a distribution with a larger variance.

An important point is that the distributions represent the population of signals detectable by the receiver. Ideally, signals exist far below kTB noise levels, but they are not detectable. The new-energy-survey distributions are for signals which exceed the ambient noise levels by the specified amplitude threshold.

C. SUMMARY OF RESULTS

The log-normal signal amplitude distribution is a good model for new-energy-present conditions. This model matches the results from the overall HF signal amplitude or channel occupancy surveys discussed in Chapter III. Figure 4.13 shows two theoretical signal amplitude probability distribution functions generated using daytime and nighttime new-energy-detection data. Figure 4.14 shows the two corresponding density functions.

General HF spectrum surveys, excluding international broadcasting, are valid predictors of new-energy levels. There appears to be little signal population difference between weekdays and weekends.

The shift in the mean signal level from day to night is significant enough to warrant using different day and night system design criteria. The nighttime signal population establishes the dynamic range requirements for the search system excluding international broadcasting signals. Design should always incorporate the best receiver sensitivity possible with practical values near -125 dBm. The new-energy signals alone require a receiver dynamic range of 85 dB (from -125 to -40 dBm). However, the overall dynamic range requirement (as shown in Chapters 2
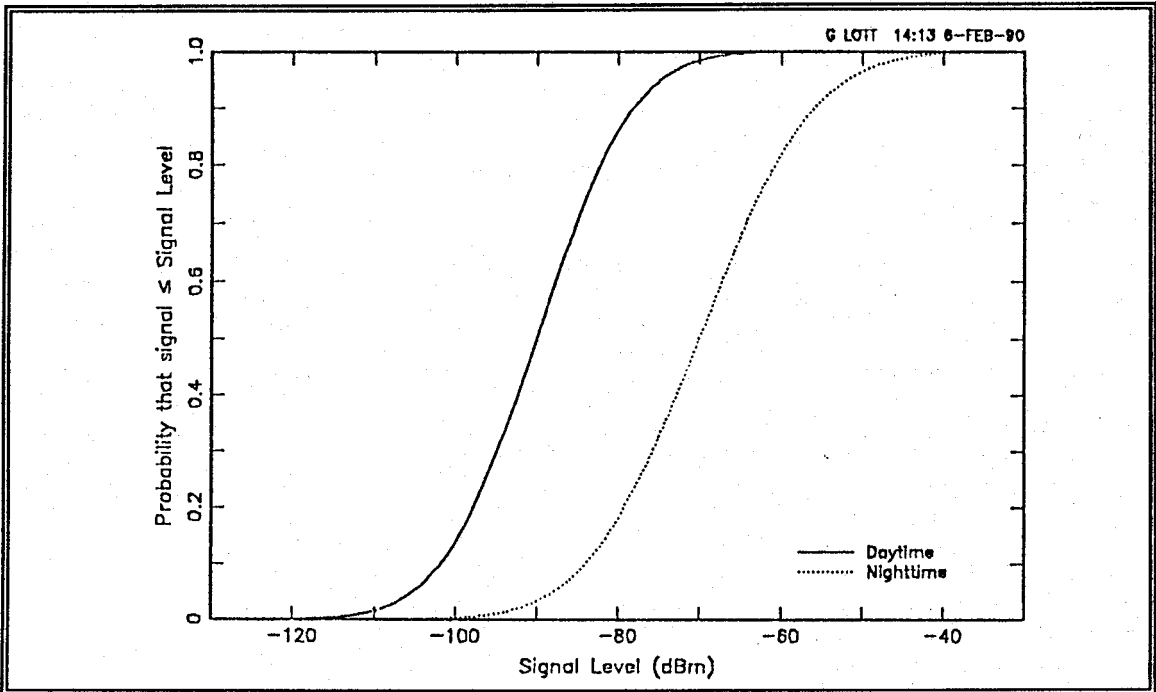
Figure 4.13 - New Energy Detection and Non-Broadcast Survey Distribution Functions
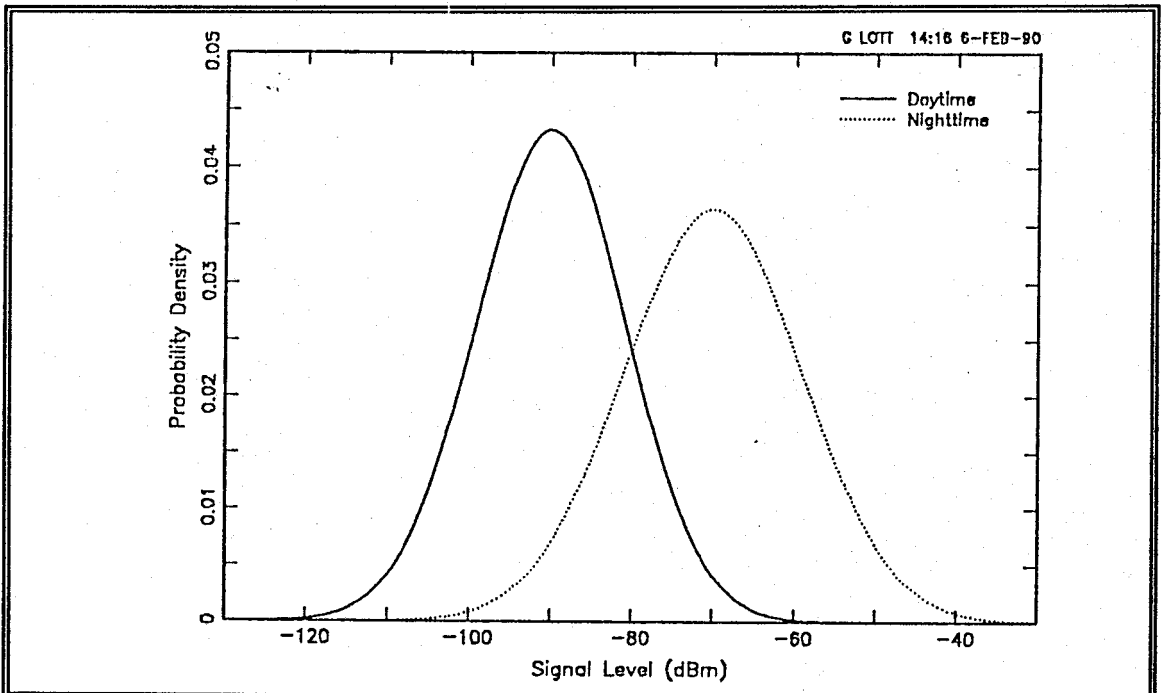
Figure 4.14 - New Energy Detection and Non-broadcast Survey Density Functions

71

and 3) remains at 120 dB (from -125 to -5 dBm) as dictated by the total HF signal population. The greater dynamic range is necessary, or one must alter the HF signal environment to remove the strongest signals.

V. HF SITE PERFORMANCE CRITERIA

The distributions of standard HF signals and new signal energies provide a basis to determine a site's ability to receive signals of interest. From distributions of signal strengths, one can determine the effects of noise and signal attenuation on the reception of signals of interest. Noise and signal path attenuation have predictable and harmful effects on signal reception.

Signal attenuation and noise levels can be related to the percentage of signals of interest lost. The signals of interest are usually the clandestine transmitters, weak mobile transmitters, and stations using low power transmitters and inefficient antennas. The search function rarely looks for international broadcast band signals.

Because of the search target characteristics, a signal distribution used to measure site performance is misleading if it includes international broadcast stations. However, the overall signal handling capability of the search receiver must include these strong signals.

Site performance quantification began with the Navy's Signal-to-Noise Enhancement Program (SNEP). Researchers at the Naval Postgraduate School observed harmful interference at various HF receiver sites. Lead by Professors Steve Jauregui and W. Ray Vincent, site noise surveys found many signals of interest being obscured by various noise sources.

There are many Department of Defense programs to reduce interference effects. These typically fall under the category of electromagnetic interference/radio frequency interference (EMI/RFI). Noise and interference, from whatever the source, reduces a receiver site's ability to perform its mission. Yet, rarely do EMI/RFI programs try to quantify a level of degradation in signals or targets lost.

EMI/RFI programs do nothing to mitigate the signal path attenuation effects. These programs tend to emphasize "noise reduction" rather than overall site performance improvement.

SNEP research revealed that there is another, equally important side to site performance improvement. Surveys found there is a baseline noise level within the radio frequency path from antenna to receiver at almost all Navy CDAA sites. This noise is the composite of externally and internally generated sources, and it is present at all receivers in the facility. A typical figure is -120 dBm in a 3 kHz bandwidth.

This noise level is present regardless of the signal attenuation characteristics within the RF signal path. This noise floor is rarely below -125 dBm in a 3 kHz bandwidth. The noise baseline varies with time-of-day, season, frequency, etc. The variable noise level is always stronger than the baseline level. The instantaneous value of the noise masks signals-of-interest. A long term average cannot truly represent the base noise value.

Given a reasonably constant noise level, suppose a signal of interest arrives within the receiving system at -110 dBm. Without amplification, a 15 dB RF system attenuation would reduce the signal strength below the demodulation threshold. For automated demodulators, only a 5 dB system loss creates a similar effect.

RF signal amplification will not help once a signal level is below the threshold of about 10 dB above the baseline noise level. Thus RF system attenuation has the same effect on weak signals as the addition of noise. Site performance improvement must address both noise reduction and signal path attenuation.

A. PERFORMANCE CURVES

Professor W. Ray Vincent and LT John O'Dwyer developed the first set of site performance curves. Chapter III discussed the origins of this curve (a preliminary amplitude distribution of all received signals). The original curve assumed a logarithmic distribution of signal amplitudes. [Ref. 16]

Using this first curve, SNEP personnel quantified the effects of man-made noise on a receiver site's ability to perform its mission [Ref 16]. Several SNEP surveys during the mid 1980's used this early means of evaluating site performance. These survey results show that man-made noise and signal attenuation degraded site performance considerably more than first estimated.

Figure 5.1 presents a set of improved signal strength distributions prepared for the determination of site performance of CDAA sites during ionospheric daytime conditions. Figure 5.2 shows a similar set for nighttime ionospheric

75

conditions. Each figure provides separate distributions for signals employing one and two ionospheric hops.

The basis for the distributions provided in Figures 5.1 and 5.2 is the spectral survey data presented in Chapter III and the new energy distributions discussed in Chapter IV. The daytime curve, one hop, has a mean of -100 dBm and a variance of 100. These values come from the cluster of daytime signals shown in Figure 4.10.

The nighttime variance is not directly provided by the nighttime new energy survey results. Weak signals are present near -120 dBm during the night,but the limited dynamic range of the new energy survey receiver's do not allow the measurement of these weak signals.

The nighttime variance should be such that the probability distribution approaches zero near the same level as the daytime observation. The nighttime mean signal amplitude is 20 dB higher than that of the daytime as shown by all referenced signal population surveys. During data collection, the detection threshold was 8 dB above the LTA value which resembles the signal-to-noise ratio requirements of automated detection systems. The performance criteria can apply to systems requiring similar signal-to-noise ratios by adjusting the mean of the signal distribution.

Hagn's research is the only study which reveals the dramatic signal strength difference between one and two hop ionospheric paths [Ref. 24]. Intuitively, one
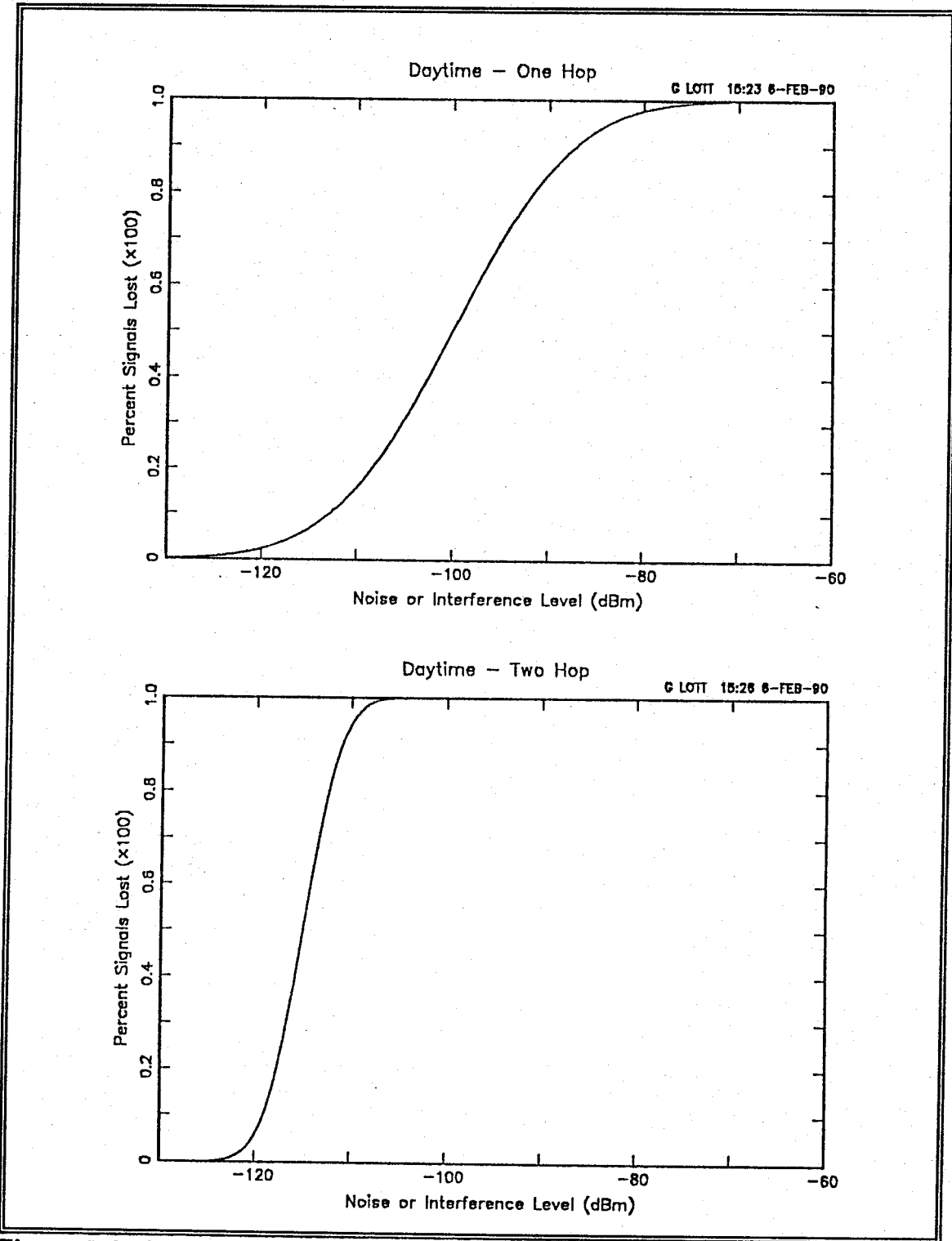
Figure 5.1 - Daytime Site Performance Criteria for One and Two Ionospheric Hop Sites
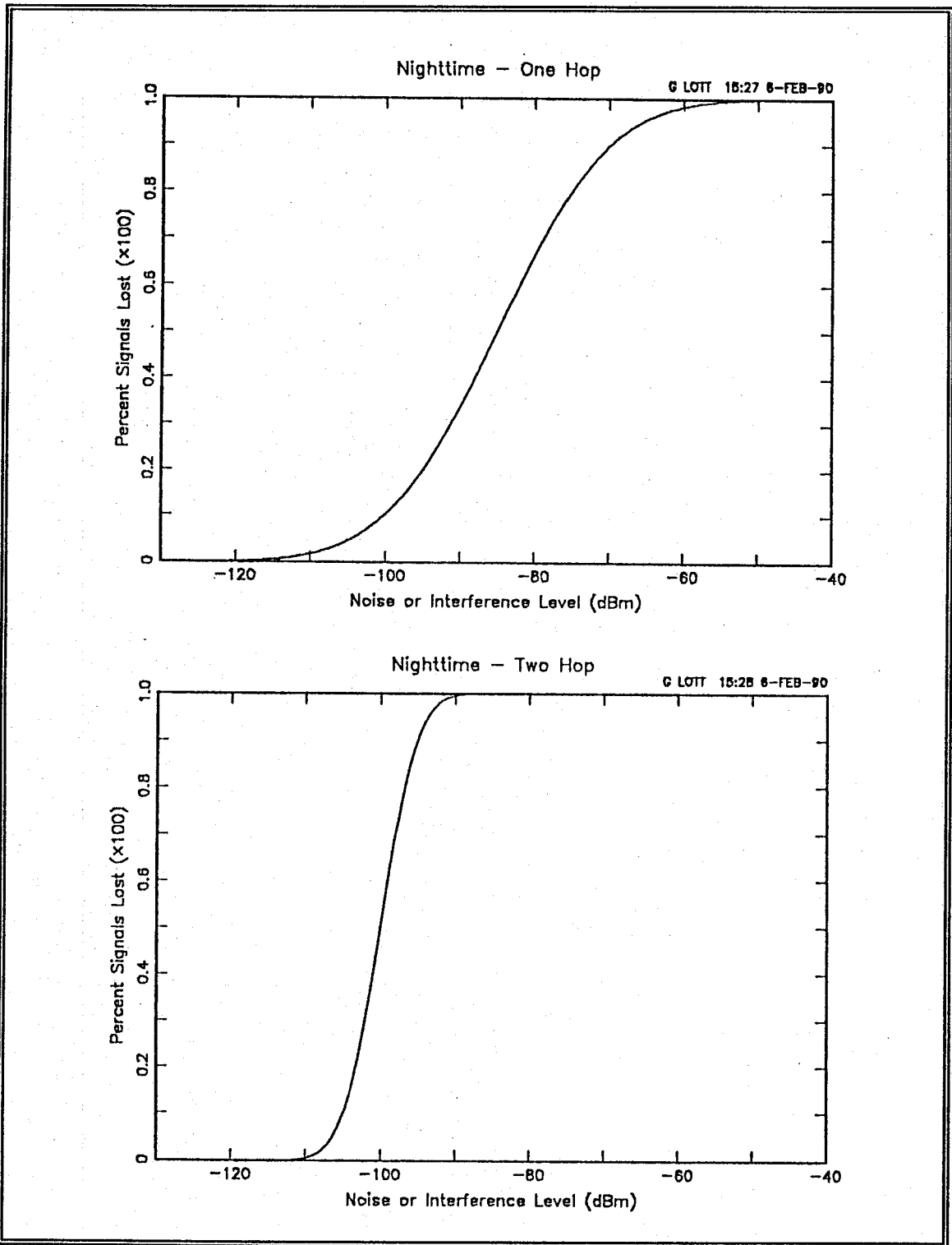
Figure 5.2 - Nighttime Site Performance Criteria for One and Two Ionospheric Hop Sites

would expect the two-hop signal to be weaker. The strongest two-hop signals should be from international broadcast stations. Even in the two-hop signal case, the weakest detectable signal must have a power level well above the instantaneous noise floor during the measurement. These characteristics of two-hop signals result in a lower mean, but the greatest effect is a smaller variance which is shown by an increased slope of the performance curve. For example, if signal path conditions result in increased signal levels, a two-hop site will hear relatively more signals than a one hop site.

B. ESTIMATING PERFORMANCE FROM SITE MEASUREMENTS

There are five steps necessary to assess HF receiver site performance. These are:

♦ Determine the distance to typical transmitters-of-interest and international broadcasters and establish the resulting number of ionospheric hops.

♦ Determine the strongest signals received.

♦ Determine internally caused baseline noise levels as seen at a receiver.

♦ Determine external noise levels and other factors which further degrade site performance.

♦ Determine the RF distribution system signal attenuation.

1. Distance and Ionospheric Path

There are two signal path distances one must determine as the first step to assess receiver site performance. One distance helps determine the maximum signal strength of signals from international broadcasting stations to establish the

total system dynamic range requirements. The other distance determines which set of performance curves to use.

The distance to international broadcasting stations requires identification of those broadcasters which target the area where the receiver is situated. A receiver site in Guam falls in the Northern Pacific Islands target area or the broader Far East, Pacific, or Oceania target areas. The current edition of the *World Radio Television Handbook* is an excellent guide for locating the international broadcast station locations.

The Voice of America schedules transmissions to "Oceania" using relay stations in the Philippines, Sri Lanka, and Thailand. The U.S.S.R. State Committee for Television and Radio Broadcasting (Radio Moscow) extensively targets the South East Asian and Pacific areas for HF coverage. Transmitter sites used for this coverage include Chita (Aleksandrovka), Pettropavlovsk-Kamchatskiy, and Vladivostok. The Australian Broadcasting Corporation (Radio Australia) uses transmitters located in Darwin, Shepparton, and Carnarvon to beam programs to East Asia, Northern Pacific Islands, and Paupa/New Guinea. Signals from all these (and many other broadcast stations) are the strongest signals received at the receiver site on Guam. [Ref. 3]

The distance from Guam to these sites is typically one ionospheric hop. However, the major target areas for broadcasts to this region are the Philippines and Indonesia. This is due to the population densities and the political situations

in the region. So Guam is on the periphery of the coverages. While signals will be single hop, the actual signal strengths should not be exceedingly high because of transmitting antenna beam effects. One could expect the strongest signals to be broadcasts targeted for evening reception in the 31, 41 and 49 meter bands [Ref. 3].

Three field techniques are available to determine the path distances. One is to take an inexpensive world globe available in most book stores. By using a string, one can mark off distances between broadcast transmitters and a receiver site along great circles centered on the receiver facility. This method provides an excellent pictorial representation for operational personnel.

The second is to use one of the many ray tracing programs available for small computers. There are several programs used by amateur radio operators that can provide bearing and distance between specified points. By entering the location of suspected transmitters-of-interest, the program can calculate the distances and display the path on a map.

A third field technique is to use the PROPHET program developed by the Naval Ocean System Center, San Diego. The specific program in PROPHET Ver. 3.2 is Raytrace. This can provide not only distances, but it can determine if the path is most likely one or two ionospheric hop. PROPHET can provide many other estimates of path conditions. [Ref. 31]

2. Strongest Signal Measurements

To establish the strongest signals present at a receiver site, one must measure the signal strengths at three locations. These are the antenna elements, the outputs of the RF distribution system, and the antenna input terminal of a typical HF receiver used in the facility.

During a visit to the Guam CDAA facility in September 1989, the SNEP team investigated the potential interference from two international shortwave broadcasting stations located on the island. KTWR, located near the town of Merizo, uses four 100 kw transmitters and two large curtain array antennas. Program target areas are China and South East Asia. KSDA, located near the town of Agat, uses two 100 kw transmitters and two curtain arrays also beamed towards South East Asia. Both transmitter sites are on the southwest end of Guam. This is some 15 miles from the receiver site located in the northwest corner of the island.

There are also two international broadcasting stations located on the island of Saipan approximately 300 miles from the Guam receiver site. KFBS near Marpi uses three 100 kw transmitters, and KYOI at Agingan Point uses one 100 kw transmitter. [Ref. 3]

This author monitored transmissions from these broadcasters throughout their broadcast schedules. The signals received at the CDAA were not any stronger than the average international broadcast signal received by ionospheric modes. The

strongest signal level from on-island stations received at the CDAA site was -40 dBm from KSDA. Ground wave propagation losses for the distance from Guam to the Saipan broadcast transmitters and the transmitting antenna beam directions prevent these stations from producing extremely strong signals at the CDAA. Mountains provide effective terrain shielding between the on-island transmitters and the CDAA.

The strongest on-island signal sources at Guam are the U.S. Navy and U.S. Air Force transmitter facilities. Both sites are six miles from the receiver site. Signals received from the Navy facility show the effectiveness of terrain shielding. Some of the transmit antennas are behind a 100 meter high hill. Other transmitting antennas, including the ionospheric sounder antenna, are within line-of-site of the CDAA. Signals transmitted from identical antennas and with the same power levels from locations behind the hill are 20 to 30 dB below those from line-of-site locations.

This survey reveals that the strongest signals received by the Guam CDAA are one-hop international broadcast transmissions from Australia, China, and the Soviet Union. The second strongest signal source is the non-terrain shielded U.S. military transmitters. Figure 5.3 shows the strongest international broadcasting signals received at -8 dBm at 0318 local time in the 31 meter band. Figure 5.4 shows the strongest signals received from the military transmitters, about -40 dBm.
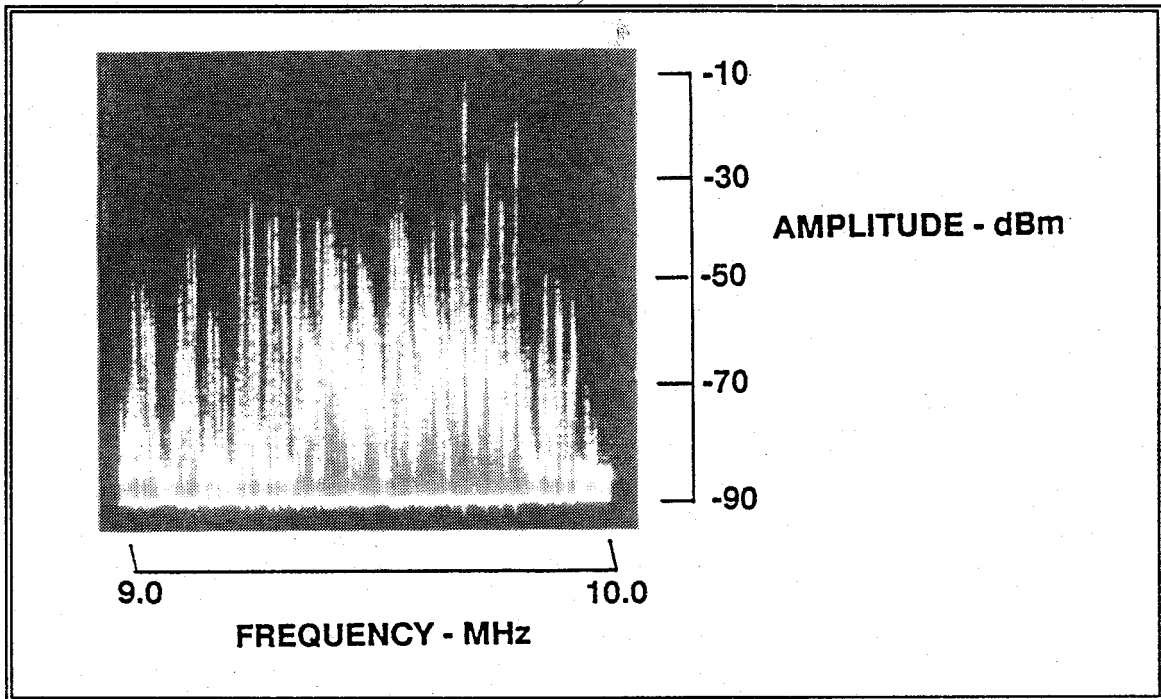
Figure 5.3 - Strongest Signal Received at the Guam CDAA
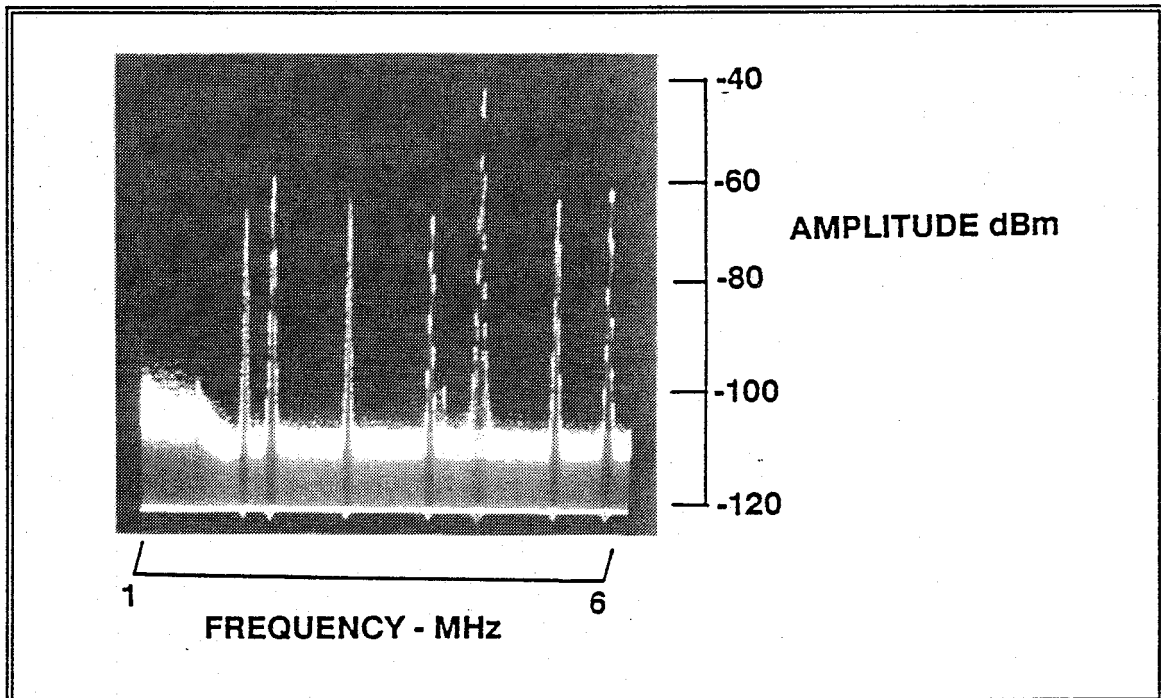
Figure 5.4 - Strong U.S. Military Signals Received at the Guam CDAA

84

By comparison, a receiver site in West Germany is within the single hop coverage of all the major international shortwave broadcasters in Europe. There, and in most of Central Europe, one would expect extremely strong signals in the international broadcasting bands. The strongest signals should be at nighttime in the 25, 31, 41, and 49 meter bands. Nighttime signal levels of +5 dBm are not uncommon at European CDAA sites.

3.   Baseline Noise Levels

Each site should be able to consistently receive and demodulate a signal of strength -115 dBm with a 10 dB signal-to-noise ratio. This would require a noise baseline of -125 dBm in a 3 to 10 kHz receiver bandwidth. This performance target requires that the noise floor at the site be externally established by non man-made sources. There must be little signal attenuation in the RF distribution system. No U.S. Navy receiving site visited by a SNEP team has met this target. One site nearly met the target but was limited in performance by internal noise sources.

Figure 5.5 shows a site with a receiver noise baseline of about -109 dBm in a 3 kHz bandwidth centered at 8.0 MHz (measured at the CDAA facility at Hanza, Okinawa, during September 1989). Internal noise sources caused the high noise baseline.

Figure 5.6 shows site-generated signals and noise coupling into a double-shielded coaxial cable within the Guam receiver site. A 50Ω coaxial terminator was
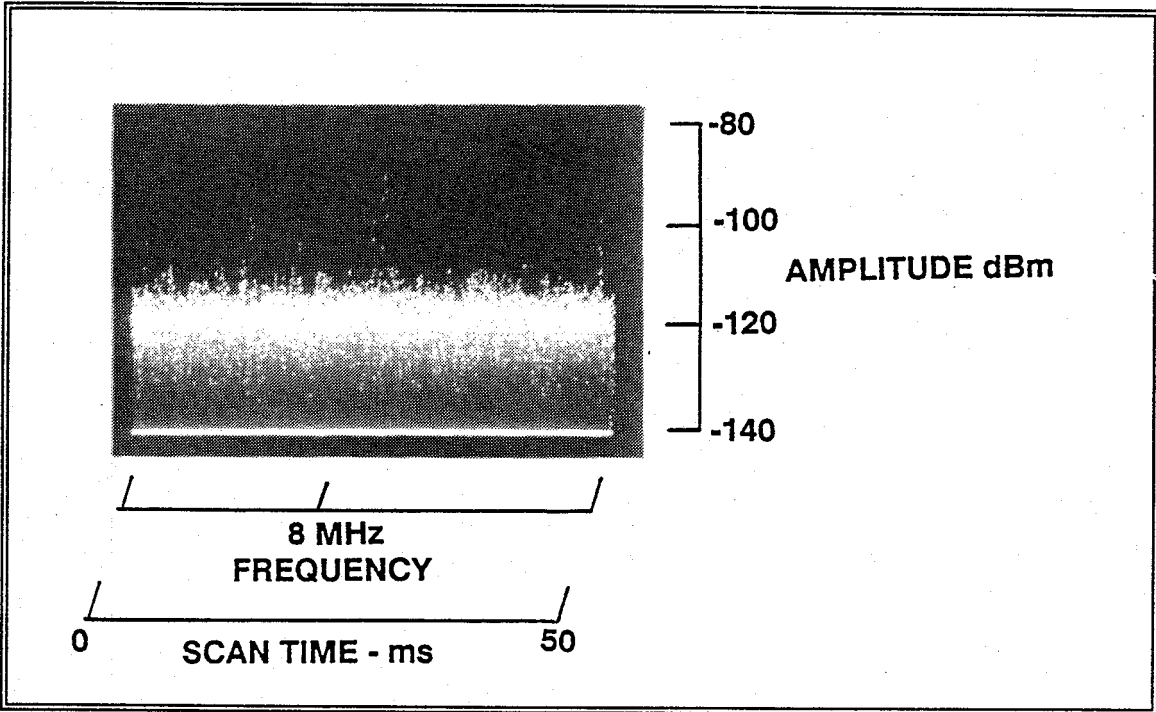
Figure 5.5 - Receiver Terminal Noise Baseline at Hanza CDAA
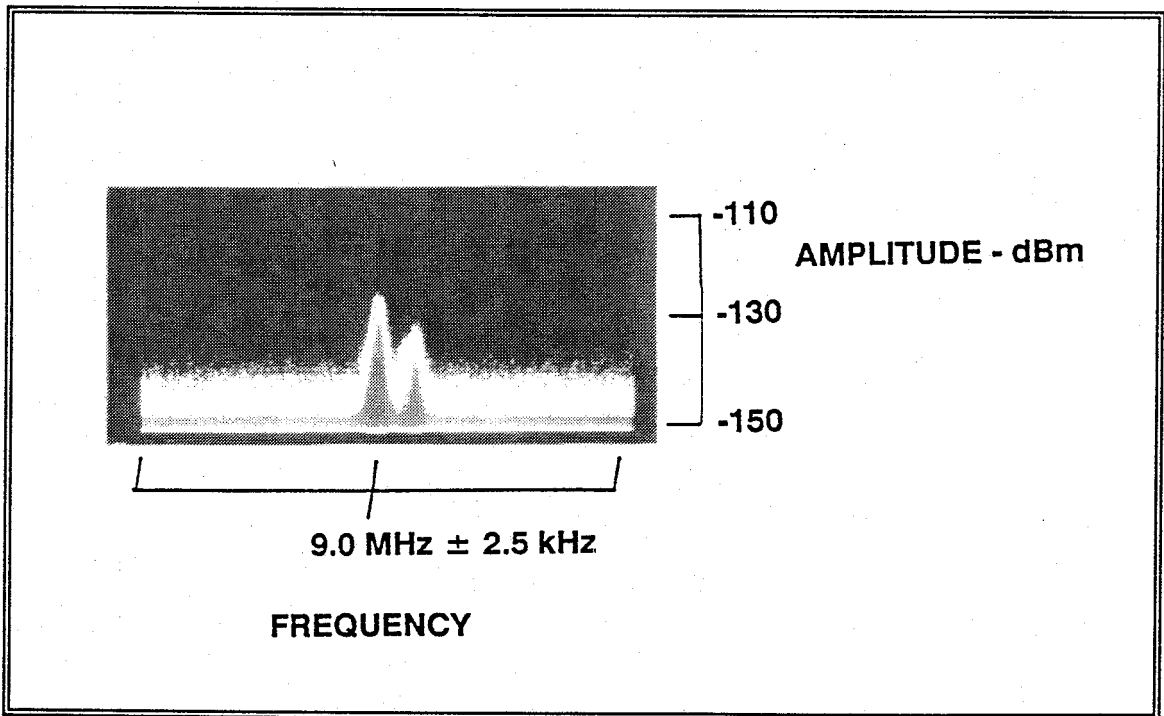
Figure 5.6 - Internal Noise Coupled into Terminated Coaxial Cables

on one end of the approximately 75 ft. length of RG-223/U cable, and the measurement equipment terminated the other end. These unwanted signals generated within the site interfere with the reception of signals of interest.

4. External Noise and Other Degradation

Externally generated noise, such as power-line related noise, adds to the site generated noise baseline. Figure 5.7 shows three kinds of power-line noise observed at the Okinawa CDAA during September 1989. Each noise source is broadband and periodic (with a 8.33 ms period) and has a maximum amplitude of -70 dBm in a 10 kHz bandwidth. During the hours when this noise source was present, the site's performance degraded to intolerable levels.

Figure 5.8 shows an in-band parasitic oscillation generated within the RF switching system in Okinawa. The oscillation was sporadic, and it was of sufficient amplitude to interfere with the reception of the two adjacent weak frequency-shift-keyed signals.

5. Signal Path Attenuation

Figure 5.9 shows weak signals centered near 12 MHz received on the Homestead, Florida, CDAA high-band monitor beam 096. The high-band monitor beam has approximately 12 dB of antenna gain.

The RF distribution system attenuates signals sufficiently so that weak signals received by an antenna element cannot be received by a receiver in the site.
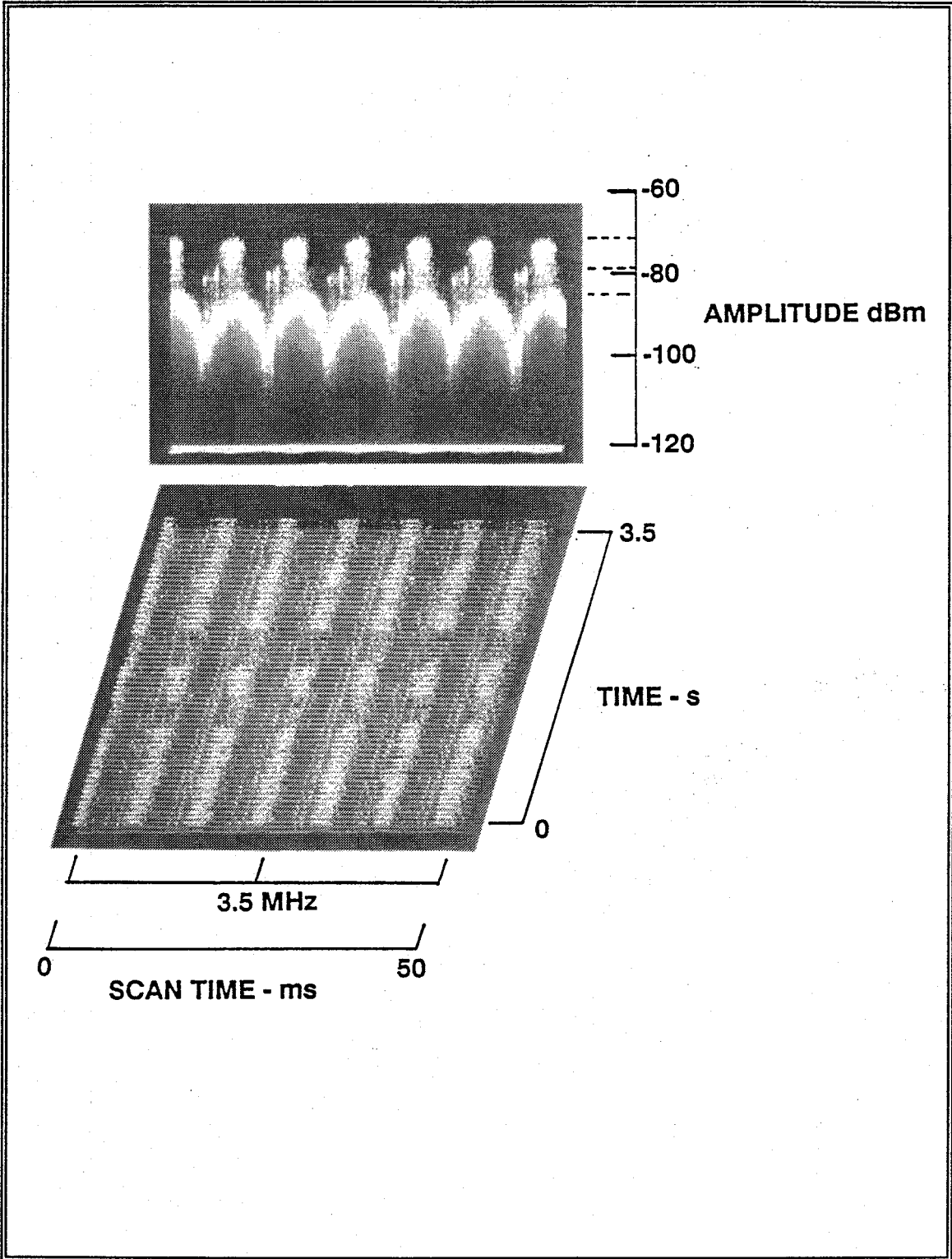
Figure 5.7 - Power-Line Related Noise

88
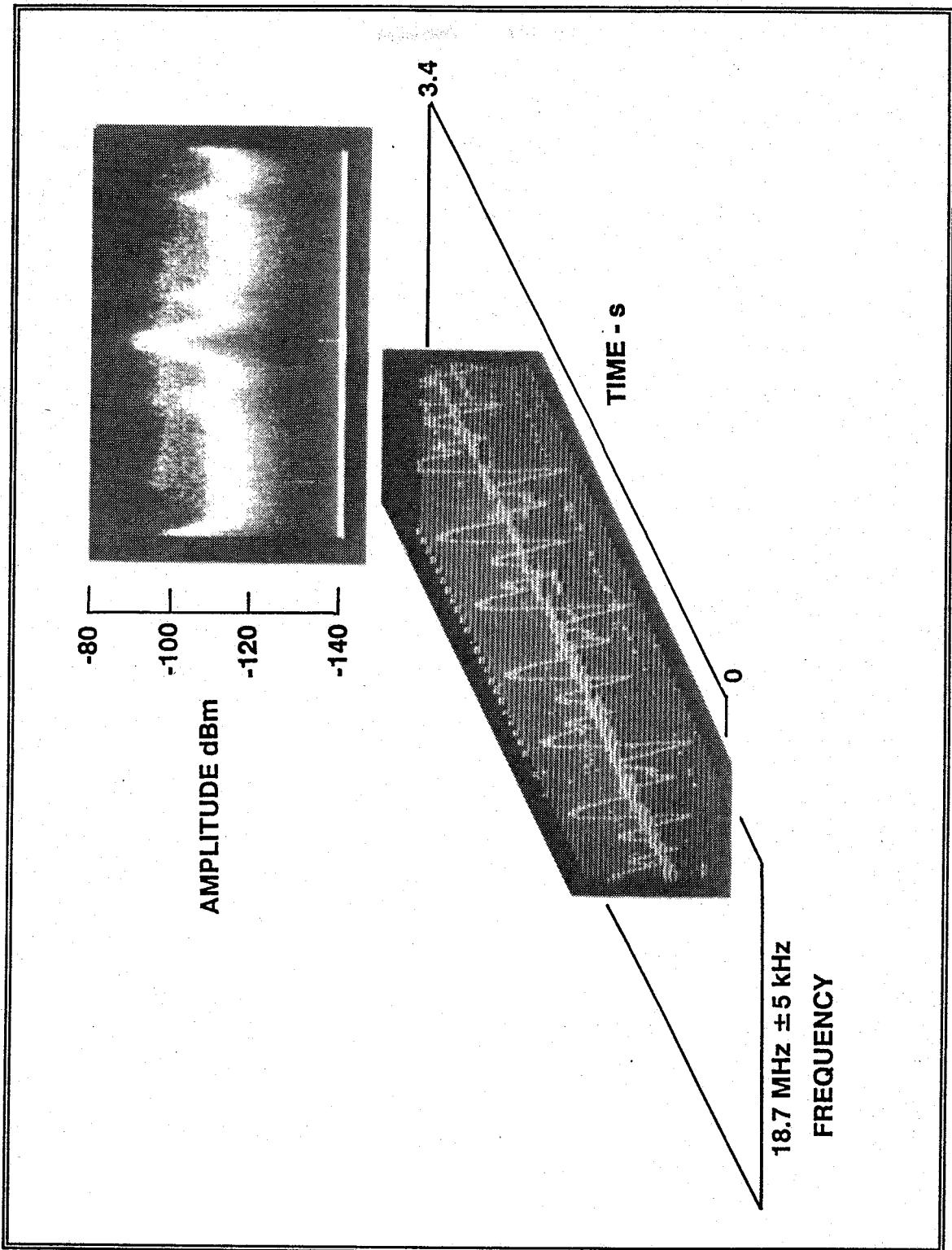
Figure 5.8 - In-Band Parasitic Oscillation

89
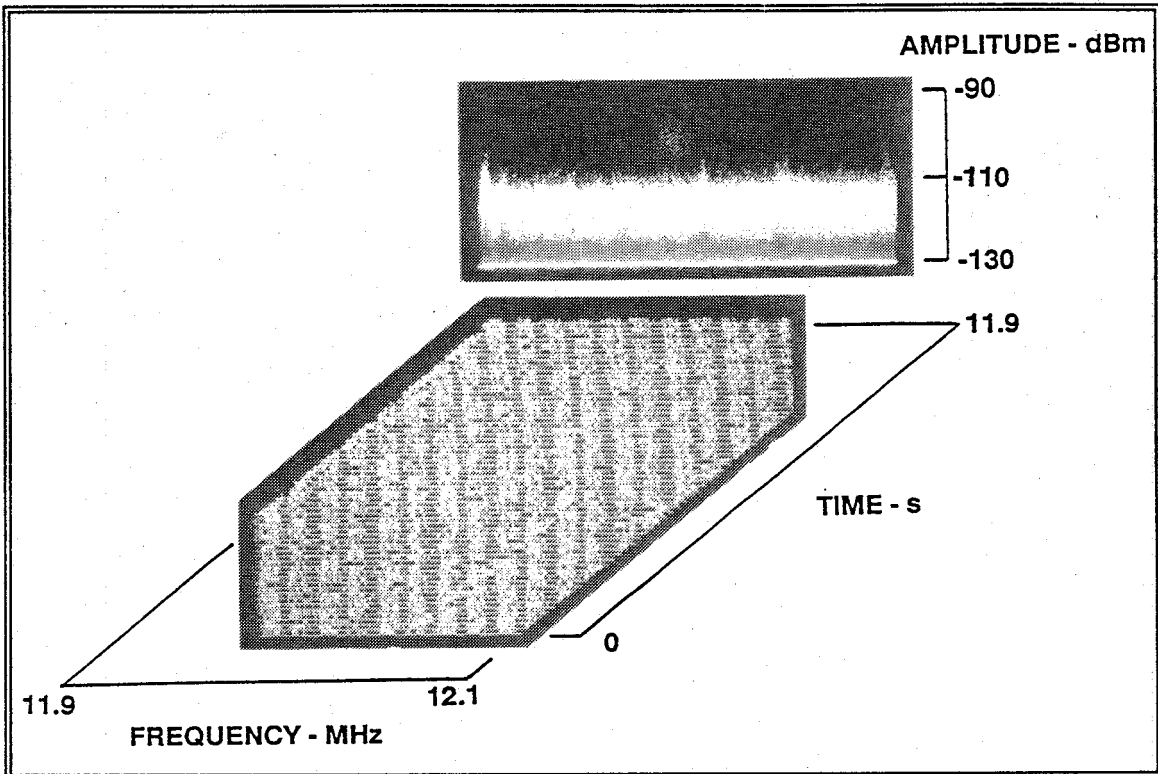
Figure 5.9 - Weak Signal Attenuation by RF Path Loss

Table 5.1 summarizes the RF distribution system losses measured at the Guam CDAA after installation of the ENLARGER RF switch. The loss through a single channel of the beamformer is expected, and it is partially recovered when all antenna elements forming the beam are used. The most significant loss is within the ENLARGER switch.

The Homestead ENLARGER antenna switching system has a constant loss of 7 dB as did the Guam system. With a consistent noise floor of -115 dBm prior to and after ENLARGER, the weak signals in Figure 5.9 should have had a signal-to-noise ratio 7 dB greater than that shown. The two signals in Figure 5.9 are not receivable without significant error.

Table 5.1 - MEASURED RF SIGNAL PATH LOSSES AT CDAA GUAM

Reference Signal: -40 dBm. injected as high band (HB) antenna element 37

Measurement Location	Measured Value	Cumulative Change
Output HB primary multicoupler 37	-38 dBm	+2 dB
Output HB beamformer 10	-49 dBm	-9 dB
Output ENLARGER Diplexer	-50 dBm	-10 dB
Output ENLARGER switch matrix	-56 dBm	-16 dB

Earlier SNEP surveys found ENLARGER to have time-varying path losses ranging from a few dB to a high of 35 dB [Ref. 32]. These losses seriously degrade site performance.

C.   GRAPHICAL SITE PERFORMANCE ESTIMATION

Upon completing a receiver facility survey, the maximum signal level, noise floor, and signal distributions provide the information needed to estimate site performance. Figures 5.1 and 5.2 provide the basis for making graphical estimates of site performance degradation. It is important that the day and night criteria and the one and two ionospheric hop criteria be used in determining site performance levels.

One must select the appropriate criteria and enter on the ordinate scale the typical noise baseline and the strongest signal level observed. The baseline noise measured in Guam in September 1989 was -115 dBm in a 3 kHz bandwidth. Detectable signals with signal amplitudes between -125 and -115 dBm are lost due
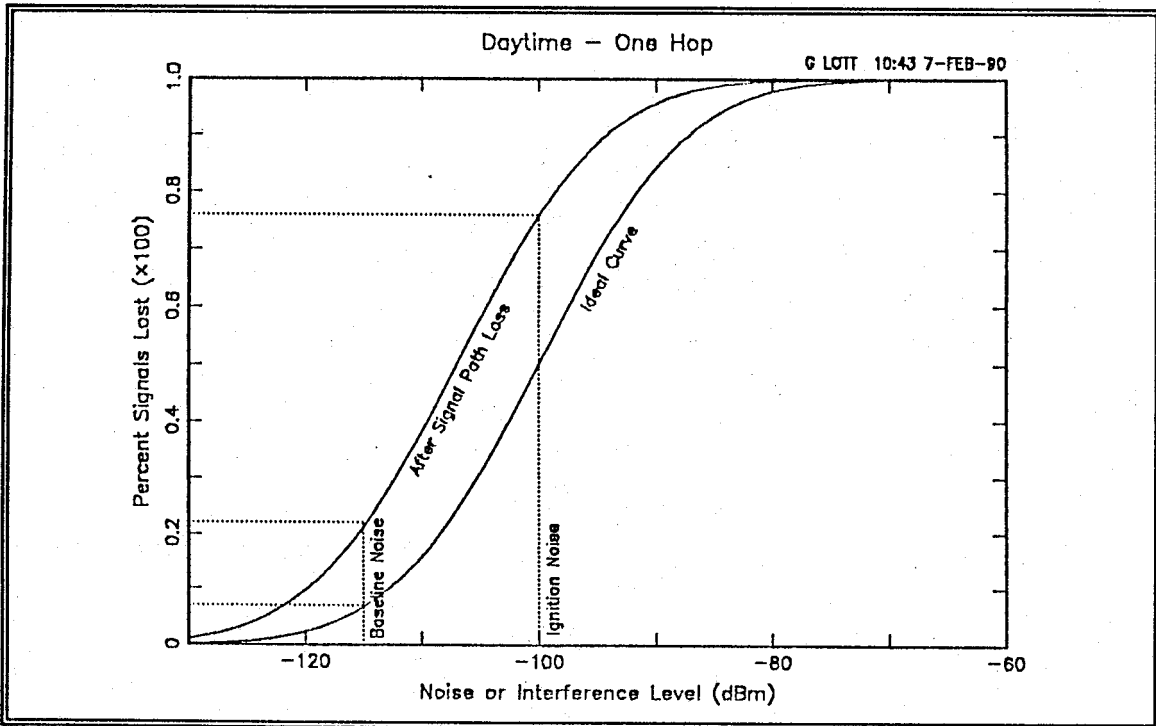
Figure 5.11 - Site Performance Estimate for Guam CDAA

performance estimate is good for the time of day and over the frequency band shown in Figure 5.12.

A similar performance estimate is possible using the same technique for the CDAA in Hanza, Okinawa, during September 1989 measurement period. The strongest signal level observed was -10 dBm, and the noise baseline observed was -109 dBm. The dynamic range requirement for the Okinawa site is 115 dB. A major difference between the ENLARGER RF switch in Guam and the RFSS RF switch in Okinawa is that there is little or no signal loss through the RFSS switch. As was found in Guam, the site's high noise floor seriously degraded weak signal reception.
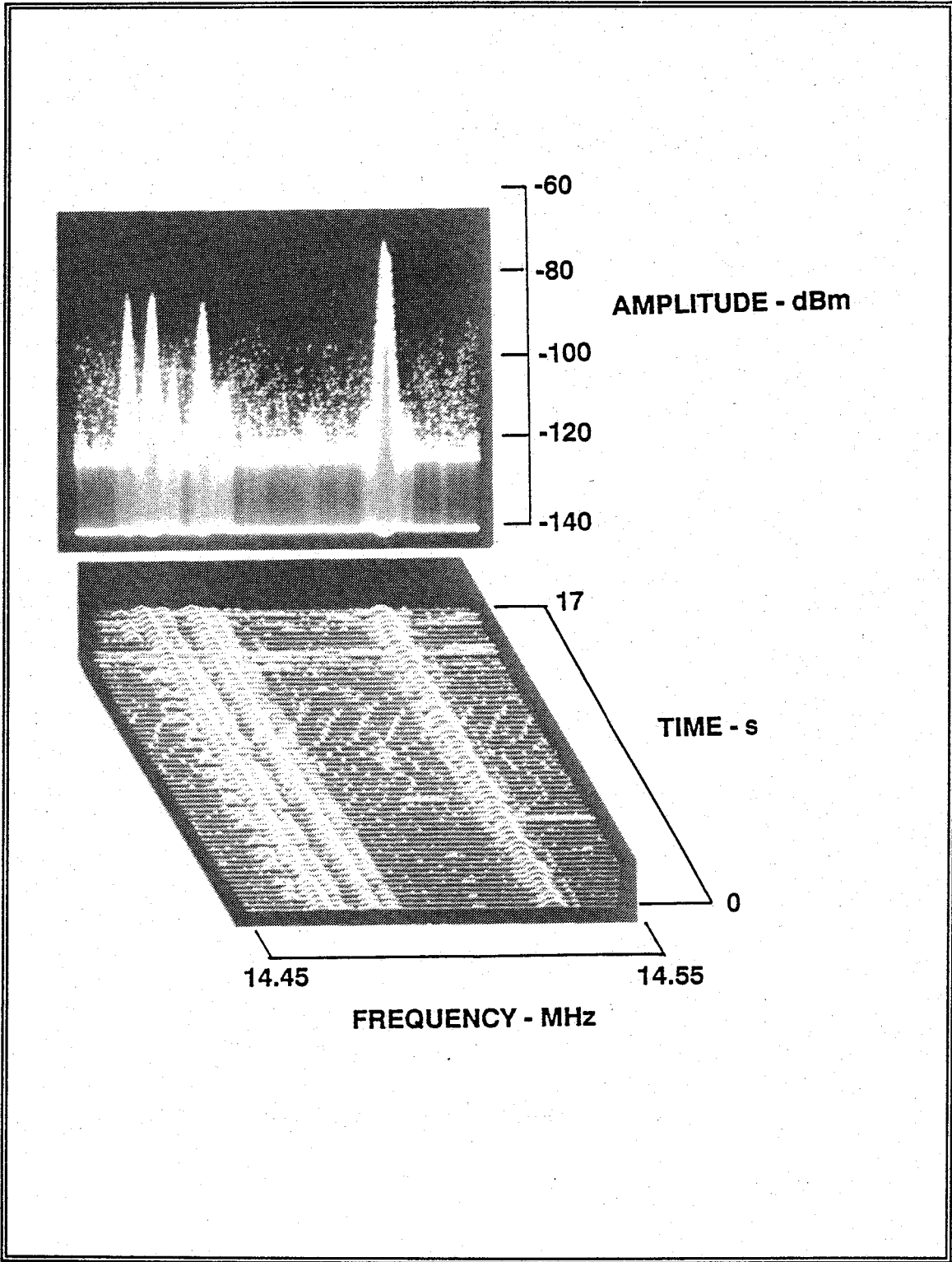
Figure 5.12 - Ignition Noise

External noise from power-line related phenomena caused severe interference at the Okinawa CDAA from 1.8 to 9 MHz. The worst power-line related noise levels were near 3.5 MHz with an amplitude of -65 dBm. Using Figure 5.1, the site cannot hear 100 percent of the daytime one hop signals of interest in the 2 to 6 MHz band while the power-line noise is present. The Hanza conditions result in losing 90 percent of the nighttime one hop signals in the same band provided the noise source was active at night. This power-line noise masks 100 percent of the two hop signals in the frequency band from 2 to 6 MHz anytime the source is active.

D. DISCUSSION

The site performance curves provide the field engineer and site personnel with the first quantitative assessment of signals of interest lost due to RF system deficiencies and noise. With performance estimates, one can prioritize problems for correction. Fix-up programs can focus on the recovery of the maximum quantity of signals lost. Site performance estimation has an important role in new antenna site location decisions. All real estate considered for a new receiver site requires a SNEP type survey before making a final site selection.

VI. A/D SELECTION AND PERFORMANCE

Figure 6.1 shows the block diagram of a possible future HF receiver site. There have been other digital receiver systems proposed, but most digital receiver schemes concentrate on converting a specific task (such as direction finding) from current analog or hybrid equipments to a fully digital system. [Refs. 33,34] Figure 6.1 generalizes the site systems and provides a multipurpose receiving capability. Analog signals appear only at the antenna, impedance matching networks, filters, preamplifiers, and any superheterodyne initial stages. The RF Distribution System becomes a digital network. Any HF receiver function requires only a dedicated processor to use the quantized HF signal environment. The dedicated processor can use common hardware with application software, or it may employ specialized hardware (such as neural networks) optimized for the specific function.

The keystone component in Figure 6.1 is the analog-to-digital converter. Figure 6.2 shows the ideal transfer characteristic of a 3-bit, bipolar, symmetric analog-to-digital converter. It quantizes voltages between $-V_{max}$ and V_{max} into eight levels. The quantized levels are Gray coded binary numbers.

The dashed straight line represents the ideal, linear transfer characteristic approximated by the stepped nonlinear transfer function of the actual quantizer. By maintaining the same voltage range and increasing the number of quantization
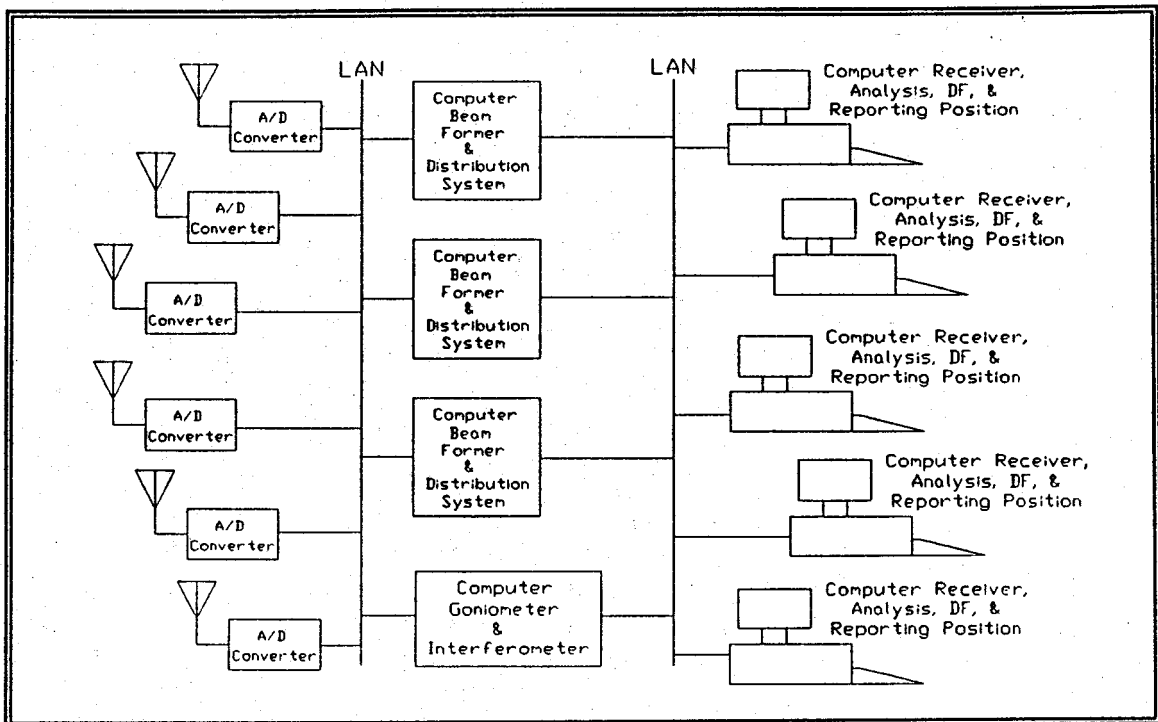
Figure 6.1 - Author's Conception of the Fully Digital HF Receiver Site

levels, the actual transfer characteristic can more closely approximate the linear transfer characteristic.

Each analog component between the antenna element and the A/D converter must have at least the same dynamic range capability as the A/D converter. All components, analog and digital, must have a sensitivity of at least -125 dBm, and they must have a dynamic range greater than that of the signal population to avoid intermodulation distortion.

Twenty years from now, the dynamic range requirements may be greater as the HF signal population continues to grow. The future HF receiver site will require extremely linear, high dynamic range analog-to-digital converters. These
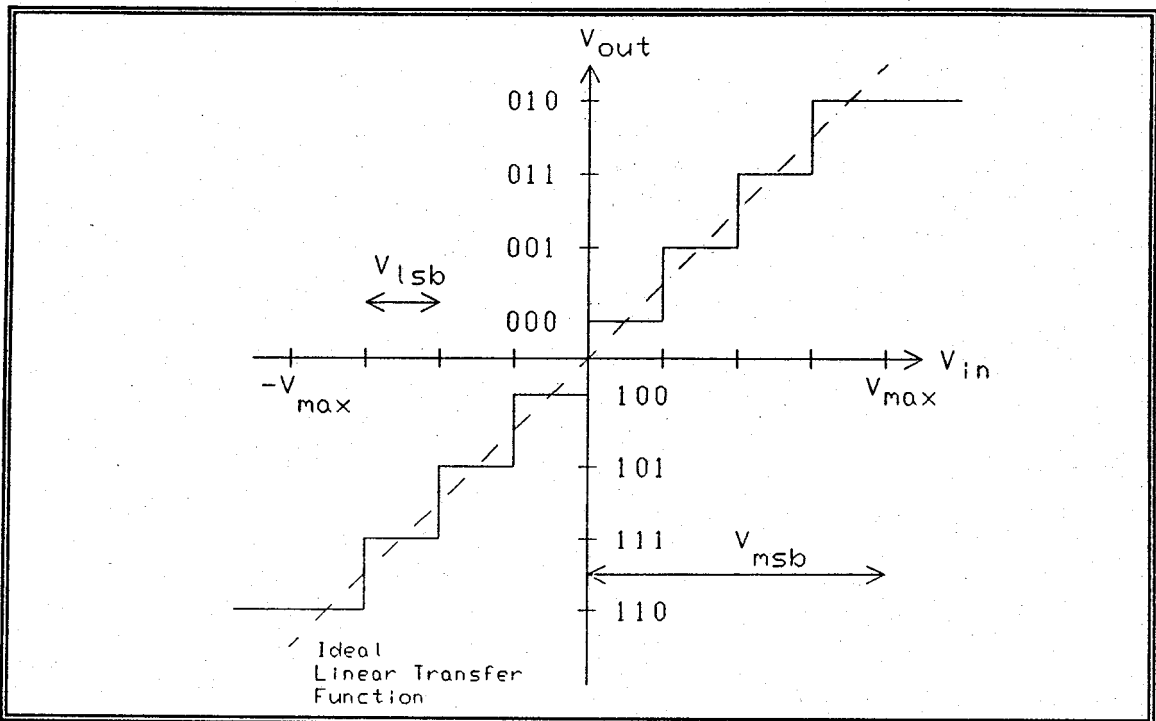
Figure 6.2 - 3-bit, Bipolar, Symmetric A/D Converter Transfer Characteristic

quantizers will need to have 20 to 22-bit resolution, have sampling rates above 90 MHz, and negligible differential and integral error.

This capability is far beyond today's technology, but improvements in high-speed sample-and-hold circuits and higher speed successive-approximation A/D's may make this possible at some future time. The computing requirements of an all-digital receiving system should be available by the time the quantizers are available.

Until technology is available, all wideband, digitizing search receivers, as shown in Figure 6.3, will use bandwidth-limited front ends. Superheterodyne techniques provide the amplification and selectivity. The primary limitations are those of

99

sampling speed and quantization resolution. This chapter reviews today's A/D converter technology, and it shows the key limiting factors of high-speed, high-resolution A/D's.
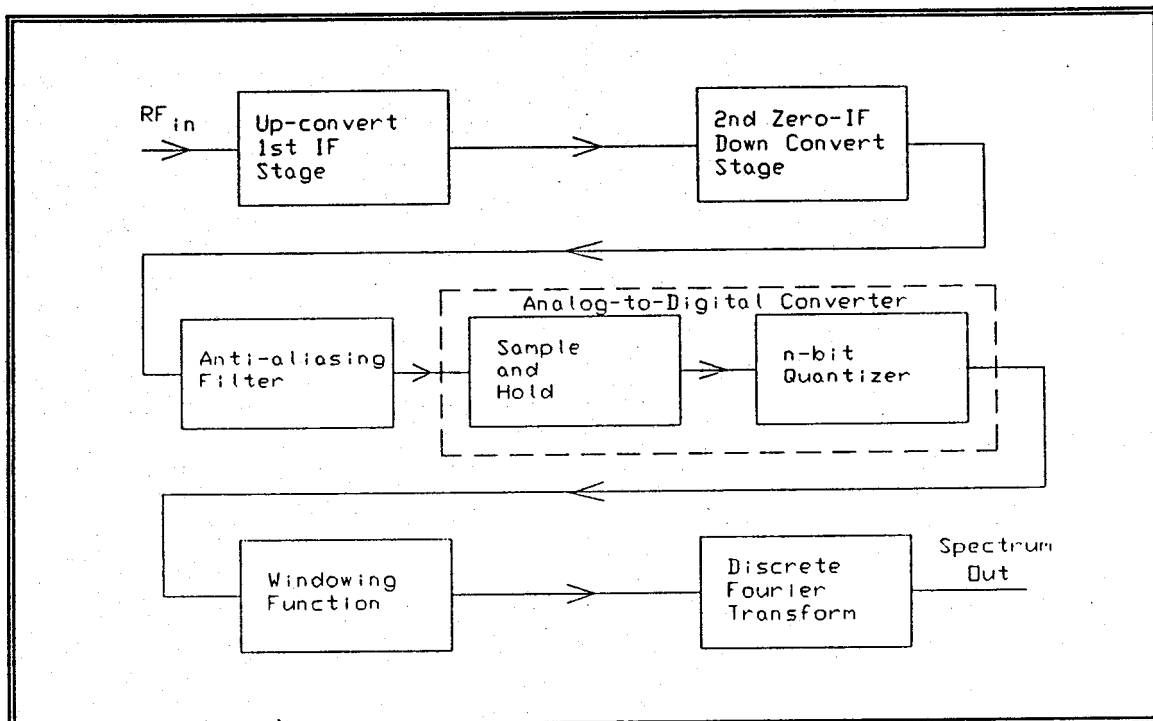
Figure 6.3 - Bandlimited Digital Search Receiver Using Superheterodyne Techniques

A. GENERAL A/D REQUIREMENTS

There are four basic architectures for A/D converters; servo or delta modulation (up-down counter), integrating or charge replacement, parallel (flash), and successive approximation. Appendix C gives a brief discussion and block diagram for each type. There are many other A/D types which are variations of one of the four basic architectures [Refs. 35,36].

100

The requirements for an HF search receiver quantizer are:

♦ Large dynamic range

♦ Large value of sampling rate

♦ Excellent linearity.

Large dynamic range value equates to high resolution or to many bits in the codeword which represents the input voltage. The highest resolution, off-the-shelf converter is the 22-bit resolution Analog Devices Model AD1175K. It uses a multi-slope integrating technique. This converter ideally provides 133 dB dynamic range with excellent linearity. [Ref. 37]

High-resolution quantization of HF signals requires receiver system computational power with more bits to reduce the effects of round-off errors. High speed 32-bit processors are just now becoming available to handle the processing requirements.

Today's technology can provide only 10 to 16-bit resolution with conversion speeds greater than 500 kHz. Rapid sampling is necessary to broaden the bandwidth of each converter and to reduce the number of converters required to cover the entire HF spectrum. The Nyquist sampling theorem requires a sampling frequency twice the bandwidth coverage, but practice indicates that an all digital receiving system requires a sampling frequency three to four times the bandwidth coverage. The higher sampling frequency allows for better anti-aliasing filtering. This is important since signals aliased into the passband reduce dynamic range.

Receiver coverage of the entire HF spectrum by dividing the 2 to 30 MHz band into 8 to 15 bandwidth-limited segments is manageable both in equipment size and overall control system requirements. This limited number of receivers requires quantization of a bandlimited HF signal voltage by an A/D converter sampling at a frequency greater than 4 MHz. The single receiver performance limitation that results from 22-bit quantizer resolution is a 10 kHz or less sampling frequency. Receivers built using 22-bit A/D converters may achieve the dynamic range needed for today's HF signal population, but the resulting system requires as many receivers as the narrowband search system mentioned in Chapter IV.

A high degree of A/D converter linearity is necessary to prevent creation of intermodulation (IM) products during quantization. IM products are less of a problem in narrowband digitizer schemes because most of the distorting signals will appear outside the passband of the receiver. In a wide bandwidth receiver, the IM products from many higher orders may fall in-band. This is particularly important in an energy detection receiver where each in-band IM product represents a new energy present condition.

With the HF spectrum's large number of signals, fading, extremely strong signals, ionospheric effects, and strong man-made noise, the number of IM products by an A/D converter without enough dynamic range could overwhelm a search receiver system's ability to process all the new energies. The large signal

population may produce hundreds of IM products from only one strong station. The result appears as broadband, white noise.

A dynamic-range-limited receiver system loses its weak signal detection capability because in-band IM products generate an increase in the system noise floor. This broadband noise from IM products increases the amplitude of the LTA for each frequency bin. Weak signal amplitudes will no longer be greater than this greater LTA value by the amount exceeding the amplitude screening threshold. The resulting site performance degradation is the same as would be observed by increasing the man-made noise level. The total noise voltage increase resulting from A/D nonlinearities must not exceed the voltage represented by the least significant bit, or about 6 dB. In a 120 dB dynamic range system with a -125 dBm noise floor, this equates to IM products being less than one microvolt.

B.   A/D PERFORMANCE LIMITATIONS

For the generalized HF new energy receiver, the following discussion assumes that the system requires this level of performance:

◆ 120 dB dynamic range in a 1 kHz bandwidth

◆ 5 to 10 MHz sampling frequency

◆ Total nonlinearity related products no greater than one half of 1-bit.

This section will discuss the bounds on receiver dynamic range performance resulting from the quantization (A/D conversion) process.

1. Aperture Uncertainty

The first device before the actual quantizer is a sample-and-hold (S/H). The S/H is a type of voltage memory that retains the analog signal value while the quantization process is underway. Much of the quantizing error results from nonlinearities in the S/H [Ref. 38].

A simplified expression for the composite input signal voltage, with a maximum frequency component f_{max}, as seen by the S/H is:

$$v_{in}(t) = M\cos(2\pi f_{max}t) \quad . \tag{6.1}$$

At the instant the sampling should take place, the incoming signal will be changing at some rate. The slope of the incoming composite signal is:

$$-M \sin(2\pi f_{max}t) \ \frac{\partial 2\pi f_{max}t}{\partial t} \quad . \tag{6.2}$$

The maximum slope occurs when:

$$t = \frac{(2m-1)}{4f_{max}} \tag{6.3}$$

where m is an integer.

In the S/H circuit, there are two operating modes, sample mode and hold mode. During the sample mode, the output voltage ideally equals the input voltage. The sample mode bandwidth of the S/H must be adequate to pass the input signal without producing distortion. Otherwise the S/H is useless for that

application. During the hold mode, the output is held constant at the value of the input signal at the instant when the S/H receives the hold command. [Ref. 39]

Aperture time is the duration of time from when the S/H receives the command to switch from the sample mode to the hold mode to when the S/H actually completes the transition and captures the input voltage level. The aperture time will vary between devices, but it ideally should be a constant for a single device. Actual S/H operation shows that the aperture time may vary within the same device. This variability in aperture time is called aperture uncertainty. If the input signal is changing rapidly, there can be a significant voltage change during the aperture uncertainty period. The resulting error voltage is the difference between the actual voltage level of the held signal from the voltage which was present when the sample-to-hold transition should have been completed. [Ref. 39]

Aperture uncertainty is a random variable, but it has a maximum value for a given physical device. This maximum time is the limiting value on the resulting aperture uncertainty error.

Regardless of the statistics of the aperture uncertainty, the maximum error should not exceed the voltage represented by one-half of the least-significant-bit (LSB) in the A/D. The one-half LSB limit assumes that the input voltage is uniformly distributed within one quantization interval.

The greatest error that can occur due to aperture uncertainty is that occurring when the amplitude of the input signal is changing most rapidly. Let τ_a

be the maximum aperture uncertainty value in seconds. The maximum error voltage, ϵ_a, due to aperture uncertainty is:

$$\epsilon_a = \frac{\partial v_{in}(t)}{\partial t} \Bigg|_{t=\frac{(2m-1)}{4f_{max}}} \cdot \tau_a \qquad (6.4)$$

which yields:

$$\epsilon_a = M \cdot 2\pi f_{max} \cdot \tau_a \quad . \qquad (6.5)$$

As shown in Figure 6.2, the maximum voltage amplitude which the A/D converter can quantize without distortion is V_{max}. Given this limitation, the voltage represented by the least significant bit is:

$$V_{LSB} = \frac{2V_{max}}{2^n} \qquad (6.6)$$

where n is the number of bits of resolution in the A/D converter. Using the worst case when $V_{max} = M$, the aperture uncertainty in the S/H establishes the bound:

$$n_{ap} \leq - \log_2(f_{max}) - \log_2(2\pi\tau_a) \quad . \qquad (6.7)$$

This relates the number of bits quantized with an error less than one-half of 1-bit (i.e., the dynamic range of the quantization system) to the highest frequency present in the voltage sampled for a specified aperture uncertainty.

Brigham and Cecchini give a similar dynamic range relationship which includes the variance of the aperture uncertainty [Ref. 40]. If one assumes that the

sample rate is the Nyquist rate, $2f_{max}$, writing the expression in terms of the number of the number of bits yields:

$$n_{ap} = \log_2\left(\frac{12}{\pi^2\sigma_z^2}\right) - 2\cdot\log_2(f_{max}) \qquad (6.8)$$

where σ_z^2 is the variance of the aperture uncertainty and the other terms are the same as in Equation 6.7.

2. Pedestal Error and Droop

Pedestal error, ϵ_p, is a shift in the hold voltage level due to charge accumulation in stray capacitance between the S/H input and the hold amplifier capacitor. This is a nonlinear function that is highly dependent on the input voltage. "The obvious result of the nonlinear pedestal-input relationship is harmonic distortion." [Ref. 38]

Assuming that pedestal error will be a linear function of the maximum voltage excursion, the goal is for:

$$\epsilon_p = a_1M+a_2 \leq \frac{V_{LSB}}{2} = \frac{V_{max}}{2^n} \qquad . \qquad (6.9)$$

Calculating the effect of pedestal error as a function of the number of bits yields:

$$n_p \leq \log_2(V_{max}) - \log_2(a_1M+a_2) \qquad (6.10)$$

where a_1 and a_2 are functions of the stray capacitance. Maximizing V_{max} and minimizing the capacitance related parameters a_1 and a_2 gives the greatest dynamic

107

range. The bound established by pedestal error is not directly dependent on the bandwidth.

Droop error results from the gradual decay or change of the held analog voltage. Many S/H devices use a charge storage device (i.e., a capacitor) to hold the voltage level being quantized, and the stored voltage level will change with time. The charge depletion results from finite resistances and parasitic capacitances to ground associated with the hold circuit.

The entire A/D conversion must occur before the droop error exceeds one half of the LSB. Droop can cause significant error when used in conjunction with slow conversion rate A/D converters. Droop causes little error when used with flash type converters since there is only one conversion cycle. Flash A/D converters are the type used in all high speed conversion systems like those in the broadband HF receiver. Current design techniques can retain a stored voltage within one part in 10^6 for a period less than 1 μs. Therefore, the error resulting from droop in the S/H is not a limitation on the HF receiver quantization process. [Ref. 38]

3. Analog Component Dynamic Range Limitations

Performance limitations in analog components which precede the S/H and A/D pair in a digitizing receiver can cause errors in the codeword generated by the A/D converter. A term used to describe this performance limitation of the analog devices is spurious-free-dynamic-range (SFDR).

Understanding the performance bound resulting from analog component nonlinearities requires the determination of two values. The first is minimum detectable signal (MDS). MDS is the input power level to the quantizer due to the kTB (thermal) noise voltage present; G, the analog front-end amplifier gain; and, F, the analog front-end noise figure. The MDS is:

$$MDS = kTB \cdot F \cdot G \qquad (6.11)$$

where B is the bandwidth of the system feeding the S/H and A/D pair. The MDS value for the HF digital search receiver should be less than -125 dBm.

The second value required is the third-order intercept point. This number is used as an indicator of distortion resulting from the lumped effect of nonlinearities in the active device. Determining the actual third-order intercept point is usually done graphically. The third-order intercept point is the intersection of the projection of the active device's linear gain characteristic and the linear projection of the device's characteristic relating the power level of third-order IM products to the input signal power level. A device's manufacturer usually specifies the third-order intercept point along with gain and noise figure.

By contrast, the values most often used to describe the lumped nonlinearity errors in an A/D converter alone are the differential error, the integral error, and the effective number of bits [Refs. 41,42,43]. These three indicators of A/D performance are independent of the limitations of other devices.

In most systems, the third-order intermodulation products produce the greatest degradation in system dynamic range. This is true in a narrowband superheterodyne receiver because the third-order IM products are those that can appear in-band and interfere with received signals. The third order intermodulation product dynamic range is given as:

$$DR_3 = \left(\frac{I_o^3}{kTFG} \right)^{\frac{2}{3}} \cdot \left(\frac{1}{B} \right)^{\frac{2}{3}} \qquad (6.12)$$

where DR_3 is the third-order limited dynamic range and I_o^3 is the third order output intercept point [Ref. 44]. As shown before, the dynamic range of the converter is 2^n bits. Equating the two expressions yields:

$$2^n = \left(\frac{I_o^3}{kTFG} \right)^{\frac{2}{3}} \cdot \left(\frac{1}{B} \right)^{\frac{2}{3}} \quad . \qquad (6.13)$$

High dynamic range testing using a 1 Hz resolution bandwidth is an increasingly common technique. The definition of SFDR for the analog devices is the ratio of the third-order-output-intercept-point to the MDS in the 1 Hz bandwidth [Ref. 45]. The SFDR is not a directly measurable value since the third-order intercept point is an extrapolated value. Using this definition, and changing the bandwidth B to f_{max}, one can write the expression:

$$n_{SFDR} \leq -\frac{2}{3} \log_2(f_{max}) + \log_2(SFDR) \quad . \qquad (6.14)$$

110

This expression equates the ideal dynamic range in bits to the measurable dynamic range. This places another bound on dynamic range performance as a function of the highest frequency sampled.

4. Quantization

Quantization error occurs because the quantization process maps a continuous voltage into a subset of the integers. Figure 6.4 shows the error voltage function resulting from the ideal A/D transfer function. Between V_{max} and $-V_{max}$, the error noise power of the ideal converter is due solely to quantization. The quantization noise power, P_q, in the uniform quantizer is:

$$P_q = \int_{-V_{max}}^{V_{max}} \epsilon^2(v_{in}) \, P_{v_{in}}(v_{in}) \, dv_{in} \qquad (6.15)$$

which when evaluated becomes:

$$P_q = \frac{V_{LSB}^2}{12} = \frac{V_{max}^2}{3 \cdot 2^{2n}} \qquad (6.16)$$

assuming that the voltage is uniformly distributed within each quantization step.

Gray and Zeoli developed an expression for A/D quantization noise based on the assumption that the input is Gaussian distributed with standard deviation σ [Ref. 46]. By letting the value of σ times a positive integer k (k≥1) be
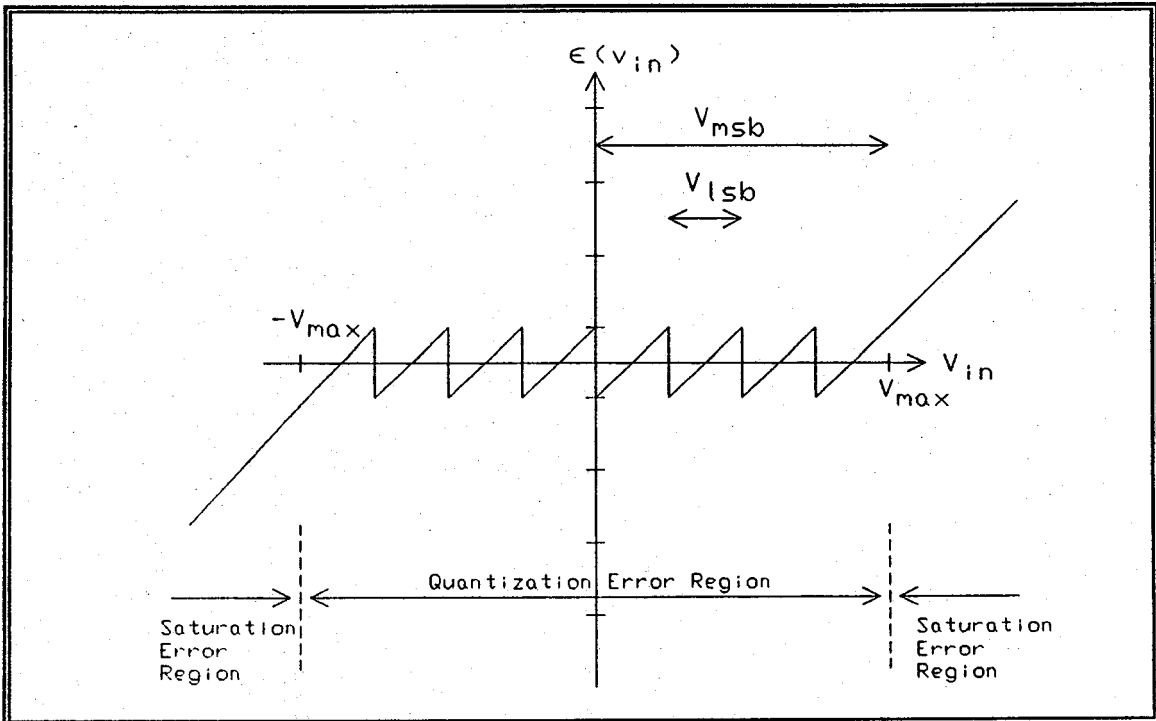
Figure 6.4 - Error Function for an Ideal, Bipolar, Symmetric A/D Converter

the maximum voltage level of the A/D, the quantization noise power expression

is given as:

$$P_q = \frac{2\sigma^2 k^2}{12(2^{n-1}-1)^2} \left(\frac{1}{2} - \int_k^\infty \frac{1}{\sqrt{2\pi}} e^{-\frac{u^2}{2}} du \right) . \qquad (6.17)$$

Since k is a positive integer, the value for the last term in the expression is such

that one can evaluate bounds on the expression as:

$$0.34 \leq \frac{1}{2} - \int_k^\infty \frac{1}{\sqrt{2\pi}} e^{-\frac{u^2}{2}} du \leq 0.50 \qquad (6.18)$$

for $1 \leq k < i$ as $i \to \infty$ and $i \in$ {integers}.

112

For the ideal quantizer, where quantization noise and saturation are the only limiting factors, the natural definition for dynamic range is the ratio of the maximum power input to the A/D without saturation, $k^2\sigma^2$, to the quantization noise power, P_q. Continuing with Gray and Zeoli's Gaussian input voltage assumption, considering the case where n is large, and choosing the worst case from Equation 6.18, one can write the number of bits required to achieve a specified dynamic range, DR, as:

$$n_q \leq \frac{1}{2} \log_2(\text{DR}) - 1.07 = 0.167 \cdot \text{DR}_{\text{dB}} - 1.07 \quad . \quad (6.19)$$

The effective number of bits is the same as in the ideal A/D case, the approximation of which was given in Equation 4.1. This function is a bound only on the number of bits, and it is not a function of bandwidth.

In the HF signals case, the amplitude of the input signals are log-normally distributed rather than being normally distributed as in the case above. By assuming ideal, uniform quantization, one can calculate the quantization noise power for the HF signals as:

$$P_{q_{HF}} \cong 2 \cdot \frac{V_{lsb}^2}{12} \cdot \int_0^{k\beta} \frac{1}{x_t \sqrt{2\pi\sigma_{ln}^2}} \, e^{-\frac{(\ln(x_t) - \mu_{ln})^2}{2\sigma_{ln}^2}} \, dx_t \quad (6.20)$$

where β is the standard deviation of the distribution in Equation 3.9 and $k\beta$ is the voltage V_{max}. In this case:

$$V_{lsb}^2 = \left(\frac{2V_{max}}{2^n}\right)^2 = \frac{k^2\beta^2}{(2^{n-1})^2} \qquad (6.21)$$

resulting in the expression:

$$DR \cong \frac{k^2\beta^2}{P_{q_{HF}}} = \frac{3 \cdot 2^{2n}}{2 \cdot \Lambda(k\beta)} \qquad (6.22)$$

where

$$\Lambda(k\beta) = \int_0^{k\beta} \frac{1}{x_t\sqrt{2\pi\sigma_{ln}^2}} \, e^{-\frac{(ln(x_t)-\mu_{ln})^2}{2\sigma_{ln}^2}} \, dx_t \quad . \qquad (6.23)$$

One can then express the number of A/D converter bits required as a function of the specified dynamic range as:

$$n_{q_{HF}} \cong \tfrac{1}{2}\log_2(DR) - 0.3 + \tfrac{1}{2}\log_2(\Lambda(k\beta)) \qquad (6.24)$$

or in dB as:

$$n_{q_{HF}} \cong 0.167 \cdot DR_{dB} - 0.3 + \tfrac{1}{2}\log_2(\Lambda(k\beta)) \quad . \qquad (6.25)$$

Since $\Lambda(k\beta) \leq 1$, the last term in Equation 6.25 will reduce the effective number of bits. For the case where $\Lambda(k\beta) \approx 1$,, the dynamic range changes at a rate of 6 dB per bit which is the ideal case given in Equation 4.1.

5. Saturation

Saturation noise caused by overloading an A/D converter is an important consideration when working with signals in the HF band. Saturation severely degrades system operation during nighttime at most HF receiver facilities. Today's best amplifiers and multicouplers can barely process the daytime HF signal population without producing intermodulation products. Since the HF signal levels increase 20 to 30 dB at night, these stronger signals can easily exceed the input voltage range for linear operation of the analog devices and the A/D converter. The devices become saturated, and the output noise level increases.

Saturation occurs when the amplitude of the input voltage being quantized exceeds V_{max}. Clipping is another term used to describe saturation. While the quantization error voltage is a bounded, periodic value, the saturation error voltage can grow without bounds. The limit on saturation is the total signal capacity of the physical electronics before damage occurs.

By keeping the quantization step size small enough to reduce quantization noise, the departure from a linear characteristic in the A/D converter transfer characteristic is kept small. While not truly a linear process, small quantization step size minimizes the performance degradation resulting from intermodulation products. Strong signal levels, which require a higher value of V_{max} for a given number of bits, result in greater quantization noise because the

quantization step size increases. Preventing saturation is a trade-off between quantization and saturation noise for a fixed quantizer resolution.

Figure 6.4 shows the region of input voltage values for which saturation error occurs. The saturation error power is:

$$P_s = \int_{-\infty}^{-V_{max}} \epsilon^2(v_{in}) \ p_{v_{in}}(v_{in}) \ dv_{in} + \int_{V_{max}}^{\infty} \epsilon^2(v_{in}) \ p_{v_{in}}(v_{in}) \ dv_{in} \quad . \quad (6.26)$$

By using symmetry, and writing the expression for the error voltage, the saturation power becomes:

$$P_s = 2 \cdot \int_{V_{max}}^{\infty} \left(v_{in} - V_{max} \cdot \left(1 - \frac{1}{2^n} \right) \right)^2 \ p_{v_{in}}(v_{in}) \ dv_{in} \quad . \quad (6.27)$$

Further simplification of Equation 6.27 is possible when n is large.

Gray and Zeoli also developed an expression for A/D saturation noise using the same assumptions as in their quantization noise case [Ref. 46]. Their expression is:

$$P_s = 2\sigma^2 \left((k^2+1) \int_{k}^{\infty} \frac{1}{\sqrt{2\pi}} \ e^{-\frac{u^2}{2}} \ du - \frac{k}{\sqrt{2\pi}} \ e^{-\frac{k^2}{2}} \right) \quad . \quad (6.28)$$

Since saturation error is unbounded, simplification techniques used to develop Equation 6.19 do not work with Equation 6.28. In the case of HF signals, the saturation noise power for large values of n becomes:

$$P_{s_{HF}} = 2 \cdot \int_{k\beta}^{\infty} (v_{in} - k\beta)^2 \frac{1}{v_{in}\sqrt{2\pi\sigma_{ln}^2}} e^{-\frac{(ln(v_{in}) - \mu_{ln})^2}{2\sigma_{ln}^2}} dv_{in} \quad . \quad (6.29)$$

As in the HF quantization noise case, there is no closed-form expression deducible from Equation 6.29 to express the effective number of bits representing true dynamic range as a function of saturation noise power. The best approach to minimize the noise resulting from both quantization and saturation is to balance the effects through the optimal selection of the variable k. This can be done numerically, and Gray and Zeoli did this for the Gaussian signal case [Ref. 46].

During the data collection described in Chapter IV, several data sets were included to test the effects of A/D saturation on the number of new energy alarms. Figure 6.5 shows the equipment configuration used where paralleled 14-bit and 12-bit A/D converters quantized the same voltage. During the tests, strong signal levels were present that would saturate either A/D without adding some front-end attenuation.

The experiment assumed that the number of new energies detected during a 15 minute observation period would not change substantially from one data set to another. This assumption requires the entire observation period to be

117
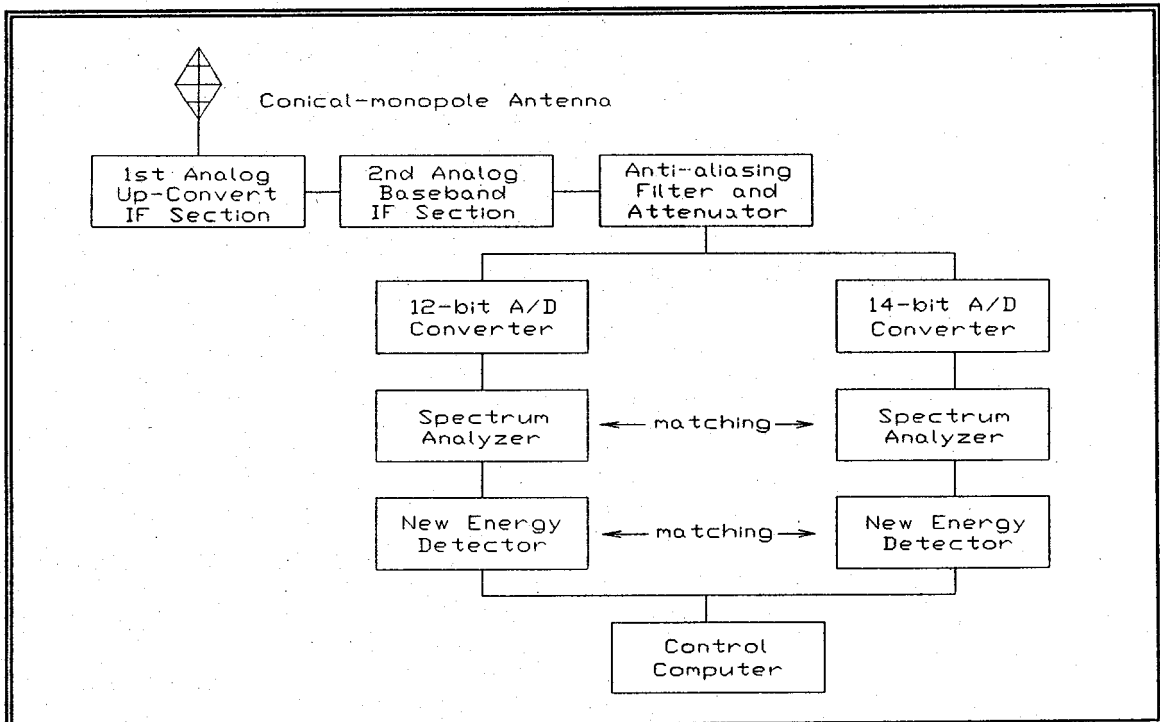
Figure 6.5 - A/D Saturation Experimental Equipment Configuration

either during day or night because of the substantial change in the signal population between the two time periods.

The experiment consisted of operating the new energy receiver system in the configuration shown in Figure 6.5 while changing only the front-end RF attenuation every 15 minutes. Calibration showed that both A/D converter systems had the same sensitivity. There were two experimental periods, data sets 8 through 18 (daytime) and data sets 19 through 26 (nighttime). The control system logged all new energies, and off-line data reduction produced histograms for each 15 minute collection period as described in Chapter IV and shown in Appendix B. Appendix B also contains surface and contour plots of data from the saturation

experiments and plots showing the ratio of the number of new energy alarms on the 14-bit converter to the number of new energy alarms on the 12-bit converter system.

Figures 6.6 and 6.7 show data which summarize the experimental findings. The solid lines are cubic-spline fits to the data points shown. There is a nearly constant ratio of 14-bit A/D new energy detections to 12-bit A/D new energy detections when both A/D converters are not saturated. The 12-bit converter performed within a few percent of the 14-bit converter in the total number of new energy detections.

During the daytime test, the 12-bit quantizer saturated with about 28 dB of front-end RF attenuation. The 14-bit began to saturate with about 24 dB of RF attenuation. Using the 6 dB per bit dynamic range rule, one would expect a 12 dB difference between attenuation levels of the two quantizers required to reach A/D saturation. System operation during the nighttime experiment revealed about the same 4 to 6 dB difference in attenuation levels to reach A/D saturation.

After reaching saturation, the number of new energy alarms generated by the 12-bit converter rose dramatically. This was expected since all the intermodulation products resulting from saturation would appear as new energies. Eventually, saturation of the 12-bit A/D converter became so complete that the LTA levels in all frequency bins rose high enough that the signals present could not exceed the amplitude screening threshold and produce new energy alarms.
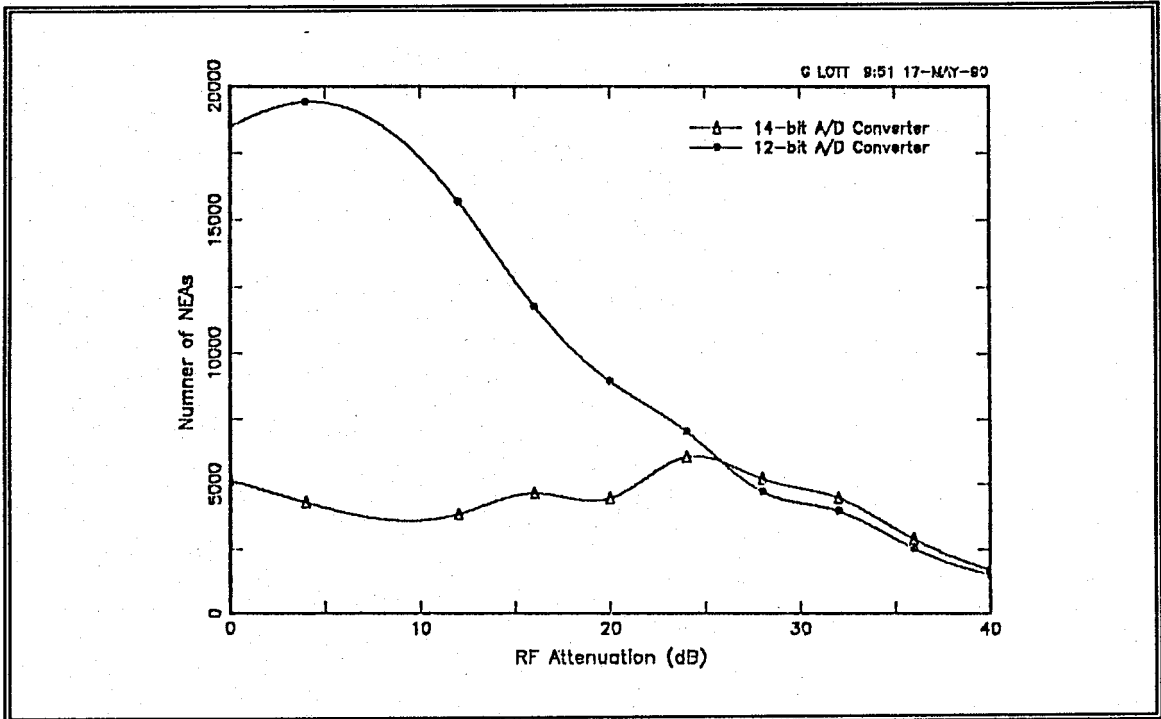
Figure 6.6 - Daytime Saturation Experiment Results
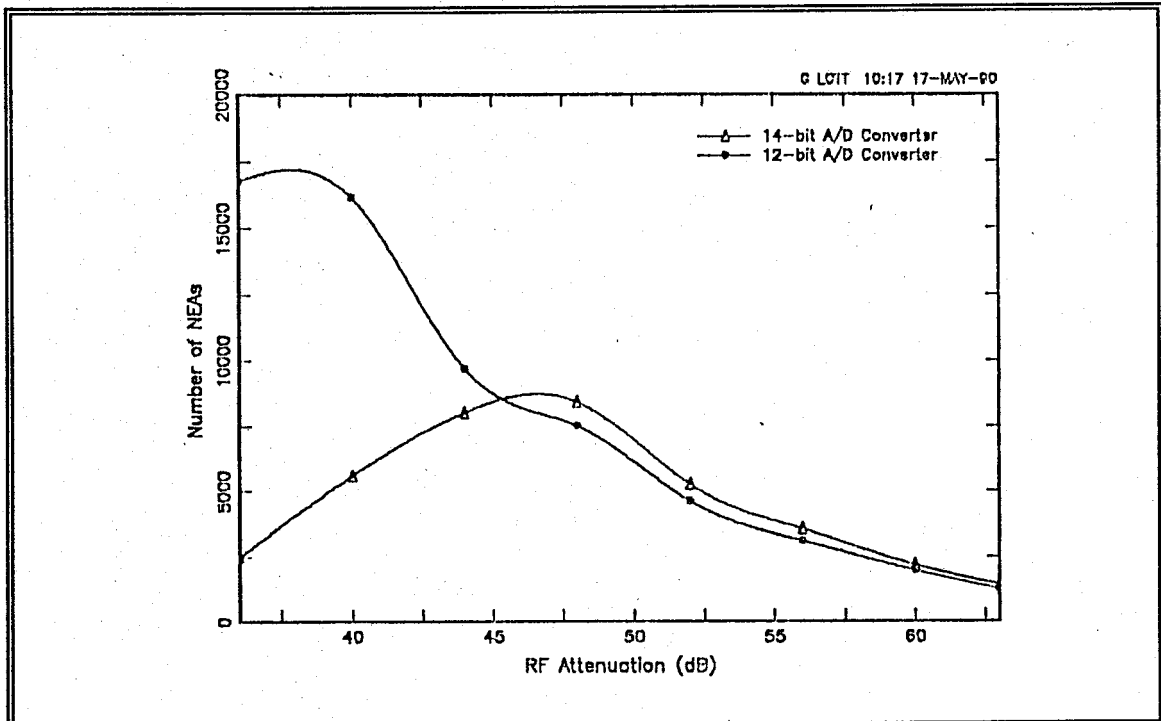
Figure 6.7 - Nighttime Saturation Experiment Results

120

The 14-bit converter responded in a different way. During the daytime test, the number of new energy alarms on the 14-bit system actually stabilized or declined after saturation. Viewing the output spectrum from the receiver revealed a different saturation phenomenon. The baseline noise level in the 12-bit converter gradually increased with each reduction of attenuation. This phenomenon continued until there were no signals observable in the noise. However, the 14-bit system had a marked jump in the baseline noise level upon reaching saturation. This sudden addition of saturation noise caused the noise floor to increase by as much as 20 to 30 dB. The result was a burst of new energy alarms activity upon reaching saturation, but the LTA value for all frequency bins was already high enough for no new alarms to occur.

The exact reason for the different saturation responses between the 12-bit and 14-bit A/D converters is not known, but one can hypothesize about the causes. Both A/D systems use different sample-and-hold amplifiers just prior to the quantizer. If the compression rate of the S/H with the 14-bit converter's is greater than that of the S/H with the 12-bit converter, the S/H with the 14-bit converter would generate stronger IM products of higher order than would the S/H amplifier with the 12-bit converter. This would explain the sudden jump in the spectrum with the 14-bit converter as explained above.

By measuring the slope of the lines in Figures 6.6 and 6.7 in the region without A/D saturation, one can write a simple expression for the change in the

number of new energy alarms as a function of added attenuation. When operating

without saturation, the rule-of-thumb is:

$$\%\Delta_{nea} = 0.8 \cdot \Delta_{RF\ Atten\ (dB)} \qquad (6.30)$$

6.   Aliasing

The performance of the lowpass filter which precedes the S/H and A/D

pair, as shown in Figure 6.3, places a limitation on the overall receiver system

dynamic range since the filter's out-of-band rejection is not infinite. Signals at

frequencies greater than one-half the sampling rate will be aliased into the receiver

passband unless attenuated by the anti-aliasing filter. A well designed filter can

substantially attenuate the voltage from the higher frequency signals, but the peak

out-of-band voltage levels must be no greater than one-half of the voltage

represented by the LSB, as shown in Figure 6.8. Otherwise, the aliased signals will

reduce system performance by interfering with weaker in-band signals.

In a digital search receiver, the final superheterodyne stage usually

translates the in-band signals to baseband (i.e., no frequencies greater than one half

the A/D sampling rate). A receiver incorporating this superheterodyne method is

said to have a zero-IF final stage. In narrowband receiver design, "...the anti-alias

filter requirements are generally more demanding in a digital radio than say for an

audio application where the signal energy above 15 kHz is small." [Ref. 47]

Traditional IF filter technology is adequate for narrowband receiver incorporating
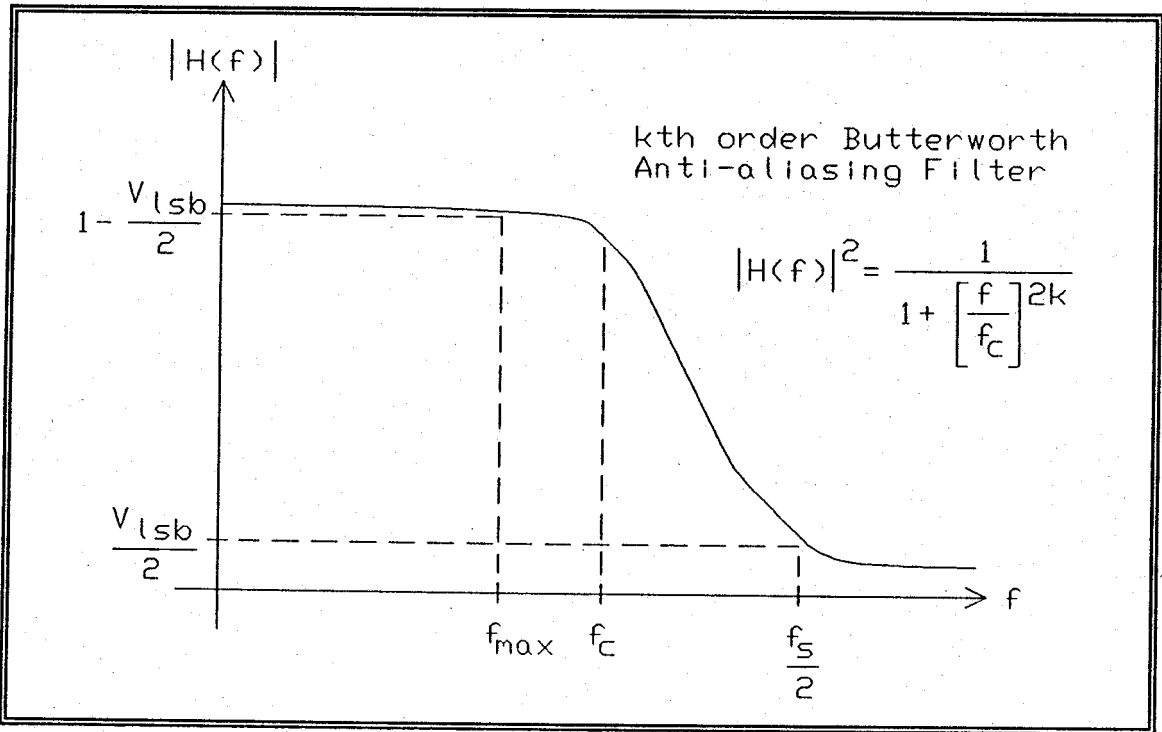
Figure 6.8 - Anti-aliasing Filter Transfer Function Requirements

digital IF technology such as that in the 3 MHz IF of the Collins/Rockwell HF-2050 HF receiver [Ref. 48].

A multiple conversion superheterodyne receiver includes IF and preselector filters which can collectively attenuate out-of-passband HF broadcasting signals before reaching the zero-IF stage. Since the strongest HF signals are 120 dB greater than the weakest detectable signals, the preselector, IF bandpass, and anti-aliasing filters must provide at least 120 dB of out-of-band rejection. Tunable preselector filters in the front-end of a wideband receiver must sacrifice high out-of-band rejection to be tunable. The first intermediate frequency in a wideband receiver is likely to be two orders of magnitude greater than the final receiver

123

bandwidth, and realizable bandpass IF filters in such an up-conversion scheme lack sufficiently steep skirts to provide the necessary out-of-band rejection. So the greatest out-of-band filter rejection requirement in a wideband HF superheterodyne receiver falls on the filter following the last frequency translation (the zero-IF stage). This final filter is the anti-aliasing filter.

In addition to the out-of-band rejection requirement, Figure 6.8 also shows that the anti-aliasing filter's passband ripple must be no greater than one-half of V_{lsb}. This places stringent requirements on Chebyshev, Bessel, and Elliptic filter designs. To eliminate the ripple constraint from the analysis, the filter form selected is the maximally-flat Butterworth form of a lowpass filter. The amplitude transfer function for a Butterworth lowpass filter of order k is [Ref. 49]:

$$|H(f)| = \frac{1}{\sqrt{1+\left(\dfrac{f}{f_c}\right)^{2k}}} \quad . \tag{6.31}$$

Given a sampling frequency f_s, the maximum out-of-band signal amplitude value requirement is:

$$\frac{1}{\sqrt{1+\left(\dfrac{f_s}{2\cdot f_c}\right)^{2k}}} \leq \frac{V_{lsb}}{2} = \frac{V_{max}}{2^n} \quad . \tag{6.32}$$

124

In the filter passband, out to a frequency value of f_{max}, the transfer characteristic must meet the condition that:

$$\frac{1}{\sqrt{1+\left(\dfrac{f_{max}}{f_c}\right)^{2k}}} \leq 1 - \frac{V_{lsb}}{2} = 1 - \frac{V_{max}}{2^n} \quad . \tag{6.33}$$

A special note is that $f_{max} < f_c$.

Rewriting Equation 6.32, with $V_{max} = 1$, yields:

$$2^{2n} - 1 = \left(\frac{f_s}{2 \cdot f_c}\right)^{2k} \quad . \tag{6.34}$$

Substituting Equation 6.34 into Equation 6.33, and rearranging terms yields:

$$n_{ail} \leq k \cdot \left(\log_2(f_s) - 1\right) - k \cdot \log_2(f_{max}) \tag{6.35}$$

For a given sampling frequency and filter order, this expression provides the bound on the dynamic range performance (in terms of the number of bits) as a function of the bandwidth.

One can develop similar expressions for various filter forms using the same criteria. Analysis of the elliptic, or Cauer, lowpass filter does not allow for a closed form expression for the number of bits of dynamic range as given in Equation 6.35. The Butterworth filter order, k, will be large to meet the 120 dB dynamic range requirements. In practice, an exponential, Chebyshev, Bessel, or Cauer form of anti-aliasing filter will be necessary.

125

For band-limited signal quantization, "...a five-times sampling rate plus a five-pole filter yields 0.5% aliasing error." [Ref. 50] This rule uses the natural roll-off phenomenon to achieve the necessary out-of-band attenuation. In any case, design should incorporate the highest sampling rate possible to further reduce dynamic range limitations caused by the anti-aliasing filter.

7. Windowing and Round-off

Windowing places two limitations on the dynamic range performance of the spectrum estimation form of the digital receiver. Sidelobes resulting from finite sample lengths and main-lobe spreading resulting from the windowing function can prevent detection of weak signals adjacent to strong signals. Rectangular windowing does not produce small enough sidelobes for the required dynamic range.

There are two window functions which provide performance that approaches the required sidelobe suppression. These are the Kaiser-Bessel (a=3.5) and the Minimum 4-Sample Blackman-Harris windows. They provide 82 and 92 dB sidelobe suppression respectively. The tradeoff for dynamic range is that these windowing functions produce main-lobe spreading. The equivalent noise bandwidth is 1.93 and 2.00 bins respectively. [Ref. 51] Neither function provides the 120 dB dynamic range necessary, so digital search receiver development must include development of higher sidelobe suppressing window functions.

Finite register lengths for computing place dynamic range limitations on the calculations required in the spectrum estimation portion of the digital search

receiver. These errors include the quantization of the windowing function itself, the rounding or scaling of the FFT butterfly calculations, and the rounding of the cosine and sine functions. There have been numerous studies of these effects. Computing power of today's processors allow 32 bit computations which provide more than enough dynamic range. [Refs. 52,53]

C. COMBINED EFFECTS ON A/D DYNAMIC RANGE

Several persons have developed methods for estimating the dynamic range of an A/D converter or a system which performs spectral estimation which has an A/D converter as a component part. Most of the estimating methods are in the form of nomographs which allow rapid estimation of the dynamic range. Only Brigham and Cecchini consider the entire system effect. [Refs. 40,54-57]

Figure 6.9 shows plots of the limiting effects on the number of bits (i.e., dynamic range) as given in Equations 6.8, 6.14, and 6.35 as a function of the bandwidth (sampling rate) required. The lines drawn in Figure 6.9 are straight lines connecting the data points calculated using the bounding equations. The shaded region shows where today's technology is capable of operating. The desired operating point marked is for a 2.5 MHz bandwidth (5 MHz sampling rate) and a 120 dB (20 bits) dynamic range. Steinbrecher performed a similar analysis of these effects without considering the overall system performance requirements of the HF digital receiver [Ref. 45]. Of the performance limiting effects mentioned in the previous sections, only three, aperture uncertainty, analog component dynamic

range, and aliasing are direct functions of the bandwidth or sampling frequency. Using values typical to today's systems, the 120 dB (20 bit) requirement is not possible at a sampling frequency greater than 5 MHz.
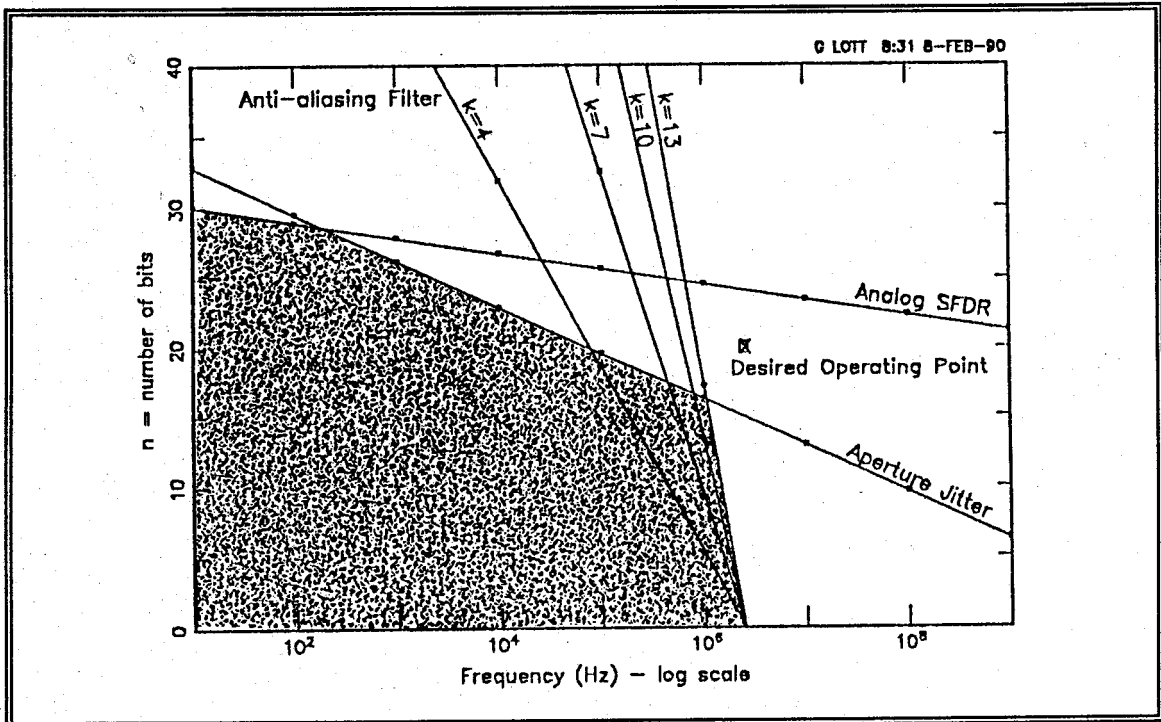
Figure 6.9 - Bounds on A/D Performance

The aperture jitter line is for τ_a = 2 ps. This is typical of the best sample-and-hold devices available. The SFDR curve is for a 96 dB SFDR which is typical of today's best HF preamplifiers. The anti-aliasing filter bound is shown for four orders of filters.

To achieve the desired operating point, the aperture jitter must be near 10 fs. The sampling rate must approach 10 MHz to allow adequate transition for a 10th order or greater anti-aliasing filter.

Story performed a survey of A/D conversion using an order-of-merit for each type of converter. He concluded that the current performance limitations are at 70 dB with a 5 MHz sampling rate. Story's estimate closely matches the bounds shown in Figure 6.9. His analysis shows about 2 dB of performance improvement per year. [Ref. 58]

An analog-to-digital conversion system providing 120 dB dynamic range and an adequate sampling rate is not likely to be available for some time. One must explore ways to expand the dynamic range of today's technology.

VII. A/D DYNAMIC RANGE EXTENSION METHODS

There is a continuing effort by both the Government and industry to produce A/D converters with high resolution and sampling rates greater than 1 MHz. A recent Government-sponsored research effort produced a 14-bit, 5-MSPS converter [Ref. 59]. Commercial development produced a 12-bit, 10-MSPS converter which received good trade reviews for RF signal processing applications [Refs. 60,61,62]. Hewlett-Packard has constructed a new A/D converter and S/H combination which provides 10-bits of resolution as 20-MSPS [Ref. 63]. There is even advance notice of a 16-bit, 0.5-MSPS converter coming to the commercial market [Ref. 64].

U.S. Naval Ocean Systems Center researchers have achieved some success with wider-bandwidth receiver systems which incorporate high resolution A/D converters. One project considered the digitization of RF signals received by a submarine towed-buoy antenna system. The quantized data from various sources, including the antennas, is then time-division-multiplexed on a fiber-optic cable connecting the towed buoy to the submarine. The project proposes with direct conversion of VLF signals with frequencies up to 150 kHz and quantization of HF signals within a 100 kHz bandwidth after being heterodyned to a lower intermediate frequency. [Ref. 65]

130

The towed system uses a 12-bit, 5-MSPS Analog Devices A/D and S/H combination. Power consumption is an important consideration in the device selection because of power limitations in the buoy, and the power consumption of the Analog Devices pair is lower than others. Experimentation shows that aperture jitter and spurious signal production from lumped nonlinearities in the A/D limited system performance. Multiple-tone and notched-noise dynamic range testing showed that the RF A/D conversion system had a 67 dB dynamic range which is within 5 dB (1-bit) of ideal device performance. [Ref. 65]

Today's hardware technology cannot produce the 20-bit, 5-MSPS converter needed in the HF digital search receiver [Ref. 66]. How does one extend the dynamic range of available conversion architectures? Is there a method which does not require returning to a narrowband receiver structure?

A. GAIN-ADJUSTING AND FLOATING-POINT CONVERSION

The most common method used to expand A/D dynamic range is that of gain adjustment. In analog receiver technology, automatic-gain-control (AGC) is an equivalent technique. The digitizing version usually takes either of two forms; floating-point with scaling or parallel-scaled conversion.

Figure 7.1 shows the block diagram of a floating-point type A/D converter. The first quantization produces a number representing the exponent of the final floating-point codeword. The second quantization produces the mantissa value. The value from the exponent determines the programming of gain or attenuation
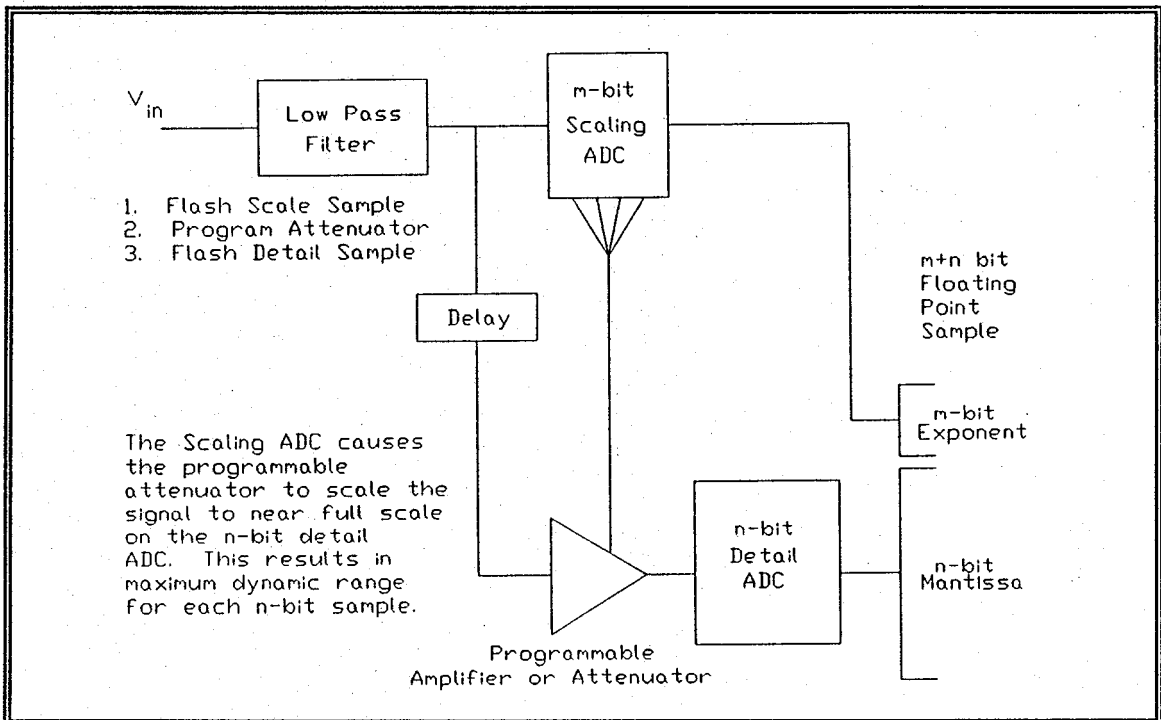
Figure 7.1 - Floating Point A/D Converter

which is added to the signal prior to mantissa determination. The programmable

device keeps the voltage at the mantissa converter from exceeding V_{max} in order to

prevent saturation. There are many variations on this technique to expand dynamic

range. Some utilize analog and digital scaling systems. [Refs. 67-71]

All these AGC techniques suffer from the lack of sensitivity in the presence

of strong signals. The strongest HF signal (i.e., the peak signal level from a

broadcast station) determines the scaling factor. The mantissa converter alone

typically has a dynamic range (on the order of 48 to 60 dB, 8 to 10-bits) which is

much less than that required for the total signal population in the HF spectrum .

The value from the exponent converter will establish the upper limit of the

132

mantissa's dynamic range. If the strongest signal level is -10 dBm, then the weakest signal quantizable by the mantissa converter will be about -70 dBm. If the system can add only attenuation prior to the mantissa converter, and if the weakest signal quantizable is -125 dBm, the exponent value would result in the addition of 55 dB of attenuation. Site performance estimation using the techniques described in Chapter V with 55 dB of signal path loss would show that the attenuation prevents detection of nearly all the signals of interest.

Figure 7.2 shows another method of increasing A/D conversion dynamic range. Instead of having variable gain adjustments, the parallel-scaled architecture has fixed scaling devices and A/D converters which quantize simultaneously. This system can use multiple parallel stages. [Refs. 72,73]

The parallel architecture suffers from the same sensitivity problem as the AGC architecture. Due to saturation products, the least significant bits of the first stage are lost. The sensitivity of the remaining stages is lost through the fixed attenuation preceding each A/D converter. The signal level can be reduced, but the noise floor is not affected by attenuation. The attenuation pushes weak signals into noise. This architecture is not suitable for the HF digital search receiver since it must retain sensitivity to detect the clandestine signal.

The internal noise of the basic A/D converter elements establishes the physical limitation in any A/D hardware schemes. The parallel-series converter provides the
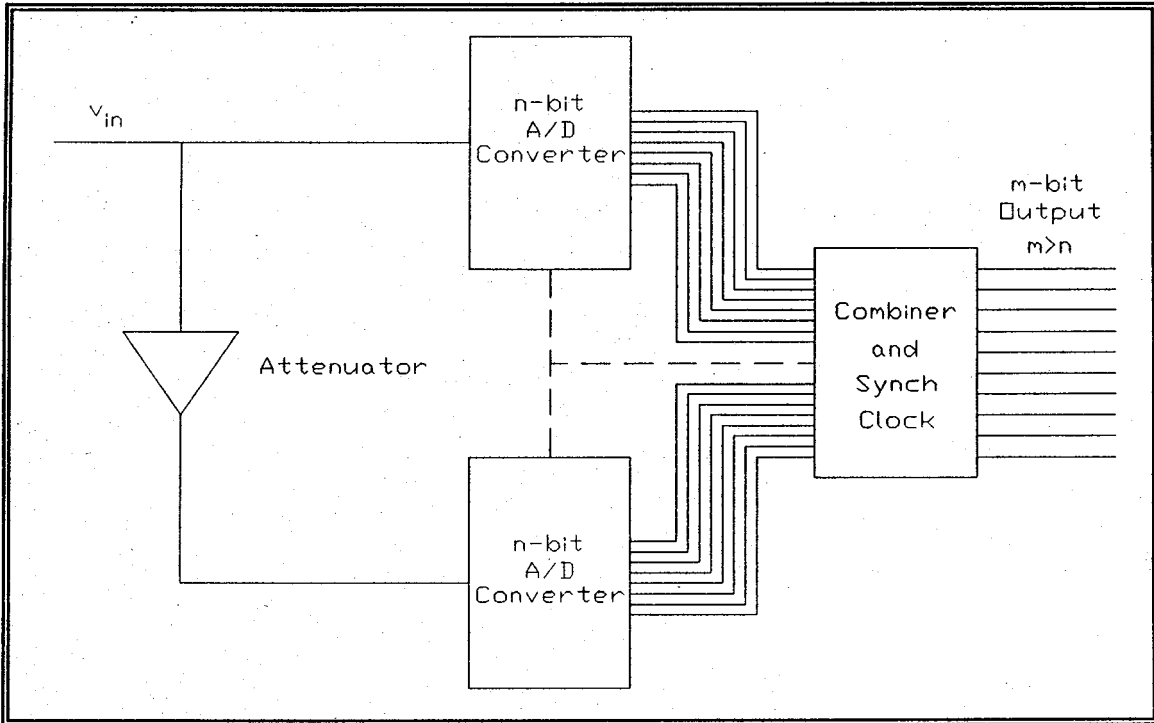
Figure 7.2 - Parallel-Scaled A/D Converter

minimum product of noise band and conversion time. However this technology can only operate with kHz sampling rates. [Ref. 74]

B. NONLINEAR QUANTIZATION

All A/D converters with finite-length codewords have nonlinear transfer characteristics. However, so called linear quantizers are those having uniform steps with the center point in each quantization level having a value which lies on the associated linear conversion characteristic. Figure 6.2 shows a 3-bit uniform-linear quantizer transfer characteristic. The term "nonlinear quantization" implies that the quantizer transfer function approximates an analytically nonlinear function.

134

Nonlinear quantization has the analog equivalent of companding. Some nonlinear quantization schemes incorporate a companding amplifier before a uniform-linear A/D. Another technique is to use linear quantization to precede a digital nonlinear function converter stored as a look-up table in read-only-memory. These two architectures are the easiest to implement. The more difficult technique is direct nonlinear quantization where the nonlinear function is built directly into the A/D converter transfer characteristic through the implementation of variable quantization step size. There are two basic techniques of direct nonlinear quantization, fixed and adaptive.

Fixed, direct nonlinear converters have quantization step sizes which are set in the hardware of the device. In an 8-bit square-root quantizer, the voltage step which causes a change in the least significant bit at full scale is 55 dB more than the voltage change causing a change in the least significant bit near zero [Ref. 75].

There have been many designs of nonlinear quantizers, and each has a particular advantage for a specified application. "An analog-to-digital converter with a square root transfer function will allow a maximum dynamic range with a fixed number of data bits." The dynamic range covered by the quadratic converter is:

$$DR_{quad} = (2^n)^2 = 2^{2n} \tag{7.1}$$

where n is the number of bits in the digital codeword. Transmitting video signals from charged-coupled-device sensors over telemetry systems with limited data rates

is an example where a quadratic quantizer is the best choice for the particular application [Ref. 75].

The logarithmic-law A/D converter is the most common form of nonlinear quantizer. This converter provides constant relative accuracy rather than a constant absolute accuracy [Ref. 76]. "Frequency accuracy in music and loudness in audio response are examples where logarithmic-law converters find usage". [Ref. 77] The logarithmic converter is easily implemented for slow conversion rates using an integrating A/D architecture [Ref. 78].

TRW uses a programmable amplifier preceding their 8-bit, 50-MSPS model TDC1046 converter to implement a nonlinear A/D converter. The transfer characteristic for the converter-amplifier arrangement is:

$$H(A) = (2^n - 1) \cdot \left(\frac{V_{in}}{V_{bias} + A \cdot V_{in}} \right) \qquad (7.2)$$

where A is the value of a programmable resistor. By varying A, one can dramatically vary the transfer characteristic. [Ref. 79]

"For an ADC that converts wide-range signals with a truncated hyperbolic distribution of levels, the optimum scale is linear-logarithmic." [Ref. 80] Implementation of the linear-logarithmic design using an 8-bit converter provides greater than 60 dB dynamic range. It also has a conversion error of less than three percent for a sinusoidal input from 30 Hz to 1.5 MHz [Ref. 81].

136

The other class of direct nonlinear quantization is that of adaptive quantizers. These devices vary the quantizer step size (i.e., transfer function shape) to fit certain criteria such as minimal mean-squared-error. Most adaptive quantizers use estimating algorithms to vary the step size.

In a backward estimating adaptive quantizer using a logarithmic algorithm, a study revealed that "...system properties of unlimited dynamic range and complete error dissipation are contradictory and cannot be realized at the same time by a linear-logarithmic algorithm." The transfer characteristic implemented was: [Ref. 82]

$$H(z) = \frac{z-\alpha}{(z-\beta)(z-\alpha) - \gamma(1-\alpha)} \quad . \tag{7.3}$$

Bell Laboratories experimented with an adaptive 2-bit quantizer for conversion of speech. The adaptation scheme varies step size by a fixed amount at each sampling time using the previous sample to predict the required step size for the next sample. The application using this 2-bit A/D conversion system for band-limited speech shows promise, but the procedure does not adapt well to non-stationary processes such as signals in the HF spectrum. [Ref. 83]

There is no doubt that nonlinear conversion can provide the 120 dB of dynamic range required for the HF digital search receiver. With as many as 800 to 1200 signals present in a 2.5 MHz portion of the spectrum, practice proves that any nonlinearity in the quantization process produces a significant level of in-band

intermodulation products that will mask weak signals. Any A/D converter used in an HF wideband receiver must have a transfer characteristic which is as close as possible to a linear function. An A/D converter with a uniform-symmetric transfer function and small quantization step size (many bits) is the optimum choice for the HF application.

C. OVERSAMPLING

Oversampling is a technique in which one samples a signal at a rate which is many times the Nyquist rate. By oversampling and decimation, one can extend dynamic range of an A/D converter by reducing quantization noise. Oversampling spreads the quantization noise power evenly over a larger frequency interval, but it does not alter the shape of the power spectrum of the noise. Decimation is an averaging technique which acts as lowpass filtering of the higher frequency quantization noise.

Practice shows that an effective dynamic range improvement of three to five bits is possible with an oversampling factor in the range of 6 to 15. Figure 7.3 shows a plot of the gain in dynamic range in number of bits, n_{os}, as a function of the oversampling factor, f_{os}, derived using Claasen's expression:

$$n_{os} = -\frac{1}{2} \log_2 \left(\frac{2}{f_{os}} \left(1 - \frac{\sin\left(\frac{\pi}{f_{os}}\right)}{\frac{\pi}{f_{os}}} \right) \right) . \qquad (7.4)$$
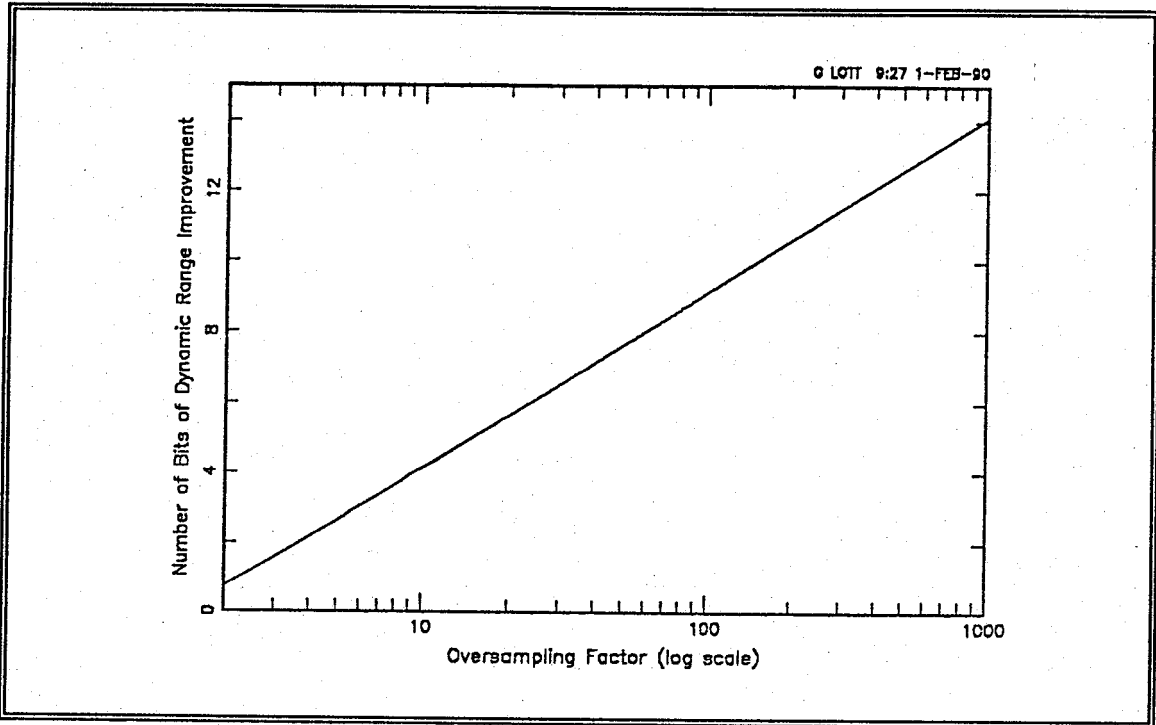
Figure 7.3 - Dynamic Range Gain by Oversampling

The solid line in Figure 7.3 is the cubic-spline fit of data points calculated using Equation 7.4. [Ref 84]

Oversampling and decimation can theoretically provide a 12-bit improvement with an oversampling factor near 400. This oversampling rate equates to using an 8-bit A/D with a 1 GHz sampling frequency to achieve 20-bits of dynamic range. There is no indication that anyone has achieved this in actual practice. 8-bit converters with sampling speeds near 1 GHz are just now becoming commercially available [Refs. 85-88].

To gain dynamic range, the system proposed by Claasen requires pre and post signal processing. The input signal is soft limited and nonlinearly transformed.

After the A/D conversion, the system takes first order differences followed by low pass filtering in the form of decimation. [Ref. 84]

The oversampling reduces the quantization noise by a factor equal to f_{os}. This technique has worked in extending dynamic range in a 12-bit, 4-MSPS converter [Ref. 89]. In a narrow-band RADAR application, oversampling and decimation are an effective dynamic range enhancing tool [Ref. 90]. In each of these applications, the system processed a single signal and noise.

In a broadband HF receiver application , the pre-processing including soft-limiting and frequency modulation of the original signal will produce in-band intermodulation products. These products are not noise in the sense of the quantization noise, and they will appear in the output spectrum.

Oversampling also does not improve the sensitivity versus dynamic range. The -125 dBm (0.2 μV) sensitivity establishes the ΔV requirement in the A/D converter (i.e., the voltage represented by the LSB). Even with quantization noise lowered by oversampling, saturation of a limited dynamic range A/D converter remains a problem. There simply is no way to achieve a large signal handling capacity and good sensitivity in an A/D converter using Claasen's technique alone.

D.   POST-CONVERSION PROCESSING

Extensive testing of A/D converters reveals that the lumped effect of nonlinearities within the device reduce the dynamic range. The lumped nonlinearities include "...nonlinear distortion, quantization error, and random noise."

140

[Ref. 91] The value given as the effective number of bits better represents the dynamic range of the system. For example, the Elsin AD1512, a 14-bit 5-MSPS converter, loses 2-bits of dynamic range due to residual errors. [Refs. 92,93]

The Elsin AD1512 was the A/D converter in the receiver system used to collect the data presented in Chapter IV. Ideally, a 14-bit A/D converter should have 84 dB of dynamic range using the six-dB-per-bit rule. Single-tone measurements on the data collection system showed that the receiver had approximately 73 dB (12-bits) of dynamic range. The performance measurement closely matches the 12 effective bits for the Elsin converter measured by Lincoln Labs [Ref. 92].

Linearization of the A/D process recovers some of the information lost due to unwanted distortion products. Compensation of the quantized signal implemented through error table correction has proven as an effective means to improve the number of effective bits. Conducting many discrete Fourier transforms on the A/D's output with a known signal input provides the statistical data needed to determine the error table entries. [Ref. 94]

Error compensation on a Burr-Brown ADC600, 12-bit, 10-MSPS, improved spurious-free-dynamic-range by 8 dB [Ref. 95]. Dent and Cowan proposed a related correction technique for each A/D before it leaves the factory [Ref. 96]. This method of dynamic range extension will bring converter performance closer to the ideal.

Error compensation is a process with potential to improve the quantization dynamic range in a digital search receiver. It will not, however, improve operation to take today's A/D technology to that required for the HF environment.

E.   OTHER TECHNIQUES

The digital new energy receiver makes signal detection decisions based on frequency domain representation of the input signal. Kay and Sudhaker presented a method of spectrum estimation based on the measurements of the signal's zero crossings. The computation speed requirements for the zero-crossing system are within the speed capability of today's processors because the number of calculations is similar to that required in the FFT algorithm. The system does not have the limited amplitude dynamic range and slow conversion rates of a conventional A/D. There is no indication of the required precision of the zero-crossing measurement needed for 120 dB dynamic range. There does not appear to be a published implementation using this spectral estimation technique in any HF spectrum search program, and it warrants further investigation since it is input signal amplitude independent. [Ref. 97]

There have been many methods derived for quantization which minimize mean squared quantization error by proper selection or adjustment of step size [Refs. 98,99]. Bounds on optimal quantizer performance are well understood for these cases [Refs. 100,101]. They do not always satisfy the sensitivity requirement, especially when symmetric-uniform quantization is a requirement.

142

Sasaki and Hataoka propose a method of quantization which minimizes intermodulation distortion when the number of signals and number of quantization levels is small. This technique does not work well with a large number of quantization levels as required for adequate sensitivity in an HF receiver. It provides no gain over the uniform-symmetric quantizer for large numbers of bits. [Ref. 102]

Other techniques under investigation include:

♦ digital Josephson circuits (SQUIDS) that do not latch into the voltage state [Ref. 103]

♦ photoconductor switched A/D converters [Ref. 104]

♦ linear prediction with oversampling techniques [Ref. 104], and

♦ spectral estimation through hard clipping circuits[Ref. 105].

None of these techniques show direct application in the near-term to the HF search receiver problem.

F. SUMMARY

Dynamic error compensation is the dynamic range enhancing technique best suited for implementation in an HF wideband receiver. Oversampling can improve dynamic range, but the resulting intermodulation distortion will negate the improvement. The HF receiver's performance requirements prohibit designs using floating-point, AGC, and nonlinear quantization.

Converters with 14-bits and 20-MSPS are the next high dynamic range improvements. 16-bit, 1-MSPS converters will also be available in the next few years. Neither of these hardware improvements alone solves the HF new energy receiver problem.

VIII. STRONG SIGNAL ELIMINATION

Chapters VI and VII show there are no A/D techniques available today which can achieve the performance required for the HF digital new energy receiver. The strongest international broadcasting signal which sometimes reaches 0 dBm, the amplitude of the weak clandestine signal-of-interest which is often near -125 dBm, and the need for a sampling speed of at least 5 MHz in order to keep the receiver's complexity manageable combine to place extreme demands on A/D performance.

The receiver sensitivity requirement is directly related to the signals of interest, and the rapid sampling rate is necessary for a receiver system which is economically realizable. Of the three extremes, only the high dynamic range requirement caused by strong broadcast signals does not result from performance needed to improve the detection of signals of interest. As proven by the results given in Chapters III and IV, if the strongest signals were not present, the dynamic range of the A/D converter could be reduced substantially without loss of detection performance.

How much of the international broadcasting energy must one remove to reduce the dynamic range requirements? During Signal-to-Noise Enhancement Program site surveys, it is SNEP team practice to examine the overall HF signal

population with special attention to the strong signals within the international broadcast bands. Figure 2.2 shows an observation where the one signal from Radio Moscow dominated all other signals. Finer frequency resolution measurements that morning in Adak revealed that even the next strongest signals in the 31 meter international broadcasting band were 20 to 30 dB below that one strong signal. Removing the extremely strong Radio Moscow signal would reduce the A/D dynamic range requirement for receivers at that site by four to five bits.

During other Signal-to-Noise Enhancement Program site surveys, the team observed similar occurrences where a few international broadcast signals or signals from nearby transmitters were 20 to 30 dB stronger than all other signals. Figures 8.1 (daytime) and 8.2 (nighttime) show observations of the strong signal populations at Hanza, Okinawa. Both show that there were a limited number of extremely strong international broadcast signals which were dominant. Experience from other SNEP surveys shows this to be the case at most CDAA sites.

How can one reduce the impact of the strongest signals? There are three ways. First, antenna beam selection is possible for those search missions which require limited geographic coverage. Antenna beam selection is not an alternative for the general, omni-directional new energy search function. Second, one can remove the strongest signals by notch filtering the international broadcasting bands before the signals reach the receiver. Since the frequency of the strong signals will change from daytime to nighttime and between different sites, each site would
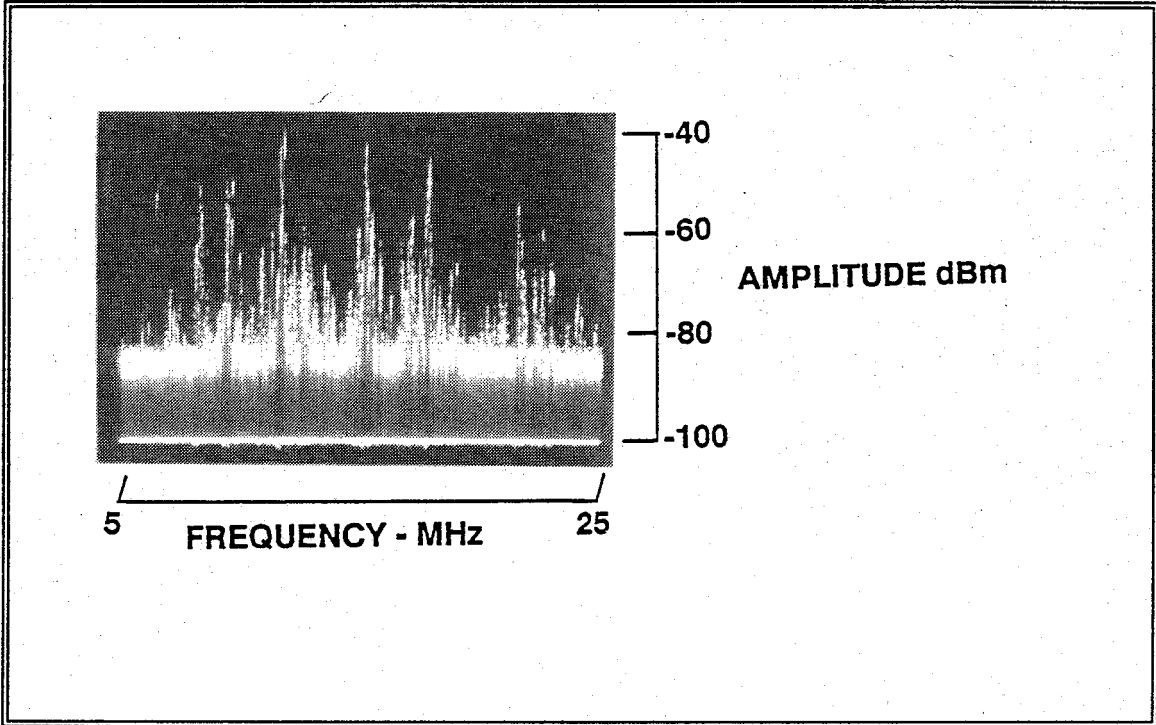
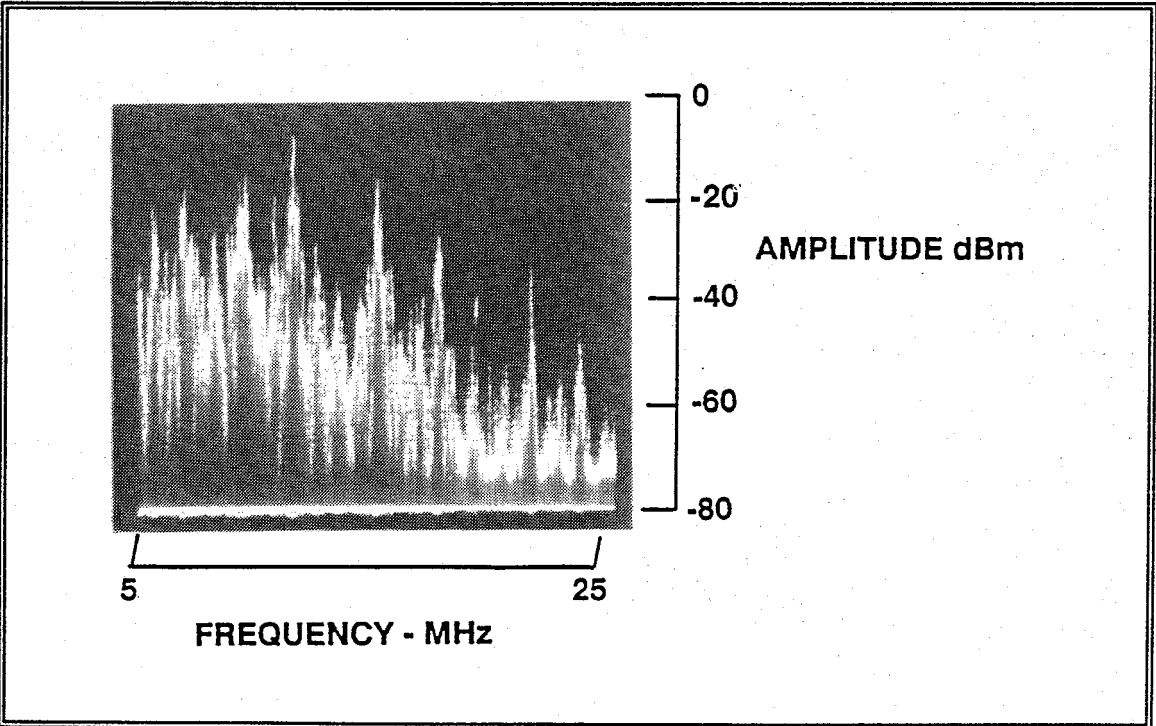**Figure 8.1** - Strong Daytime International Broadcast Signals

Figure 8.2 - Strong Nighttime International Broadcast Signals

147

require a set of notch filters for all the international broadcast bands. If signals of interest were present in the international broadcasting bands, these notch filters would prevent detection of those transmissions. In Section B of this chapter is presented a third alternative of selectively removing the strongest signals without sacrificing signal-of-interest detection.

A. FREQUENCY COVERAGE PLAN AND NOTCH FILTERING

Given a 2.5 MHz receiver bandwidth (corresponding to a 5 MHz A/D sampling rate), proper frequency selection can place only one international broadcasting band in the receiver coverage at any one time. Figure 8.3 shows a plan for covering the entire HF band from 1.75 to 30 MHz using 12 receivers, each with a 2.5 MHz bandwidth. There is little frequency coverage duplication. The four lower frequency international broadcasting bands, known as the Tropical Bands, rarely include the strongest signals seen at an HF receiver site. These four lower bands are not significantly used outside the tropical regions, and station transmitter power is typically less than 10 kw.

One can further reduce the strong signal impact on each receiver by notch filtering the international broadcasting band within the current frequency coverage. The broadcasting band allocations from 49 meters to 12 meters range in bandwidth from 200 kHz to 500 kHz, and most of these bands have adjacent frequency allocations which include fixed, marine, and aeronautical services. Figure 2.1 shows such a situation where a fixed service band is adjacent to the 31 meter international
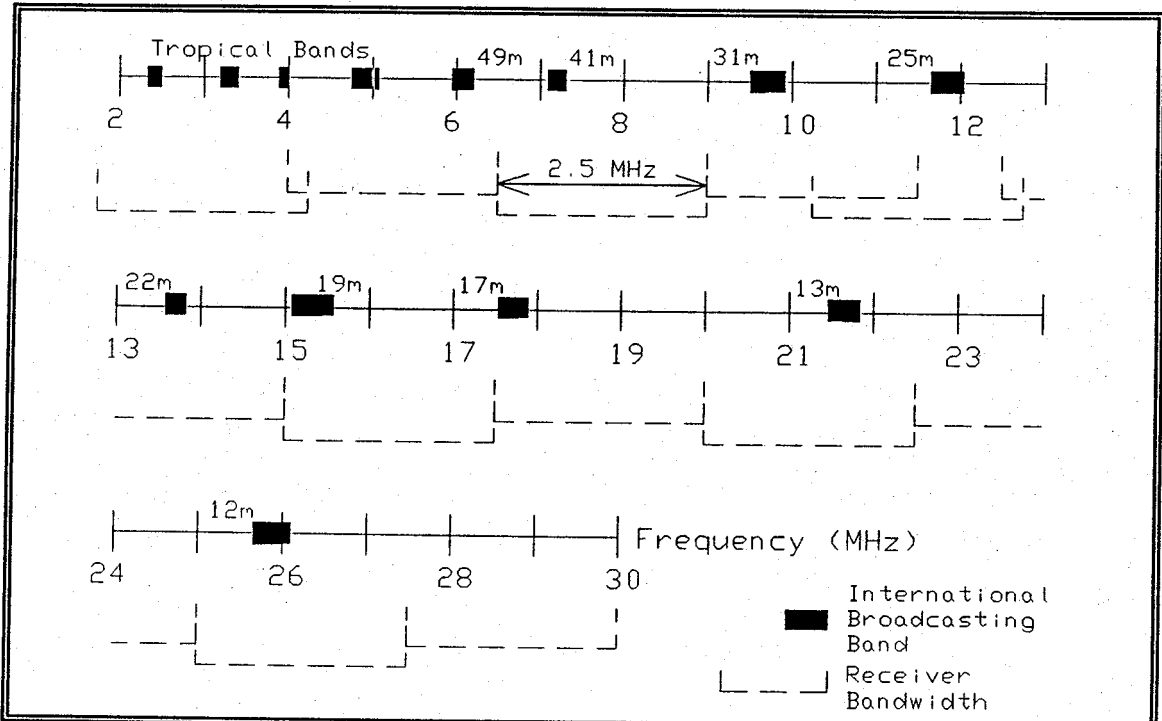
Figure 8.3 - Receiver Coverage to Minimize International Broadcast Overloading

broadcasting band. The notch, or band-stop, filter for each band must be of relatively high order to achieve steep skirts in order to prevent unwanted attenuation of signals in the adjacent bands. Notch band attenuation should reduce the receiver dynamic range requirements by four to six bits (24 to 36 dB). A 14 or 16-bit converter, which is becoming available, could then provide the performance needed.

One can design an elliptic, or Cauer, band-stop filter which covers the 19 meter international broadcasting band and meets these requirements:

♦ 50 Ω input and output impedance

♦ 5% reflection coefficient

149

♦ band-stop attenuation >40 dB

♦ 15.1 to 15.6 MHz notch.

The filter, the schematic of which is shown in Figure 8.4, is a ninth-degree filter with 13 capacitors and 13 inductors. Table 8.1 lists the calculated component values. The design is based on techniques given in Reference 1. The final notch frequencies are 15100 kHz and 15600 kHz, and final pass frequencies are 15072 kHz and 15629 kHz. Maximum notch attenuation is near 50 dB.
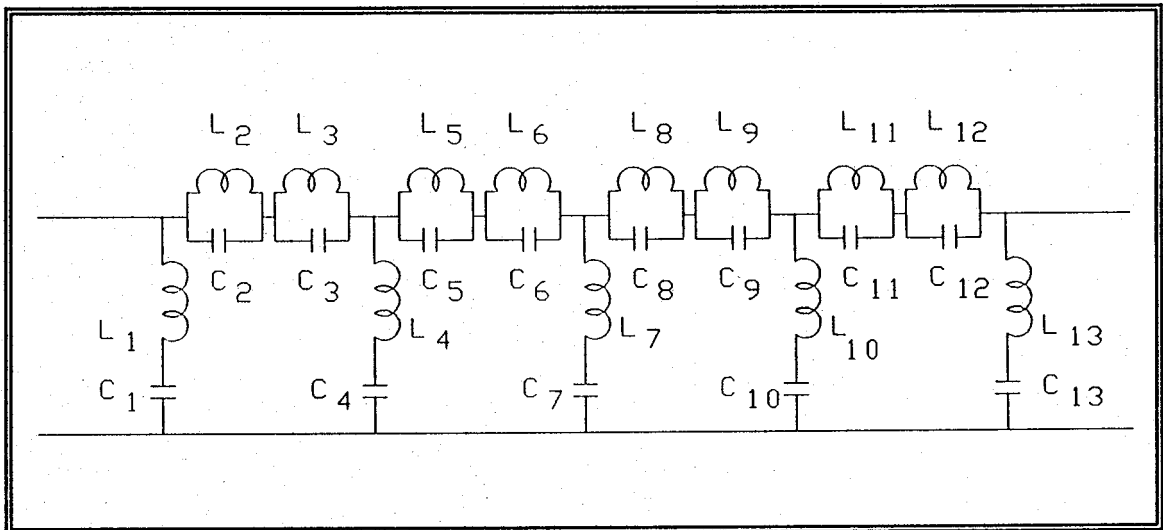
Figure 8.4 - 19 Meter Band Elliptic Notch Filter

Actual physical construction of this filter would be difficult, but skilled RF designers can produce such a filter. To minimize signal attenuation, construction should include distributed coaxial components, hand-trimmed silver-plated components, and other low-loss RF techniques.

Good system engineering would place this filter before any active stage, digital or analog. If design included notch filtering only in the final zero-IF stage, the

Table 8.1 - 19 METER BAND ELLIPTIC FILTER COMPONENT VALUES

L1 = 20.1	C1 = 534	f1 = 15348
L2 = 0.012	C2 = 9013	f2 = 36336
L3 = 0.012	C3 = 9153	f3 = 36336
L4 = 11.6	C4 = 928	f4 = 15348
L5 = 0.008	C5 = 13544	f5 = 18233
L6 = 0.008	C6 = 13964	f6 = 18233
L7 = 12.2	C7 = 662	f7 = 15348
L8 = 0.006	C8 = 16597	f8 = 17184
L9 = 0.006	C9 = 17516	f9 = 17184
L10 = 14.6	C10 = 737	f10 = 15348
L11 = 0.008	C11 = 13390	f11 = 21813
L12 = 0.008	C12 = 14091	f12 = 21813
L13 = 35.2	C13 = 305	f13 = 15348

Inductor values are in μH, capacitor values are in pF, and frequency values are in kHz.

strong signals would cause intermodulation products in the IF stages prior to the filter.

Using a notch filter can reduce the dynamic range requirements some 30 to 40 dB. However, as mentioned before, notch filtering effectively eliminates search coverage in the notch. One can argue that an adversary would experience similar strong signal interference trying to receive a clandestine transmission in the international broadcasting band, so an adversary would not be likely to transmit amidst the strong broadcasting signals.

B.   STRONG SIGNAL ELIMINATION SYSTEM

HF search coverage ideally should not eliminate detection of weak signals in the broadcasting bands.   As shown above, removing a few very strong signals can

151

reduce the receiver analog and A/D converter dynamic range requirements by 20 to 30 dB. One can conceive of a system which tracks the frequency of the strongest few signals, isolates them, and subtracts them from the spectrum. The elimination architecture must automatically switch from one signal to another as the signals fade or as ionospheric propagation conditions change. Figure 8.5 is a conceptual block diagram of such a system.
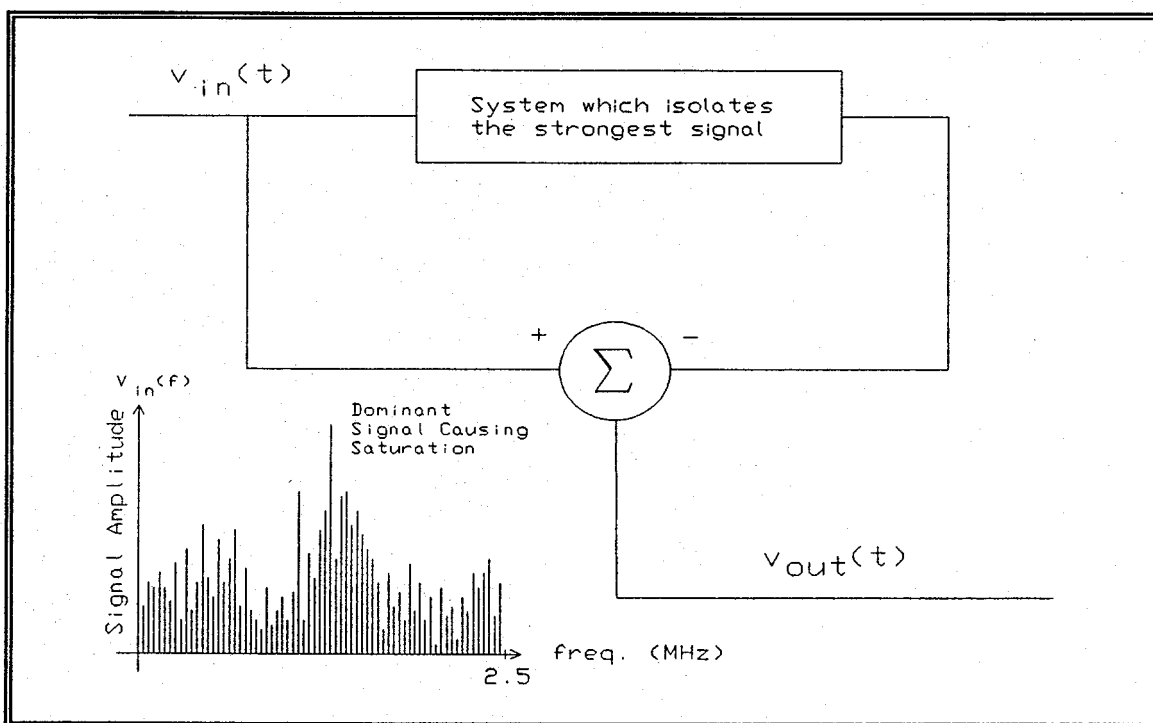

Figure 8.5 - Ideal Signal Subtraction System

In most cases, the strongest signal will be a double-sideband, with carrier, AM signal from an international broadcasting station. Given this, one can represent the composite HF voltage, $v_{in}(t)$, as:

$$v_{in}(t) = v_a(t) + v_b(t) \qquad (8.1)$$

where $v_a(t)$, the strongest signal, is:

$$v_a(t) = A(t)\cos(\omega_c t) \qquad (8.2)$$

and $v_b(t)$, the sum of the remaining HF signals, is:

$$v_b(t) = B(t)\cos(\omega_c t + \phi(t)) \quad . \qquad (8.3)$$

The ideal circuit design would allow for the isolation and complete elimination of the strongest signal leaving the remaining components of the HF spectrum intact. There will always be some error voltage since no system can reproduce $v_a(t)$ exactly. The elimination system must generate a carrier frequency signal in phase with the carrier of the strongest signal. Isolation of the strongest signal also requires detection of the signal's envelope with minimal corruption from the other signals.

1. **Carrier Reconstruction**

Some device in the strong signal elimination system must reproduce a signal in-phase with the carrier of the strongest signal. Prof. Glen A. Myers has developed such a phase tracking system [Ref. 106]. The complete system includes

153

a hard-limiter before the phase tracking device. The hard-limiter removes the AM

on the strongest signal, but it maintains the zero-crossings of the composite signal.

The zero crossings of the strongest signal's carrier will dominate the

locations of the zero-crossings of the composite signal. Using the zero-crossings as

a reference, the phase tracking network processes the hard-limited input voltage

and generates a sinusoidal (or square) voltage which is 180° out-of-phase with the

carrier of dominant signal. The remaining signals in the composite voltage may

cause a slight frequency modulation of the zero-crossings, and this can produce

some error in carrier reconstruction.

Another source of signal subtraction error results from carrier phase

tracking error. Considering the case where there is only one signal to eliminate,

any signal power which remains at that frequency after subtraction is due to the

phase tracking error. Define the RMS signal power remaining after strong signal

subtraction as:

$$\epsilon_{ph} = \sqrt{\frac{1}{\Delta t} \int_{t_1}^{t_2} \left(\cos(\omega_c t) - \cos(\omega_c t + \Delta\phi(t)) \right)^2 dt} \qquad (8.4)$$

where $\Delta\phi(t)$ is the phase error and $\Delta t = t_2 - t_1$, f_s is the sampling frequency which

satisfies the Nyquist criteria, and N is the total number of samples. Evaluating

Equation 8.4 for a non-time-varying phase error using a discrete approximation:

$$\epsilon_{ph} = \sqrt{\frac{1}{N} \sum_{i=1}^{N} \left(\cos\left(2\pi \frac{i}{f_s} \right) - \cos\left(2\pi \frac{i}{f_s} + \Delta\phi \right) \right)^2} \qquad (8.5)$$

provides a simple rule for the amount of unwanted signal power which remains in the single signal case. If one expresses the phase error in dB as:

$$\Delta\phi_{dB} = 20 \cdot \log_{10}(\Delta\phi) \quad , \tag{8.6}$$

the unwanted signal power which remains, in dBW, calculated using Equation 8.5 is:

$$\epsilon_{ph_{dB}} = 20 \cdot \log_{10}(\epsilon_{ph}) \cong \Delta\phi_{dB} - 3 \quad . \tag{8.7}$$

Using the rule given in Equation 8.7 requires $0 < \Delta\phi \leq 0.1$ radians. Using Equation 8.5, a constant phase difference, $\Delta\phi$, of 0.01 radians, is a phase difference of -40 dB. The unwanted signal power which remains after subtraction is -43.1 dBW.

Since the goal of the strong signal elimination system is to decrease the A/D dynamic range requirements of the receiver by about 6 bits, the phase reconstruction must be within 0.01 radians of the phase of the carrier of the strongest signal. Testing proves that the device can lock well within the 0.01 radian requirement when the signal is 10 dB or more greater than any other signal.

Can a filtered hard-limiter output alone adequately track the phase of the strongest signal? If so, the circuit would be much simpler. Appendix D shows a MATHCAD work sheet which simulates the complete large-signal-elimination system using only a filtered hard-limiter output. Using a scaling value of 0.776 with

the hard limiter, the model showed that the filtered hard-limiter system could not adequately remove the strongest signal. The weaker signal which was 20 dB down remained undetectable because of the remaining unwanted signal energy. An iterative process minimizing the error power identified the scaling factor of 0.776 as the value which produced the best subtraction of the strong signal.

2. Envelope Reconstruction

The second half of the strong signal reconstruction process is to isolate the envelope of the strongest signal, $A(t)$. This voltage is present in, but not easily isolatable from, the composite signal envelope, $E(t)$.

A preferred method requires an AM detector which exhibits capture similar to that found in an FM detector. Then the output would allow construction of $A(t)$ alone. Yet there are no amplitude detectors developed which exhibit capture.

Another method is to tune to the strongest signal using a conventional AM receiver. Fading and multipath will result in the strongest signal changing between several stations, so this electronically-tuned narrowband receiver would need an extremely rapid tuning system.

One can describe the effect of errors in the envelope on the ability to eliminate the strongest signal. Define the unwanted signal power which remains due to a difference in envelopes as:

$$\epsilon_{amp} = \sqrt{\frac{1}{\Delta t} \int_{t_1}^{t_2} \left[A(t)\cos(\omega_c t) - (1 - \epsilon(A,B,\phi,t)) \cdot A(t)\cos(\omega_c t) \right]^2 \, dt} \quad (8.8)$$

where $\epsilon(A,B,\phi,t)$ is the amplitude error factor. This is defined in more detail later. The other terms are as defined previously. By allowing ϵ to be a constant amplitude difference defined as ΔA, and when:

$$A(t) = 1 + m_a(t) = 1 + \cos(2\pi f_a t) \quad (8.9)$$

analysis of the unwanted signal power suggests an identical rule as in the phase tracking error case. After using a discrete model similar to that used in the phase error case, the signal power remaining from the strongest signal is:

$$\epsilon_{amp_{dB}} = 20 \cdot \log_{10}(\epsilon_{amp}) \cong \Delta A_{dB} - 3 \quad (8.10)$$

where the terms are amplitude equivalents to those used in Equation 8.7. While this analysis produces a simple rule as a first order estimation, just as with phase tracking, the difference in amplitude will not be a constant for the case with real signals.

157

How does one isolate the envelope of the strongest signal? First, combining Equations 8.1 through 8.3, one can write the composite input signal voltage in complex envelope form as:

$$v_{in}(t) = E(t)\cos(\omega_c t + \theta(t)) \qquad (8.11)$$

where the envelope term is:

$$E(t) = A(t) \cdot \sqrt{1 + \frac{B^2(t)}{A^2(t)} + 2 \cdot \frac{B(t)}{A(t)} \cdot \cos(\phi(t))} \qquad (8.12)$$

which can also be written as:

$$E(t) = A(t) \cdot \epsilon(A,B,\phi,t) \quad . \qquad (8.13)$$

The goal for any envelope reconstruction system is to have $\epsilon(A,B,\phi,t)=1$. Examination of the envelope term shows that as $A(t)$ increases, ϵ approaches one. The stronger the signal to be eliminated, the more its voltage dominates the composite envelope.

There are three common AM detectors which can be used as the detectors in the envelope isolation system. These are:

♦ coherent, product detector

♦ envelope detector

♦ square-law detector.

In the coherent, product detector, the system multiplies the reconstructed carrier with $v_{in}(t)$. A lowpass filter follows the multiplier to remove the newly

158

generated signals at twice the carrier frequency of the strongest signal, ω_c. After filtering, the product detector's error factor, $\epsilon_p(A,B,\phi,t)$, is:

$$\epsilon_p(A,B,\phi,t) = \left(\frac{1}{2} + \frac{1}{2} \frac{B(t)}{A(t)} \cos(\phi(t)) \right) \quad . \qquad (8.14)$$

The ideal envelope detector recovers the envelope exactly as given in Equation 8.12. The envelope detector's error factor, $\epsilon_e(A,B,\phi,t)$, is:

$$\epsilon_e(A,B,\phi,t) = \sqrt{1 + \frac{B^2(t)}{A^2(t)} + 2 \cdot \frac{B(t)}{A(t)} \cdot \cos(\phi(t))} \quad . \qquad (8.15)$$

The square-law detector recovers the square of the voltage recovered by the envelope detector. The square-law detector's error factor, $\epsilon_s(A,B,\phi,t)$ is:

$$\epsilon_s(A,B,\phi,t) = A(t) \cdot \left(1 + \frac{B^2(t)}{A^2(t)} + 2\frac{B(t)}{A(t)} \cos(\phi(t)) \right) \quad . \qquad (8.16)$$

As stated before, the best recovery system is one where $\epsilon(A,B,\phi,t) \approx 1$. With A(t) defined as in Equation 8.9, and with:

$$B(t) = k_b(1 + \cos(2\pi f_b t)) \qquad (8.17)$$

one can compare the envelope error factor's effect on the ability to isolate A(t).

An initial guess was made to select the detector which results in ϵ being closest to one. However using the RMS value of envelope error factor can be a quite misleading measure for detector selection. Figure 8.6 shows a plot of the logarithm of the RMS values of the three forms of ϵ as a function of the logarithm

159

of the scaling factor k_b with $k_a=1$. The lines in Figure 8.6, and the remaining graphs in this chapter, are cubic-spline fits of the data points shown.

For $k_b \geq -35$ dB of k_a, the RMS values indicate that the product detector is the choice to keep ϵ closest to one. For -65 dB$\leq k_b \leq$-35 dB referenced to k_a, the square-law device has an a value of ϵ closest to one. Only for $k_b \leq$-65 dB from k_a does the envelope detector appear as the choice. This technique turned out to be to be the incorrect method for selecting the best detector.
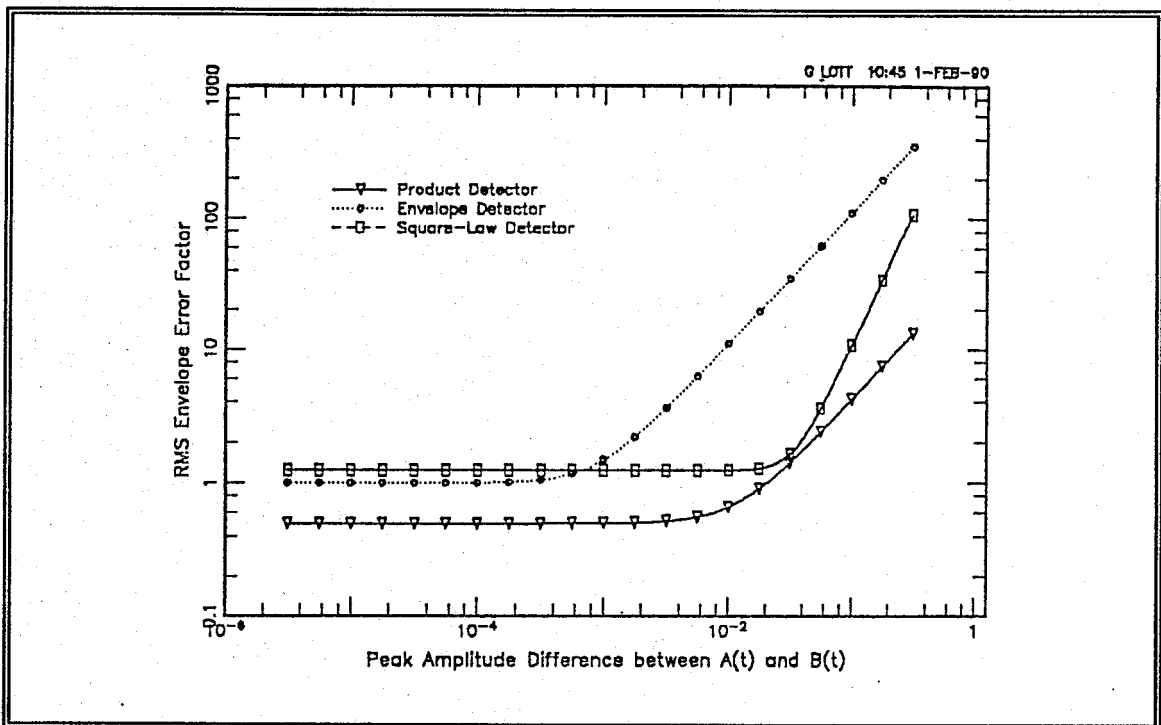
Figure 8.6 - RMS of Envelope Error Factor versus Peak Amplitude Difference

The residual value is the correct indicator to use in the selection of the best detector for envelope isolation. The value of the residual is given as:

$$\text{residual} = A(t) - A(t) \cdot \epsilon(A, B, \phi, t) \qquad (8.18)$$

which indicates the detector's ability to track the instantaneous envelope of the strongest signal. Using the definitions of $A(t)$ and $B(t)$ in Equations 8.9 and 8.17, one can calculate the RMS value of the residual as:

$$\text{res}_{RMS} = \sqrt{\frac{1}{(t_2 - t_1)} \int_{t_1}^{t_2} (A(t) \cdot (1 - \epsilon(A, B, \phi, t)))^2 \, dt} \qquad (8.18)$$

As shown in Figure 8.7, the envelope detector tracks the instantaneous envelope better than the other two detectors where the strongest signal is at least 10 dB above the other signals. For even greater amplitude differences between the strongest signal and the other signals, the instantaneous residual value gets progressively smaller for the envelope detector.

Figure 8.8 shows data representing the instantaneous residual values for all three detector types for the case where the peak amplitude of $v_b(t)$ is 40 dB below the peak amplitude of $v_a(t)$. The envelope detector produces an instantaneous residual which is already an order of magnitude below the other two residuals. For this calculation, $f_a = 2$ Hz, $f_b = 5$ Hz, $\phi = 11$ Hz, and the sampling frequency was 251 Hz.

161
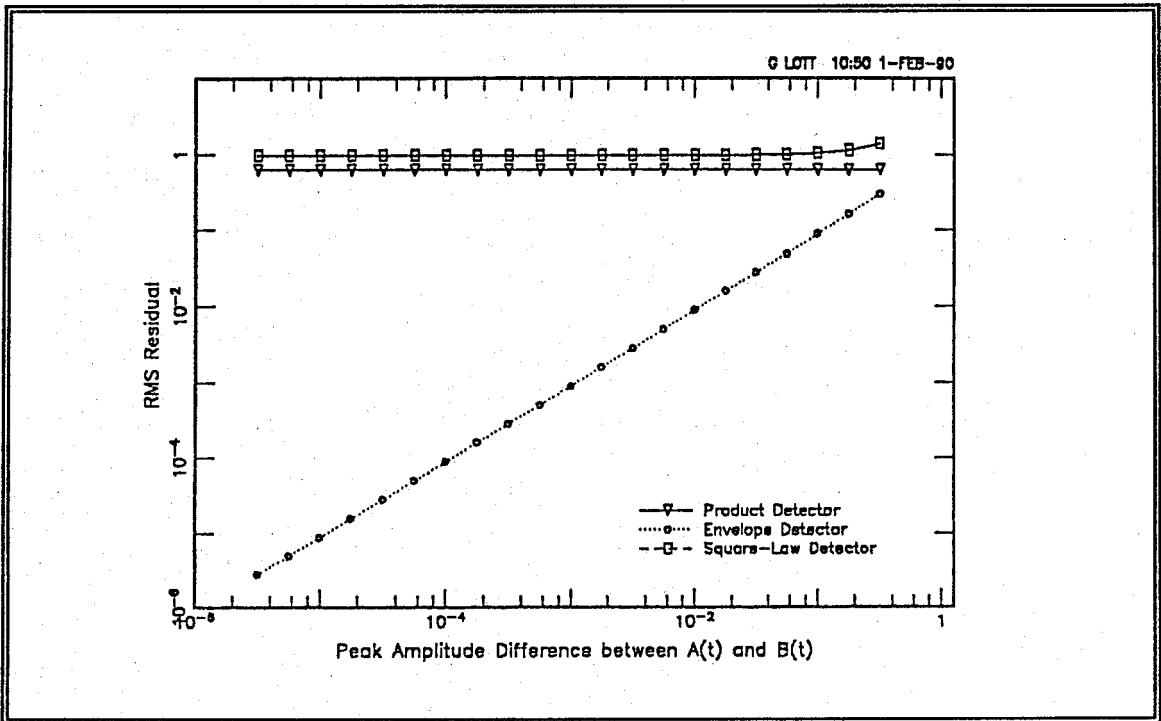
Figure 8.7 - RMS Residual Values versus Peak Amplitude Difference
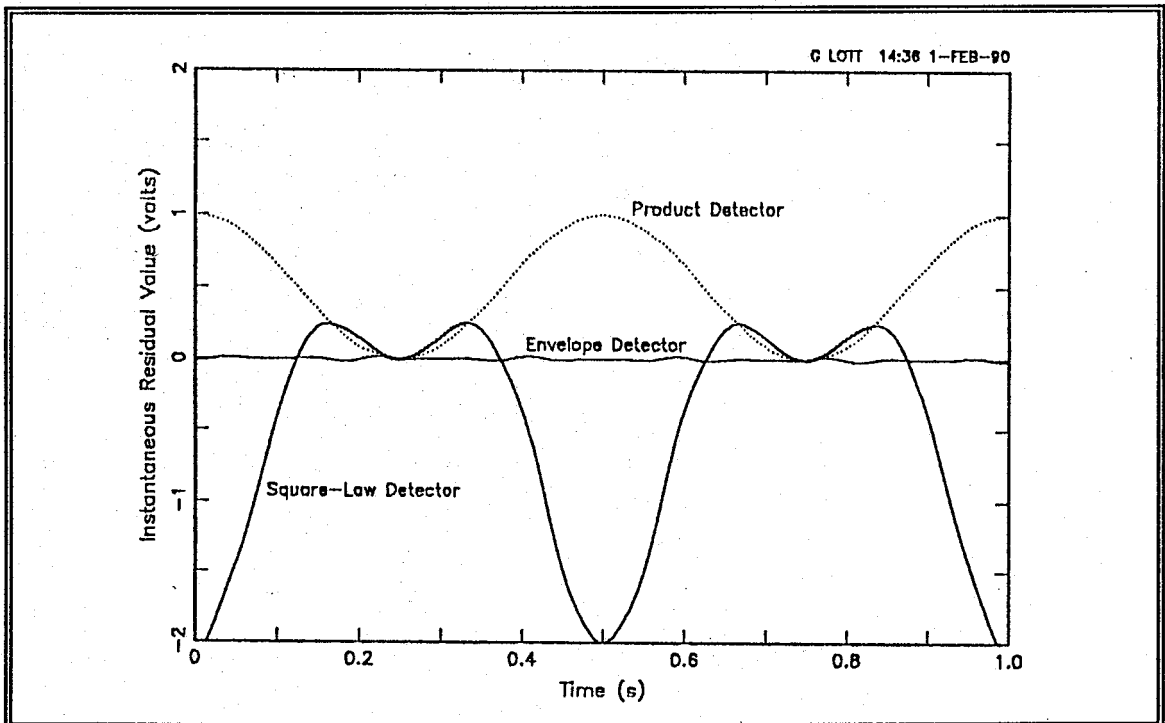
Figure 8.8 - Instantaneous Residual Value

162

Since no available AM detector exhibits capture, the envelope detector is the best choice. Figure 8.9 shows a strong signal elimination system incorporating the phase tracking network and the envelope detector. Appendix D also includes a MATHCAD work sheet showing voltage calculations and voltage spectral densities for the circuit configuration shown in Figure 8.9. The system removed the stronger signal, and the spectrum of the residual voltage clearly shows that the weaker signal is detectable as a new energy.
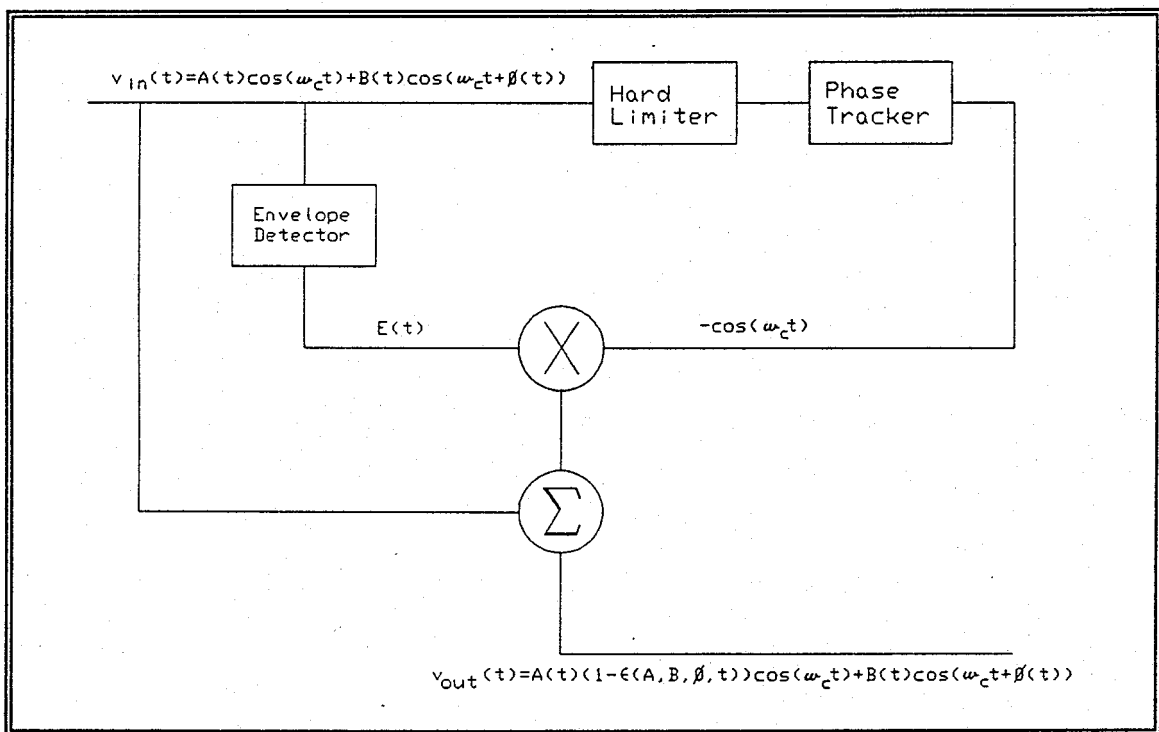
Figure 8.9 - Block Diagram of Basic Strong Signal Elimination System

The signal created by the strong signal elimination system shown in Figure 8.9 is a double-sideband signal centered on the carrier frequency of the strongest signal. Since there was no filtering prior to the envelope detector, the

163

envelope voltage contains energy from all the signals present in the receiver's passband. This results in the creation of the mirror images of all the weaker signals in the other sideband. This unwanted mirror sideband appears as a new set of unwanted signals in the receiver passband.

Even by using the I-Q method of generating single-sideband, one cannot avoid this mirroring. For each real new energy in the 2.5 MHz receiver final IF section, there will be potentially two new energies due to the unwanted sideband. This depends on the strongest signal's location in the 2.5 MHz passband and the relative position of the new signal to the strongest signal.

The problem with this system configuration shown in Figure 8.9 is that a mirrored HF signal may mask the presence of a weaker signal located at the mirrored frequency. If the strongest signal is at 1450 kHz, and another strong signal is at 1200 kHz, there will be a strong mirror signal at 1700 kHz within the 2.5 MHz passband. If the strongest signal had originally been at 15.450 MHz, a strong signal at 15.200 MHz will mask any Fixed Service signal at 15.700 MHz. This could severely inhibit detection of new energies caused by signals of interest.

The problem can be eliminated by further isolating A(t) by a means other than with an unfiltered envelope detector. Figure 8.10 shows a superheterodyne network where the output of the phase tracking system controls the receiver tuning.
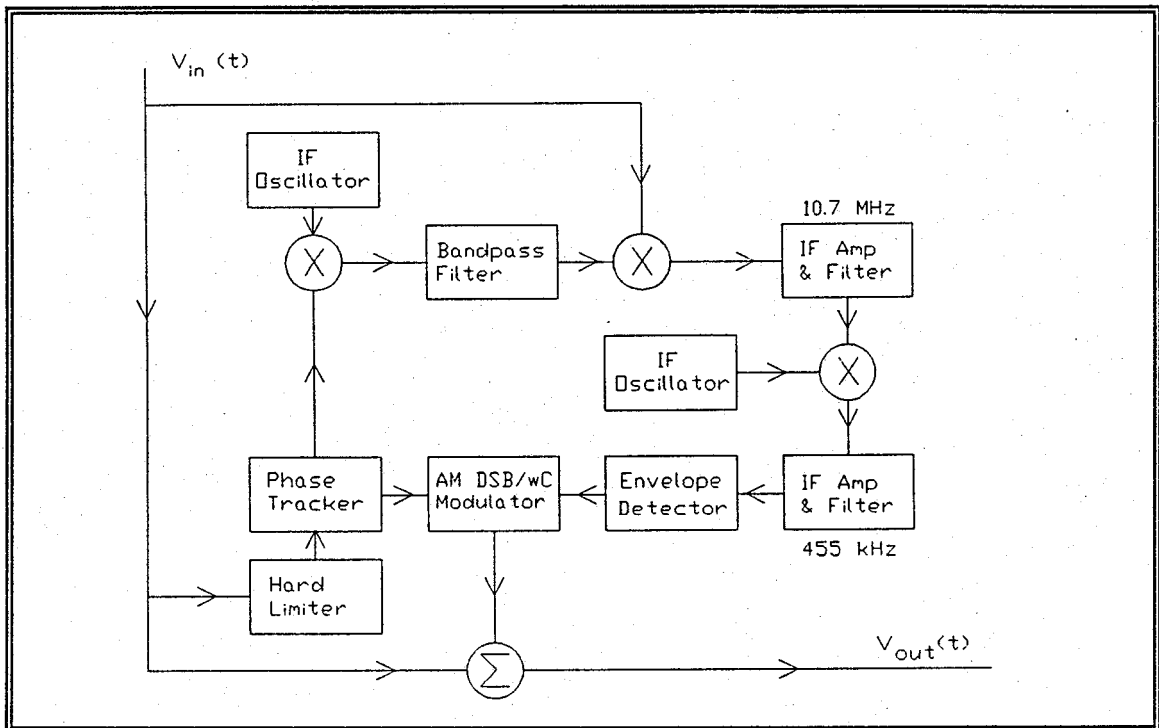
Figure 8.10 - Superheterodyne Strong Signal Eliminator

The phase tracker locks onto the carrier frequency of the strongest signal, using a passband frequency of, say, 1.5 MHz. If the IF oscillator is at 10.7 MHz, the output of the bandpass filter would be at 9.2 MHz using the difference frequency. This 9.2 MHz multiplies the incoming signal, and it produces a 10.7 MHz IF voltage with the strongest signal always at the first IF frequency.

The second IF stage, with an IF frequency of 455 kHz, functions as does any superheterodyne receiver. The IF filter bandwidth should be about 10 kHz since international broadcasting uses a 10 kHz bandwidth. Design should optimize selectivity at the sacrifice of some sensitivity. The only signal passed by the IF

165

stage will be the strongest signal. There are many high-order filters available for both the intermediate frequencies mentioned.

After the heterodyning and filtering, the envelope detector sees a voltage which should contain only the IF form of $v_a(t)$ and little, if any, other voltage additionally from the other signals. The voltage from the envelope detector ideally would be A(t).

The remaining design for subtraction is the same as shown in Figure 8.9. The system reconstructs $v_a(t)$ and subtracts it from the composite voltage $v_{in}(t)$. There may be a phase error added due to delay in the IF circuits. If so, the system may require an RF delay before the RF summer.

The system acts as the fast tuning receiver proposed earlier where the tuning is slaved to the phase tracker. There is an order of magnitude increase in the system's complexity, but there will be no mirroring of other signals. This system can remove the strongest signal with little or no corruption of the other signals.

C. MULTIPLE-STAGE STRONG SIGNAL ELIMINATION

Figure 8.11 shows the application of multiple levels of strong signal elimination in the RF system. The RF signals pass around the entire system until the peak voltage level exceeds a threshold. The system switches in the strong signal eliminators until the peak RF voltage drops below the saturation level. This system can effectively expand the dynamic range of the digital receiver by altering the HF signal environment before quantization takes place.

166
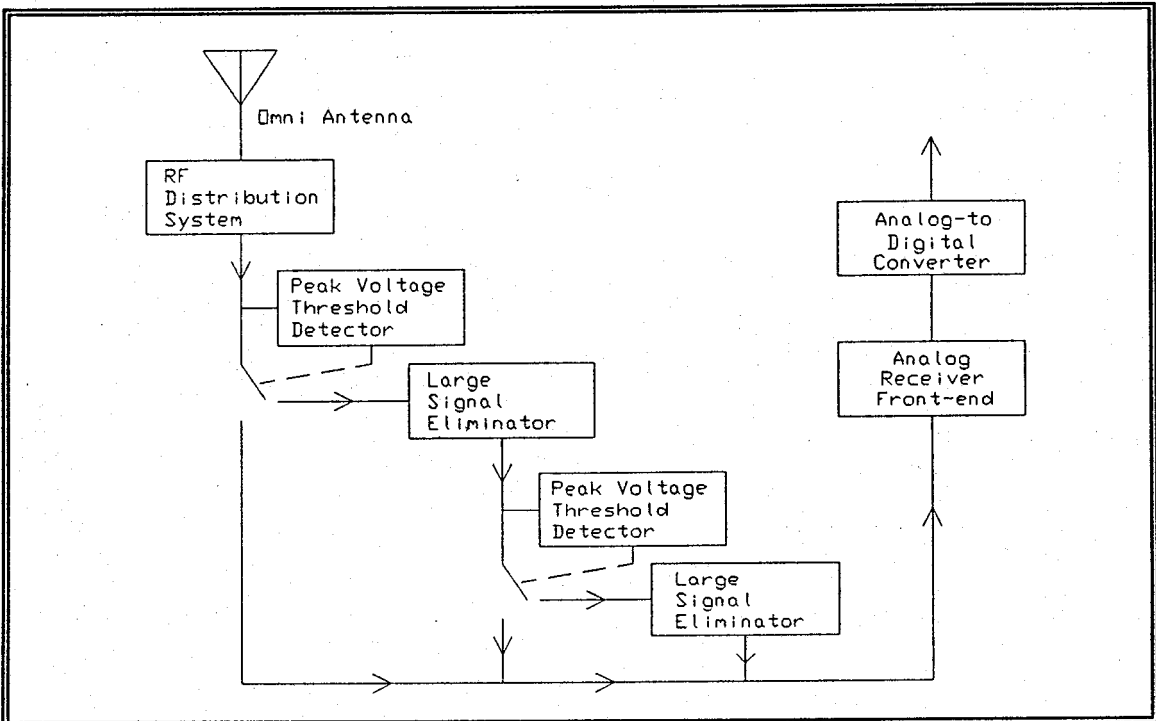
Figure 8.11 - Multiple Stage Strong Signal Elimination Architecture

IX. CONCLUSIONS AND RECOMMENDATIONS

HF signal amplitudes are log-normally distributed. Their mean is 30 dB higher at night than in the daytime. The nighttime variance is also higher. The nighttime variance will range from about 40 to 140 depending on many variables.

Results from general HF spectrum surveys which target non-broadcasting bands provide a good statistical description of the amplitude distribution of military signals-of-interest. During daytime at a CDAA receiver facility, the mean level of non-broadcast signals will be about -100 dBm. The nighttime mean will be near -85 dBm. The probability distribution function for the military signals of interest shows that the daytime signal amplitudes range over some 50 dB (-125 dBm to -75 dBm), and the nighttime signal amplitudes range over 70 dB (-125 dBm to -55 dBm). Since the receiver front-end will receive energy from the international broadcasting stations, the actual dynamic range required of an HF receiver is much greater than that required only by the signals of interest. The receiver's dynamic range must be at least 120 dB.

International broadcasting operations continue to grow, and broadcasting signals are clearly the strongest signals in the spectrum. The strongest international broadcasting signals will be 30 to 50 dB stronger than the strongest non-broadcasting signals. Intermodulation products in the RF Distribution System and

receivers resulting from these strongest signals corrupt the nighttime RF environment at every Navy CDAA facility.

New energy receivers require a sensitivity of -125 dBm (0.2 μV). The same receiver must simultaneously process -5 dBm signals without intermodulation distortion. Current receivers require large front-end attenuation to prevent overload, and this attenuation causes a substantial performance loss.

The distribution of HF signal amplitudes provides a method of measuring HF receiver site performance. Noise, interference, and signal path attenuation cause poor performance. The peak value of noise and interference determines the number of signals lost. Noise levels, temporally averaged, do not indicate the level of degradation caused by man-made noise. RF Distribution System signal loss from the antenna to the receiver should be kept to a minimum since it will reduce site performance in a manner similar to increasing the external noise level.

In a digital, new-energy receiver, design should minimize the number of analog devices (i.e., amplifiers, switches) prior to the analog-to-digital converter. There should be no electronic switching systems anywhere in the RF path as these generate noise or attenuate the incoming signals. Where essential, analog systems require special design to maximize their dynamic range in order to exceed the dynamic range capability of the A/D converter. Otherwise, IM distortion will be present when the input voltage is quantized. These IM products can interfere with actual signal detection.

Aperture uncertainty, saturation, aliasing, and intermodulation products bound the performance capability in A/D converters used in wideband HF receiver applications. There currently exist A/D converters with adequate dynamic range for the HF spectrum, but these have slow sampling rates. Within the next ten years, a 16-bit 5-MSPS converter will be available. A system built around a 16-bit converter will have a 90 to 94 dB dynamic range.

Every quantizer in the new energy system should include dynamic error compensation networks. Oversampling using the 1 GHz sampling converters will reduce the quantization noise, but oversampling cannot provide the sensitivity and dynamic range required in the HF new energy receiver.

Today, the only way to improve weak signal detection is to operate at the A/D converter performance threshold and to alter the HF signal environment. Notch filtering can whiten the HF spectrum. Attenuating the international broadcasting band signals by 40 dB reduces the dynamic range to about 80 dB. However, weak signals of interest in the notched frequency bands are also attenuated. So using notch filtering removes new-energy search coverage within the stopband.

Altering the HF signal environment is the preferred way to improve performance. Surveys show that a few signals constitute the front-end and A/D converter overloading. Frequency coverage should include only one international broadcasting band within the receiver passband.

170

Large signal elimination is possible using a superheterodyne system. By detecting the strongest signal's envelope, one can subtract the strongest signal before quantization.

Many areas for research remain in this area. Future research should include:

♦ HF path-specific amplitude distribution studies. These should concentrate on polar, auroral, and trans-equatorial paths. There should be more work on the differences in one- and two-hop distributions.

♦ HF signal-specific amplitude distribution studies. The goal should be to create a subset of the non-broadcast signals including only military signals-of-interest.

♦ HF receiver site performance improvement verification. Studies should select one or two HF receiver sites which have measured poor performance. Work should identify and correct the problems. Operators should keep careful logs before and after the work. The experiment should define two or three operational performance indices. Using the performance curves in Chapter V, one should compare the operational indices to verify the improvement.

♦ Installation of broadcast band notch filters at a CDAA site. Studies should look carefully at before and after intermodulation products present in the receiver.

♦ Construction and testing of the large signal eliminator system.

APPENDIX A

Figure A.1 shows the equipment configuration used to provide detailed time- and frequency-domain measurements. The input voltage is the voltage present on the coaxial cable feeding signals to a typical receiver. The receiver is usually fed by the facility's RF distribution system which may include primary multicouplers, beam-forming networks, secondary multicouplers, path switching, and connecting cabling.
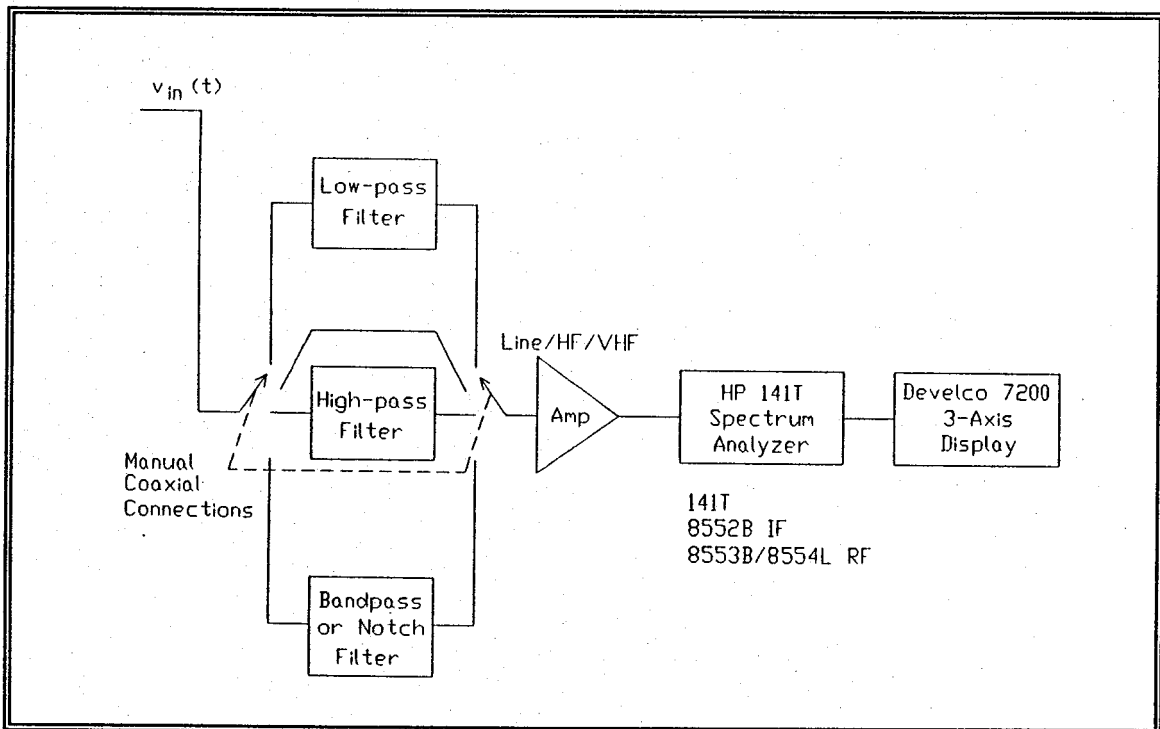
Figure A.1 - Block Diagram of Equipment Used to Make Noise and Interference Measurements

While measurements are made with the spectrum analyzer connected directly to the RF distribution system, filters and amplifiers can modify the input voltage. The filters commonly used include a lowpass filter with a cutoff frequency of 1 MHz, a highpass filter with a 35 MHz cutoff frequency, and a bank of bandpass filters designed to pass non-international broadcast bands from 2 to 30 MHz. Strong signals may require the use of an external attenuator.

The amplifiers include a low frequency (10 Hz to 500 kHz) line amplifier, an HF amplifier (such as the Olektron Model B-HIA-11-HF, 500 kHz to 50 MHz), and a VHF amplifier (50 MHz to 500 MHz). The line and VHF amplifiers are used primarily to make intermodulation products measurements above and below the HF spectrum. The HF amplifier must have a large dynamic range, requiring a third order intercept point of at least +52 dBm.

As shown in Figure A.1, the Hewlett-Packard (HP) Model 140/141 spectrum analyzer acts as a scanning receiver. Along with the HP 141T Display Section, typical HF measurements require two plug-in modules, the HP 8552B Intermediate Frequency Section and the HP 8553B RF Section. The operator can adjust the RF attenuation, scan rate, scan width, IF gain, IF bandwidth, and other controls to give the best presentation of the noise or signal under observation.

The Develco 7200 3-axis display provides a real time display of noise and signals received with the spectrum analyzer. As shown in Figure A.2, the three axes are usually frequency (horizontal axis), signal or noise power (vertical axis),

173

and time (depth or Z axis). The horizontal axis is also the time for each spectrum

analyzer sweep which allows measurement of repetition rate and duration of

wideband interference such as distribution power-line related noise.
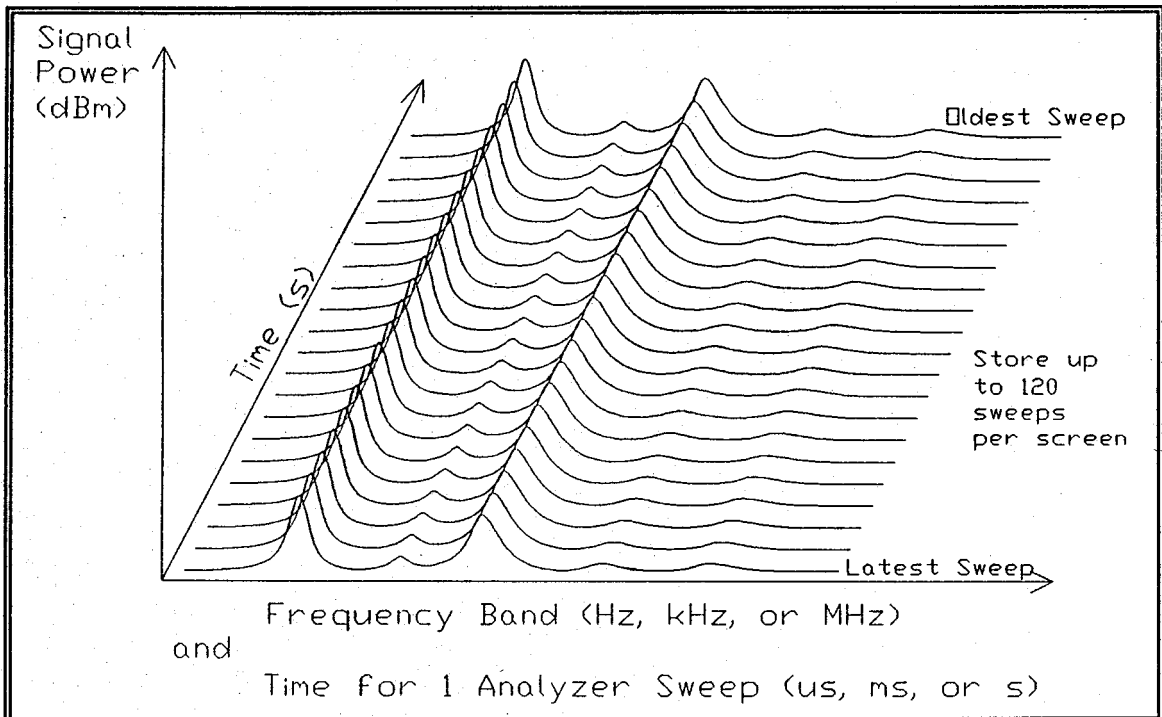
Figure A.2 - Units of Measure Associated with Each Axis in Photographs Made
with the 3-Axis Display System

The HP141 spectrum analyzer provides two signals to the 3-axis display, video

and synch. The 3-axis display takes 512 equally spaced samples of the video signal

from each complete analyzer scan, and the sample resolution is eight bits. As

shown in Figure A.3, the Develco 7200 is a first-in, first-out (FIFO) display. The

latest scan appears as line one. Line one moves to line two with the newest scan

again appearing as line one. The 3-axis display can typically store up to 60

174

spectrum analyzer scans. There are 120 line versions of the Develco 7200. With each scan update, the oldest scan data on the top line is discarded.
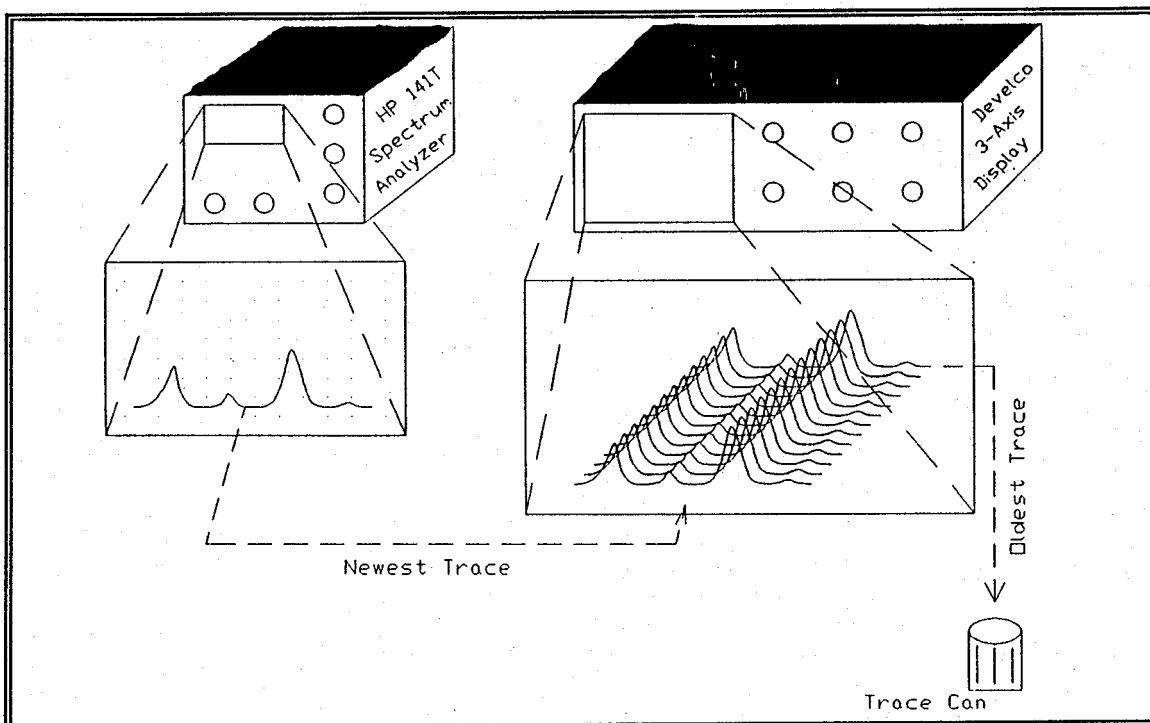
Figure A.3 - Combined Operation of HP 141T and Develco 7200 Showing FIFO Movement of Spectrum Analyzer Scans

The time (depth) axis is the elapsed time for the 60 traces. However, spectrum analyzer retrace time adds to the total. Measurements show that on one HP 8553B with a scan rate of 5 ms per division (50 ms per scan), the actual time for one scan and retrace in the auto synch mode was 56.5 ms. For the same unit with the same setting, the actual time for one scan and retrace in the line synch mode was 66.94 ms. When displayed on the Develco 7200, the depth time axis limit for measurements made with a 5 ms per division scan rate on the specific HP

8553B are 60 times the actual time for one scan plus retrace, or 3.4 s and 4.0 s respectively.

There is no simple expression that one can use to determine the actual scan time as a function of the instrument control scan rate. Prior to making measurements, the operator must measure the actual scan times for each scan rate in both the auto and line synch modes. The actual scan times will be different for each HP 8553B, and experience shows that the times will change each time a unit undergoes calibration.

Measurements require accurate frequency, amplitude, and time calibrations for use as standards for manually scaling the photographs taken of the 3-axis display's screen. Calibrations include the total scan time measurements and a 10 dB step amplitude calibration photograph. Calibrations are good only for the specific instruments used. Operators should make daily checks to ensure that the calibration photographs are accurate. Changing the oscilloscope camera may require a new amplitude calibration photograph because image compression may occur due to small differences in the camera lens.

Figure A.4 shows a sketched example for 25 spectrum analyzer scans as displayed on the Develco 7200. The figure shows the temporal changes for six signals in the 50 kHz part of the HF spectrum. Actual signal identification for some modulation types is difficult using only the 3-axis display. To make signal identification easier, a separate HF communications receiver augments the measurement system.
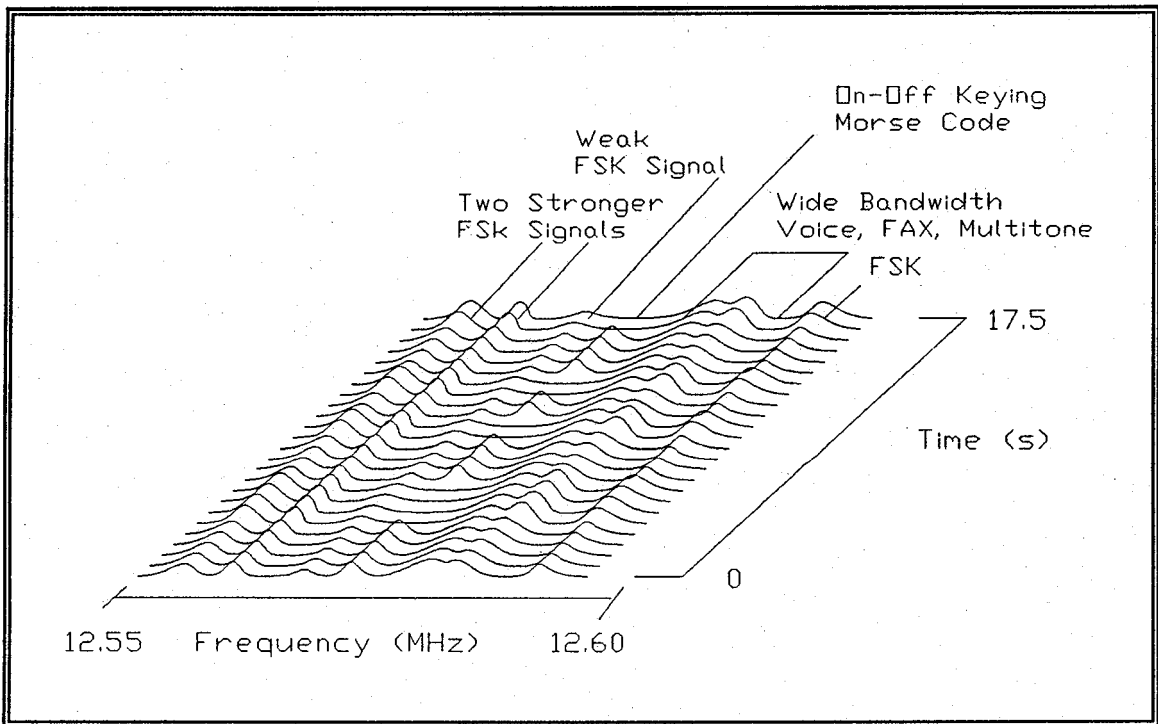
Figure A.4 - Example of 3-Axis Display of HF Signals

The 3-axis display controls allow for:

♦ freezing the data in memory for photographing or detailed viewing

♦ changing amplitude compression

♦ changing the elevation and azimuth of the depth axis

♦ adjusting the background level.

To make photographs for amplitude measurements, the display elevation and azimuth are set to zero. This results in viewing all 60 traces as if they were superimposed into one trace. Using a card made from the 10 dB calibration step photograph, knowing the equipment settings, and using the trace baseline as a reference, one can manually scale the amplitude photographs.

Controls also allow for the selection and display of subsets of the 60 spectrum analyzer scans stored in 3-axis display memory. Experience using the 3-axis display while viewing various types of signals and noises results in the operator being able to adjust the 3-axis display controls to optimize the presentation. A typical measurement requires two photographs, one for amplitude measurement and one with the time (depth) axis elevated to show temporal variations.

APPENDIX B

This appendix contains histograms from data sets collected at the CDAA HF receiver facility in Edzell, Scotland, during the period 10 - 22 April 1989. The main discussion of this data is found in Section B of Chapter IV. Immediately after the data set number are the date and the starting and ending times (both in UTC) of the observation. The other parameters for the observation are identified as:

♦ CF - center frequency of the 2.5 MHz passband

♦ AT - receiver front-end attenuation

♦ ADT - Amplitude Detection Threshold

♦ b - number of bits in the A/D codeword (either 14 or 12)

♦ NEAs - number of New Energy Alarms

♦ CSF - Cubic-spline fit to data points

Figures 6.6 and 6.7 summarize the results given in Figures B.7 through B.42.
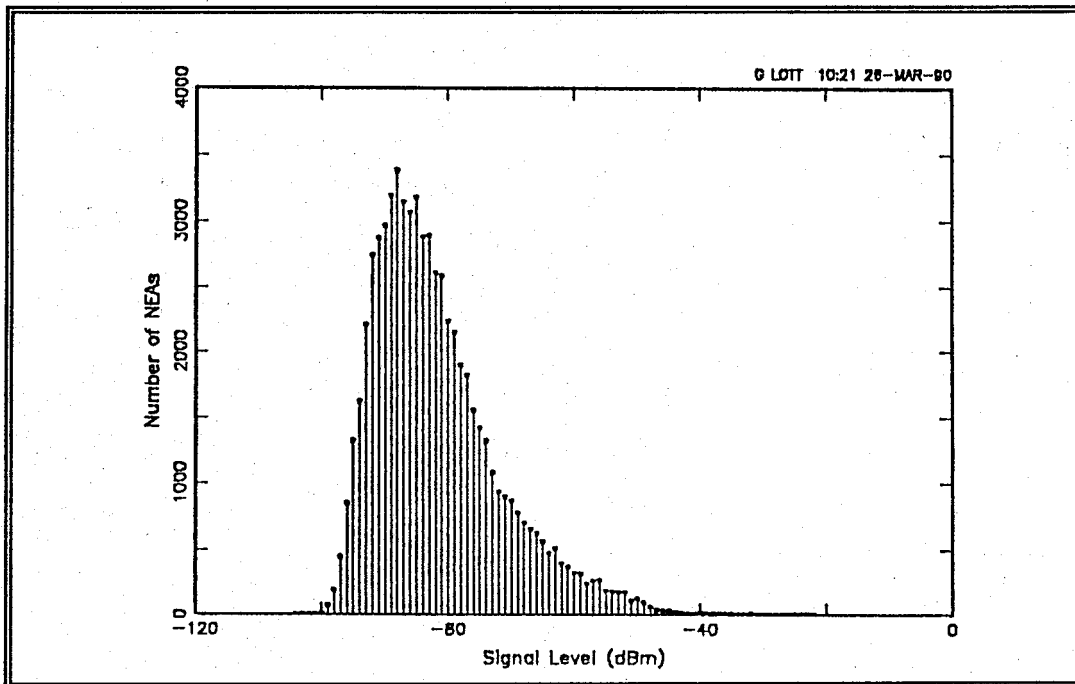
Figure B.1 - Histogram for Data Set 1, 11 Apr 89, 1342-1415, CF=14750 kHz, AT=16 dB, ADT=8 dB, b=14
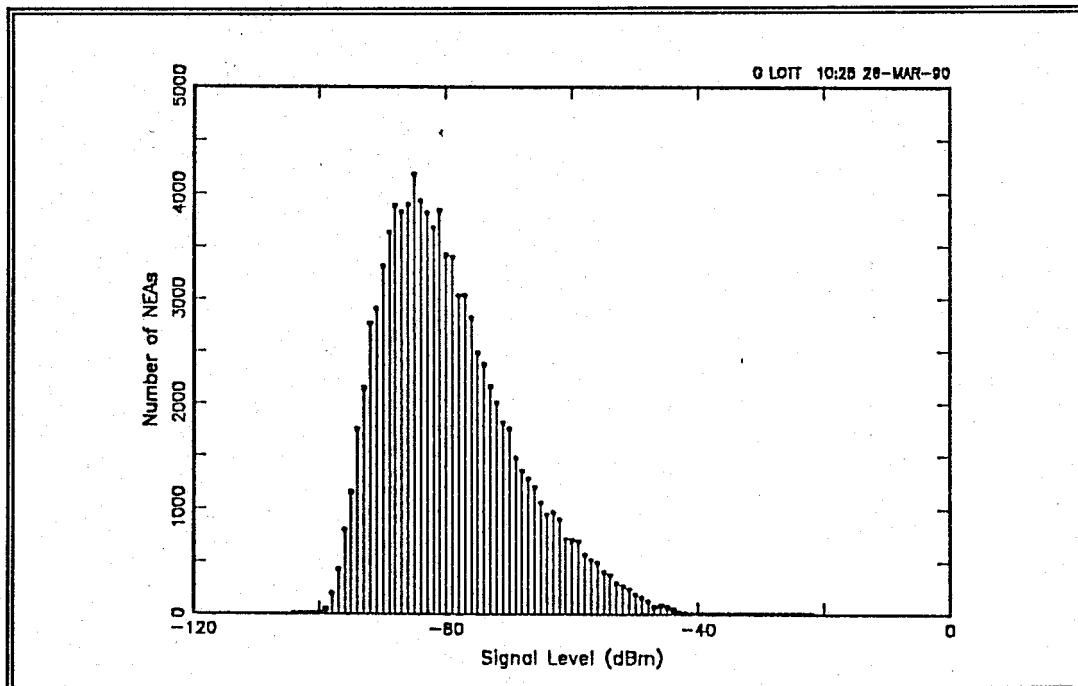
Figure B.2 - Histogram for Data Set 2, 11 Apr 89, 1450-1533, CF=11250 kHz, AT=16 dB, ADT=8 dB, b=14

180
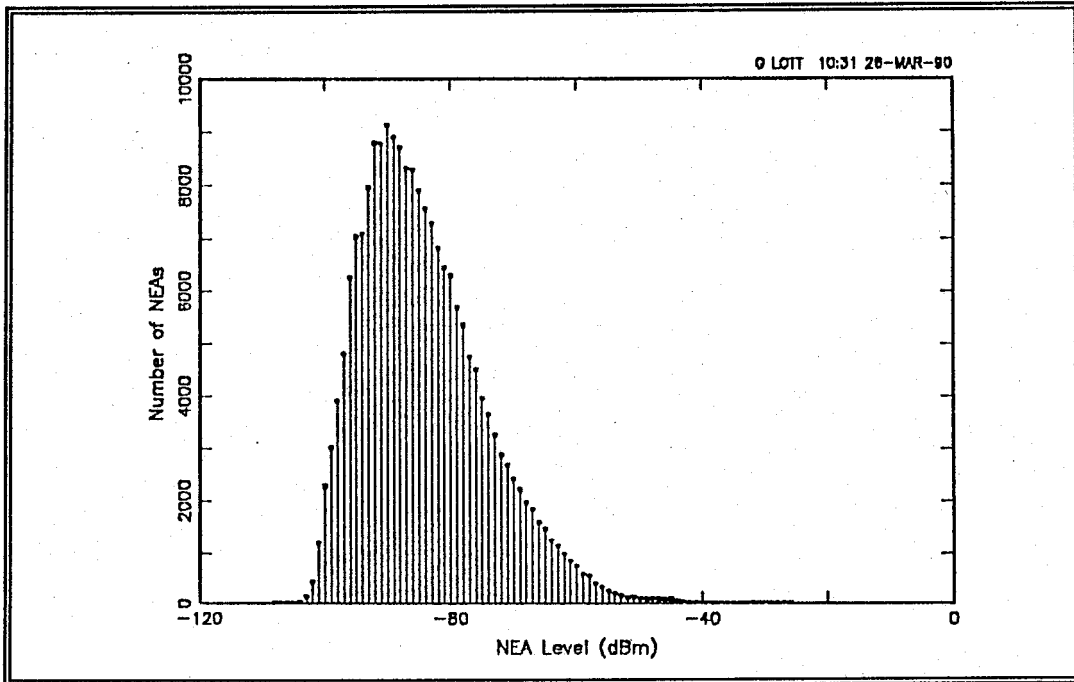
Figure B.3 - Histogram for Data Set 4, 11 Apr 89, 1727-1957, CF=13750 kHz, AT=12 dB, ADT=8 dB, b=14
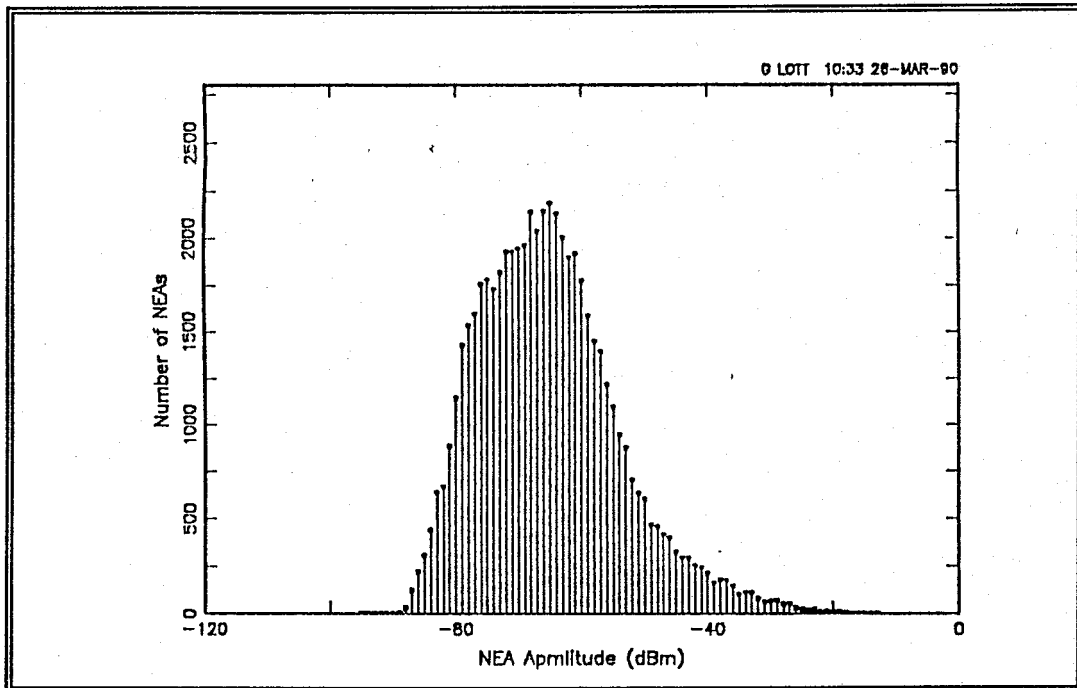
**Figure B.4** - Histogram for Data Set 5, 11 Apr 89, 2006-2123, CF=5250 kHz, AT=25 dB, ADT=8 dB, b=14
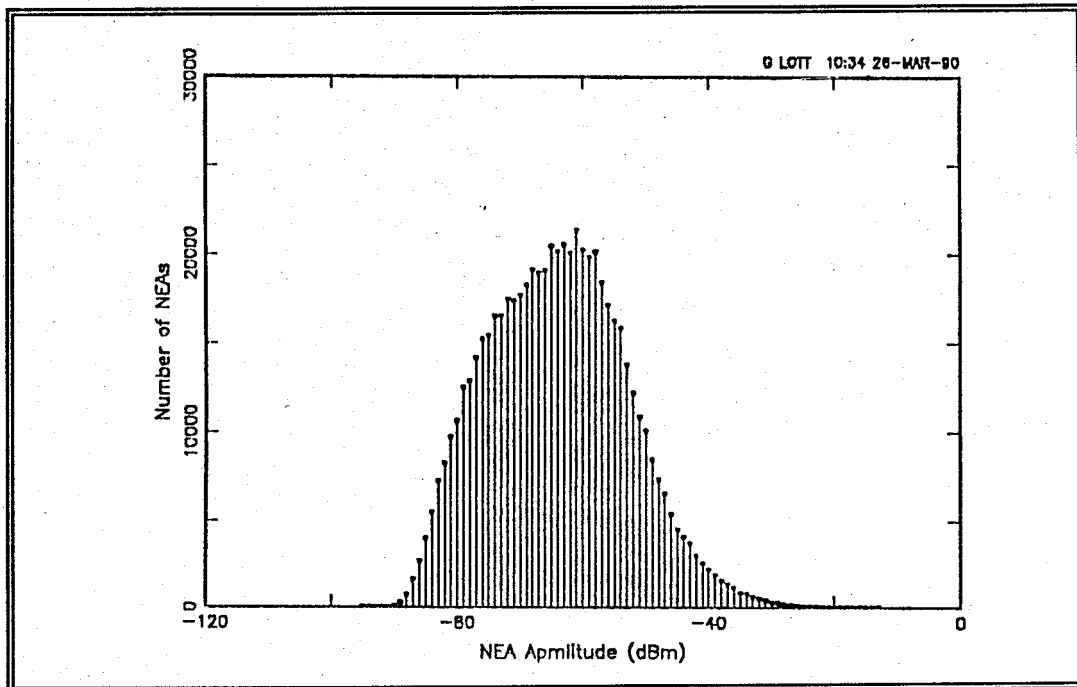
Figure B.5 - Histogram for Data Set 6, 11-12 Apr 89, 2126-0527, CF=4500 kHz, AT=25 dB, ADT=8 dB, b=14
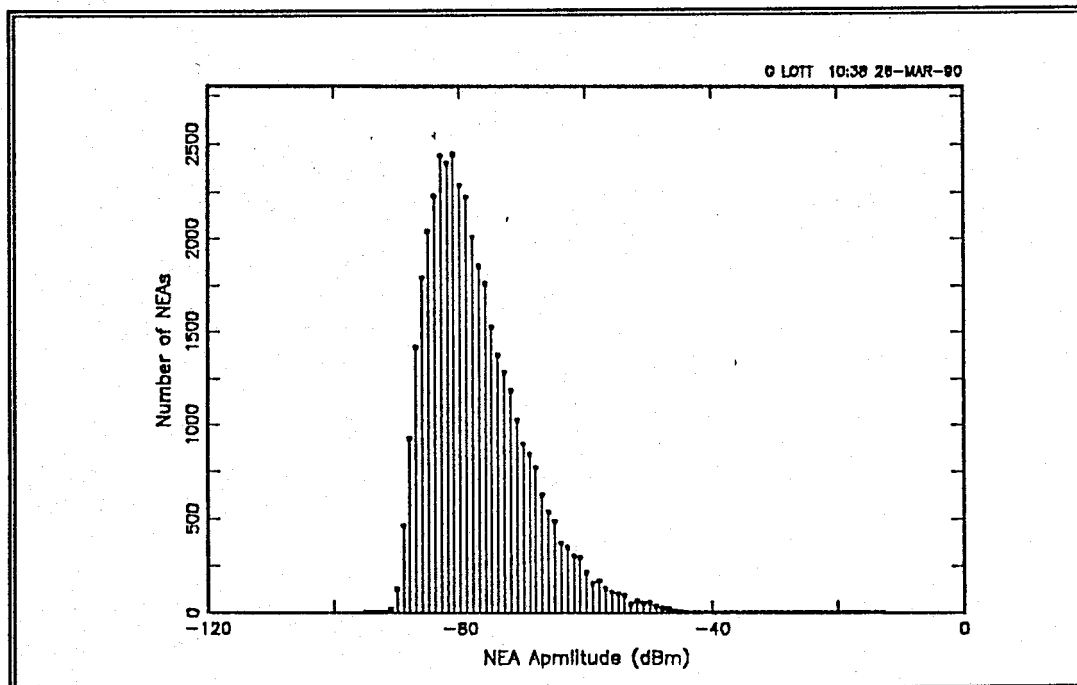
Figure B.6 - Histogram for Data Set 7, 19 Apr 89, 0942-1142, CF=13750 kHz, AT=25 dB, ADT=8 dB, b=14
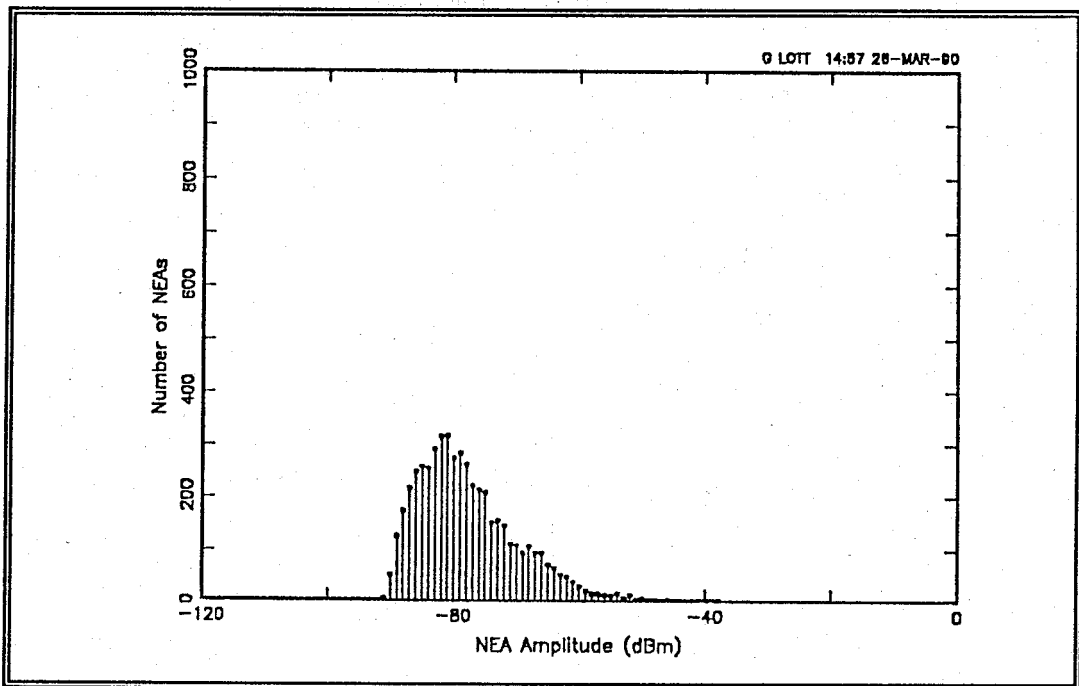
Figure B.7 - Histogram for Data Set 8, 19 Apr 89, 1209-1224, CF=13750 kHz, AT=0 dB, ADT=8 dB, b=14
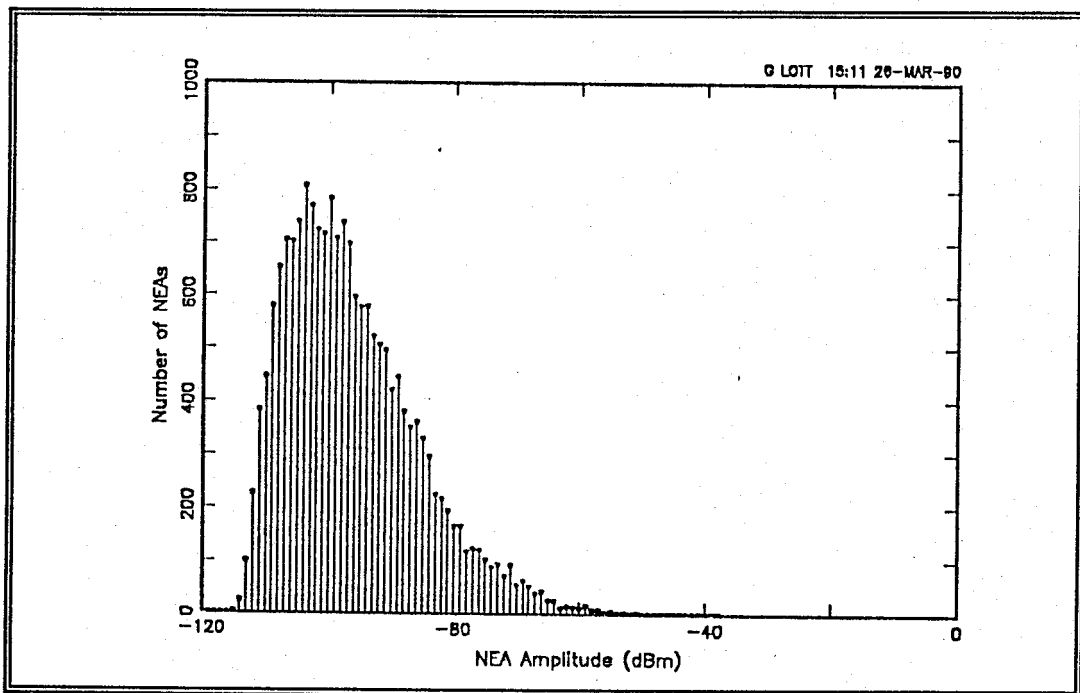
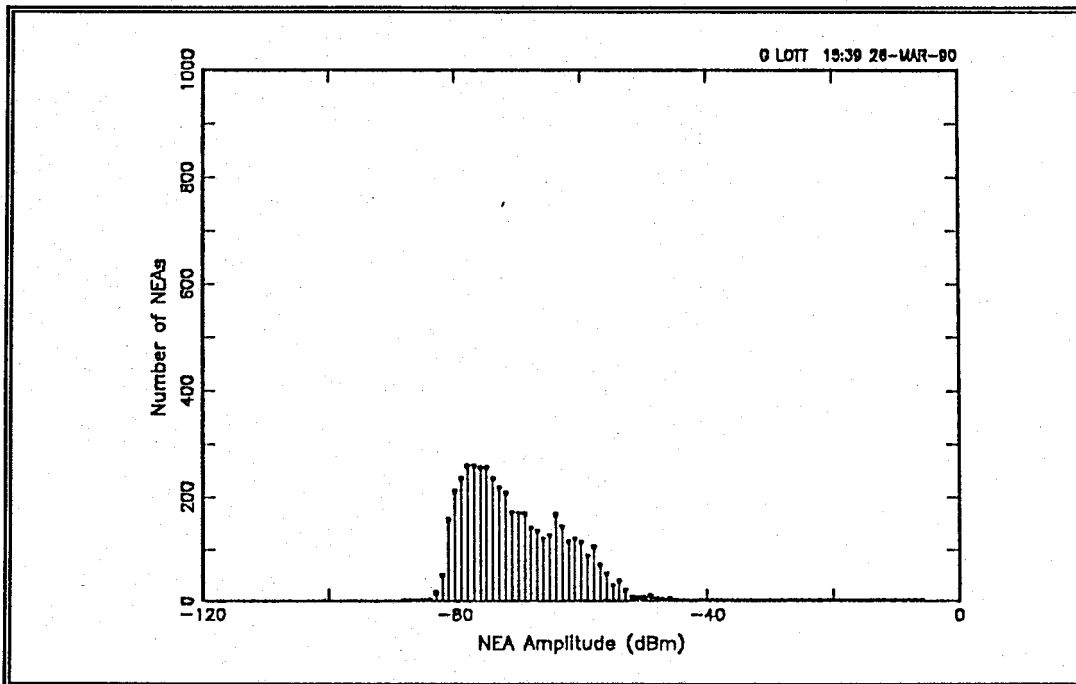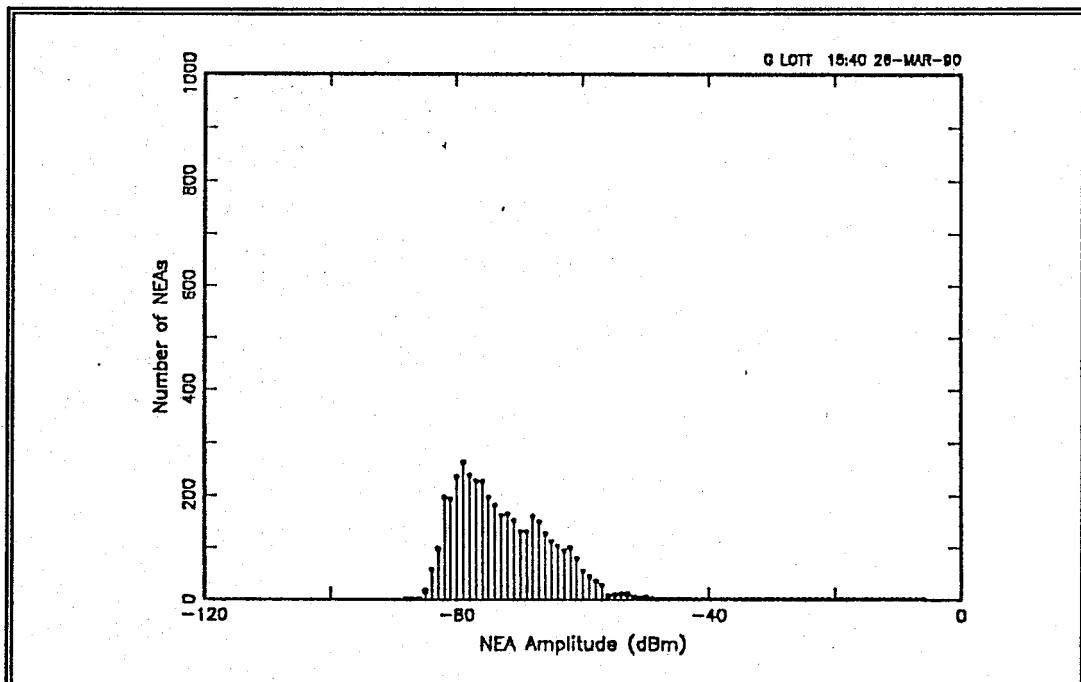**Figure B.8** - Histogram for Data Set 8, 19 Apr 89, 1209-1224, CF=13750 kHz, AT=0 dB, ADT=8 dB, b=12

183
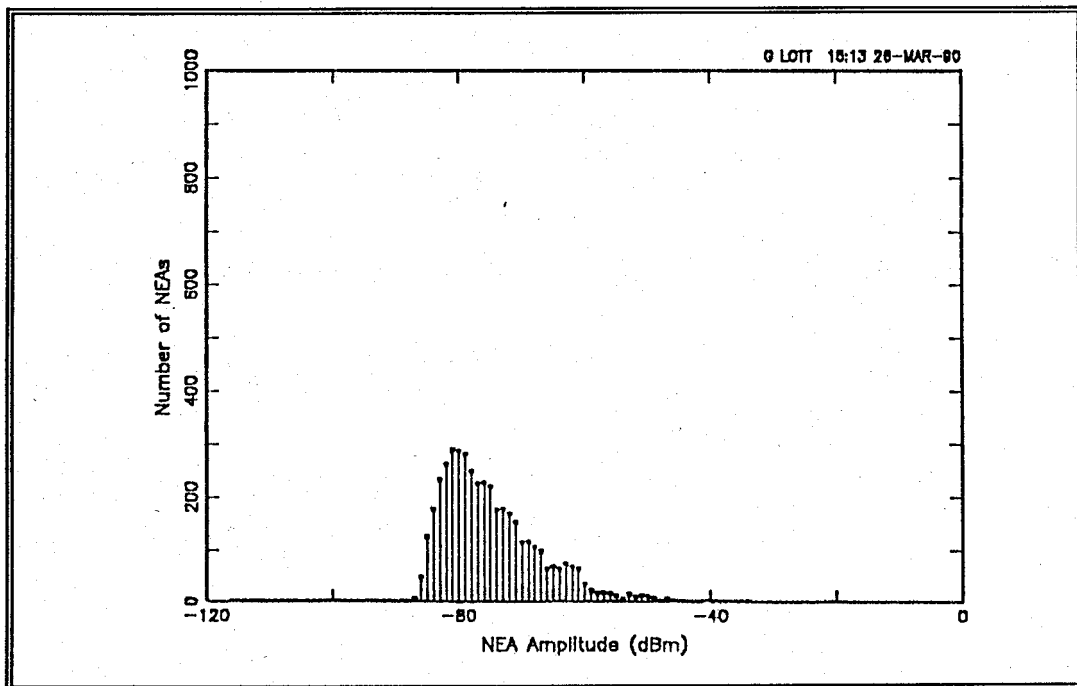
Figure B.9 - Histogram for Data Set 9, 19 Apr 89, 1225-1241, CF=13750 kHz, AT=4 dB, ADT=8 dB, b=14
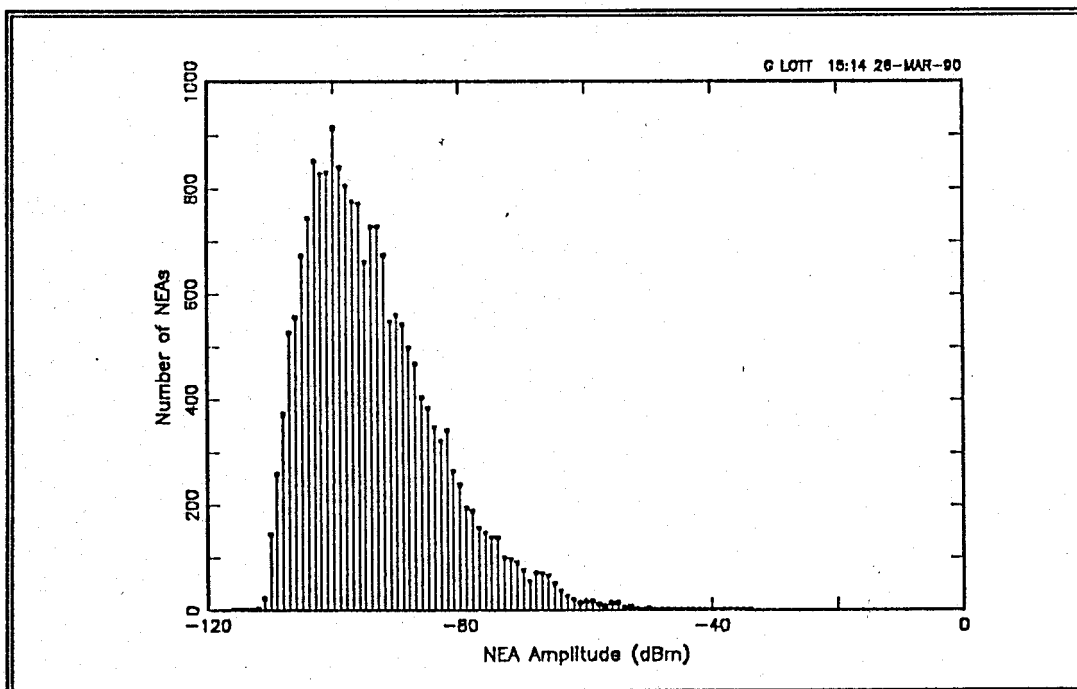
Figure B.10 - Histogram for Data Set 9, 19 Apr 89, 1225-1241, CF=13750 kHz, AT=4 dB, ADT=8 dB, b=12
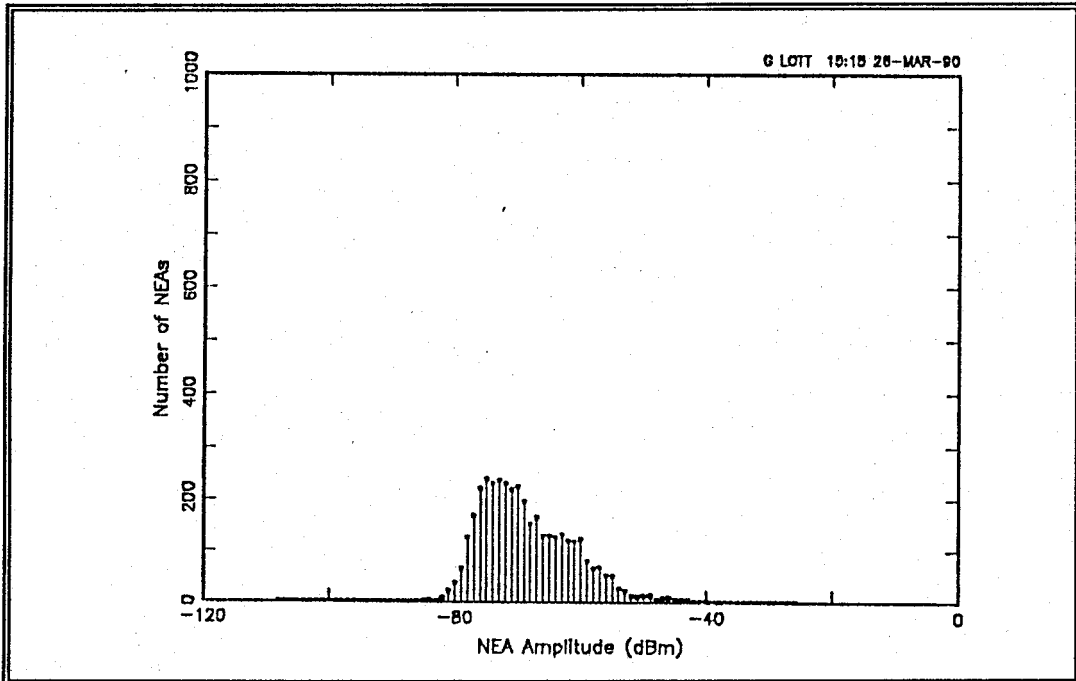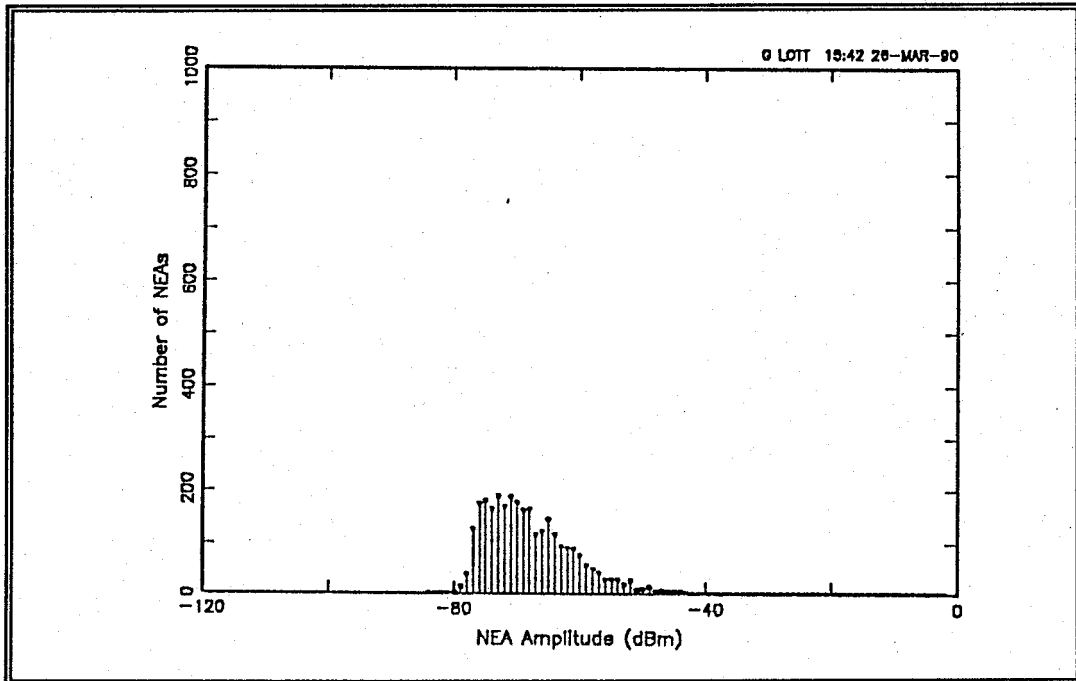
Figure B.11 - Histogram for Data Set 11, 19 Apr 89, 1301-1319, CF=13750 kHz, AT=12 dB, ADT=8 dB, b=14
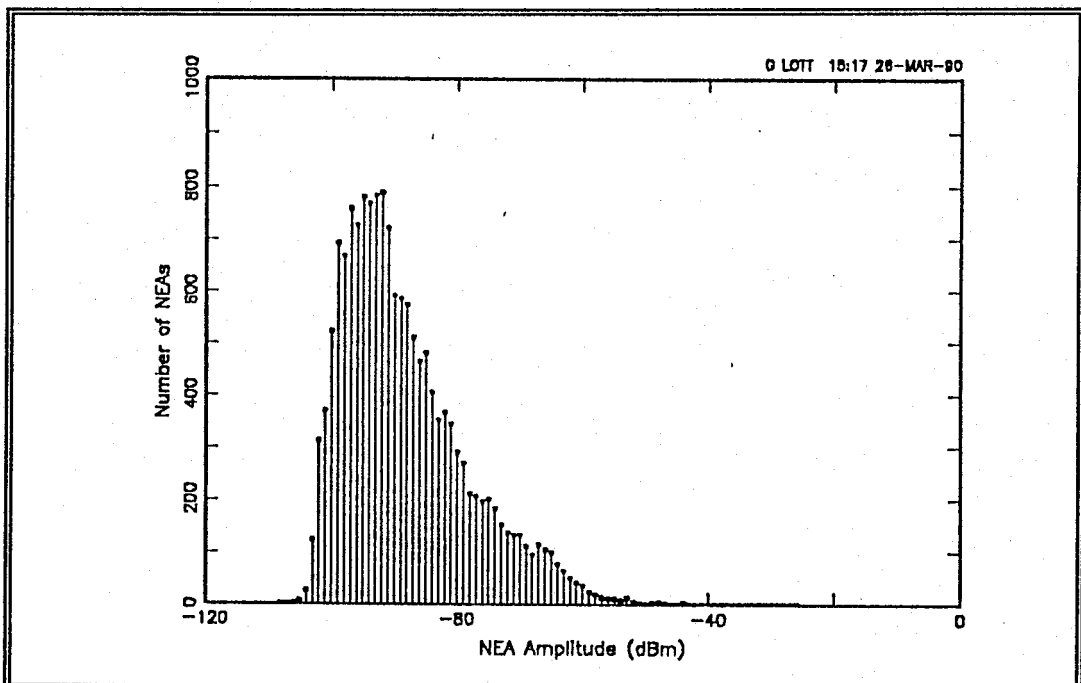
Figure B.12 - Histogram for Data Set 11, 19 Apr 89, 1301-1319, CF=13750 kHz, AT=12 dB, ADT=8 dB, b=12
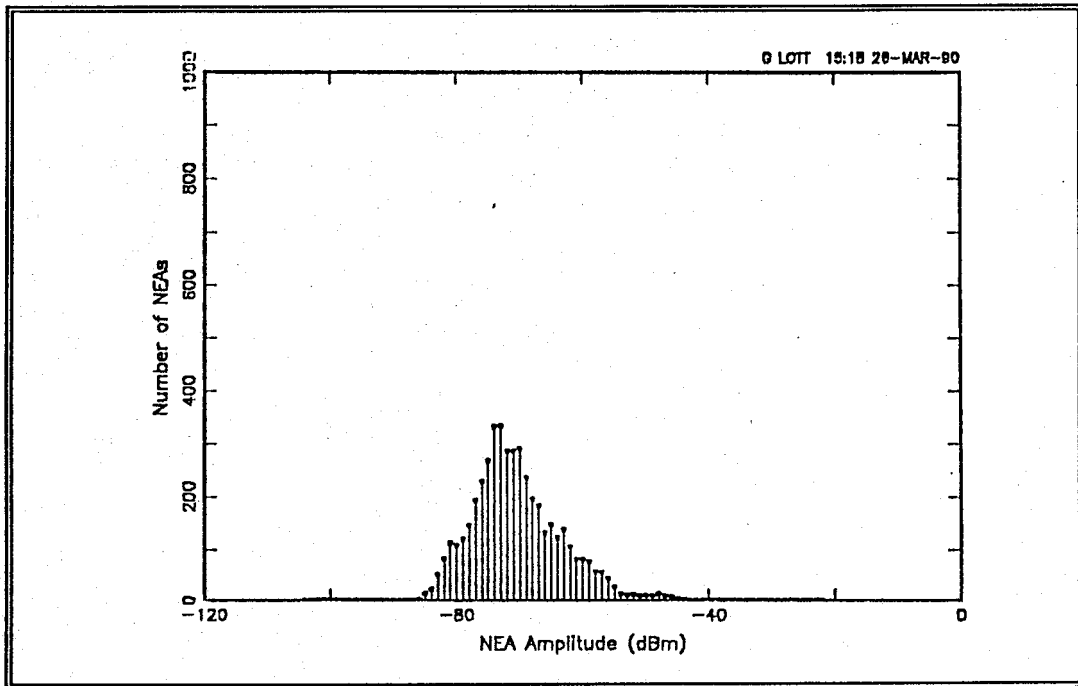
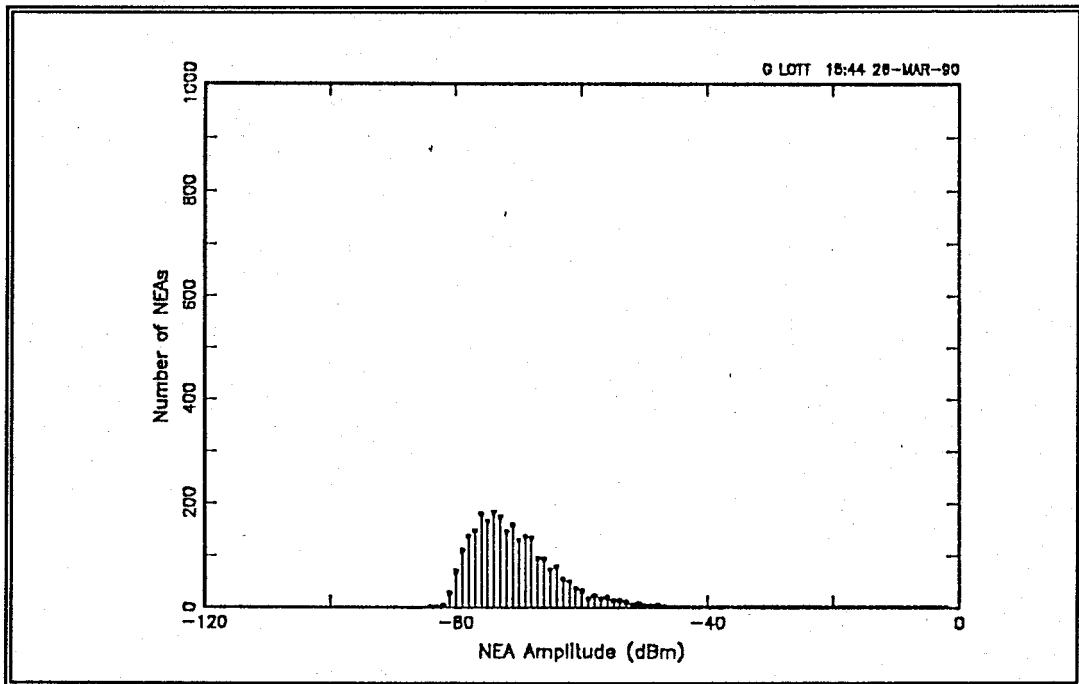**Figure B.13** - Histogram for Data Set 12, 19 Apr 89, 1319-1335, CF=13750 kHz, AT=16 dB, ADT=8 dB, b=14
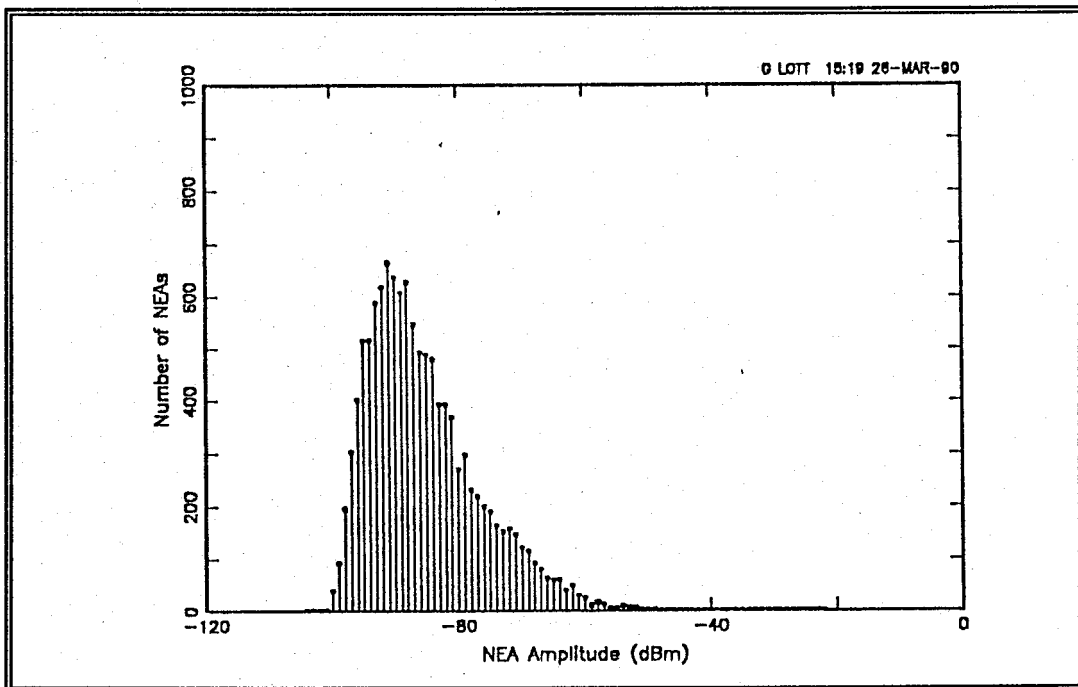
Figure B.14 - Histogram for Data Set 12, 19 Apr 89, 1319-1335, CF=13750 kHz, AT=16 dB, ADT=8 dB, b=12

186
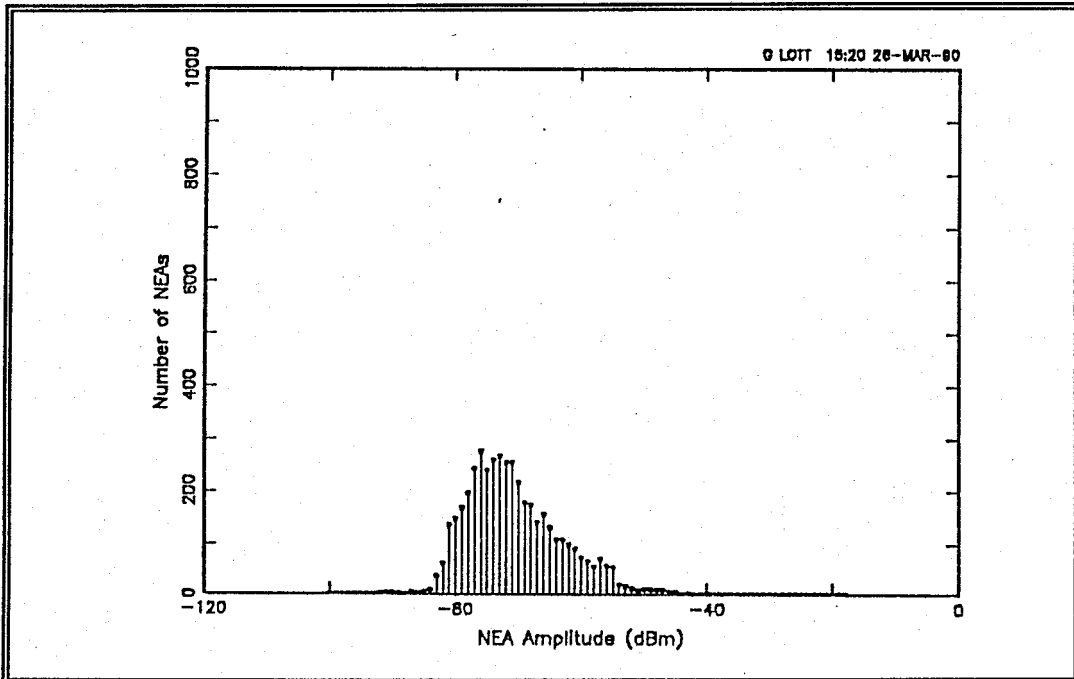
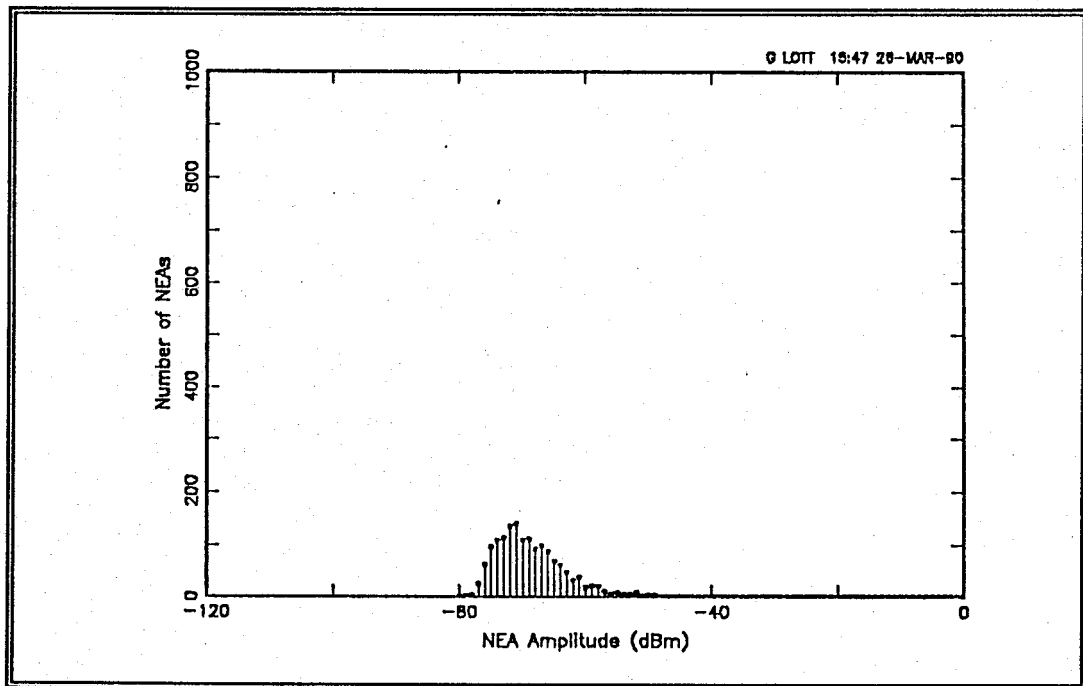**Figure B.15** - Histogram for Data Set 13, 19 Apr 89, 1335-1351, CF=13750 kHz, AT=20 dB, ADT=8 dB, b=14
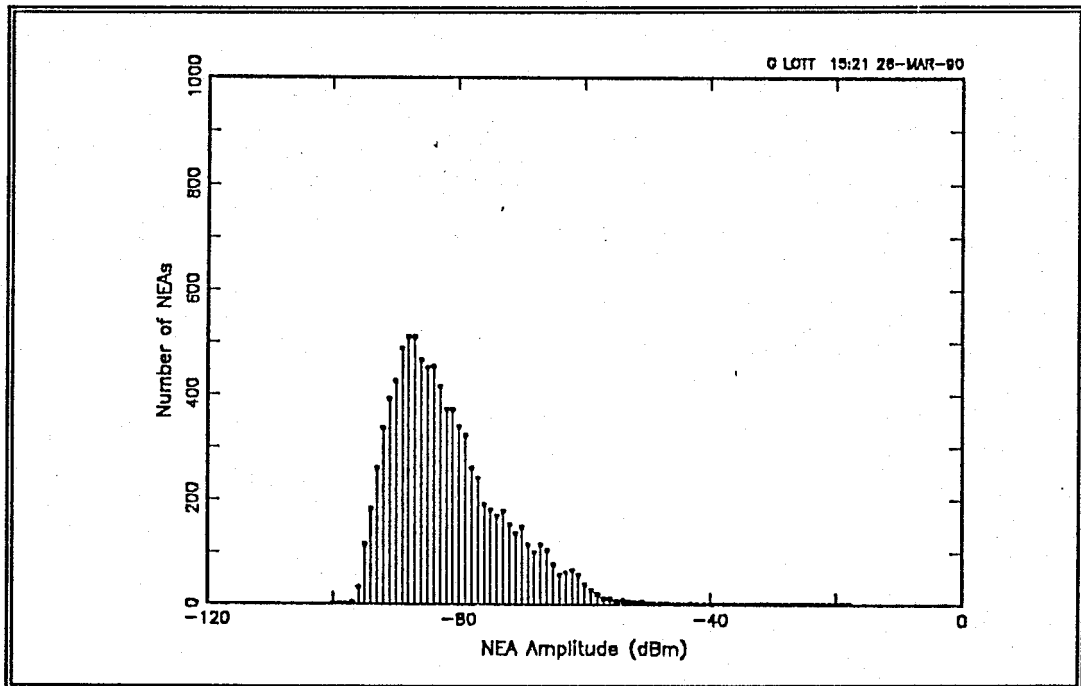
Figure B.16 - Histogram for Data Set 13, 19 Apr 89, 1335-1351, CF=13750 kHz, AT=20 dB, ADT=8 dB, b=12

187
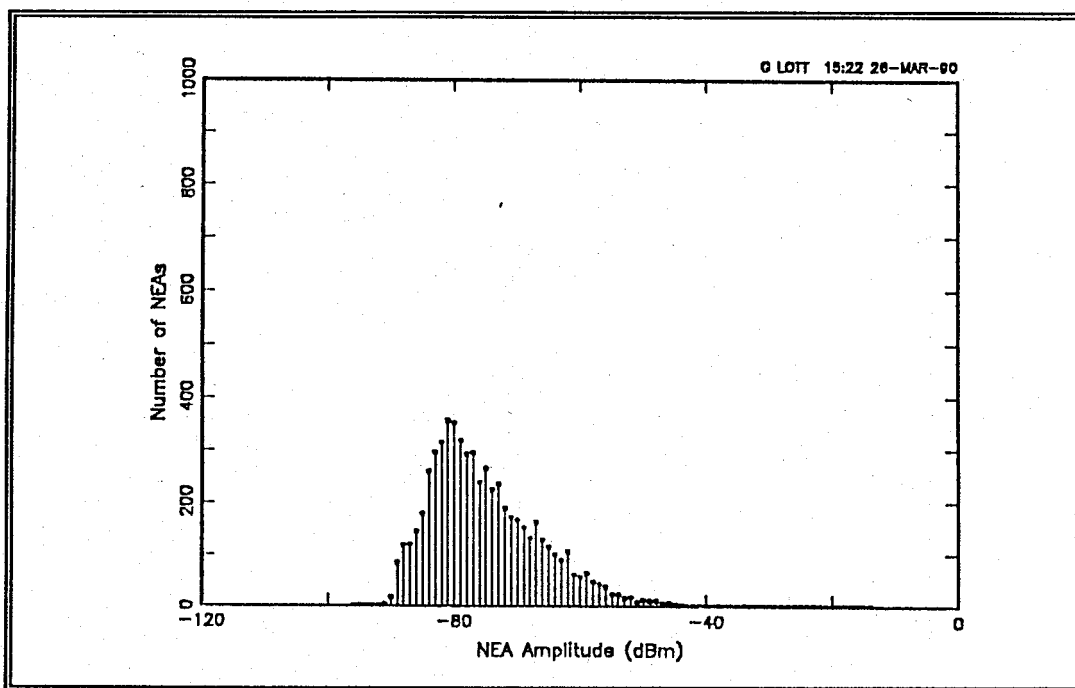
Figure B.17 - Histogram for Data Set 14, 19 Apr 89, 1351-1408, CF=13750 kHz, AT=24 dB, ADT=8 dB, b=14
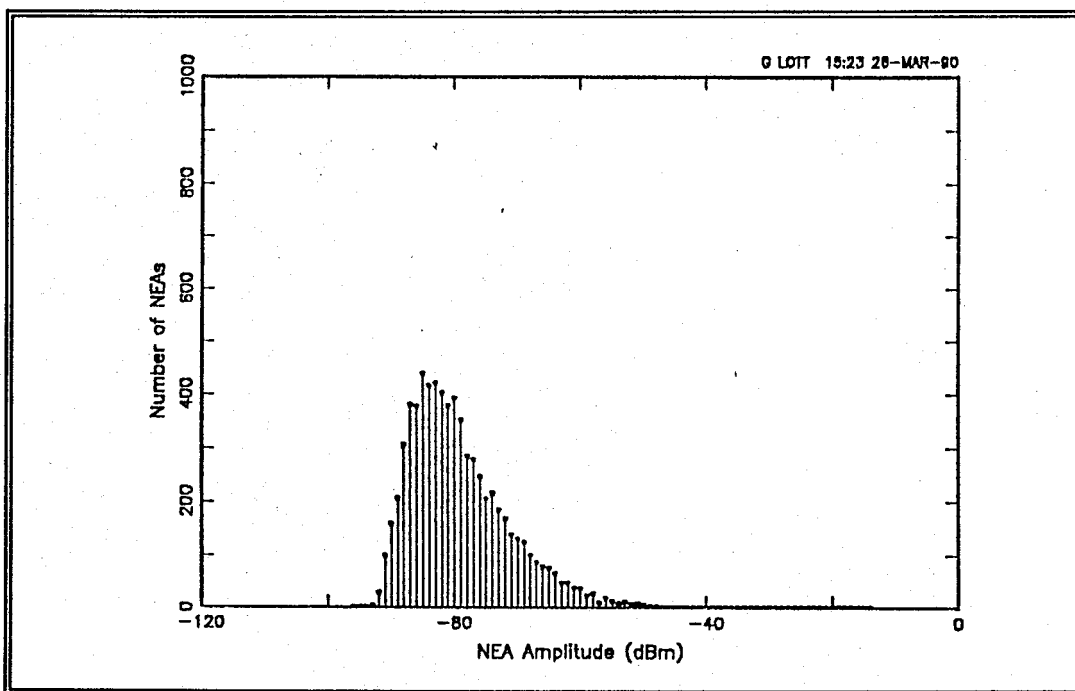
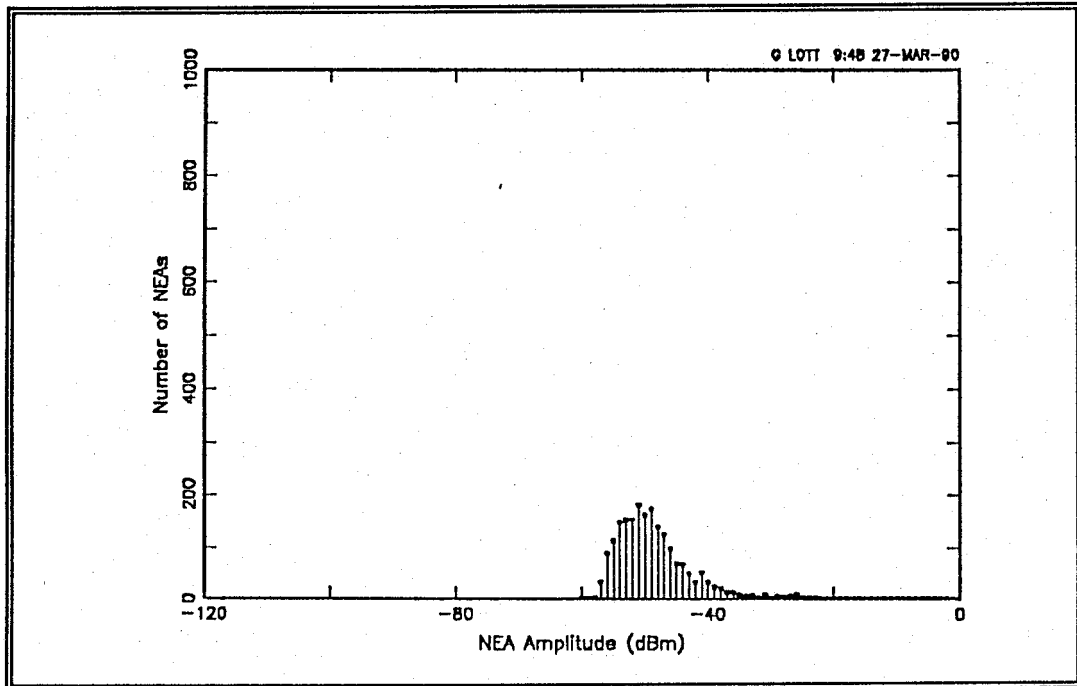**Figure B.18** - Histogram for Data Set 14, 19 Apr 89, 1351-1408, CF=13750 kHz, AT=24 dB, ADT=8 dB, b=12
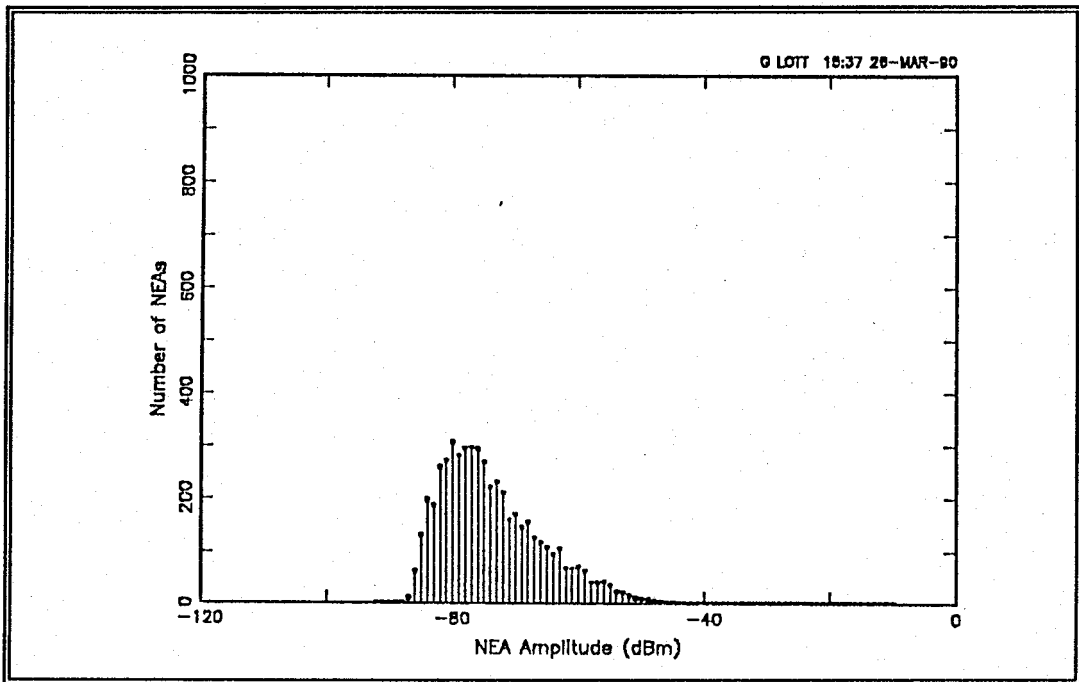
Figure B.19 - Histogram for Data Set 15, 19 Apr 89, 1409-1424, CF=13750 kHz, AT=28 dB, ADT=8 dB, b=14
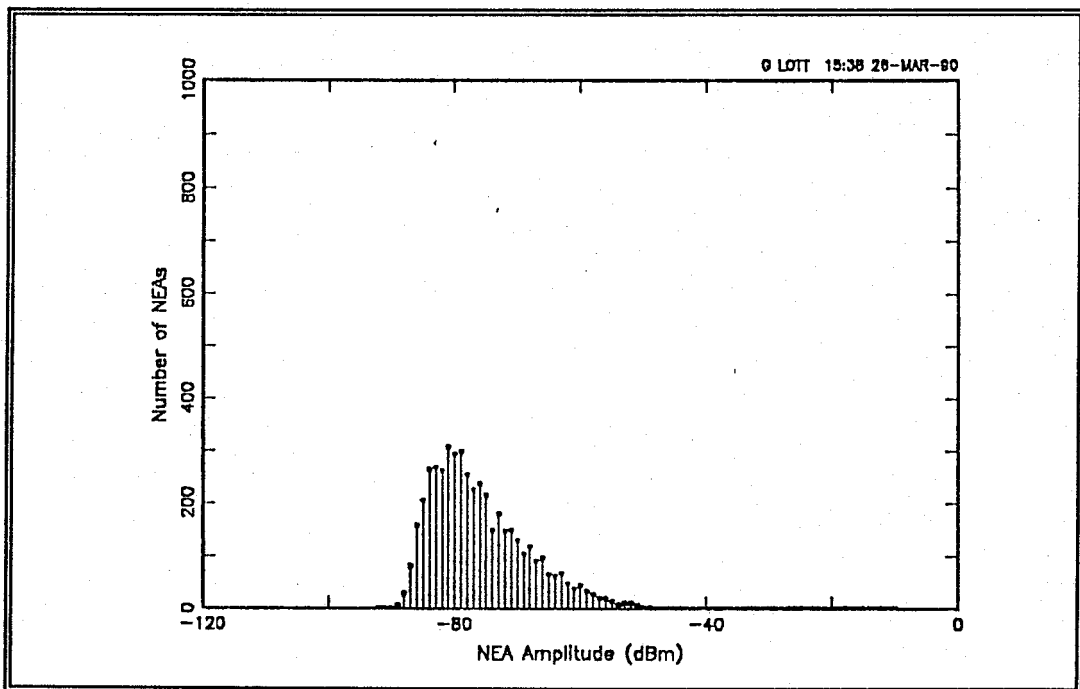
Figure B.20 - Histogram for Data Set 15, 19 Apr 89, 1409-1424, CF=13750 kHz, AT=28 dB, ADT=8 dB, b=12

Figure B.21 - Histogram for Data Set 16, 19 Apr 89, 1424-1441, CF=13750 kHz, AT=32 dB, ADT=8 dB, b=14
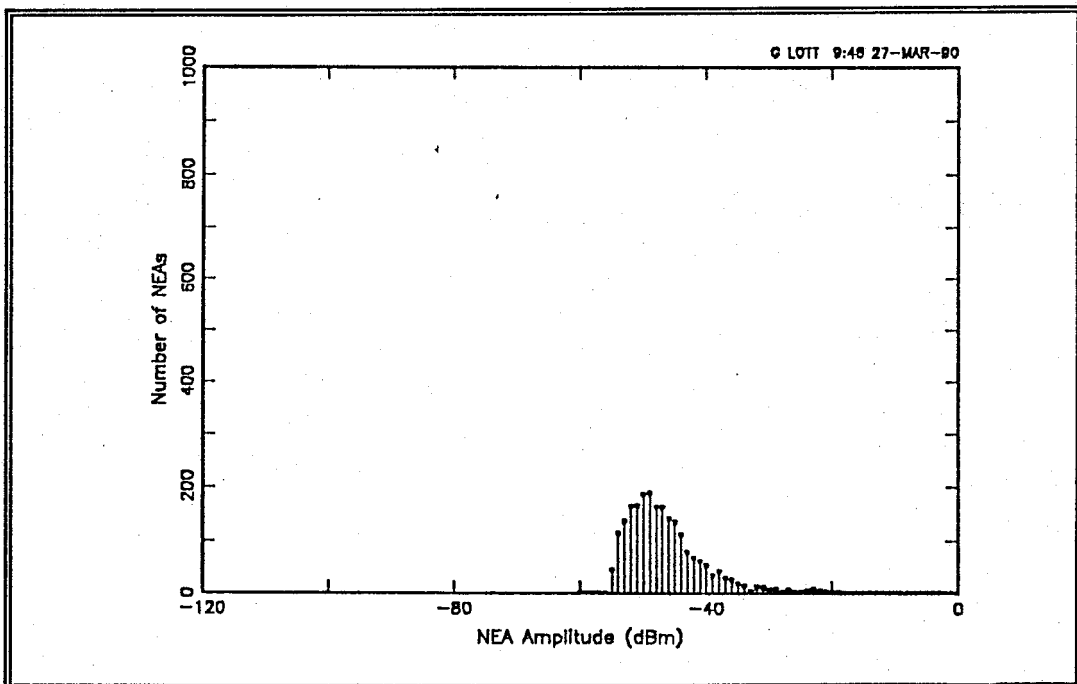

Figure B.22 - Histogram for Data Set 16, 19 Apr 89, 1424-1441, CF=13750 kHz, AT=32 dB, ADT=8 dB, b=12

Figure B.23 - Histogram for Data Set 17, 19 Apr 89, 1442-1457, CF=13750 kHz, AT=36 dB, ADT=8 dB, b=14

Figure B.24 - Histogram for Data Set 17, 19 Apr 89, 1442-1457, CF=13750 kHz, AT=36 dB, ADT=8 dB, b=12

191
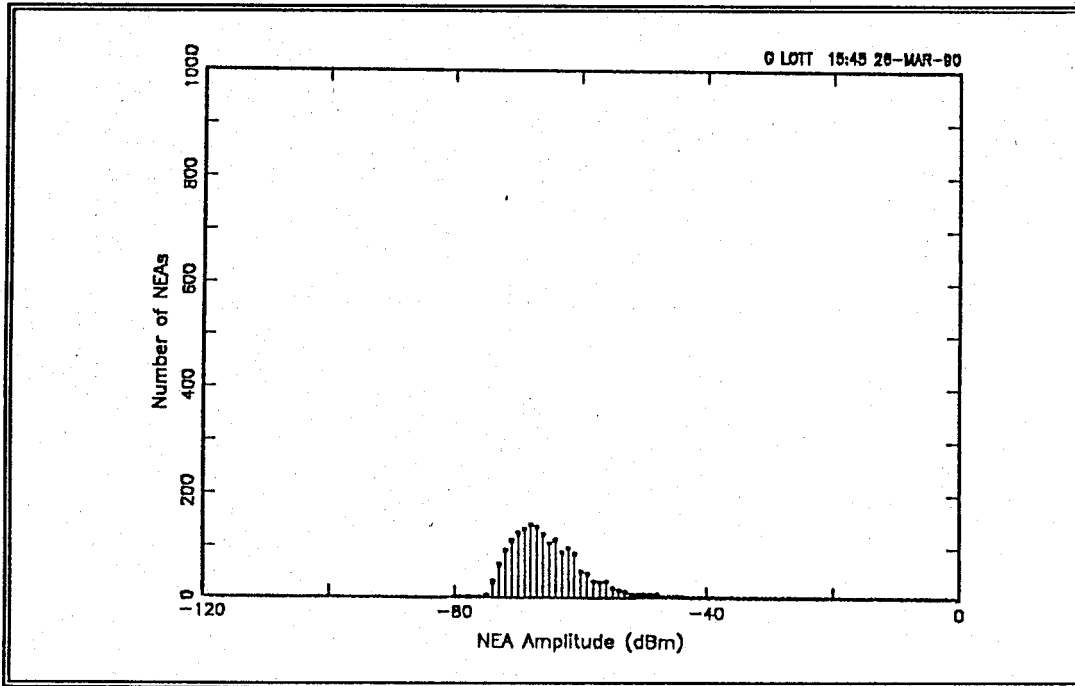
Figure B.25 - Histogram for Data Set 18, 19 Apr 89, 1457-1512, CF=13750 kHz, AT=40 dB, ADT=8 dB, b=14

Figure B.26 - Histogram for Data Set 18, 19 Apr 89, 1457-1512, CF=13750 kHz, AT=40 dB, ADT=8 dB, b=12

Figure B.27 - Histogram for Data Set 19, 19 Apr 89, 2024-2039, CF=4500 kHz, AT=60 dB, ADT=8 dB, b=14

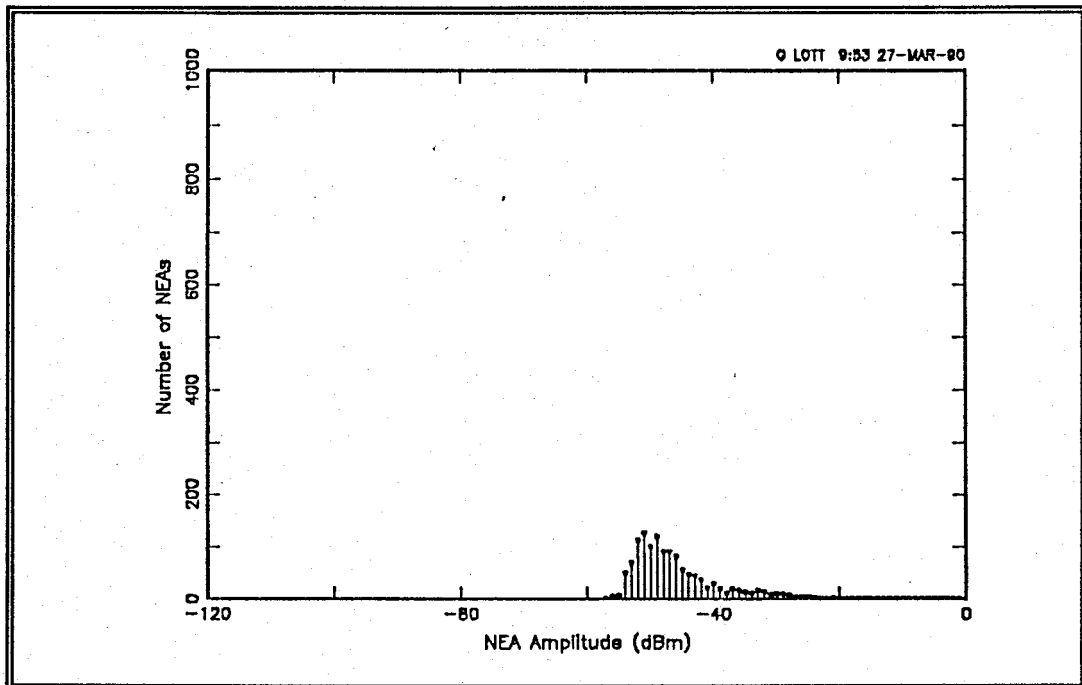**Figure B.28** - Histogram for Data Set 19, 19 Apr 89, 2024-2039, CF=4500 kHz, AT=60 dB, ADT=8 dB, b=12
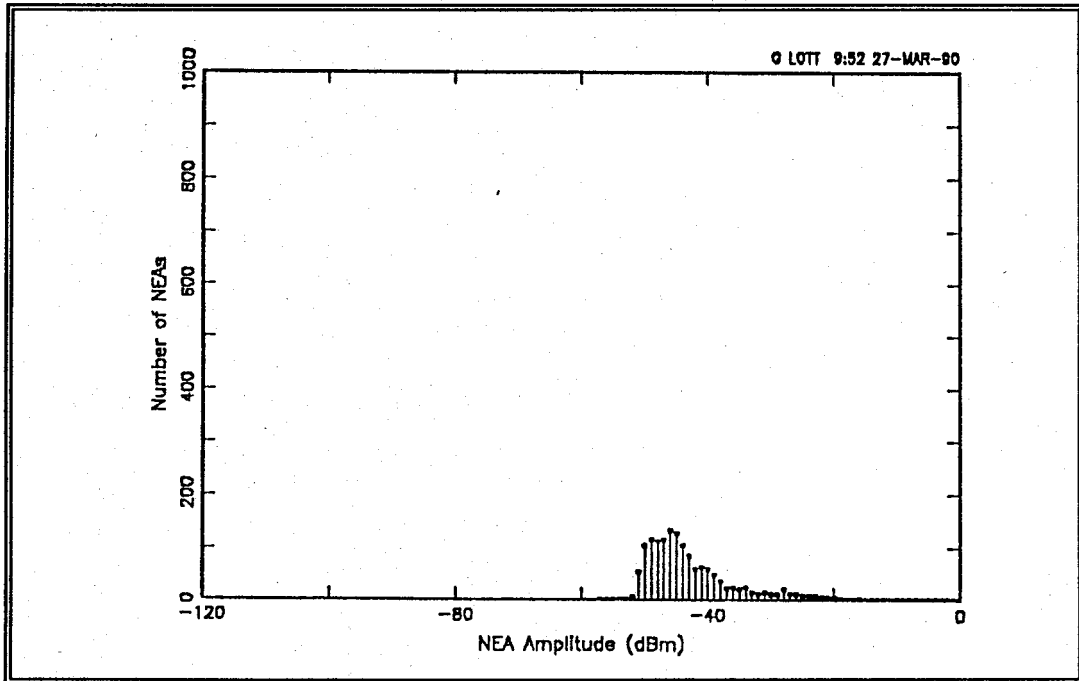
Figure B.29 - Histogram for Data Set 20, 19 Apr 89, 2040-2055, CF=4500 kHz, AT=63 dB, ADT=8 dB, b=14

Figure B.30 - Histogram for Data Set 20, 19 Apr 89, 2040-2055, CF=4500 kHz, AT=63 dB, ADT=8 dB, b=12
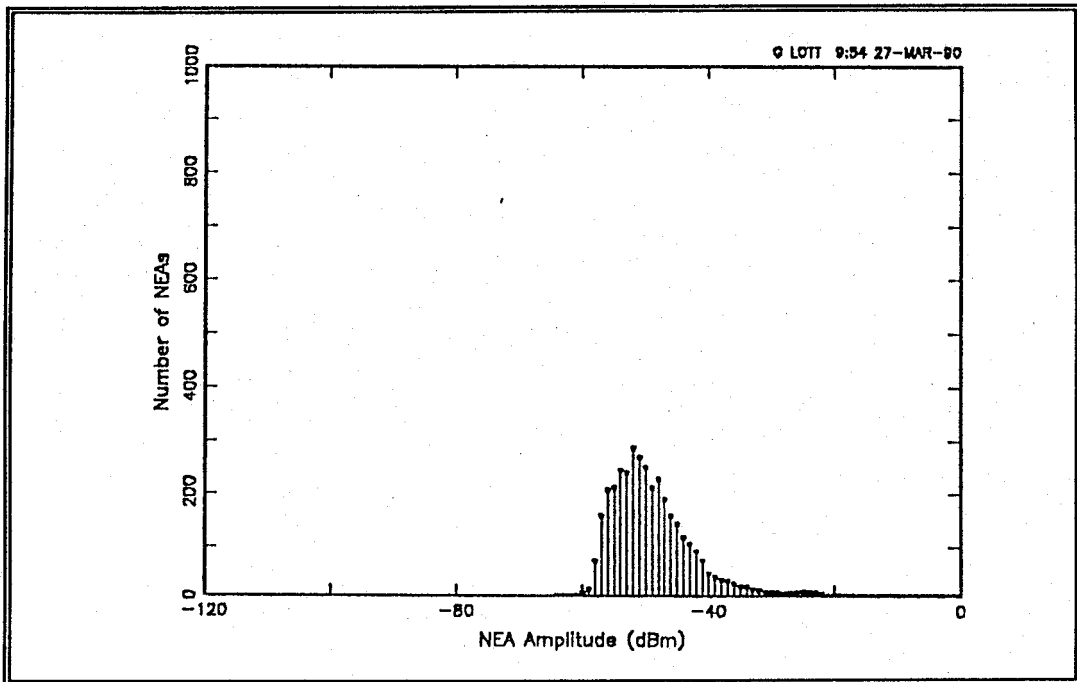
194

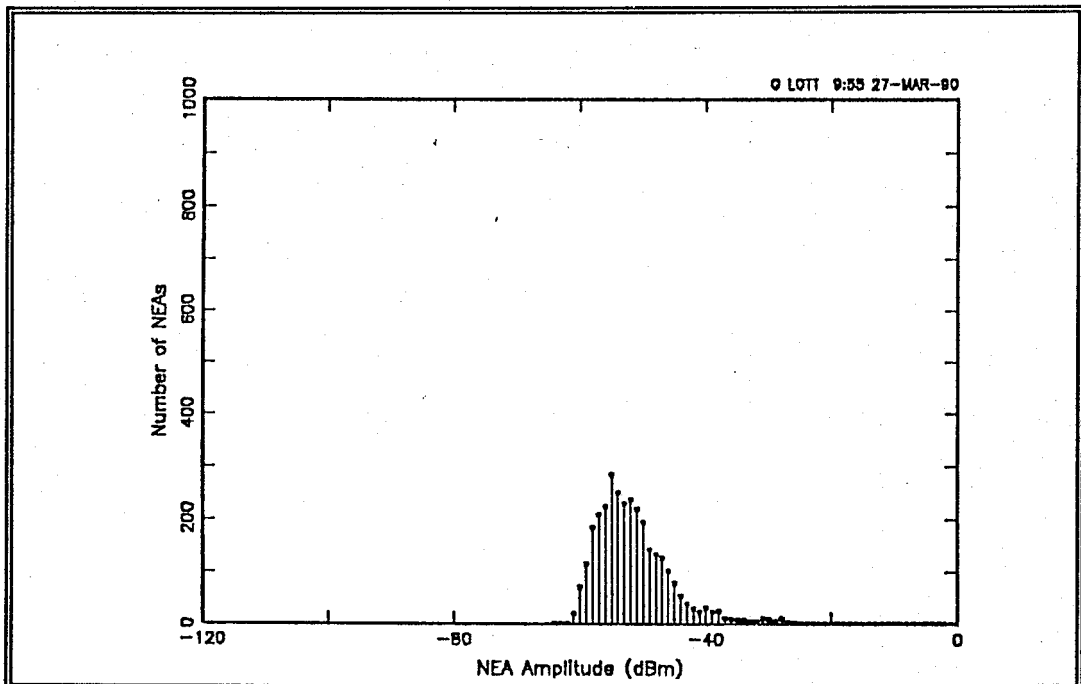**Figure B.31** - Histogram for Data Set 21, 19 Apr 89, 2056-2111, CF=4500 kHz, AT=56 dB, ADT=8 dB, b=14

Figure B.32 - Histogram for Data Set 21, 19 Apr 89, 2056-2111, CF=4500 kHz, AT=56 dB, ADT=8 dB, b=12
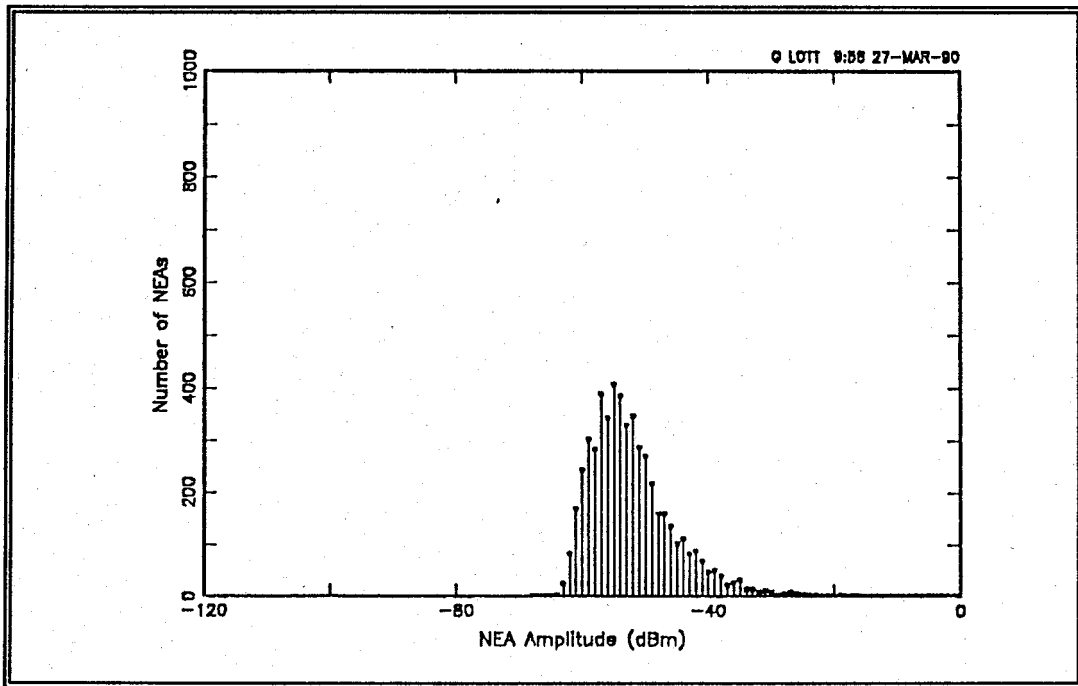
195

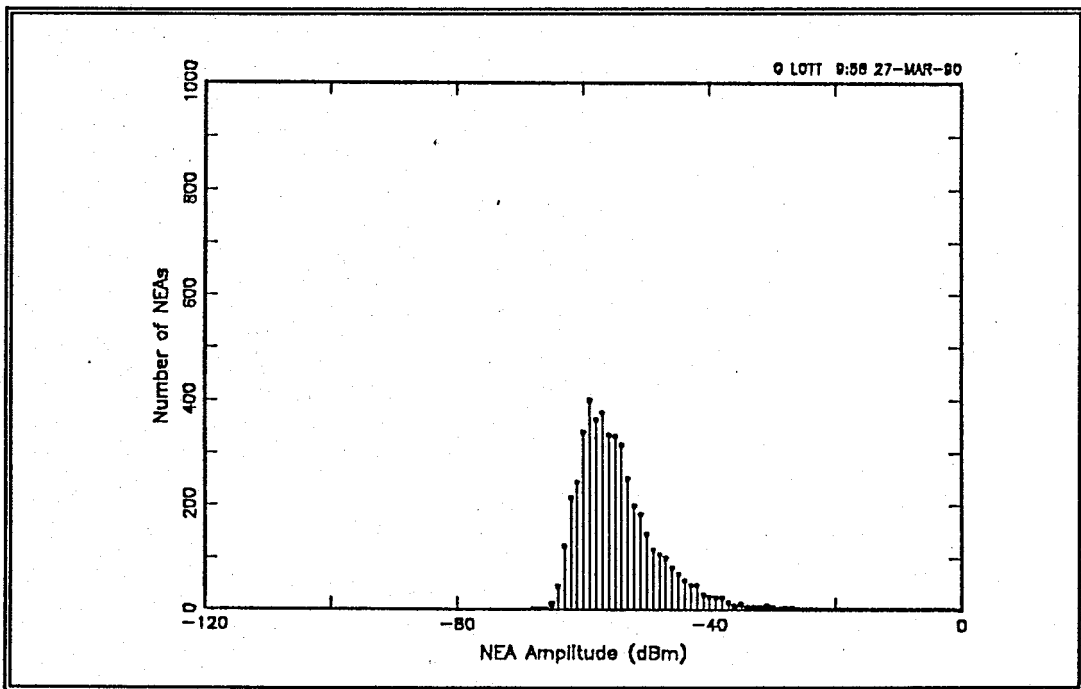**Figure B.33** - Histogram for Data Set 22, 19 Apr 89, 2111-2126, CF=4500 kHz, AT=52 dB, ADT=8 dB, b=14

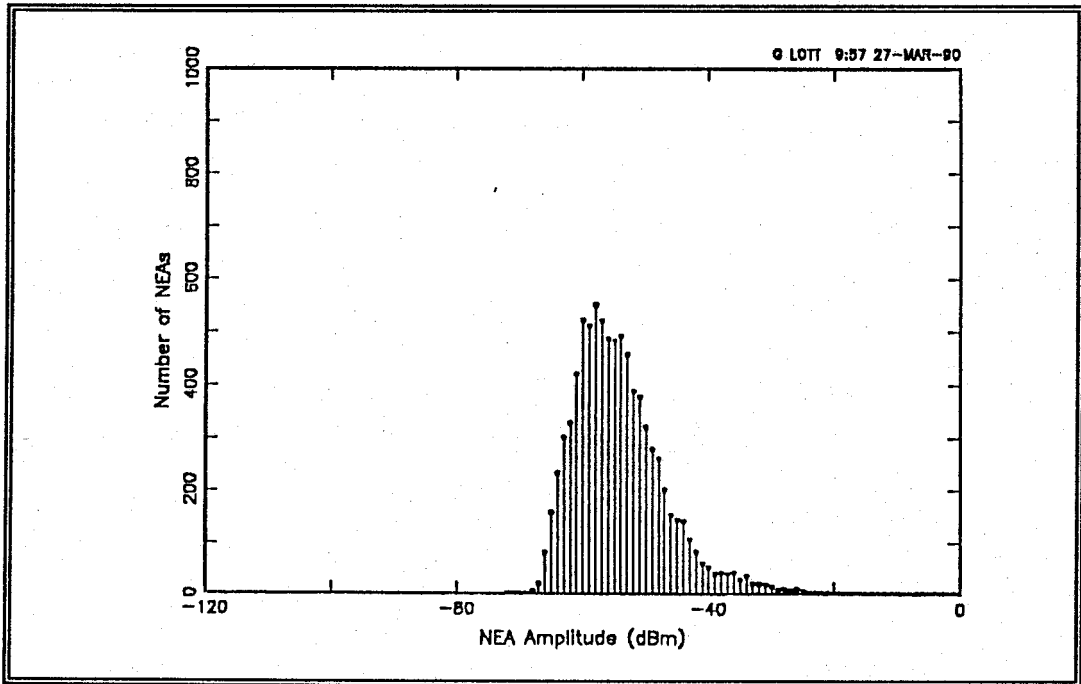**Figure B.34** - Histogram for Data Set 22, 19 Apr 89, 2111-2126, CF=4500 kHz, AT=52 dB, ADT=8 dB, b=12

196

Figure B.35 - Histogram for Data Set 23, 19 Apr 89, 2127-2142, CF=4500 kHz, AT=48 dB, ADT=8 dB, b=14
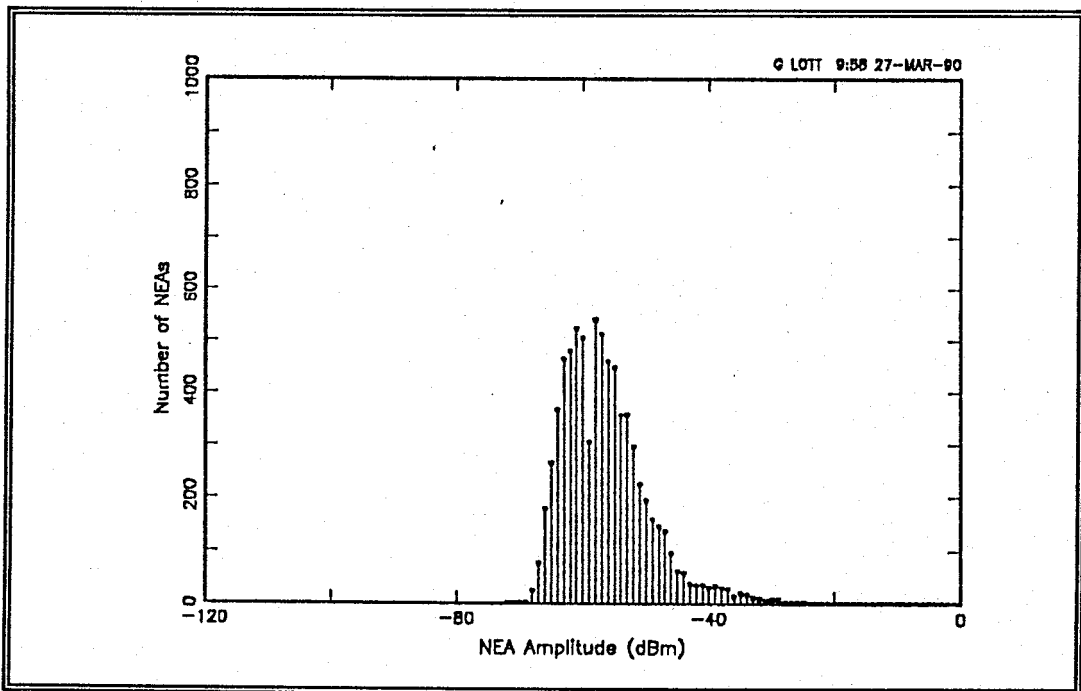

Figure B.36 - Histogram for Data Set 23, 19 Apr 89, 2127-2142, CF=4500 kHz, AT=48 dB, ADT=8 dB, b=12
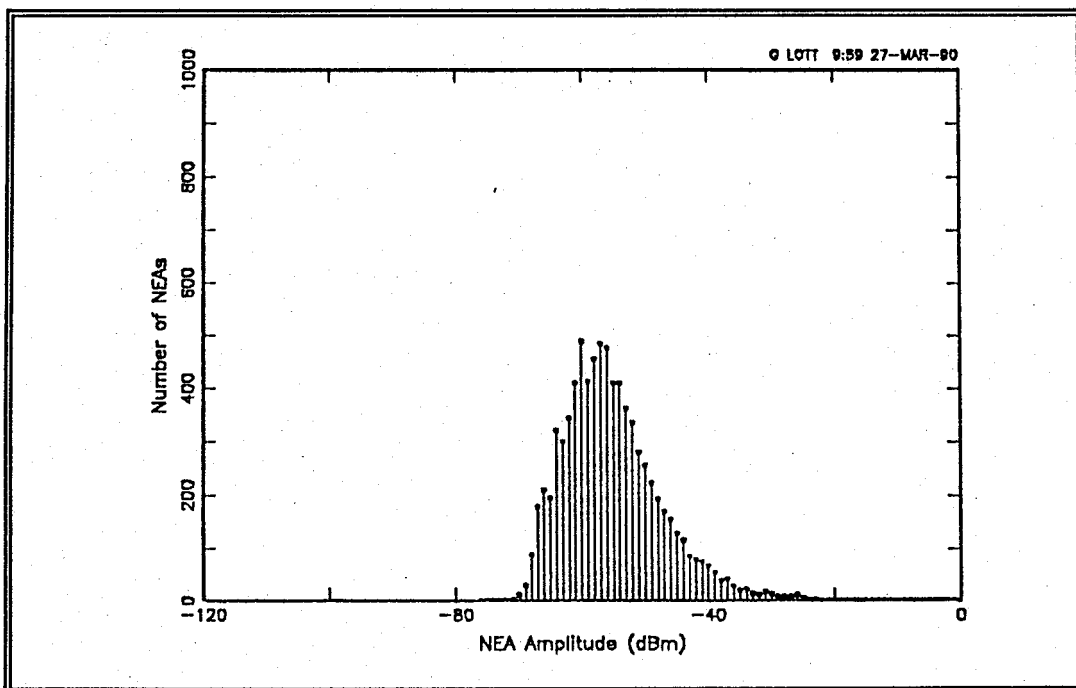
Figure B.37 - Histogram for Data Set 24, 19 Apr 89, 2142-2157, CF=4500 kHz, AT=44 dB, ADT=8 dB, b=14
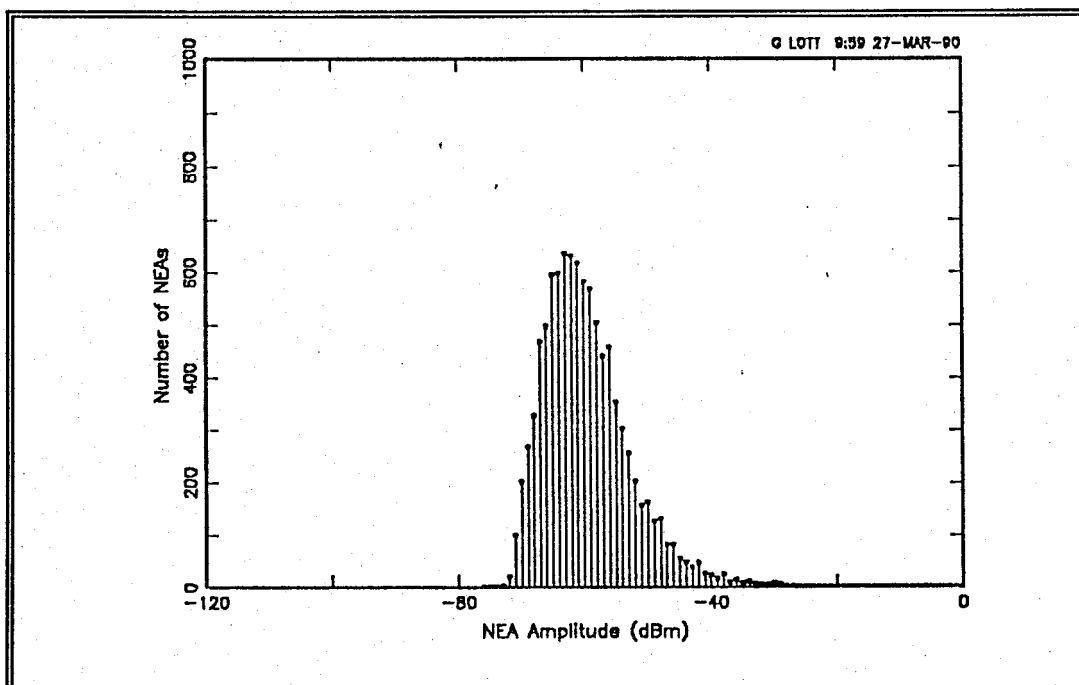

Figure B.38 - Histogram for Data Set 24, 19 Apr 89, 2142-2157, CF=4500 kHz, AT=44 dB, ADT=8 dB, b=12

Figure B.39 - Histogram for Data Set 25, 19 Apr 89, 2158-2213, CF=4500 kHz, AT=40 dB, ADT=8 dB, b=14
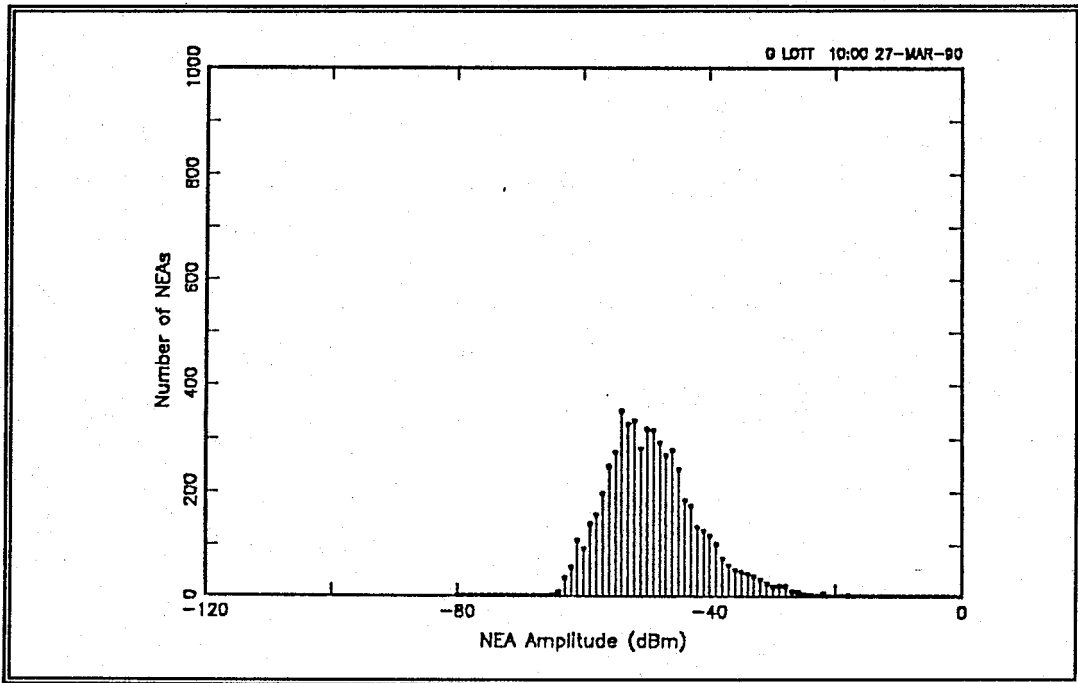

Figure B.40 - Histogram for Data Set 25, 19 Apr 89, 2158-2213, CF=4500 kHz, AT=40 dB, ADT=8 dB, b=12

199
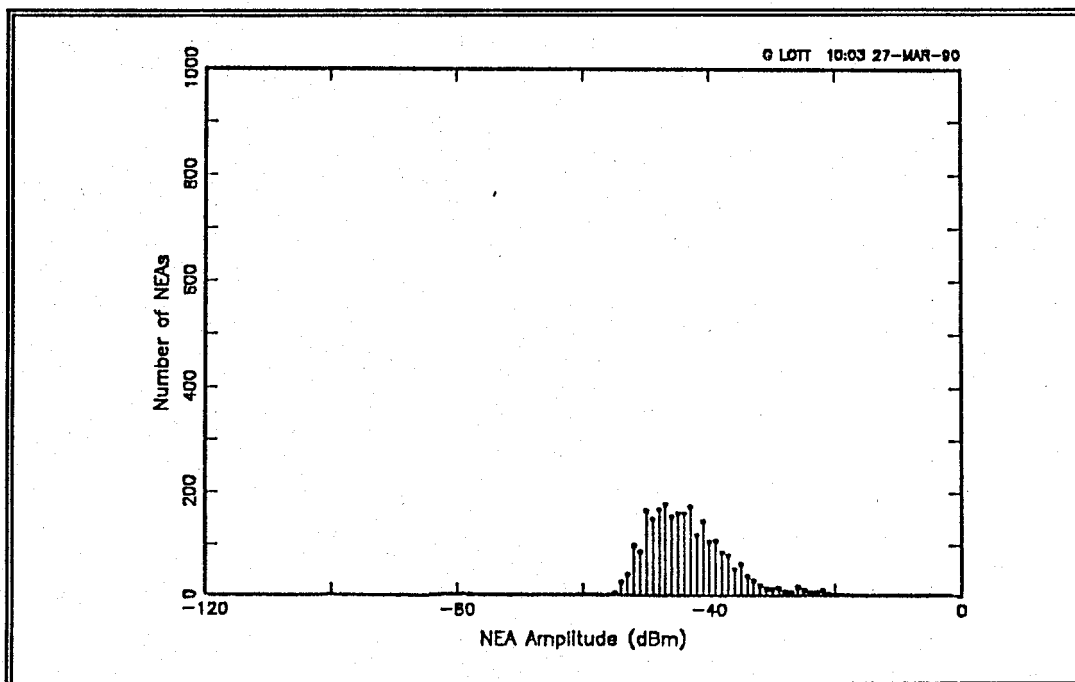
Figure B.41 - Histogram for Data Set 26, 19 Apr 89, 2213-2228, CF=4500 kHz, AT=36 dB, ADT=8 dB, b=14
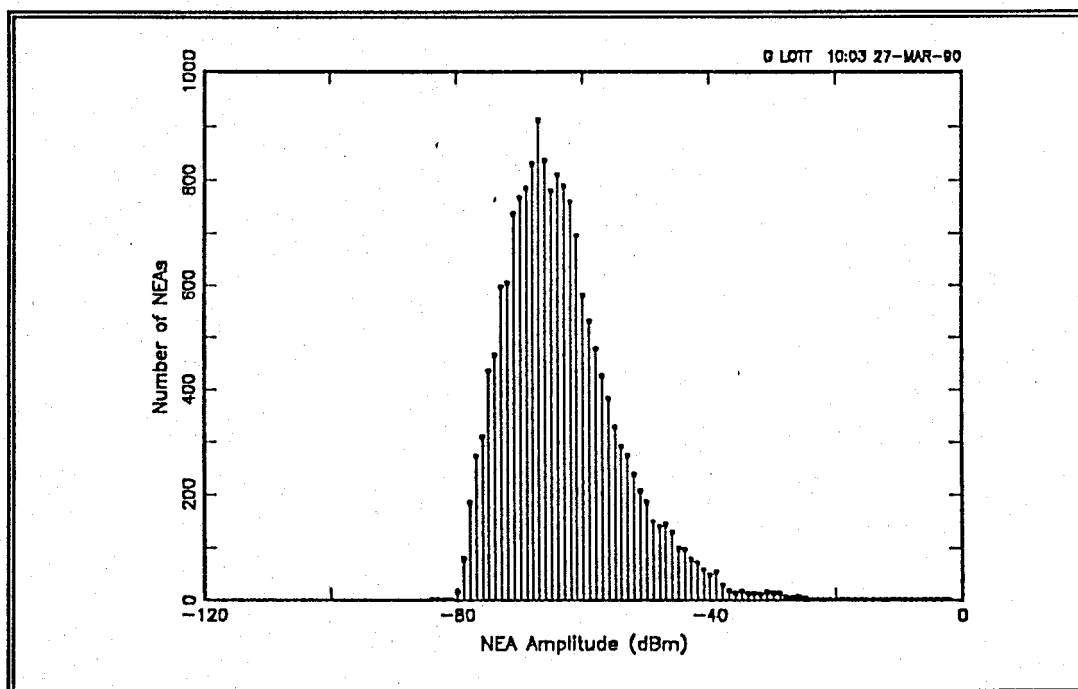
Figure B.42 - Histogram for Data Set 26, 19 Apr 89, 2213-2228, CF=4500 kHz, AT=36 dB, ADT=8 dB, b=12
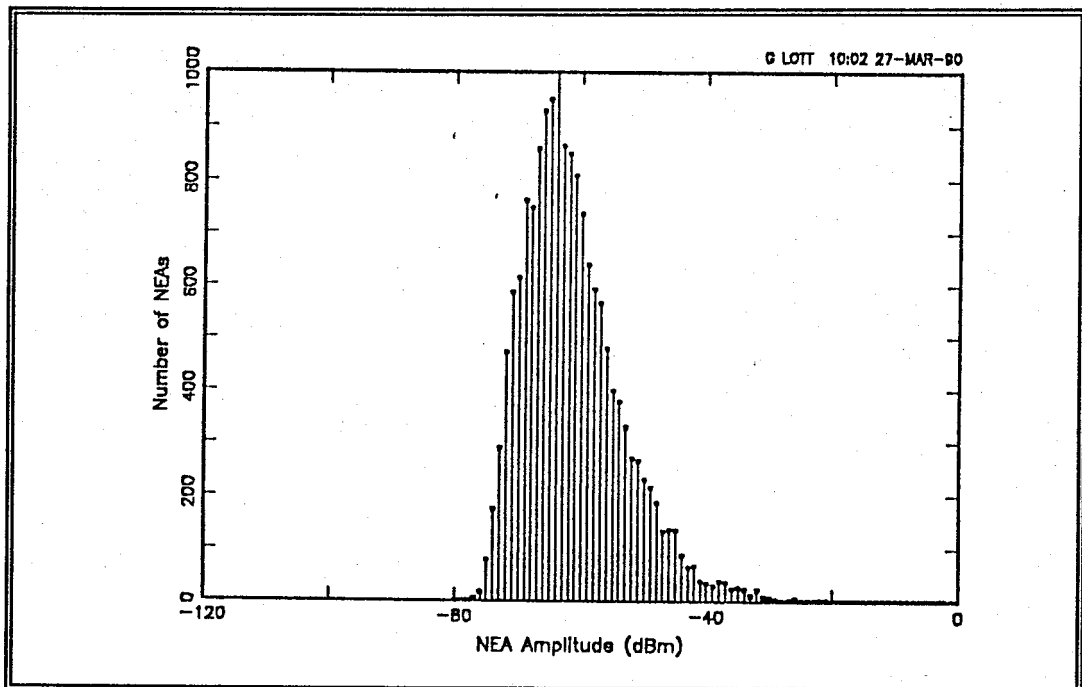
200

Figure B.43 - Histogram for Data Set 30, 22 Apr 89, 1136-1253, CF=14750 kHz, AT=12 dB, ADT=8 dB, b=14
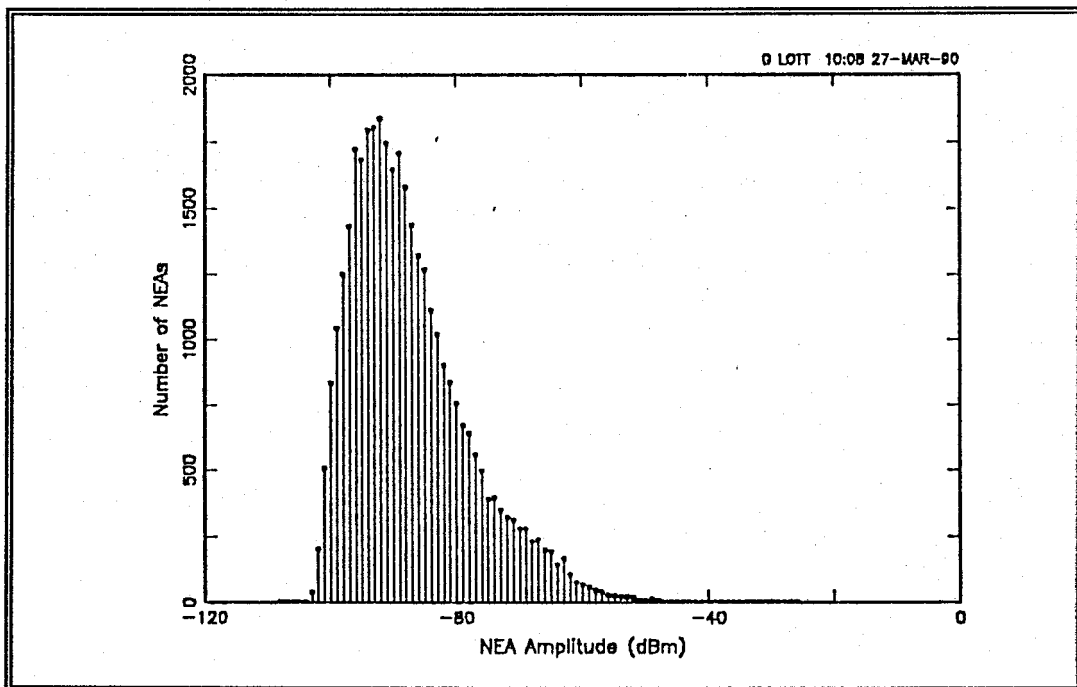
Figure B.44 - Histogram for Data Set 31, 22 Apr 89, 1259-1344, CF=13750 kHz, AT=12 dB, ADT=8 dB, b=14
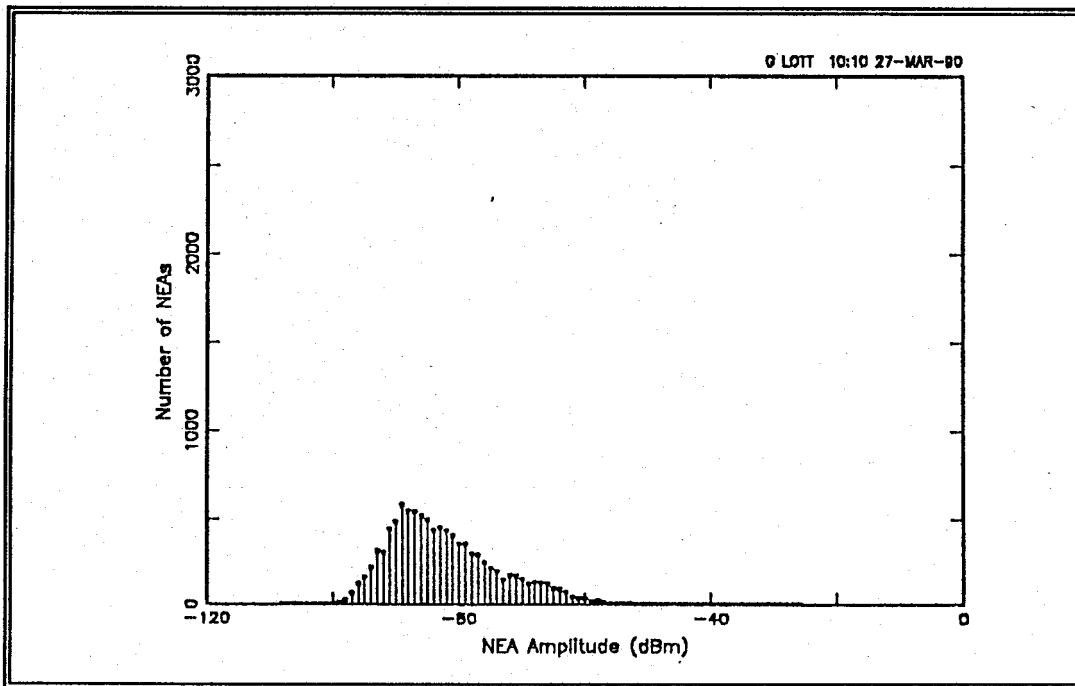
Figure B.45 - Histogram for Data Set 32, 22 Apr 89, 1346-1434, CF=13750 kHz, AT=12 dB, ADT=16 dB, b=14
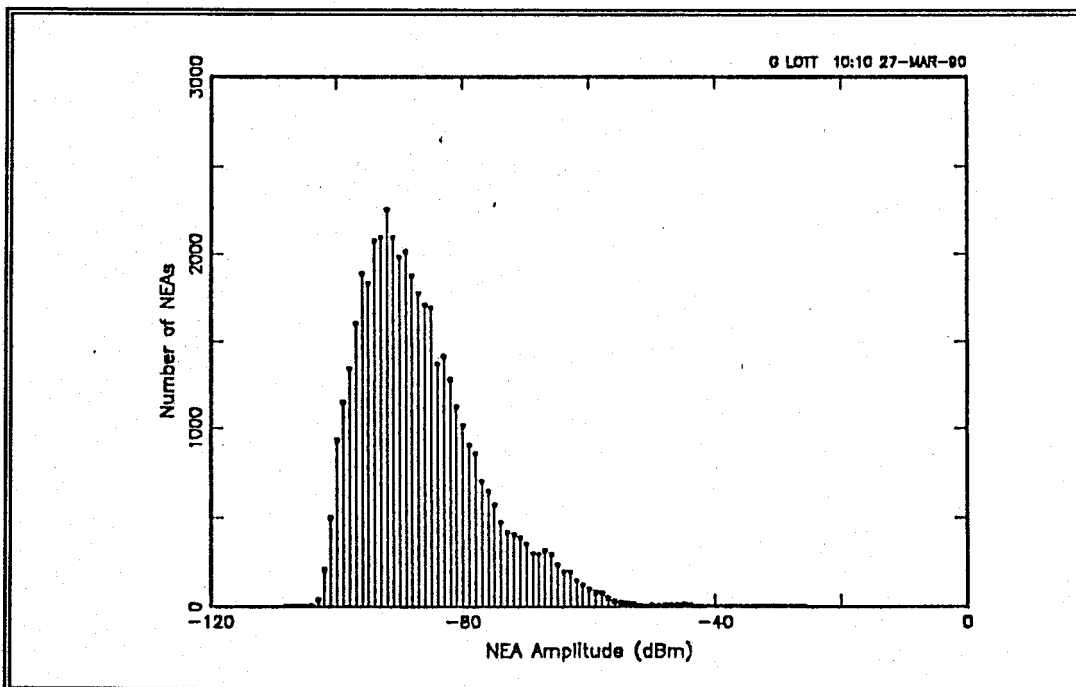
Figure B.46 - Histogram for Data Set 32, 22 Apr 89, 1346-1434, CF=13750 kHz, AT=12 dB, ADT=8 dB, b=14
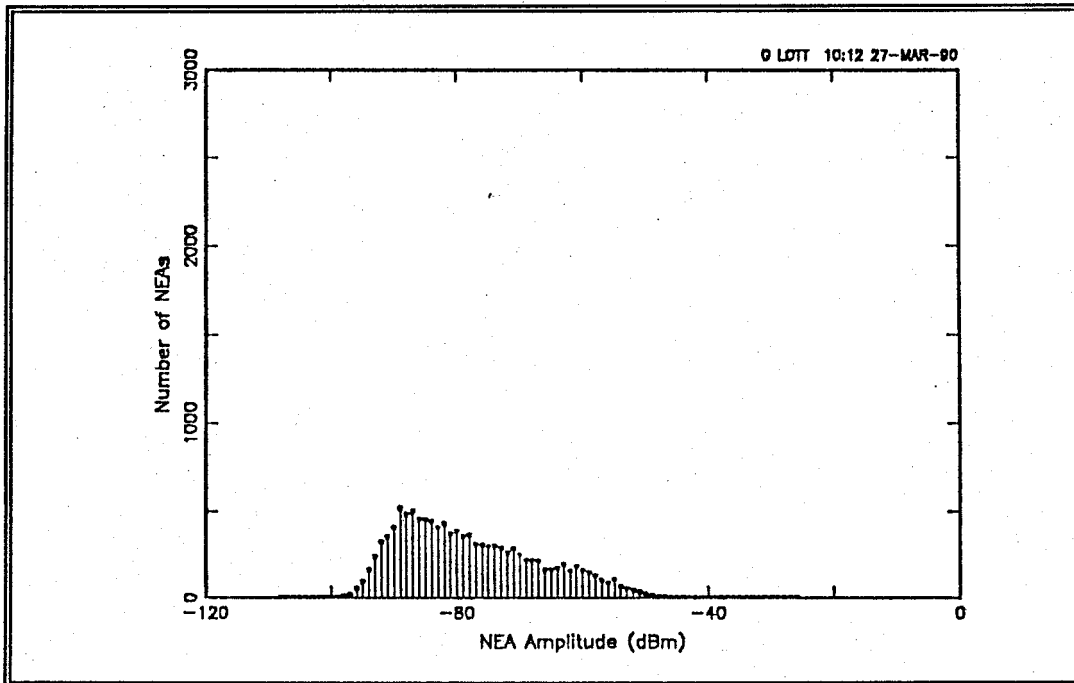
Figure B.47 - Histogram for Data Set 33, 22 Apr 89, 1435-1521, CF=7750 kHz, AT=12 dB, ADT=16 dB, b=14

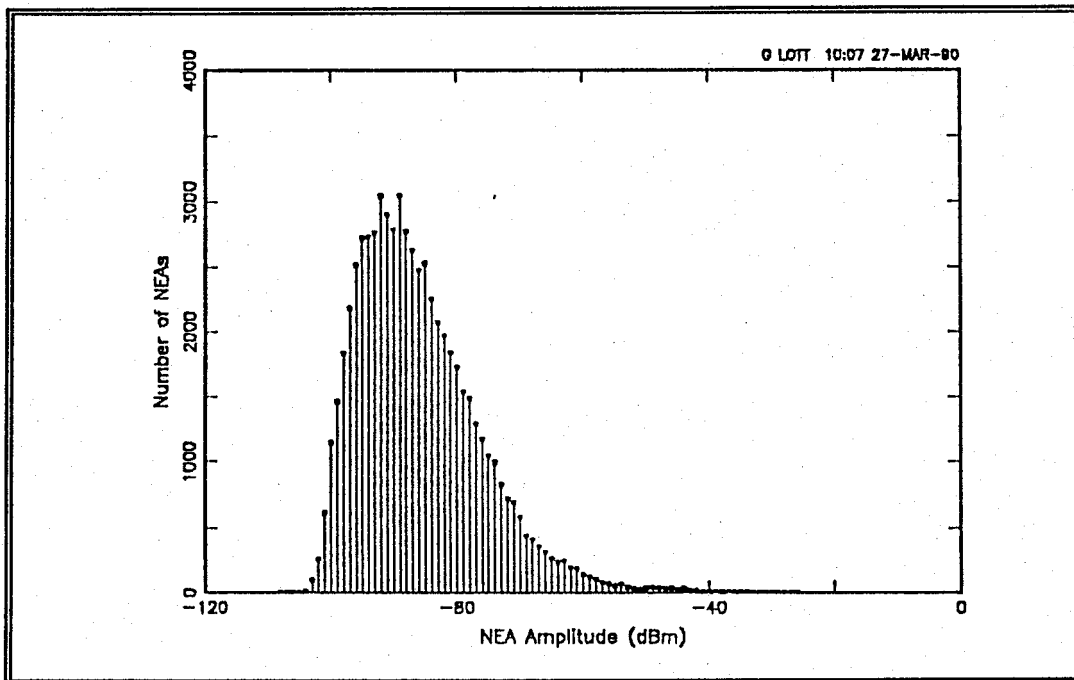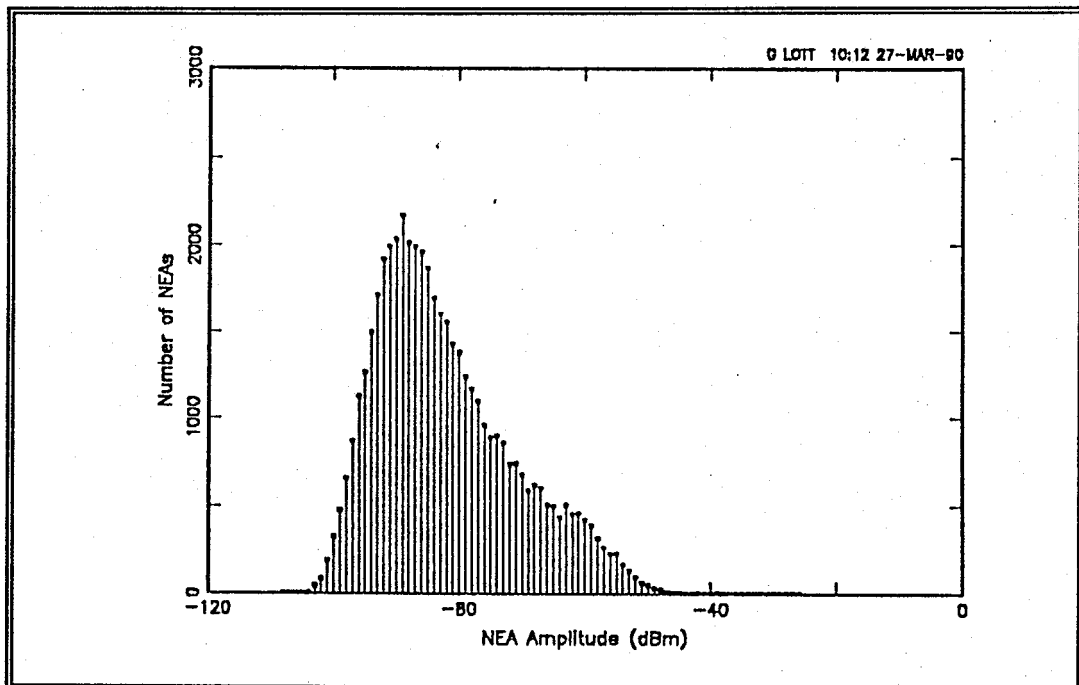**Figure B.48** - Histogram for Data Set 33, 22 Apr 89, 1435-1521, CF=7750 kHz, AT=12 dB, ADT=8 dB, b=14
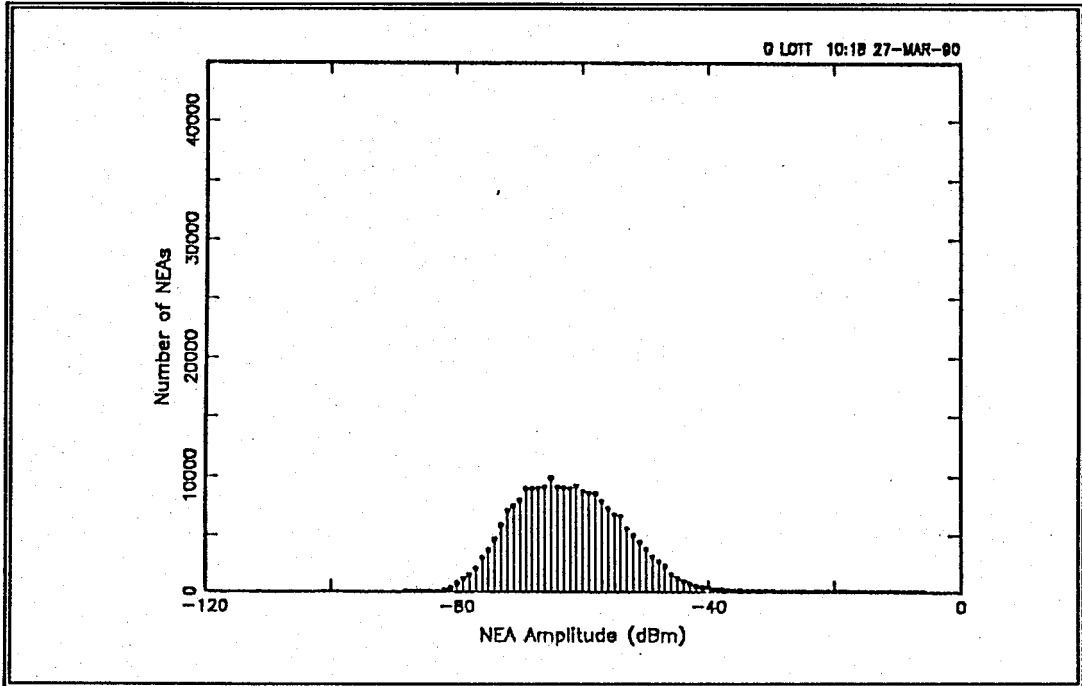
Figure B.49 - Histogram for Data Set 34, 22-23 Apr 89, 1524-0559, CF=7750 kHz, AT=32 dB, ADT=16 dB, b=14
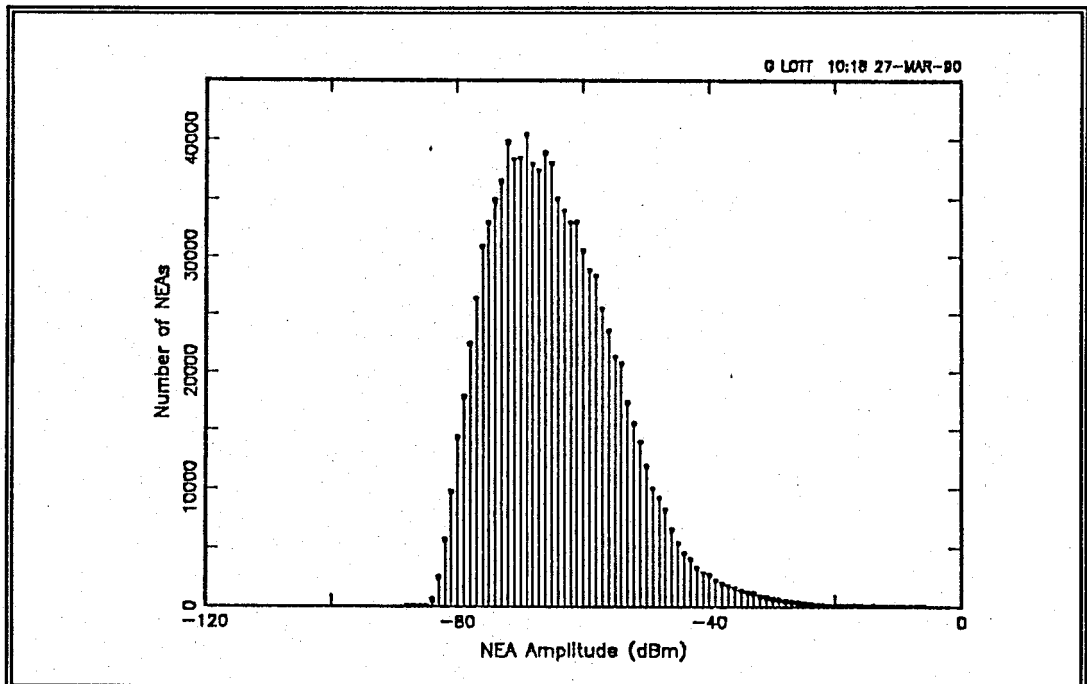
Figure B.50 - Histogram for Data Set 34, 22-23 Apr 89, 1524-0559, CF=7750 kHz, AT=32 dB, ADT=8 dB, b=14

204
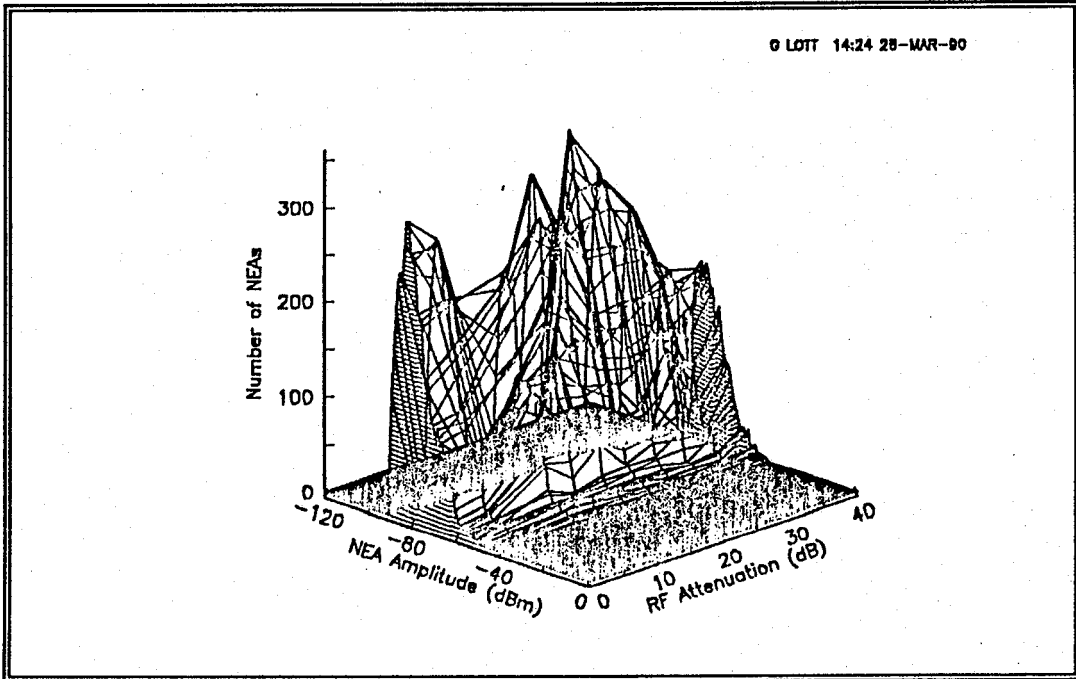
Figure B.51 - Surface Plot of Histograms for Data Sets 8-18, 19 Apr 89, CF=13750 kHz, AT=see plot, ADT=8 dB, b=14
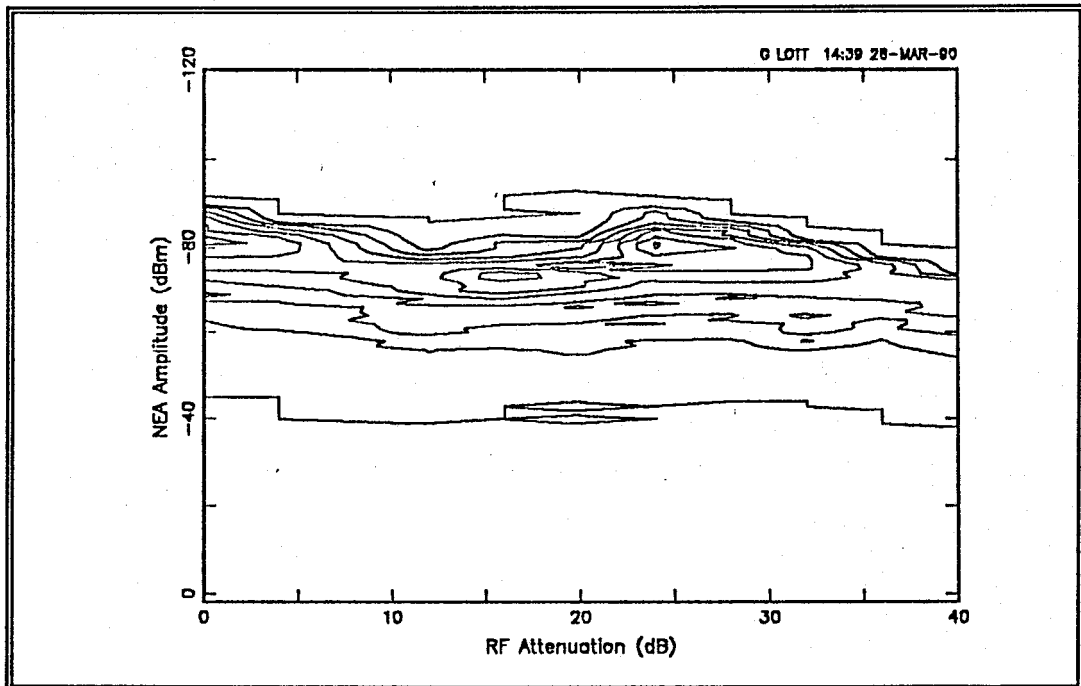
Figure B.52 - Contour Plot of Histograms for Data Sets 8-18, 19 Apr 89, CF=13750 kHz, AT=see plot, ADT=8 dB, b=14, Contour Levels = 50 NEAs
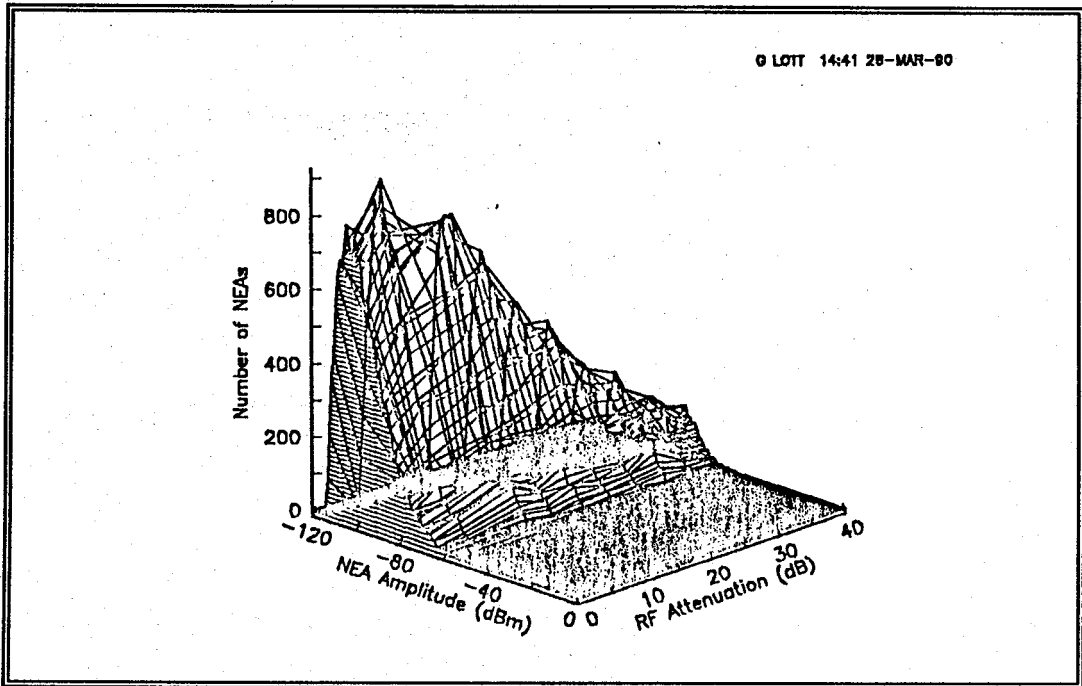
Figure B.53 - Surface Plot of Histograms for Data Sets 8-18, 19 Apr 89, CF=13750 kHz, AT=see plot, ADT=8 dB, b=12
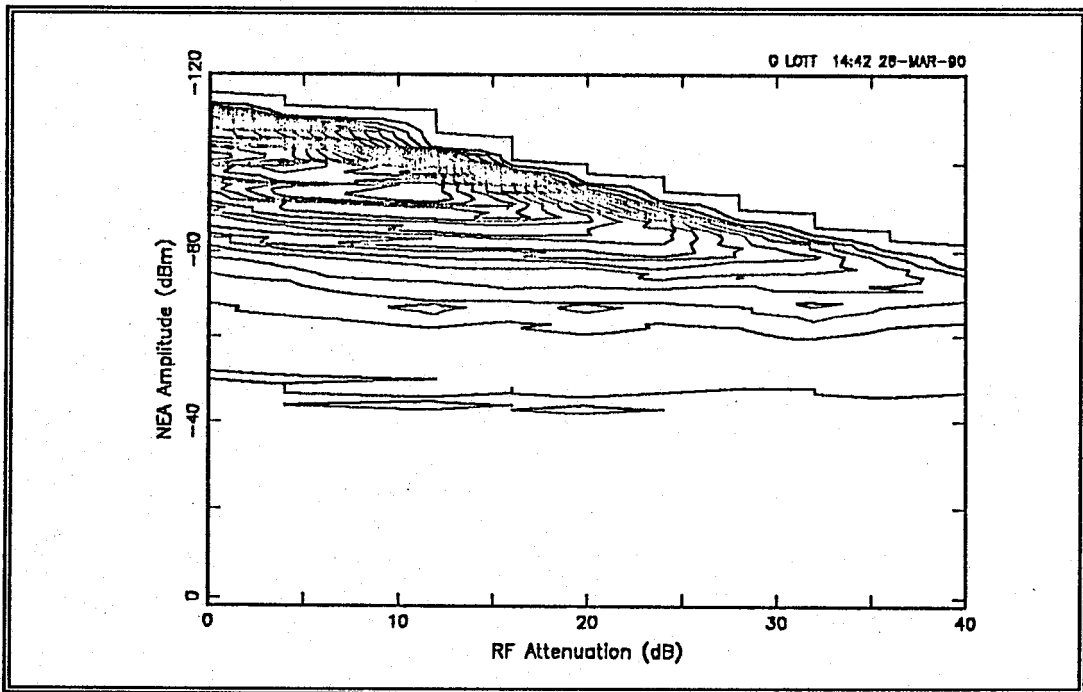
Figure B.54 - Contour Plot of Histograms for Data Sets 8-18, 19 Apr 89, CF=13750 kHz, AT=see plot, ADT=8 dB, b=12, Contour Levels = 50 NEAs

206
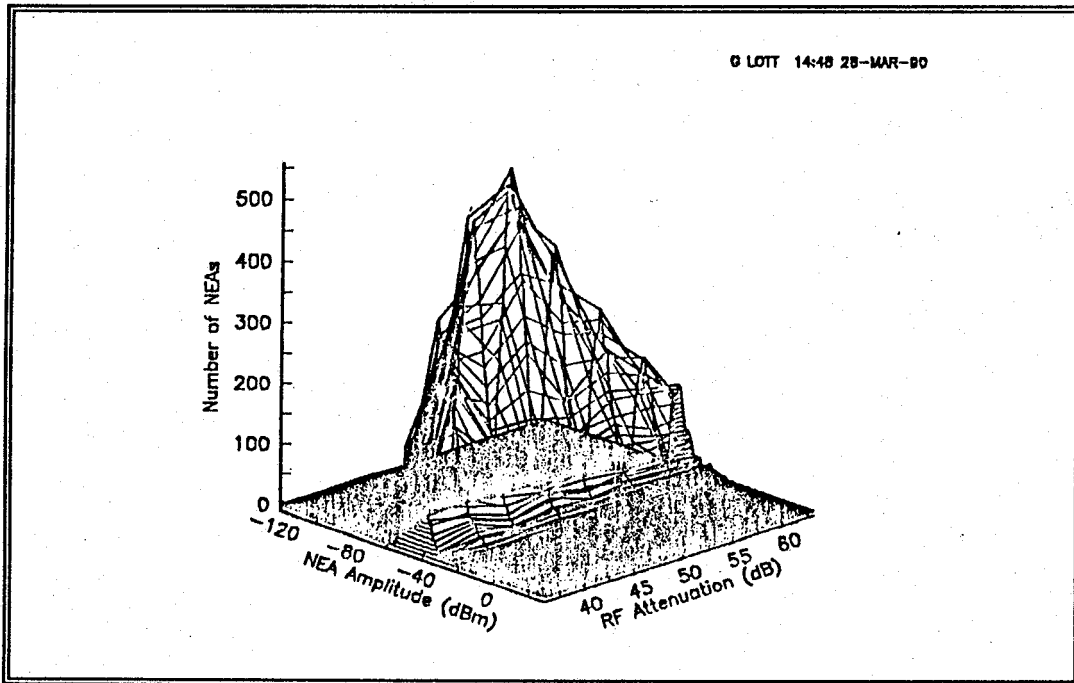
Figure B.55 - Surface Plot of Histograms for Data Sets 19-26, 19 Apr 89, CF=4500 kHz, AT=see plot, ADT=8 dB, b=14
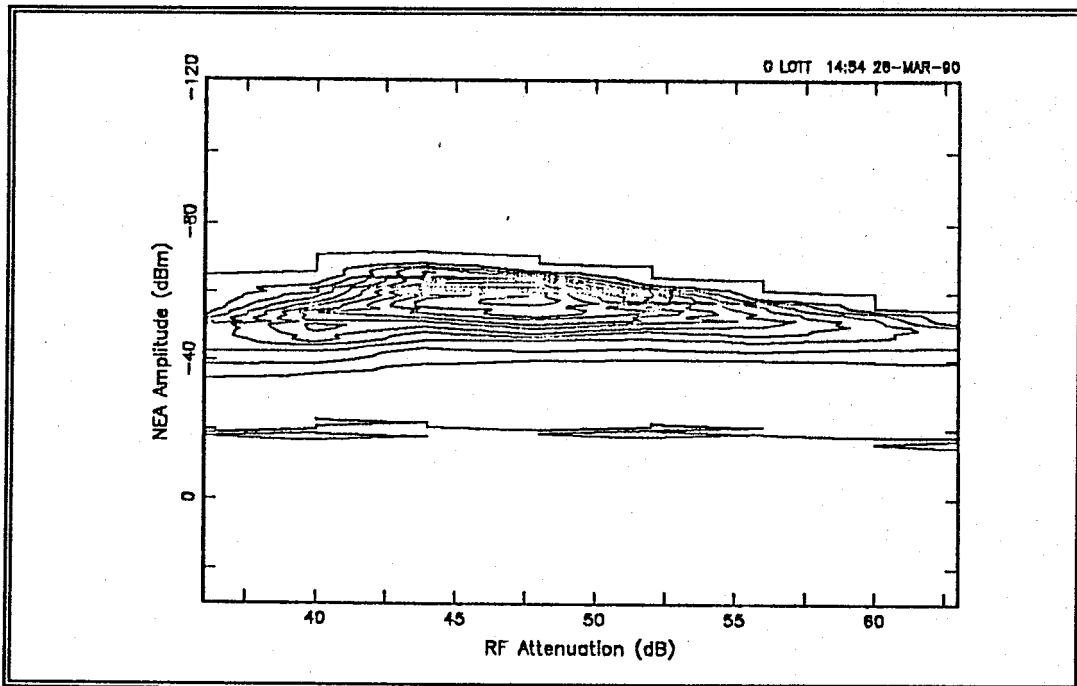
Figure B.56 - Contour Plot of Histograms for Data Sets 19-26, 19 Apr 89, CF=4500 kHz, AT=see plot, ADT=8 dB, b=14, Contour Levels = 50 NEAs

207
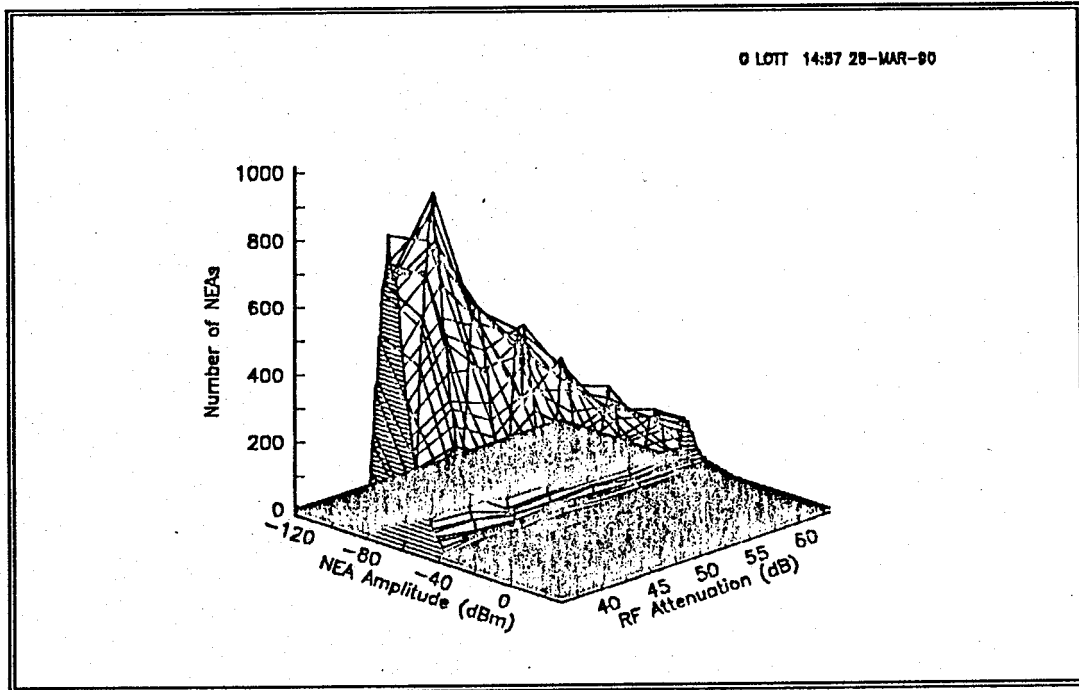
Figure B.57 - Surface Plot of Histograms for Data Sets 19-26, 19 Apr 89, CF=4500 kHz, AT=see plot, ADT=8 dB, b=12
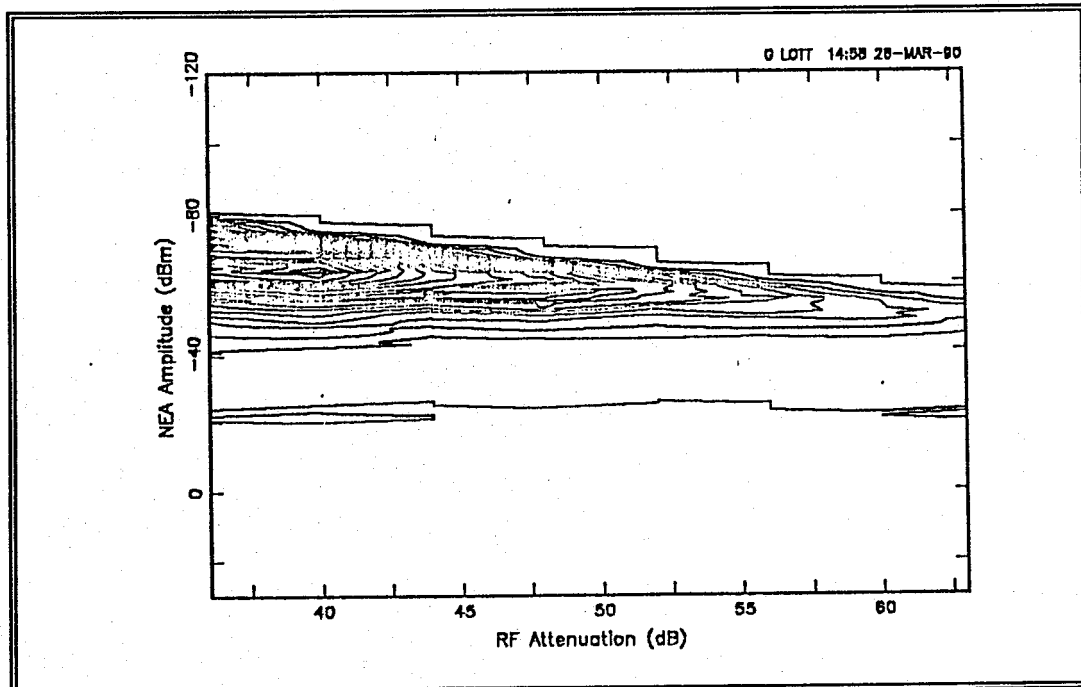
Figure B.58 - Contour Plot of Histograms for Data Sets 19-26, 19 Apr 89, CF=4500 kHz, AT=see plot, ADT=8 dB, b=12, Contour Levels = 50 NEAs
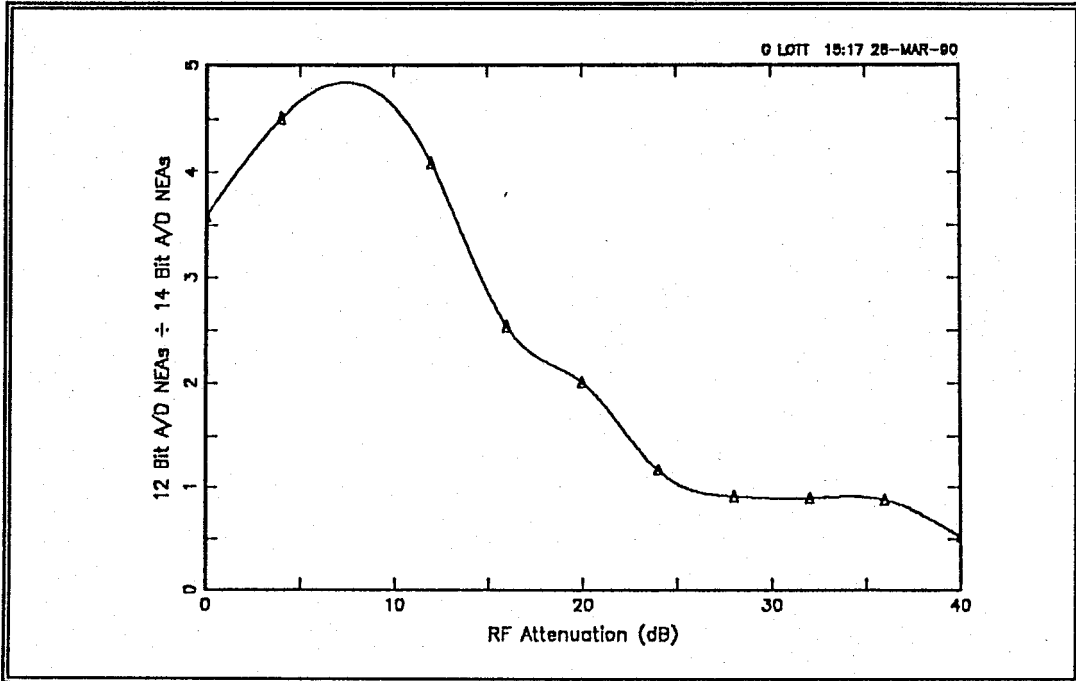
Figure B.59 - Ratio of NEAs on 14-bit A/D to NEAs on 12-bit A/D, Data Sets 8-18, 19 Apr 89, CF=13750 kHz, AT=see plot, ADT=8 dB, CSF
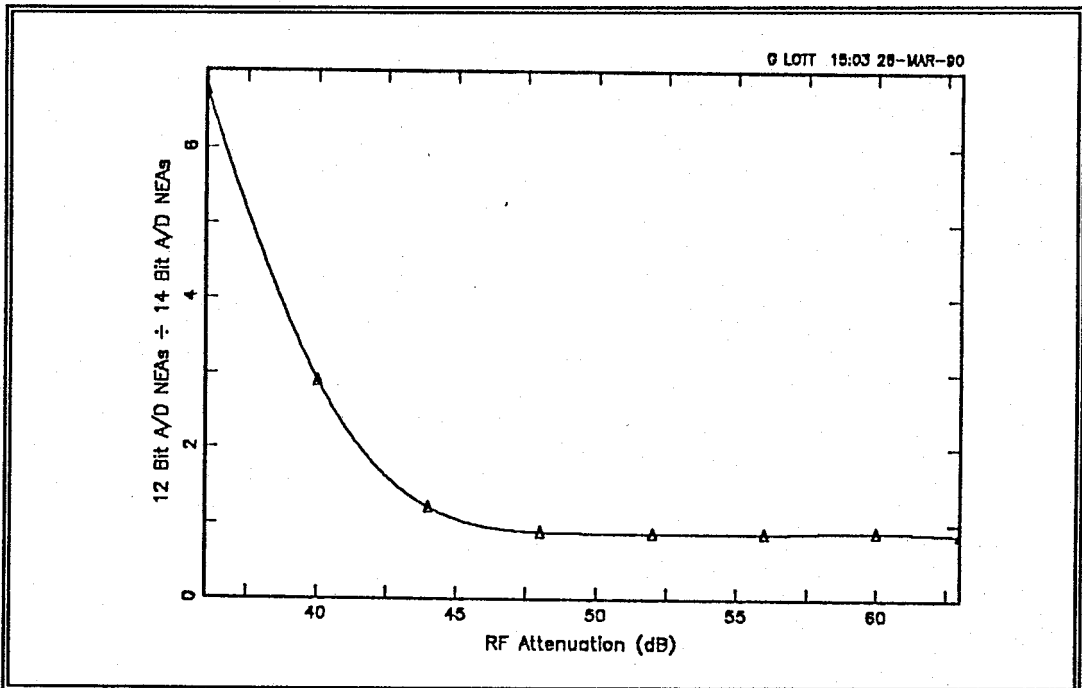
Figure B.60 - Ratio of NEAs on 14-bit A/D to NEAs on 12-bit A/D for Data Sets 19-26, 19 Apr 89, CF=4500 kHz, AT=see plot, ADT=8 dB, CSF

209

APPENDIX C

There are four main classifications of A/D converters. These are:

♦ Servo or delta modulation

♦ Integrating or charge replacement

♦ Parallel threshold

♦ Successive approximation.

The earliest patent filing for a practical electronic A/D converter was in 1948 for an integrating type. There are many variations on these basic structures. This appendix provides an overview of the basic types by combining descriptions from multiple references. [Refs. 35,36,43,107,108]

Figure C.1 diagrams the structure of a servo or delta modulation type A/D converter. Upon each clock pulse, the counter counts up or down depending on the difference between the input voltage and the output of the digital-to-analog (D/A) converter. When the count stops, the counter output is the parallel codeword for that voltage level. This converter scheme is most efficient for monitoring a single signal, and it is simple to implement. The main disadvantage is the slow conversion rate. For a 14-bit converter, conversion could require up to 16384 clock cycles. D/A errors will propagate through the system and appear as codeword errors.
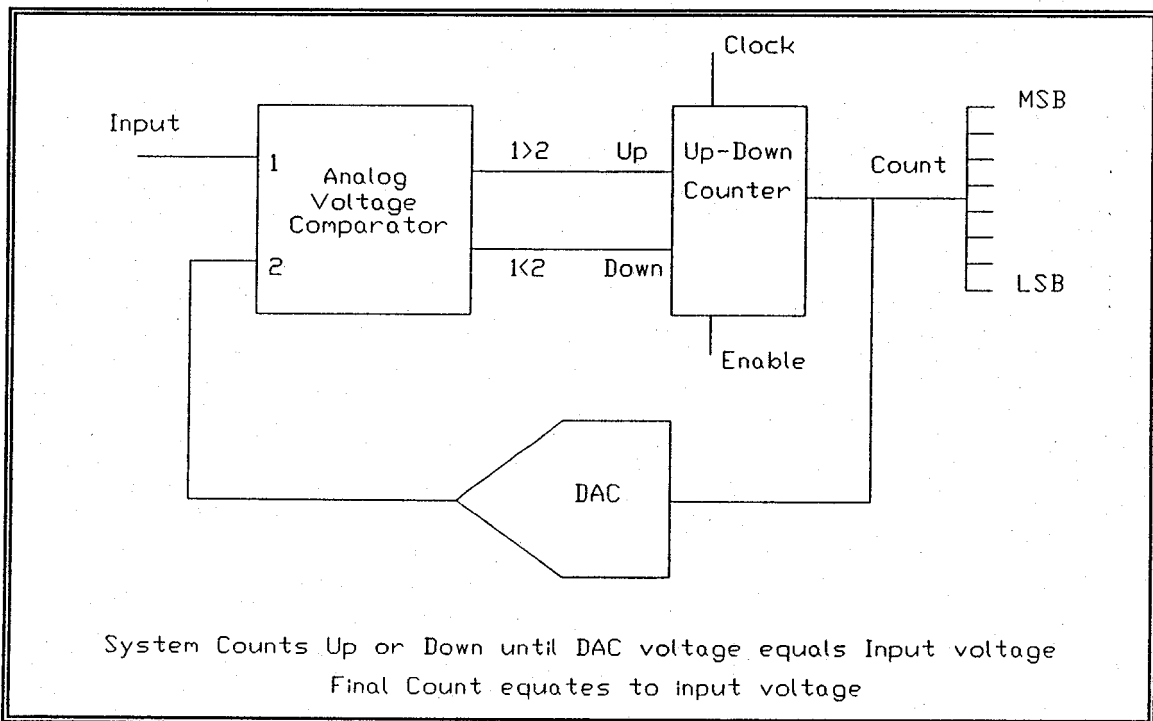
Figure C.1 - Servo or Delta Modulation Structure

Figure C.2 diagrams the structure of an integrating or charge replacement

A/D converter. The input signal, V_{in}, is applied to an integrating device. After a

predetermined time, T_{charge}, the device applies a reference voltage, V_{ref}, of the

opposite polarity to the charge holding device. A counter is used to determine the

time, $T_{discharge}$, from when the discharging voltage is applied to when the charged

device voltage reaches zero. One can determine the value of V_{in} since:

$$\frac{T_{discharge}}{T_{charge}} \propto \frac{V_{in}}{V_{ref}} \qquad (C.1)$$

Conversion is independent of the charged capacitor value and the clocking rate.

The charge replacement structure has excellent differential linearity, and the

211

integrating process filters out high frequency noise. The main disadvantage of the
integrating structure is the slow conversion time.
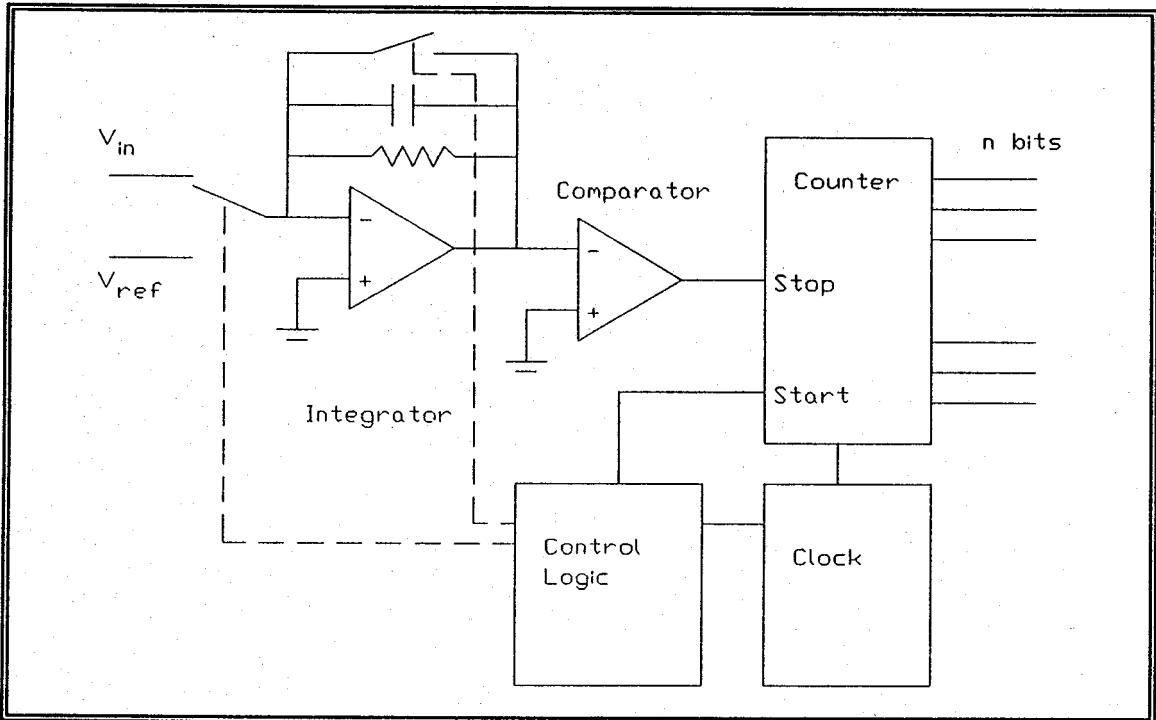
Figure C.2 - Integrating or Charge Replacement Structure

Figure C.3 shows the structure of the parallel or flash type A/D converter.
The tree of voltage comparators acts as a voltage thermometer allowing conversion
in one clock cycle. The tree of resistors divides the reference voltage into 2^n
voltage levels. Comparators with a reference voltage higher than the input voltage
output a positive voltage, usually considered the binary digit one. The comparators
with a reference input voltage less than the input voltage output a negative voltage,
usually considered the binary digit zero. A combinational logic circuit combines the
2^n comparators into a n-bit codeword. The parallel structure provides the fastest
conversion structure, and all higher speed (1 MHz and above) converters

incorporate this conversion technique. The main disadvantage is the circuit complexity. A 16-bit flash converter requires 65536 resistors and 65536 comparators. Differences in resistor values and comparator thresholds result in an increase in differential and integral linearity error.
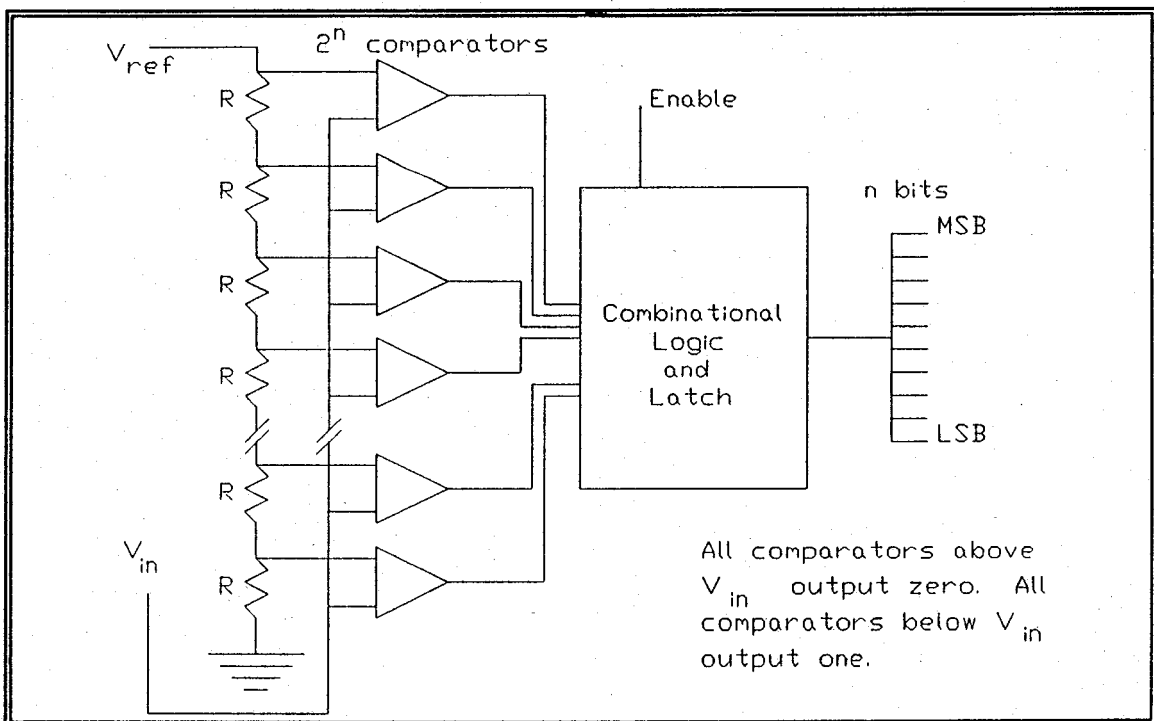
Figure C.3 - Parallel or Flash Structure

Figure C.4 shows the structure of the successive approximation type A/D converter. N-bit conversion involves n successive guesses as to the value of the input voltage. The converter sets the most significant bit (MSB) of the D/A converter to a one. If the input voltage is greater (comparator value positive), the control circuit retains the value of one for the MSB. Otherwise, the control circuit sets the MSB to zero. This same guess-and-compare scheme continues until the n-bit codeword is complete. The conversion time is fixed, and each conversion is

213

independent of previous conversions. The advantage of the successive approximation technique is that conversion resolution, or the number of bits in the codeword, is dependent only on the D/A resolution. A/D converters with 16 or more bits usually employ the successive approximation structure. The main disadvantage results from conversion errors caused by settling time, differential non-linearities, and missing codes of the D/A. Almost all successive approximation converters require a companion sample-and-hold device.
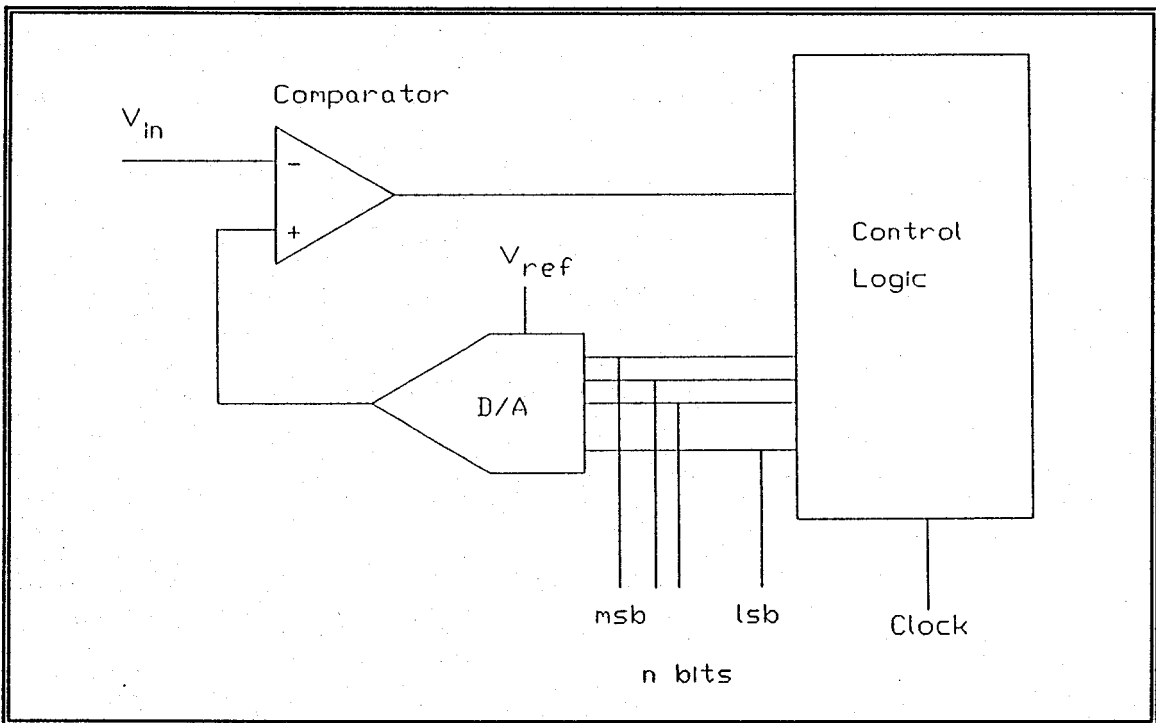
Figure C.4 - Successive Approximation Structure

APPENDIX D

This appendix contains two work sheets developed using the IBM-PC software

MATHCAD, Ver. 2.5. The discussion about the systems modeled in the work

sheets is found in Chapter VIII.

Number of Samples	$k1 := 2048$		$k := 0 .. (k1 - 1)$
Sampling Frequency	$fs := 2039$		
Carrier Frequency	$\omega_c := 2 \cdot \pi \cdot 50$	Signal Strength Difference	
		$r := 0.95$	
Modulation Frequencies	$\omega_a := 2 \cdot \pi \cdot 3$	$s := 0.01$	
		Modulation Indicies	
	$\omega_b := 2 \cdot \pi \cdot 4.1$	$k_a := 0.9$	
Carrier Offset	$\omega_\delta := 2 \cdot \pi \cdot 11$	$k_b := 0.5$	

Define two modulations, resulting envelope, & resulting PM

$$A_k := r \cdot \left[1 + k_a \cdot \cos\left[\omega_a \cdot \frac{k}{fs}\right]\right] \qquad B_k := s \cdot \left[1 + k_b \cdot \cos\left[\omega_b \cdot \frac{k}{fs}\right]\right]$$

The input signal is:

$$Vin_k := A_k \cdot \cos\left[\omega_c \cdot \frac{k}{fs}\right] + B_k \cdot \cos\left[\left[\omega_c + \omega_\delta\right] \cdot \frac{k}{fs}\right]$$
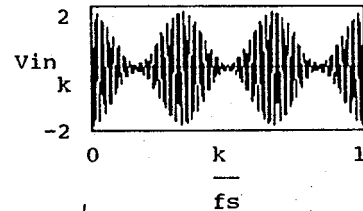
Calculate the Complex Envelope and Phase terms

$$Env_k := A_k \cdot \sqrt{1 + \frac{B_k^2}{A_k^2} + 2 \cdot \frac{B_k}{A_k} \cdot \cos\left[\omega_\delta \cdot \frac{k}{fs}\right]} \qquad \Phi_k := atan\left[\frac{B_k \cdot \sin\left[\omega_\delta \cdot \frac{k}{fs}\right]}{A_k + B_k \cdot \cos\left[\omega_\delta \cdot \frac{k}{fs}\right]}\right]$$

216

Put the input through
a hard limiter, & filter

$$Vlim_k := if\left[Vin_k > 0, 1, if\left[Vin_k < 0, -1, 0\right]\right]$$

SVlim := fft(Vlim)

$$SVfil_j := if\left[j \le 100, SVlim_j, 0\right]$$

Vfil := ifft(SVfil)
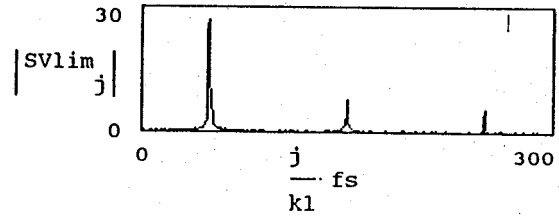
Determine the output by
scaling of the filtered signal

$$V(a,b,c,d) := a - b \cdot c \cdot d \qquad scale := 0.776$$

$$Vout_k := V\left[Vin_k, Env_k, scale, Vfil_k\right]$$

Sin := fft(Vin)

$\left|\text{Sin}_j\right|$

$\frac{j}{k1} \cdot \text{fs}$

Sout := fft(Vout)

$\left|\text{Sout}_j\right|$

$\frac{j}{k1} \cdot \text{fs}$

Sb := fft(Vb)

$\left|\text{Sb}_j\right|$

$\frac{j}{k1} \cdot \text{fs}$

218
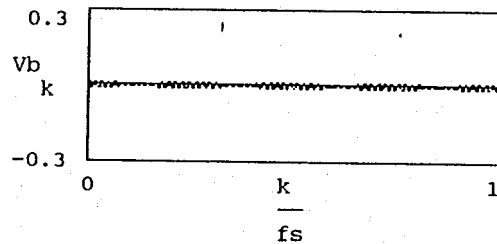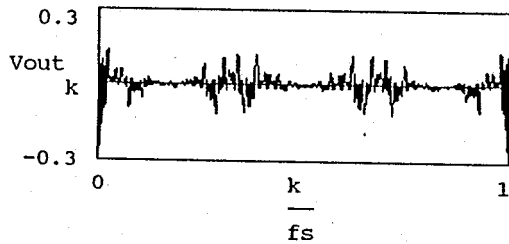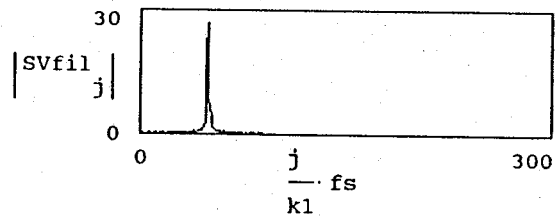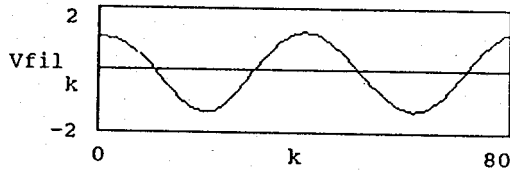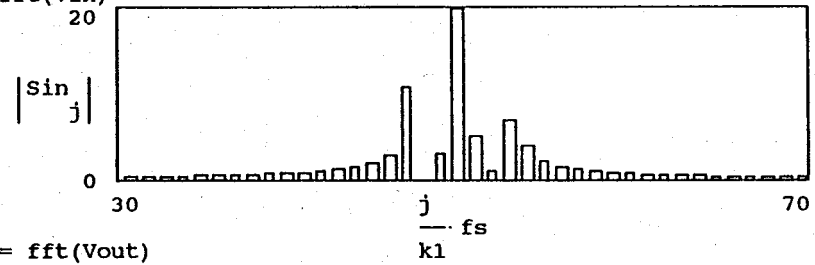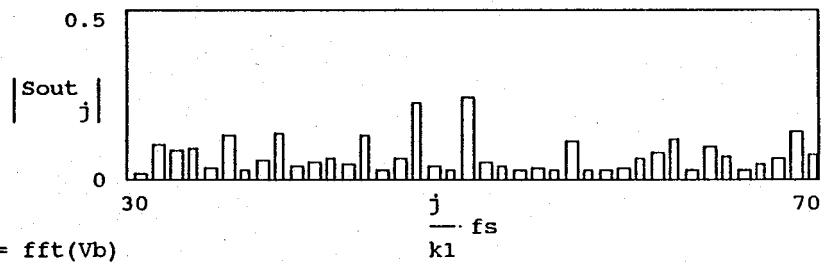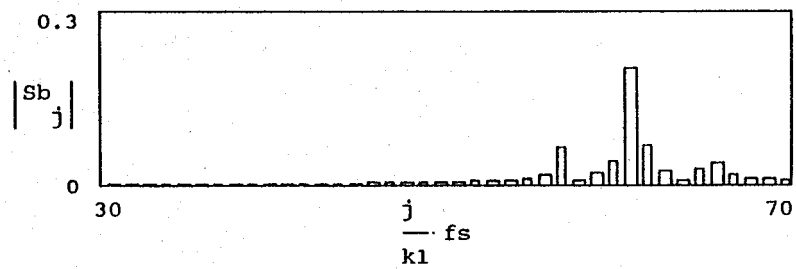
Large Signal Suppressor - Gus Lott & G.A. Myers - 13 Dec 89

Number of Samples $\quad$ $k1 := 2048$ $\qquad$ $k := 0 .. (k1 - 1)$

Sampling Frequency $\quad$ $fs := 2039$ $\qquad$ $j := 0 .. \dfrac{k1}{2}$

Carrier Frequency $\qquad$ $\omega_c := 2 \cdot \pi \cdot 50$ $\qquad$ Signal Strength Difference
$$r := 0.95$$
$$s := 0.01$$

Modulation Frequencies $\qquad$ $\omega_a := 2 \cdot \pi \cdot 3$

$\omega_b := 2 \cdot \pi \cdot 4.1$ $\qquad$ Modulation Indicies

$\qquad\qquad\qquad\qquad$ $k_a := 0.9$

Carrier Offset $\qquad$ $\omega_\delta := 2 \cdot \pi \cdot 11$ $\qquad$ $k_b := 0.5$

Define two modulations, resulting envelope, & resulting PM

$$A_k := r \cdot \left[1 + k_a \cdot \cos\left[\omega_a \cdot \frac{k}{fs} \right] \right] \qquad B_k := s \cdot \left[1 + k_b \cdot \cos\left[\omega_b \cdot \frac{k}{fs} \right] \right]$$

$$Va_k := A_k \cdot \cos\left[\omega_c \cdot \frac{k}{fs} \right] \qquad Vb_k := B_k \cdot \cos\left[\left[\omega_c + \omega_\delta \right] \cdot \frac{k}{fs} \right]$$

$$Vin_k := Va_k + Vb_k$$

$$Env_k := A_k \cdot \sqrt{1 + \frac{B_k^2}{A_k^2} + 2 \cdot \frac{B_k}{A_k} \cdot \cos\left[\omega_\delta \cdot \frac{k}{fs} \right]}$$

219
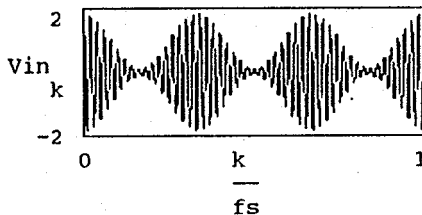
min(Env) = 0.080247   min(Φ) = -0.097799
max(Env) = 1.82   max(Φ) = 0.106054

$$\epsilon rms := \sqrt{\frac{1}{k1} \cdot \sum_k \left[A_k - Env_k\right]^2}$$

$\epsilon rms = 0.007609$
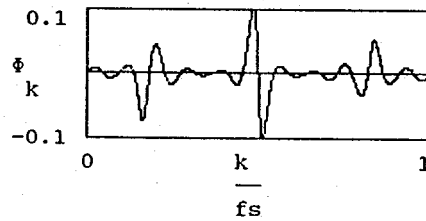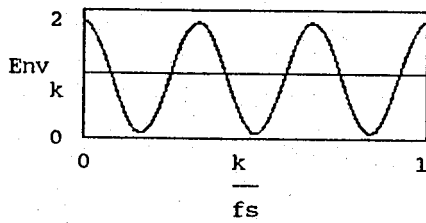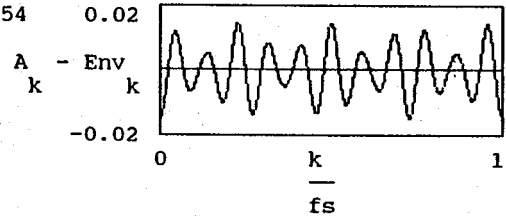
Determine the output

$$Vout_k := Vin_k - Env_k \cdot \cos\left[\omega_c \cdot \frac{k}{fs}\right]$$

$$\epsilon 1rms := \sqrt{\frac{1}{k1} \cdot \sum_k Vout_k^2}$$

min(Vout) = -0.014812

max(Vout) = 0.014514

$\epsilon 1rms = 0.005355$
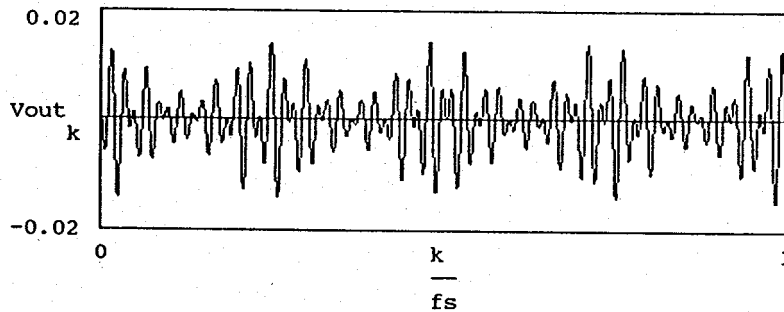
$$j := 0 \, .. \, \left[\frac{k1}{2}\right]$$

Sin := fft(Vin)
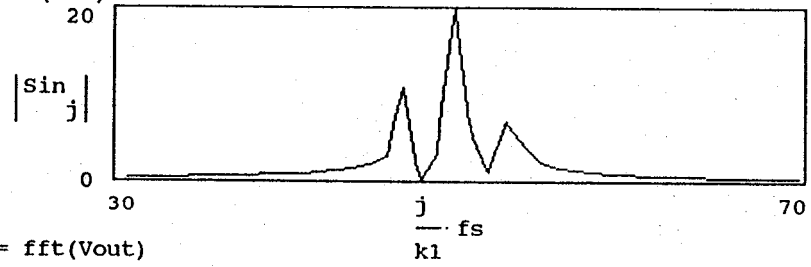
Sout := fft(Vout)
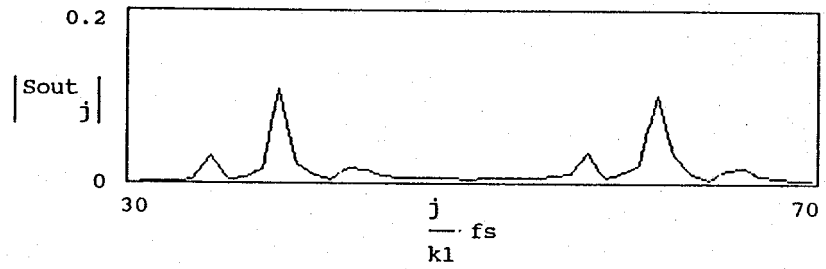
LIST OF REFERENCES

1. *Reference Data for Engineers: Radio, Electronics, Computer, and Communications,* 7th Ed., Howard W. Sams & Co., Inc., Indianapolis, IN, 1988.

2. International Telecommunications Union (ITU), *Radio Regulations,* Geneva, Switzerland, 1959, as ammended.

3. *World Radio Television Handbook,* v. 43, Billboard A.G., 1989.

4. Wong, N.F., Gott, G.F., and Barclay, L.W., "HF spectral occupancy and frequency planning," *IEE Proceedings,* Part F, v. 132, n. 7, pp. 548-557, Dec 1985.

5. British Broadcasting Corporation, "World service frequencies," *London Calling,* v. 17, n. 11, pp. 1-28, Nov 1988.

6. Sanders Associates, Inc., Technical Report No. SP-87-07926, *Analysis Report for WARS Interference Study (U),* 25 Oct 1988. SECRET.

7. Sowers, Mary W., Hand, Gregory, and Rush, Charles M., "Jamming to the HF broadcasting service," *IEEE Transactions on Broadcasting,* v. 34, n. 2, pp. 109-114, Jun 1988.

8. U.S. Department of Commerce, National Telecommunications and Information Administration, NTIA Report 86-206, *Monitoring of Harmful Interference to the HF Broadcasting Service: II. Results of the January 1986 Coordinated Monitoring Period,* pp. 1-48, National Technical Information Service, Springfield, VA, 1986.

9. Gott, G.F., Dutta, S., and Donay, P., "Analysis of HF interference with application to digital communications," *IEE Proceedings on Communications, Radar, and Signal Processing,* Part F, v. 130, n. 5, pp. 452-458, 1983.

10. Sosin, B.M., "H.F. communication receiver performance requirements and realization," *The Radio and Electronic Engineer,* v. 41, n. 7, pp. 321-329, Jul 1971.

11. Shumpert, T.H., Honnell, M.A., and Lott, G.K., "Measured spectral amplitude of lightning sferics in the HF, VHF, and UHF bands," *IEEE Transactions on Electromagnetic Compatability*, v. EMC-24, n. 3, pp. 368-369, Aug 1982.

12. International Radio Consultative Committee (CCIR), CCIR Report 322, "World distribution and characteristics of atmospheric radio noise," 10th Plenary Assembly, Geneva, Switzerland, 1963.

13. Cummings, Eugene J. Jr., Jauregui, Stephen Jr., and Vincent, Wilbur Ray, "Time and frequency domain characteristics of man-made radio noise affecting HF-communications sites," *IEEE Transactions on Electromagnetic Compatability*, v. EMC-21, n. 3, pp. 182-189, Aug 1979.

14. Pearce, T.H. and Baker, A.C., "Analogue to digital conversion requirements for H.F. radio receivers," *IEE Colloquium on Systems Aspects and Applications for ADCs for RADAR, SONAR, and Communications*, pp. 4-1 - 4-5, 3 Nov 1987.

15. Pearce, T.H., Baker, A.C, and Carter, C.G., "The application of DSP techniques in HF radio receiver design," *IEE 4th International Conference on HF Communication Systems and Techniques*, pp. 205-209, Apr 1988.

16. Vincent, Wilbur Ray, Jauregui, Stephen, and Adler, Richard W., Training Manual 890110-1, *A SNEP Team Training Manual (Draft)*, May 1989.

17. Dutta, S. and Gott, G.F., "HF spectral occupancy," *IEE 2nd Conference on HF Communication Systems and Techniques, Conf. Pub. No. 206*, pp. 96-100, Feb 1982.

18. Wilkinson, R.G., "A statistical analysis of HF radio interference and its application to communication systems," *IEE 2nd Conference on HF Communication Systems and Techniques, Conf. Pub. No. 206*, pp. 101-105, Feb 1982.

19. Gibson, A.J., Bradley, P.A., and Schlobohm, J.C., "HF spectrum occupancy measurements in southern England," *IEE 3rd International Conference on HF Communication Systems and Techniques, Conf. Pub. 245*, pp. 71-75, Feb 1985.

20. Moulsley, T.J., "HF data transmission in the presence of interference," *IEE 3rd International Conference on HF Communication Systems and Techniques, Conf. Pub. No. 245*, pp. 67-70, Feb 1985.

21. Gibson, A.J. and Arnett, L., "New HF spectrum occupancy measurements in southern England," *IEE 4th International Conference on HF Radio Systems and Techniques, Conf. Pub. No. 284*, pp. 159-164, Apr 1988.

22. Laycock, P.J. and others, "A model for HF spectral occupancy," *IEE 4th International Conference on HF Communication Systems and Techniques, Conf. Pub. No. 284*, pp. 165-171, Apr 1988.

23. Perry, B.D, and Abraham, L.G., "A wideband HF interference and noise model based on measured data," *IEE 4th International Conference on HF Communication Systems and Techniques*, pp. 172-176, Apr 1988.

24. Hagn, George H., Stehle, Roy H., and Harnish, Lawrence O., "Shortwave broadcasting band spectrum occupancy and signal levels in the continental United States and western Europe," *IEEE Transactions on Broadcasting*, v. 34, n. 2, pp. 115-125, Jun 1988.

25. Aitchison, J. and Brown, J.A.C., *The Lognormal Distribution*, Cambridge University Press, London, 1957.

26. Croxton, Fredrick E., Cowden, Dudley J., Klein, Sidney, *Applied General Statistics*, 3rd Ed., Prentice-Hall, Englewood Cliffs, NJ, 1967.

27. Sachs, Lothar, *Applied Statistics, a Handbook of Techniques*, 5th Ed., Springer-Verlag, NY, 1982.

28. Hart, William C. and Malone, Edgar W., *Lightning and Lightning Protection*, Don White Consultants, Inc., Gainnesville, VA, 1979.

29. Maslin, Nicholas M., *HF Communications: A Systems Approach*, Plenum Press, NY, 1987.

30. Ziemer, Rodger E. and Peterson, Roger L., *Digital Communications and Spread Spectrum Systems*, Macmillan Publishing Co., NY, 1985.

31. IWG Corp. Report IWG-FR-087-12, *Operators Manual for the United States Coast Guard Advanced PROPHET System*, prepared for Naval Ocean Systems Center (Code 542), San Diego, CA, pp. 96-102,201-202, 1 Nov 1987.

32. Harthcock, Clyde T., *An Examination of the Radio Frequency Switching Matrix at U.S. Army Field Station Augsburg, U.S. Army Field Station Berlin, and U.S. Naval Security Group Activity Edzell*, Master's Thesis, Naval Postgraduate School, Monterey, CA, Sep 1989.

33. Hurley, J.M. Jr., *HF Digital Subcarrier Receiver System*, Master's Thesis, Naval Postgraduate School, Monterey, CA, Dec 1985.

34. Carson, M.H., *Consideration for an All-Digital HFDF System*, Master's Thesis, Naval Postgraduate School, Monterey, CA, Dec 1982.

35. Jenkins, A., "D-A and A-D conversion," *Microelectronics and Reliability*, v.21, n. 3, pp. 329-341, 1981.

36. Gordon, Bernard M., "Linear electronic analog/digital conversion architectures, their origins, parameters, limitations, and applications," *IEEE Transactions on Circuits and Systems*, v. CAS-25, pp. 391-418, Jul 1978.

37. Schweber, B. and Labs, W., "A/D converters: 16-bit resolution isn't always enough," *Chilton's IC&S (USA)*, v. 61, n. 2, pp. 51-52, Feb 1988.

38. Little, Al and Burnett, Bob, "S/H amp-ADC matrimony provides accurate sampling," *EDN*, v. 33, n. 3, pp. 153-166, 4 Feb 1988.

39. Tewksbury, Stuart K. and others, "Terminology related to the performance of S/H, A/D, and D/A circuits," *IEEE Transactions on Circuits and Systems*, v. CAS-25, pp. 419-426, Jul 1978.

40. Brigham, E.O. and Cecchini, L.R., "A nomogram for determining FFT system dynamic range," *Proceedings of the IEEE International Conference on Acoustics, Speech, and Signal Processing*, Hartford, CT, pp. 623-627, 9-11 May 1977.

41. Doernberg, Joey, Lee, Hae-Seung, and Hodges, David A., "Full-speed testing of A/D converters," *IEEE Journal of Solid-State Circuits*, v. SC-19, n. 6, pp. 820-827, Dec 1984.

42. Naylor, Jim R., "Testing digital/analog and analog/digital converters," *IEEE Transactions on Circuits and Systems*, v. CAS-25, pp. 526-538, Jul 1978.

43. Sheingold, D.H., *Analog-Digital Conversion Hankbook*, Analog Devices, Inc., 1972.

44. Aiken Advanced Systems, Technical Note SDS-101, *Output Intercept Point Calculations*, pp. 1-4, not dated.

45. Steinbrecher, Donald H., "Fundamental limitations on Accuverter performance," unpublished internal Steinbrecher Corporation, Woburn, MA, paper discussed with author during interview at the Naval Postgraduate School, Monterey, CA, on 4 Nov 1988.

46. Gray, G.A. and Zeoli, G.W., "Quantization and saturation noise due to analog-to-digital conversion," *IEEE Transactions on Aerospace and Electronic Systems*, Jan 1971.

47. Gaskell, P.S., "Evaluating ADC's for zero-IF digital radios," *IEE Colloquium on Systems Aspects and Applications of ADC's for RADAR, SONAR, and Communications*, pp. 5-1 - 5-4, 3 Nov 1987.

48. Anderson, D.T. and Whikehart, "A digital signal processing HF receiver," *IEE 3rd International Conference on HF Communication Systems and Techniques, Conf. Pub. No. 245*, pp. 89-93, Feb 1985.

49. Ghausi, M.S. and Laker, K.R., *Modern Filter Design*, Prentice-Hall, 1981.

50. Morgan, S. Kent, "Modern data aquisition is complex," *Electronic Design*, v. 22, pp. 60-66, 25 Oct 1977.

51. Harris, F.J., "On the use of windows for harmonic analysis with the discrete Fourier transform," *IEEE Proceedings*, v. 66, n. 1, pp. 51-83, Jan 1978.

52. Oppenheim, A.V. and Weinstein, C.J., "Effects of finite register length in digital filtering and fast Fourier transform," *IEEE Proceedings*, v. 60, n. 8, pp. 957-976, Aug 1972.

53. Welch, Peter D., "A fixed point fast Fourier transform error analysis," *IEEE Transaction on Audio and Electroacoustics*, pp. 151-157, Jun 1969.

54. Tarver, Raymond J., "Graphs aid selection of A-D converters," *Electronics*, v. 47, n. 4, pp.110-111, 21 Feb 1974.

55. Hariharan, P.R., "Note on dynamic range of quantizers," *IEEE Transactions on Aerospace and Electronic Systems*, v. AES-5, n. 5, pp. 875-877, 5 Sep 1969.

56. Fogarty, John D., "Know your A/D converter's dynamic range," *Electronic Design*, v. 23, n. 3, pp. 76-78, 1 Feb 1975.

57.   Labutin, V.K., "Nomogram for finding the parameters of an analog-digital signal converter," *Telecommunications and Radio Engineering*, v. 35-36, n. 3, pp. 108-109, Mar 1981.

58.   Story, M.J., "Hardware costs of systems aspects of ADCS," *IEE Colloquium on Systems Aspects and Applications of ADCs for RADAR, SONAR, and Communications*, pp. 1-1 - 1-9, 3 Nov 1987.

59.   deGraaf, K., Air Force Wright Aeronautical Laboratories, Technical Report AFWAL-TR-83-1090, *High Speed A/D Converter Development Phase I*, Jun 1983.

60.   Burr-Brown Inc., Technical Data Sheet ADC600, *12-Bit Ultra-High Speed A/D Converter*, pp. 1-18, 1987.

61.   Albaugh, Neil, "New ADCs for RF signal processing," *RF Design*, v. 10, n. 12, pp. 33-38, Nov 1987.

62.   Breed, G.A. "High speed A/D and D/A conversion," *RF Design*, v. 11, n. 1, pp. 39-40, Jan 1988.

63.   Muto, Arthur S., Peetz, Bruce E., and Rehner, Robert C., "Designing a ten-bit, twenty-megasample-per-second analog-to-digital converter system," *Hewlett-Packard Journal*, v. 33, n. 11, pp. 9-20, Nov 1982.

64.   Burr-Brown Inc., Advance Technical Data Sheet ADC701/SHC702, *High Speed 16-bit Sampling A/D Converter System*, p. 1, Dec 1987.

65.   Althouse, E.L., Mesias, S., and Kopp, D.M., Naval Research Laboratory, Memorandum Report 5518, *The Use of a High-Speed 12-bit A/D Converter for Digital Sampling of Communication Signal Carriers*, 31 Dec 1984.

66.   Bagwell, D.J. and Considine, V., "Digital processing architectures for HF radio receivers," *IEE 3rd International Conference on HF Communication Systems and Techniques, Conf. Pub. No. 245*, pp. 86-88, Feb 1985.

67.   Burrier, Richard and others, "Floating-point converter used hardware to get a 20-bit dynamic range," *Electronic Design*, v. 32, n. 18, pp. 175-186, 6 Sep 1984.

68.   Davies, Kirk E., *Floating-Point A/D and D/A Converter*, U.S. Patent 4,393,369, 12 Jul 1983.

69. Lacy, James and McMullin, Finbarr, "Enhancing the dynamic range of an A/D converter," *Electronic Engineering (GB)*, v. 55, n. 680, pp.49-52, Aug 1983.

70. Nguyen, Chieu, "Digital automatic level control for analog-to-digital conversion," paper presented at the 76th Convention of the Audio Engineering Society, New York City, NY, 8-11 Oct 1984.

71. Morgan, Dennis R., "AGC extends the range of A/D converters," *Electronic Design*, n. 22, pp. 108-110, 25 Oct 1975.

72. Carpenter, Robert J. and Yee, Kenneth W., *High Speed, Wide Dynamic Range Analog-to-Digital Conversion*, U.S. Patent 4,129,864, 12 Dec 1978.

73. Carpenter, Robert J. and Yee, Kenneth W., *High Speed, Wide Dynamic Range Analog-to-Digital Conversion*, U.S. Patent 4,069,479, 17 Jan 1978.

74. V'yukhin, V.N. and Kasperovich, A.N., "Designing analog-to-digital converters for an extremely large number of digits," *Optoelectron Instrumentation and Data Processing*, n. 5, pp. 1-10, 1985.

75. Harrison, D.C. and Staples, M.H., "A quadratic analog-to-digital converter," *IEEE Transactions on Nuclear Science*, v. NS-27, n. 1, pp. 396-398, Feb 1980.

76. Cantarano, S. and Pallottino, G.V., "Logarithmic analog-to-digital converters: a survey," *IEEE Transactions on Instrumentation and Measurement*, v. IM-22, n. 3, pp. 201-213, Sep 1973.

77. Nimmo, R., "Companding D/A and A/D converters," *Microelectron Reliability*, v. 21, n. 3, pp. 343-353, 1981.

78. Ferrie, Ronald, "Analog-to-digital converter produces logarithmic output," *Electronics*, v. 46, n. 14, pp. 98-99, 5 Jul 1973.

79. Friend, Brian W., "Extending the dynamic range of flash A/D converters," *New Electronics*, v. 12, n. 22, pp. 47-48, 11 Nov 1986.

80. Doroshev, V.P. and others, "Wide-range high-speed analog-to-digital converter," *Instruments and Experimental Techniques*, v. 28, n. 1, pt. 1, pp. 106-110, Jan 1985.

81.   Doroshev, V.P., Belov, A.M., and Yamnyi, V.E., "High-speed analog-to-digital converter with 60-dB dynamic range," *Instruments and Experimental Techniques*, v. 28, n. 5, pt. 1, pp. 1082-1085, Sep 1985.

82.   Einarsson, Göran H., "Dynamic range and error dissipation of adaptive quantizers," *IEEE Transactions on Acoustics, Speech, and Signal Processing*, v. ASSP-33, n. 4, pp. 1073-1075, Oct 1985.

83.   Mitra, Debasis, "Mathematical analysis of an adaptive quantizer," *The Bell System Technical Journal*, v. 53, n. 5, pp. 867-898, May-Jun 1974.

84.   Claasen, Theo A.C.M. and others, "Signal processing method for improving the dynamic range of A/D and D/A converters," *IEEE Transactions on Acoustics, Speech, and Signal Processing*, v. ASSP-28, n. 5, pp. 529-537, 5 Oct 1980.

85.   Corcoran, J.J., Poulton, K., and Knudsen, K.L., "A one-gigasample-per-second analog-to-digital converter," *Hewlett-Packard Journal*, v. 39, n. 3, pp. 59-66, Jun 1988.

86.   Cake, Brian, Ems, Stephen, and Lentsch, David W., "Waveform digitizer snares single-shot events at 1.348 Gsamples/s," *Electronic Design*, v. 34, n. 5, pp. 117-126, 6 Mar 1986.

87.   Tektronix Bipolar Products Data Sheet TKAD20C, *250 MSPS 8-bit A/D Converter with Track-and-Hold*, pp. 1-16, 1987.

88.   Frohring, Brian J. and others, "Waveform recorder design for dynamic performance," *Hewlett-Packard Journal*, v. 39, n. 1, pp. 39-48, Feb 1988.

89.   Gee, Alvert, and Young, Ronald W., "Signal conditioning and analog-to-digital conversion for a 4-MHz, 12-bit waveform recorder," *Hewlett-Packard Journal*, v. 39, n. 1, pp. 15-22, Feb 1988.

90.   Bradsell, P., "Analogue-Digital converter requirements for RADAR systems," *IEE Colloquium on Systems Aspects and Applications of ADCs for RADAR, SONAR, and Communications*, pp. 7-1 - 7-4, 3 Nov 1987.

91.   Asta, D., Lincoln Laboritories, Project Report AST-5, *Evaluation of High-Speed Waveform Digitizers for Spectral Analysis Applications*, 14 Jun 1988.

92.   Spencer, N.W., Lincoln Laboratories, Project Report AST-4, *Comparrison of State-of-the-Art Analog-to-Digital Converters*, 4 Mar 1988.

93.   Irons, F.H. and Rebold, T.A., Lincoln Laboratories, Project Report AST-2, *Characterization of High-Frequency Analog-to-Digital Converters for Spectral Analysis Applications*, 28 Nov 1986.

94.   Rebold, T.A. and Irons, F.H., "A phase-plane approach to the compensation of high-speed analog-to-digital converters," *Proceedings of the IEEE International Symposium on Circuits and Systems*, pp. 455-458, 4-7 May 1987.

95.   Asta, Daniel and Irons, Fred H., "Dynamic error compensation of Analog-to-Digital Converters," *The Lincoln Laboratory Journal*, v. 2, n. 2, pp. 161-182, Summer 1989.

96.   Dent, A.C. and Cowan, C.F.N., "High linearity, high resolution analogue to digital conversion for telecommunications," *IEE Colloquium on Systems Aspects and Applications for ADCs for RADAR, SONAR, and Communications*, pp. 2-1 - 2-5, 3 Nov 1987.

97.   Kay, Steven M. and Sudhaker, R., "A zero crossing-based spectrum analyzer," *IEEE Transactions on Acoustics, Speech, and Signal Processing*, v. ASSP-34, n. 1, pp. 96-104, 1 Feb 1986.

98.   Lu, Fu-Sheng and Wise, Gary L., "A simple approximation for minimum mean-square error symetric uniform quantization," *IEEE Transactions on Communications*, v. COM-32, n. 4, pp. 470-474, Apr 1984.

99.   Max, Joel, "Quantizing for minimum distortion," *IRE Transactions on Information Theory*, v. IT-6, n. 1, pp. 7-12, Mar 1960.

100. Elias, Peter, "Bounds and asymptotes for the performance of multivariate quantizers," *The Annals of Mathematical Statistics*, v. 41, n. 4, pp. 1249-1259, 1970.

101. Elias, Peter, "Bounds on performance of optimum quantizers," *IEEE Transactions on Information Theory*, v. IT-16, n. 2, pp. 172-184, Mar 1970.

102. Sasaki, Tai, and Hataoka, Hiroshi, "Quantization for minimum intermodulation distortion," *International Journal on Electronics (GB)*, v. 57, n. 3, pp. 361-369, Sep 1984.

103. Hurrell, John P., Pridmore-Brown, David C., and Silver, Arnold H., "Analog-to-digital conversion with unlatched SQUID's," *IEEE Transactions on Electron Devices*, v. ED-27, n. 10, Oct 1980.

104. McKnight, W.H. and others, Naval Ocean Systems Center, Technical Document 1034, *Wide-Dynamic-Range Analog-to-Digital Conversion for HFDF*, Nov 1986.

105. DePrimo, John G., Naval Underwater Systems Center, Technical Report 5769, *Measurements of Noise, Signal, and Signal-Plus-Noise Spectra through a 5-Bit-Plus-Sign A/D Converter*, 5 Jan 1978.

106. Myers, Glen A. and Petersen, Stephen C., *Method and Apparatus for Frequency Independent Phase Tracking of Input Signals in Receiving Systems and the Like*, U.S. Patent Application, number not yet assigned.

107. Hnatek, Eugene R., *A User's Handbook of D/A and A/D Converters*, Robert E. Krieger Publishing Co., 1988.

108. Hoeschele, David F. Jr., *Analog-to-Digital/Digital-to-Analog Conversion Techniques*, John Wiley & Sons, Inc., 1968.

BIBLIOGRAPHY

Assard, Gerald A., *A/D Dynamic Range Enhancing Technique*, U.S. Patent 4,352,095, 28 Sep 1982.

Bedmarek, Chris, "Dynamic characterization of A/D converters," *Handshake*, Tektronix Corp., pp. 8-11, Summer 1988.

Brierley, S.K., Rome Air Development Center, Technical Report No. RADC-TR-78-237, *High Speed High Dynamic Range A/D Converter*, Nov 1978.

Chapman, P.S., "Comparison of 10 BPS MODEM with man-read morse," *IEE 3rd International Conference on HF Communication Systems and Techniques*, pp. 136-145, Feb 1985.

CNR, INC., Naval Research Laboratory, Final Technical Report for Contract No. N00173-79-C-0090, *Wideband HF Channel Analyzer*, Jan 1981.

Dybitskiy, L.A., Shvetskiy, B.I., and Yuzevich, Yu.V., "Ways for providing a high-speed analog-to-digital converter with wide dynamic range," edited translation of *Regional'nyy Nauchno-Tekhnicheskiy Seminar po Statisticheskomu Analizu, Modelirovaniyu 1 Avotmatizatski Kontrolya Ob"yektov a Konstruktivno Slozhnoy Strukuroy*, nr. 6, pp. 86-90, 1972.

Fast, Saul, Air Force Avionics Laboratory, Final Technical Report AFAL-TR-76-265, *Advanced Receiver Modeling Methods*, pp. 2-10, Sep 1977.

Garrett, Patrick H., *Analog I/O Design, Aquisition; Conversion; Recovery*, Reston Publishing Co., Inc., 1981.

Gerace, G.C., *Spectral Analysis of Digital Radio Frequency Memory and Its Effects on a Superheterodyne RF Receiver*, Master's Thesis, Air Force Institute of Technology, Air University, Wright Patterson AFB, OH, Dec 1985.

Howarth, G.L., *Fourier Analysis of Broadband, Low-Level Signals using Switched Inputs*, Engineer's Thesis, Naval Postgraduate School, Monterey, CA, Jun 1981.

Jain, V.K., Rome Air Development Center, Final Technical Report, RADC-TR-80-343, *Advanced Techniques for Black Box Modeling (Effect of Signal Quantization; Multirate Sampling of Wideband Systems*, Nov 1980.

Jenq, Y.C., "Asynchronous dynamic testing of A/D converters," *Handshake*, Tektronix Corp., v. 13, n. 2, pp. 4-7, Summer 1988.

Luiz, R., Defense Research Establishment Ottawa, Technical Note 81-17, "HF/VHF spectrum surveillance ESM receiver," pp. 1-25, Sep 1981.

Natali, Francis D. and Magill, David T., Rome Air Development Center, Technical Report No. RADC-TR-68-163, *Digital Processing Receiver Study*, May 1968.

O'Dwyer, John Mark, *Power Line Noise Models and Energy Detection in the High Frequency Radio Band*, Ph.D. Dissertation, Naval Postgraduate School, Monterey, CA, Jun 1986.

Pearce, T.H. and Rogers, S.D., "Design considerations for an HF digital radio receiver," *Proceedings from the IEE Conference on Radio Receivers and Associated Systems*, conference 09506, publication n. 68, pp. 207-212, 1-4 Jul 1986.

Pickands III, J., Raghavachari, M., "Exact and asymptotic inference for the size of a population," *Biometrika*, v. 74, n. 2. pp. 355-363, 1987.

Ramirez, Robert W., *The FFT: Fundamentals and Concepts*, Prentice-Hall, Inc., 1985.

Susskind, Alfred K. editor, *Notes on Analog-Digital Conversion Techniques*, MIT Press, 1957.

Sylvan, J., "Monolithic DAC for RF signal processing," *RF Design*, v. 11, n. 1, pp. 44-46, Jan 1988.

Telsa, D.D., "A method of channel occupancy monitoring in adaptive HF systems," *IEE 3rd International Conference on HF Communication Systems and Techniques, Conf. Pub. No. 245*, pp. 76-80, Feb 1985.

Watson, A.W.D, Simpson, S.H.W., and Jackson, T., "Digital conversion and signal processing for high performance communications receivers," *Proceedings of the International Conference on Digital Processing of Signals in Communications*, Loughborough, England, pp. 367-373, 22-26 Apr 1985.

Wise, G.L., Air Force Office of Scientific Research, Interim Report No. AFOSR-TR-84-1184, *The Study of Certain Aspects of Probability with Applications in Communications Theory*, 28 Nov 1984.

INITIAL DISTRIBUTION LIST

1. Defense Technical Information Center   2
    Cameron Station
    Alexandria, VA 22304-6145

2. Library, Code 0142   2
    Naval Postgraduate School
    Monterey, CA 93943-5002

3. Superintendent   1
    Naval Postgraduate School
    Attn: Director of Research Administration, Code 012
    Monterey, CA 93943-5000

4. Superintendent   1
    Naval Postgraduate School
    Attn: Chairman, Department of Electronic and Computer
            Engineering, Code EC
    Monterey, CA 93943-5000

5. Superintendent   5
    Naval Postgraduate School
    Attn: Prof. S. Jauregui, Code EC/Ja
    Monterey, CA 93943-5000

6. Superintendent   1
    Naval Postgraduate School
    Attn: Prof. R. Adler, Code EC/Ab
    Monterey, CA 93943-5000

7. Superintendent   2
    Naval Postgraduate School
    Attn: Prof. R. Vincent, Code EC/Ja
    Monterey, CA 93943-5000

8.   Superintendent   2
      Naval Postgraduate School
      Attn: Prof. R. Myers, Code EC/Mv
      Monterey, CA 93943-5000

9.   Superintendent   2
      Naval Postgraduate School
      Attn: Prof. P. Moose, Code EC/Me
      Monterey, CA 93943-5000

10.   Superintendent   1
      Naval Postgraduate School
      Attn: Prof. H. Fredricksen, Code MA/Fr
      Monterey, CA 93943-5000

11.   Superintendent   1
      Naval Postgraduate School
      Attn: Prof. M. Zyda, Code CS/Zy
      Monterey, CA 93943-5000

12.   Commander   2
      Space and Naval Warfare Systems Command
      Attn: Code PMW-143
      Washington, DC 20360

13.   Commander   2
      Space and Naval Warfare Systems Command
      Attn: Code PMW-144
      Washington, DC 20360

14.   Commander   1
      Naval Security Group Command
      Attn: G40
      3801 Nebraska Ave., N.W.
      Washington, DC 20390

15.   Commander   2
      Naval Security Group Command
      Attn: G433
      3801 Nebraska Ave., N.W.
      Washington, DC 20390

16. Commander   1
    Naval Security Group Command
    Attn: G80
    3801 Nebraska Ave., N.W.
    Washington, DC 20390

17. Commander   1
    Naval Security Group Command
    Attn: G81
    3801 Nebraska Ave., N.W.
    Washington, DC 20390

18. Commander   3
    Naval Security Group Command
    Attn: G8132
    3801 Nebraska Ave., N.W.
    Washington, DC 20390

19. Commander   1
    Naval Electronic Systems Security Engineering Center
    Attn: Code 042
    3801 Nebraska Ave., N.W.
    Washington, DC 20390

20. Commander   1
    Naval Surface Warfare Center
    Code F32, Attn: Dave Hovey
    Ft. George G. Meade, MD 20755

21. Director   1
    National Security Agency
    Attn: R641/Dr. Jeff Friedhoffer
    Ft. George G. Meade, MD 20755

22. Director   1
    National Security Agency
    Attn: R6
    Ft. George G. Meade, MD 20755

23. Commander   1
    Naval Ocean Systems Center
    Attn: Code 772 (R.B. Rose)
    San Diego, CA 92152-5000